

Project Acronym:
SOUNDPET(INTEGRATED/0918/0008)

MRI-guided Focused ultraSOUND system for cancer in PETs (dogs and cats).

Deliverable number: 6.3

Title: MRI Evaluation of the Thermal Heating of the Transducer

Prepared by:

Theocharis Drakos (MEDSONIC)

Michalis Kassinopoulos (CUT)

Andreas Georgiou (CUT)

Nikolas Evripidou (CUT)

Antria Filippou (CUT)

Anastasia Nikolaou (CUT)

Christakis Damianou (CUT)

Date: 12/15/2023



Ευρωπαϊκή Ένωση
Ευρωπαϊκά Διαρθρωτικά
και Επενδυτικά Ταμεία



Κυπριακή Δημοκρατία



Διαρθρωτικά Ταμεία
της Ευρωπαϊκής Ένωσης στην Κύπρο

Table of Contents

Executive summary	5
Laboratory Experiments	7
Materials and Methods	7
Degassing of water	7
FUS system	7
Wood-powder based phantom	8
Freshly excised tissue	9
Experimental set-up	9
Temperature increase in phantom and excised tissue using thermocouple	9
Temperature increase in phantom and excised tissue using the robotic device (version 1)	11
Temperature increase in phantom and excised tissue using the robotic device (version 2)	13
Multiple ablations on excised tissue using manual movement of the transducer	14
Ablation of excised tissue using movement of the robotic device (version 1)	15
Ablation of small tumour-like excised tissue using movement of the robotic device (version 1)	16
Ablation of excised tissue using movement of the robotic device (version 2)	18
Ablation of excised tissue using movement of the robotic device (version 3)	19
Ablation of excised tissue using movement of the robotic device (version 4)	19
SOUNDPET system evaluation using a thermal imaging camera	20
Results	22
Degassing of water	22
Temperature increase in phantom using thermocouple	25
Temperature increase in excised tissue using thermocouple	28
Temperature increase in phantom using the robotic device (version 1)	31
Temperature increase in excised tissue using the robotic device (version 1)	33
Temperature increase in phantom using the robotic device (version 2)	34
Temperature increase in excised tissue using the robotic device (version 2)	36
Multiple ablations on excised tissue using manual movement of the transducer	38
Thermal and cavitation lesions.....	41
Ablation of excised tissue using movement of the robotic device (version 1)	45
Formation of discrete lesions.....	45
Formation of overlapping lesions	49
Ablation of small tumour-like excised tissue using movement of the robotic device (version 1) 50	
Ablation of excised tissue using movement of the robotic device (version 2)	52
Formation of discrete lesions.....	52
Formation of overlapping lesions	58
Ablation of excised tissue using movement of the robotic device (version 3)	60
Formation of discrete lesions.....	60
Formation of overlapping lesions	65
Ablation of excised tissue using movement of the robotic device (version 4)	67
Formation of discrete lesions.....	67
Formation of overlapping lesions	71

SOUNDPET system evaluation using a thermal imaging camera.....	73
Temperature increase of the X-axis motor during movement of the robotic device (version 1)	73
Temperature increase of the X-axis driver during movement of the robotic device (version 1).....	74
Temperature increase in plastic films during sonications using movement of the robotic device (version 1)	75
Temperature increase in excised tissue during sonications using movement of the robotic device (version 2)	76
Discussion	78
MRI Experiments	95
Assessment of lesion detection using a 1.5 T MRI scanner	95
Results	96
Conclusions	100
Assessment of the effect of the imaging coil in thermal heating detection.....	100
Results	101
Conclusions	Error! Bookmark not defined.
Assessment of robotic movement of SOUNDPET version 1 during 3×3 grid sonications	103
Results	104
Conclusions	Error! Bookmark not defined.
Assessment of robotic movement of SOUNDPET version 2 during 6×6 grid sonications	106
Results	107
Conclusions	Error! Bookmark not defined.
Optimizing the echo time (TE) and repetition time (TR) in T1-W and T2-W sequences for enhanced lesion detection	108
Results	110
Conclusions	Error! Bookmark not defined.
Optimizing the echo time (TE), repetition time (TR) and echo train length (ETL) of T1-W and T2-W sequences for lesion detection	111
Results	113
Conclusions	Error! Bookmark not defined.
Assessment of the SOUNDPET version 2 robotic system during grid sonications on a tumor-like agar phantom	118
Results	119
Conclusions	Error! Bookmark not defined.
Assessing the performance of a software for MRI guided transducer navigation	121
Results	122
Conclusions	Error! Bookmark not defined.
Assessing the performance of a new software for MRI monitoring and planning	125
Results	126
Conclusions	Error! Bookmark not defined.
Examining the effect of power on lesion detection based on T1-W and T2-W images.....	130
Results	131
Conclusions	Error! Bookmark not defined.
Assessment of the SOUNDPET version 2 robotic system for 2×2 and 3×3 grid sonications.....	134
Results	136
Conclusions	Error! Bookmark not defined.
Assessment of lesion detection using a 3 T MRI scanner.....	139
Results	141
Conclusions	Error! Bookmark not defined.

**Measurement of MR relaxation times of tumor-like phantom and lesion at 1.5 T and 3 T MRI
scanners 149**
 Results 151
 ConclusionsError! Bookmark not defined.

References..... 159

Executive summary

In this deliverable (D6.3), the evaluation of the thermal heating of the transducers described in Deliverable 3.2 is presented. Evaluation was performed using excised porcine tissue as well as an agar/wood powder-based phantom containing 6 % w/v agar and 4 % w/v wood powder, described in Deliverable 4.1. The evaluation was also performed using agar-based phantoms containing agar and silicon dioxide. Excised tissues were used because of their ability to form lesions after sonications, while agar-based phantoms were preferred since they provide data repeatability. Evaluation experiments were performed in both a laboratory setting and a Magnetic Resonance Imaging (MRI) environment.

Different experimental set-ups were used for evaluation of the focused ultrasound (FUS) robotic devices (version 1, 2, 3, 4). Different transducers with varied focal length and frequency have been progressively introduced in the various versions of the robotic device. Each version of the robotic device is fully described in Deliverable 3.1. The robotic device (version 1) includes an acoustic window where the testing material has direct contact with water. In the robotic device (version 2), a membrane was added on the acoustic window resulting in a stable water level during robotic motion. The robotic device (version 3) uses a top-to-bottom approach for ultrasonic beam propagation, while the robotic device (version 4) does not have a bellow.

The first experimental set-up used in laboratory experiments was designed for localisation of the focal point of the transducer within the phantom and excised tissue using low acoustical power. After localisation of the focal point, sonications using high acoustical power were performed for the formation of lesions in both excised tissue and agar-based phantoms. The formed lesions were illustrated, and their dimensions were measured.

The second experimental set-up presented, was used for the formation of multiple lesions on excised tissue using manual movement of the transducer. By varying the sonication parameters (acoustical power, sonication time) and focal depth of the transducer, lesions of different dimensions were formed. A scanning electron microscope was used to obtain morphological characteristics of normal and tadpole shaped lesions. After confirmation that the transducers could induce high temperatures and create lesions on excised tissue, movement of the 4 degrees of freedom (DOF) robotic device (all versions) was used for tissue ablation. Movement of the transducer was performed in various grid patterns and focal depths for the creation of discrete and overlapping lesions. The dimensions of the formed lesions were measured, and any dimensional characteristics based on focal depth, and amount of applied ultrasonic energy (acoustical power \times sonication time) were analysed. Overlapping lesions on a small piece of excised tissue were performed using the robotic device (version 1), with a focused transducer of 2.6 MHz central frequency to model the case of a small tumour-like model in preclinical experiments. Discrete and overlapping lesions of varying acoustic parameters and grid patterns were also performed using the robotic device (version 2) where a membrane existed between the transducer and the excised tissue to test whether the focused ultrasound waves are transmitted unaffected from the thin membrane. Varying sonications parameters and grid patterns were also used for the formation of discrete and overlapping lesions using the robotic

device (version 3) and the robotic device (version 4). The dimensions of the formed lesions as well as the minimum ultrasonic energy required for lesion formation were investigated.

Moreover, a series of experiments were performed inside the MRI environment to assess the thermal heating of the transducer and the overall functionality of the SOUNDPET robotic system. Experiments were performed using the first two versions (version 1 and version 2) of the 4 DOF SOUNDPET robotic system (Deliverable 3.1), with sonications executed on excised pork tissues and agar-based phantoms.

Sonications executed on excised pork tissue were initially performed to assess the ability of detecting and imaging the lesions inflicted by the sonications using both a 1.5 T (Signa HD16, GE Healthcare, Chicago, Illinois, USA) and 3 T (Magnetom Vida, Siemens Healthineers, Erlangen, Germany) MRI systems. The effect of acoustic power on lesion detection using MRI images was also examined through sonications executed with varied power and monitored with a 1.5 T MRI (Signa HD16, GE Healthcare). Moreover, T1-Weighted and T2-Weighted sequences were employed with varied parameters for imaging the tissue after sonications, examining their effect on the optimal detection of the formed lesions. Additionally, a range of grid sonications were performed inside the 1.5 T MRI scanner for assessing the accuracy of robotic movement based on MRI images acquired during and after the sonications.

The agar-based phantoms were used mainly within the 1.5 T MRI scanner (Signa HD16, GE Healthcare) for assessing the accuracy of robotic motion during grid sonications and the functionality of both versions of the software (Deliverable 5.1) for MRI-guided transducer navigations. Moreover, several MR imaging coils (lumbar or surface) were employed for MR imaging during the sonications in order to find the optimal coil for the detection of thermal heating inside the 1.5 T MRI scanner. In addition, for both the agar-based phantoms and excised tissues, T1 and T2 relaxation times were measured within both the 1.5 T and 3 T MRI scanners. Relaxometry measurements as derived within the two scanners of varied magnetic field strength are essential for the MRI evaluation of the robotic system and the ultrasonic protocols since they mainly affect the contrast of the MR images used in therapy monitoring.

Laboratory Experiments

Materials and Methods

Degassing of water

Oxygen content measurements were performed using degassed and non-degassed water in order to evaluate the degassing process of water. The oxygen content of degassed and non-degassed water, which is used as the medium for transmission of ultrasound, was measured using an oxygen meter (HI5421, Hanna Instruments, Limena, Italy). Regarding degassed water, degasification was performed using a two-stage vacuum pump (VP260, Vacuum Chambers, Jodlowa, Poland) and a vacuum chamber (VC2523AG, Vacuum Chambers) with a 12.5 L capacity. Figure 1 shows a photo of the complete experimental set-up used for the evaluation of the water degassing process. The oxygen meter probe was immersed in the water sample (degassed or non-degassed) and the meter was set to the dissolve oxygen (DO) mode. The water sample was continuously stirred with a magnetic stirrer (SBS A160, Steinberg Systems, Hamburg, Germany) to provide accuracy in DO measurements. Continuous water stirring ensures that the oxygen meter probe surface continuously measures a representative sample. The speed of the stirrer was set to 300 revolutions per minute (rpm).



Figure 1: Experimental set-up for measuring the oxygen content of water.

FUS system

The FUS system was composed of a signal generator (HP 33120A, Agilent Technologies, Englewood, CO, USA) and an RF amplifier (AG1012, AG Series amplifier, 750 W, 20 kHz-6 MHz, T & C Power Conversion Inc., Rochester, NY, USA). The transducer used had a frequency of 1.1 MHz (radius of curvature (ROC)=70 mm, diameter (D)=60 mm) and was manufactured by MEDSONIC LTD (Limassol, Cyprus). Figure 2 shows the signal generator. Figure 3 shows the RF amplifier, while Figure 4 shows the proposed transducer that was included in the SOUNDPET robotic device version 1.



Figure 2: Signal generator (HP33120A, Agilent Technologies).



Figure 3: AG amplifier (model AG1012, T & C Power Conversion Inc.).



Figure 4: SOUNDPET transducer, frequency = 1.1 MHz, diameter = 60 mm, radius of curvature = 70 mm (MEDSONIC LTD).

Nevertheless, several transducers with different characteristics have been progressively used in the several versions of the SOUNDPET robotic device. Specifically, a 1.1 MHz transducer (D=50 mm, ROC=80 mm), a 2.6 MHz transducer (D=38 mm, ROC=61 mm), and a 2.75 MHz transducer (D=50 mm, ROC=65 mm) have been used.

Wood-powder based phantom

An agar/wood powder-based phantom was used to evaluate the thermal heating of the SOUNDPET transducer with frequency 1.1 MHz (D=60 mm, ROC=70 mm). The phantom contained de-ionized, degassed water, 6 % w/v agar (10164, Merck, Darmstadt, Germany) which is responsible for the bonding that forms between inclusions and background material, and 4 % w/v wood powder (Swedish pine). The development procedure of the phantom as well as measurements of any acoustic (speed, attenuation etc.), thermal (conductivity, heat capacity etc.) and MR properties (T1 and T2 relaxation times) are fully described in Deliverable 4.1. The phantom was developed having similar attenuation with human fat and muscle tissues. Additionally, its propagation speed, thermal conductivity and MR properties have been found

close to human soft tissue, making it ideal as a tissue mimicking material. For the purposes of the evaluation experiments, the phantom was developed having dimensions 60 mm (w) \times 60 mm (l) \times 80 mm (h). The phantom mold was designed with the aforementioned dimensions using Inventor Professional (Autodesk, California, USA). The computer-aided design (CAD) was then sent to an industrial 3D printer (F270, Stratasys, Minnesota, USA) that produces parts of Acrylonitrile Butadiene Styrene (ABS). The developed agar/wood-powder phantom is shown in Figure 5.

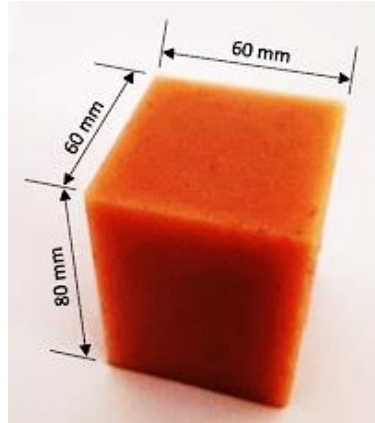


Figure 5: Photo of phantom consisting of 6 % w/v agar and 4 % w/v wood powder.

Freshly excised tissue

Freshly excised pork loin tissue was also used to evaluate the thermal heating of the transducer and its ability in forming lesions. The tissue was chosen to be homogeneous with minimal fat parts so as to allow for maximal transmission of ultrasonic beam. The tissue was provided from a local butcher shop before conduction of the experiments.

Experimental set-up

Temperature increase in phantom and excised tissue using thermocouple

A structure that holds the transducer and the phantom/excised tissue was designed to fit in an acrylic water tank with dimensions 15 cm (w) \times 18 cm (l) \times 23 cm (h). The structure was developed with ABS using an industrial 3D printer (Stratasys). The structure includes a transducer holder which is placed at the bottom, facing upwards on the phantom/excised tissue holder. The transducer holder provides ability of modifying the transducer-phantom distance in the range of 20-80 mm in 5 mm or 10 mm steps. The phantom/tissue holder was developed so that a thermocouple (5SC-TT-K-30-36, type K insulated beaded wire, 100 μ m thick, Omega Engineering, Norwalk, Connecticut, USA) could be placed at set distances of every 5 mm within the phantom/tissue to provide measurements of temperature increase during sonications so as to compare these records with MR thermometry measurements. Figure 6 shows the developed ABS structure used for the evaluation of the transducer using a thermocouple, while Figure 7 shows a photo of the complete experimental set-up. The acrylic tank was filled with deionized, degassed water, thus providing good acoustical coupling between the transducer and the phantom/tissue. The water was degassed using a two-stage vacuum pump (VP260, Vacuum Chambers) able to completely degas water at 0.3 Pa and a vacuum chamber (VC2523AG, Vacuum Chambers) with a 12.5 L capacity.

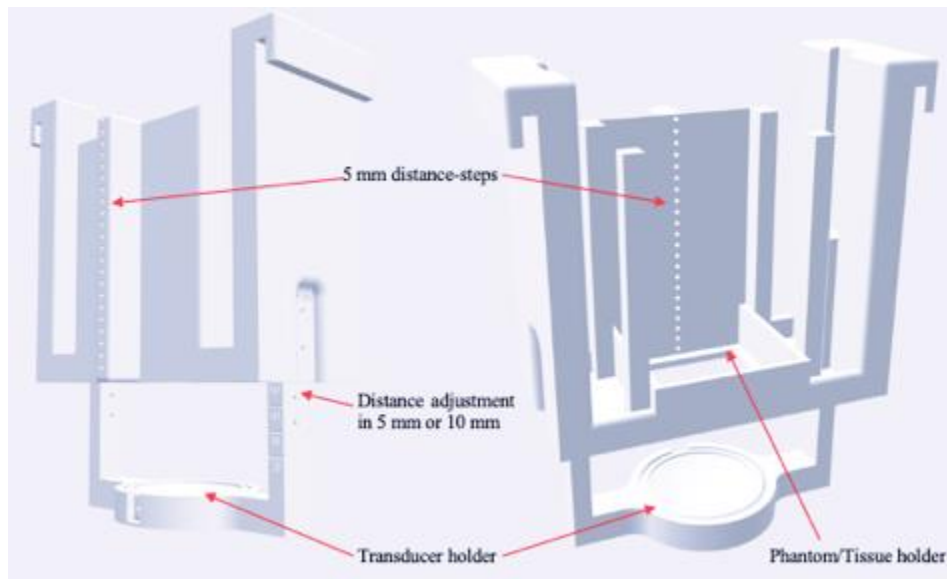


Figure 6: CAD drawing of the mechanical design used for the evaluation of the SOUNDPET transducer using a thermocouple.

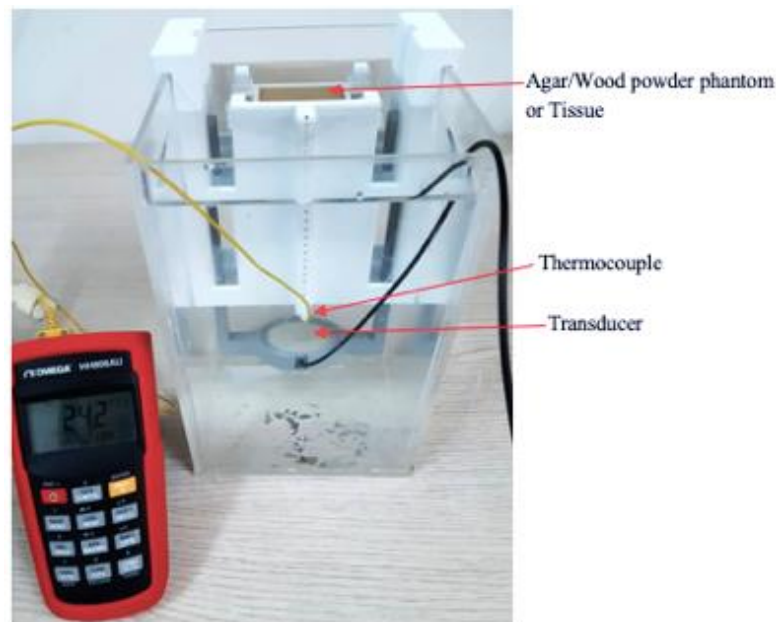


Figure 7: Experimental set-up for measuring temperature elevation in phantom/tissue using a thermocouple.

Figure 8 shows a photo of the experimental set-up with an excised porcine tissue used as a sample and the 1.1 MHz transducer ($D=60$ mm, $ROC=70$ mm) used for sonications. Experiments in excised tissue were mainly performed to estimate the temperature change after application of low acoustical power. This was necessary since during MR thermometry, application of low power is required for identifying the focal spot in coronal MRI images. This permits axial slicing of the MRI image at the focal spot to investigate the temperature change in a plane parallel to the ultrasonic beam. The distance between the transducer and the front interface of the excised tissue was 60 mm, resulting in a focal depth of 10 mm. The thermocouple was inserted in the excised tissue at a depth of 10 mm. Sonications were performed at varying acoustical power for a sonication time of 30 s to record the temperature change.

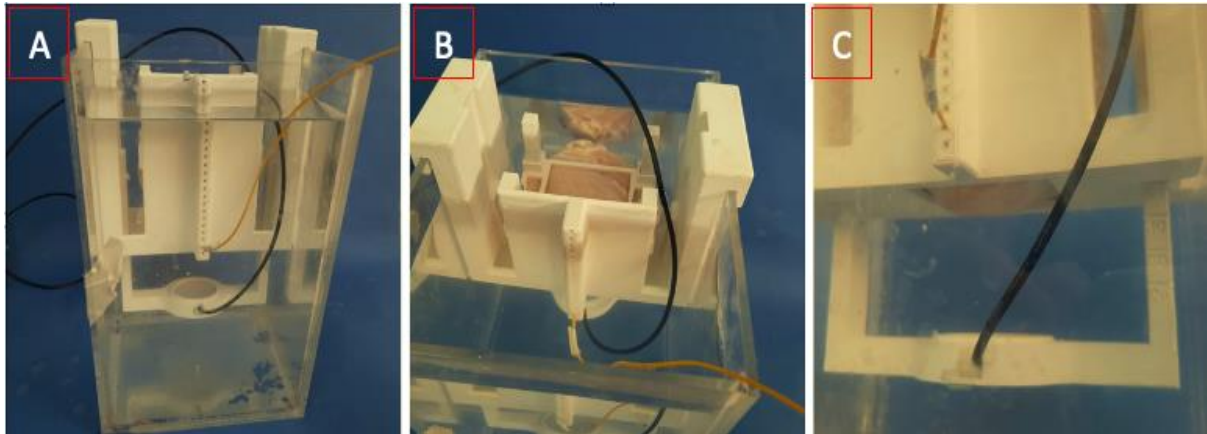


Figure 8: Experimental set-up used for measurement of temperature change at 10 mm within the excised tissue during sonications with the 2.6 MHz transducer ($D=38$ mm, $ROC=61$ mm) at 10 mm focal depth. A) Side view, B) Top view, and C) Bottom view.

Temperature increase in phantom and excised tissue using the robotic device (version 1)

The temperature change in an agar-based phantom (6 % w/v agar and 4 % w/v silica) was recorded using a thermocouple (5SC-TT-K-30-36, type K insulated beaded wire, 100 μ m thick, Omega Engineering) for grid sonications performed at different acoustical power using the robotic device (version 1). A grid pattern was performed using the MRgFUS software (Deliverable 5.1) to estimate the near-field heating of the transducer. The thermal dose induced by the different sonication protocols was also estimated. Figure 9 shows the CAD drawing of a 3D printed part (FD270, Stratasys) that was used as a phantom holder offering precise thermocouple insertion at set distances of every 5 mm within the phantom. Before placement of the phantom on the holder, the center of the transducer was set to be at the center of the phantom as shown in Figure 10. Figure 11 shows a photo of the temperature measurements during the sonications, with the thermocouple placed at 10 mm within the phantom. The distance between the 2.6 MHz transducer ($D=38$ mm, $ROC=61$ mm) and the bottom surface of the phantom was set at 50 mm resulting in a focal depth of 10 mm. Sonications of 10 s and 60 s duration at varying acoustical power were performed to record the temperature change.

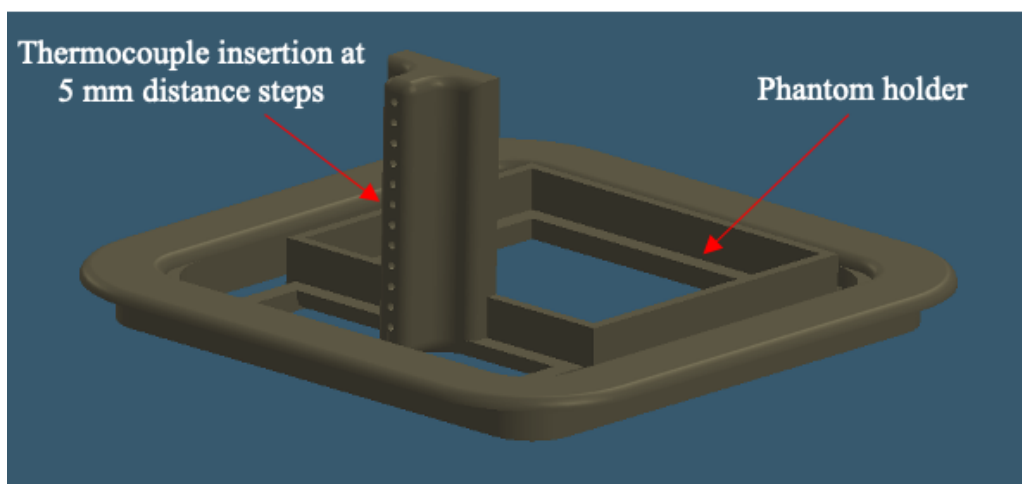


Figure 9: CAD drawing of the phantom holder offering precise thermocouple insertion at every 5 mm steps for temperature measurements.



Figure 10: Adjustment of the center of the transducer at the center of the phantom.

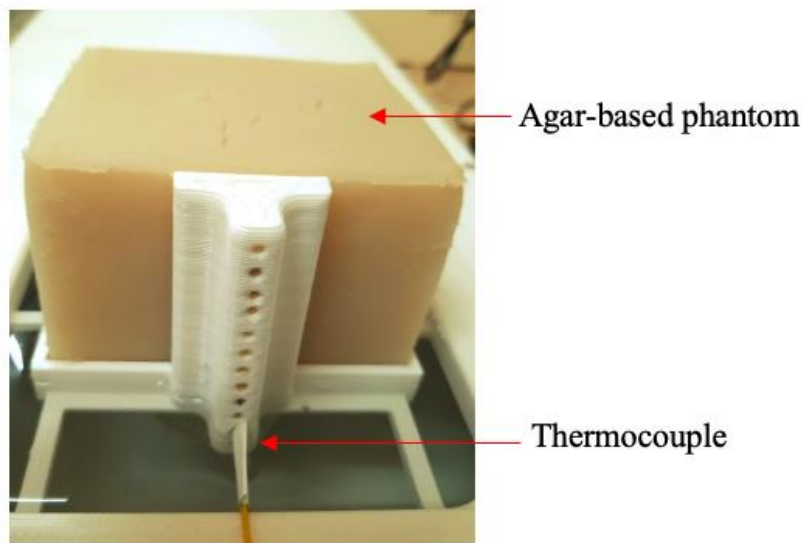


Figure 11: Experimental set-up used for thermocouple measurements of temperature change at 10 mm depth within the agar-based phantom.

For estimation of the near-field heating, two thermocouples were placed at 5 mm and 20 mm depths within the phantom, respectively, as shown in Figure 12. The distance between the transducer and the phantom was set at 40 mm resulting at a focal depth of 20 mm. Sonications were performed in a 5×5 grid with a 3 mm step using acoustical power of 23 W for a sonication time of 10 s at each grid point. A delay of 60 s was used between sonications at each grid point.

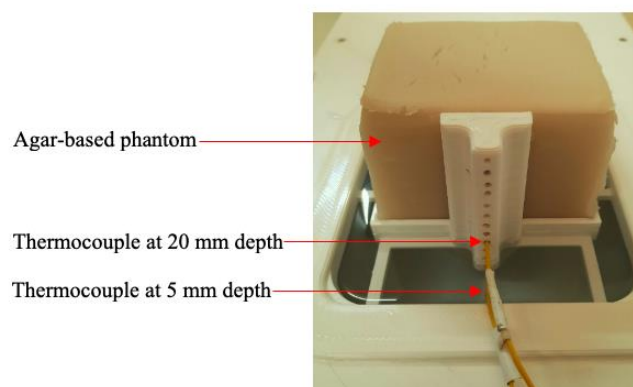


Figure 12: Placement of two thermocouples at different depths within an agar-based phantom for near-field heating estimations during 5×5 grid sonications.

Temperature measurements were also recorded during sonications on excised tissue. The tissue was placed on the holder with the thermocouple placed at 10 mm within the tissue. The distance between the 2.6 MHz transducer (D=38 mm, ROC=61 mm) and the bottom surface of the tissue was set at 50 mm resulting in a focal depth of 10 mm. Sonications of 10 s and 40 s duration at varying acoustical power were performed to record the temperature change at the focal point.

Temperature increase in phantom and excised tissue using the robotic device (version 2)

The temperature change in an agar-based phantom (6 % w/v agar) was recorded using the thermocouple (5SC-TT-K-30-36, type K insulated beaded wire, 100 μ m thick, Omega Engineering) during sonications executed at different acoustical power using the robotic device (version 2). The acoustic window of the robotic device version 2 is covered with a membrane. A part was designed, and 3D printed (FD270, Stratasys) for placement on the membrane of the robotic device for use as a phantom holder, offering precise thermocouple insertion at set distances of every 5 mm within the phantom. Figure 13 shows the CAD drawing of the part that was used as a phantom holder. Before placement of the phantom, the center of the transducer was set to be at the center of the phantom as shown in Figure 14. Figure 15 shows a photo of the temperature measurements during sonications with the thermocouple placed at 20 mm deep in the phantom. Ultrasound gel and degassed water were placed between the membrane of the robot and the agar-based phantom to achieve good coupling. The distance between the 1.1 MHz transducer (D=50 mm, ROC=80 mm) and the bottom surface of the phantom was set at 60 mm resulting in a 20 mm focal depth. Sonications of 60 s duration using varying acoustical power were performed to record temperature changes. The 2.75 MHz transducer (D=50 mm, ROC=65 mm) was also employed for sonications. Temperature changes within the phantom were recorded at the focal point for sonications executed at 20 mm focal depth using varying acoustical power for a constant sonication time of 120 s. The phantom was replaced with excised tissue. Temperature increase within the excised tissue was recorded for sonications with the 2.75 MHz transducer (D=50 mm, ROC=65 mm) executed at 20 mm focal depth using varying acoustical power for a sonication time of 60 s.

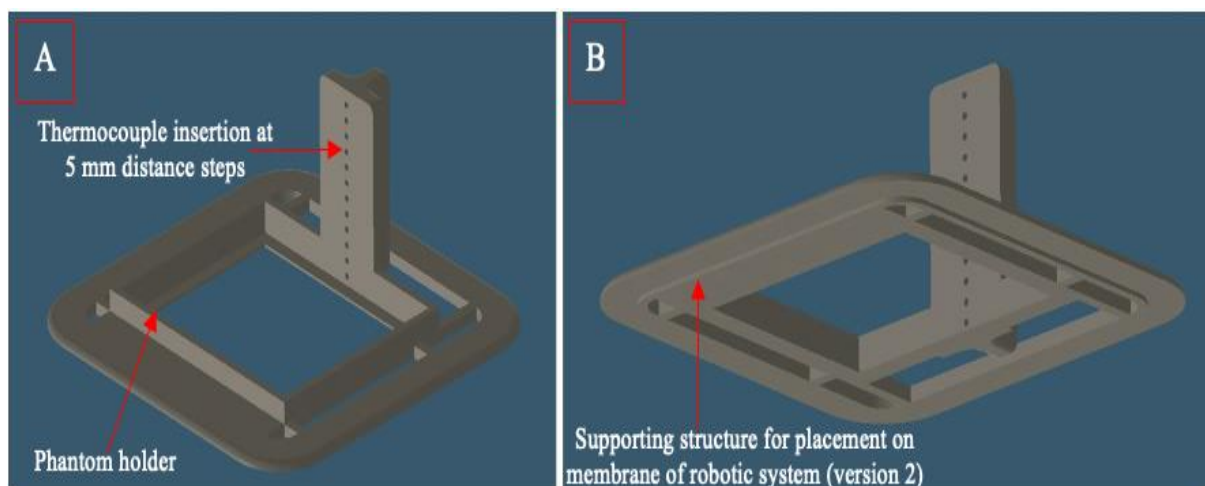


Figure 13: CAD drawing of the phantom holder offering precise thermocouple insertion at 5 mm steps for temperature measurement using the robotic device version 2. A) Side view, and B) Bottom view.

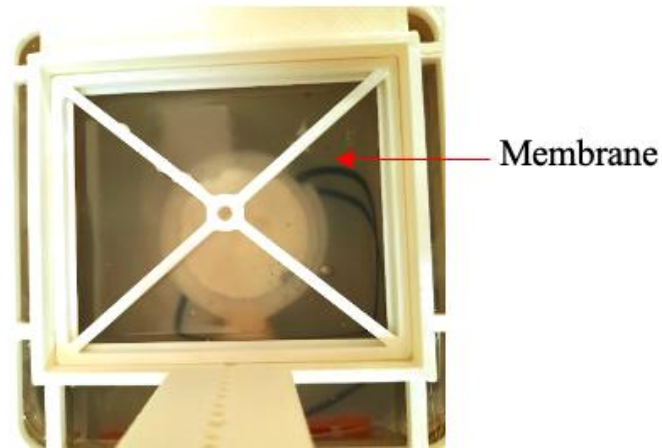


Figure 14: Adjustment of the focus to be at the center of the phantom.

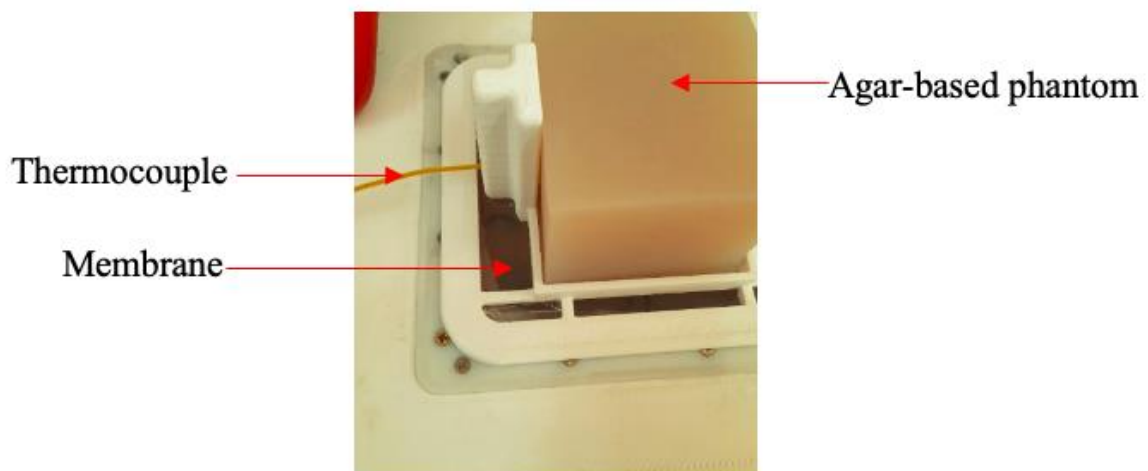


Figure 15: Experimental set-up for measurements of temperature change during sonications at 20 mm focal depth.

Multiple ablations on excised tissue using manual movement of the transducer

A different experimental set up was used to create multiple ablations on a piece of excised tissue using manual movement of the transducer. A specially designed transducer holder and an enclosure for the tissue were printed using an ABS 3D printer (FD270, Stratasys). The tissue enclosure was situated at the bottom of an acrylic water tank filled with degassed/deionized water. The transducer holder was designed so that the transducer was facing downwards on the upper surface of the tissue. The transducer holder was specially designed to allow for manual movement of the transducer in 2 degrees of freedom (X and Y axes). Movement in the Z axis was achieved by vertical movement of a cylindrical screw allowing for variation of the distance between the transducer and the upper surface of the tissue. The part allowing manual movement in the X axis included marks at every 10 mm distances for accurate movement. Figure 16 shows the CAD drawing of the mechanical design used to create multiple ablations in the excised tissue using manual movement of the transducer, while Figure 17 shows a photo of the complete experimental set-up.

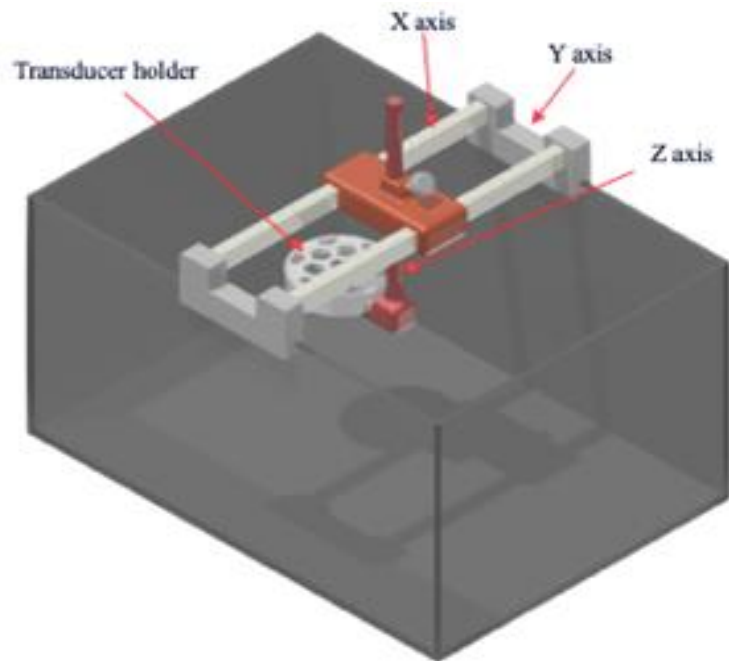


Figure 16: CAD drawing of the mechanical design used for the creation of multiple ablations using manual movement of the transducer.

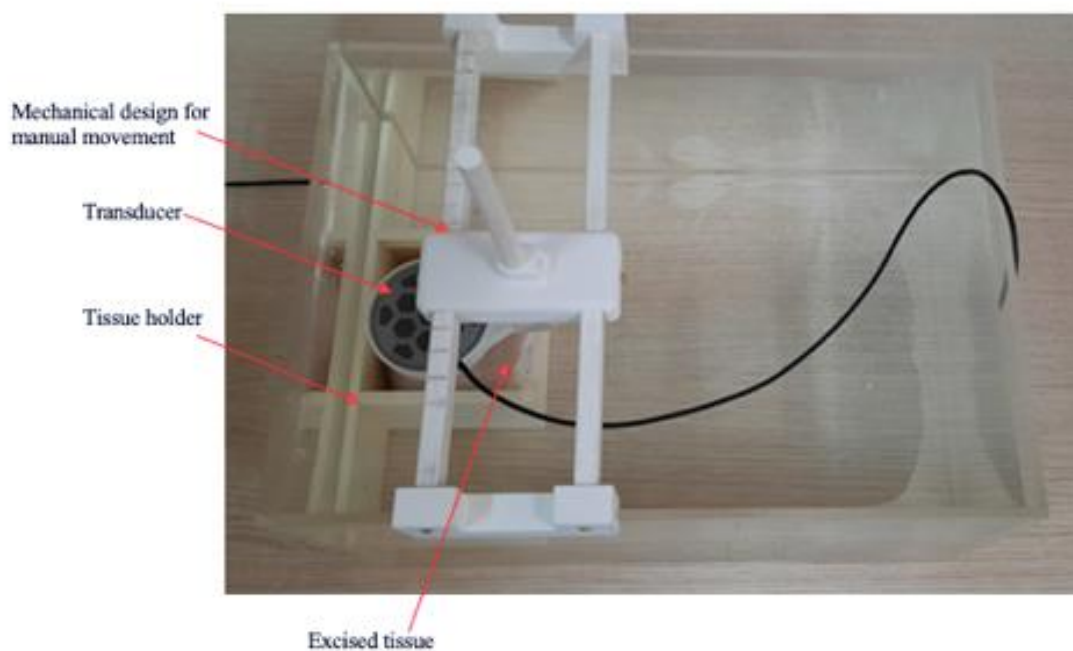


Figure 17: Experimental set-up used for the creation of multiple ablations using manual movement of the transducer.

Ablation of excised tissue using movement of the robotic device (version 1)

The 4 DOF robotic device was used for the formation of discrete and overlapping lesions using movement of the ultrasonic transducer. The robotic system which is fully described in Deliverable 3.1 provides movement in 3 linear stages (X, Y, Z) and one angular stage (Θ). Figure 18 shows a photo of the developed SOUNDPET robotic device.

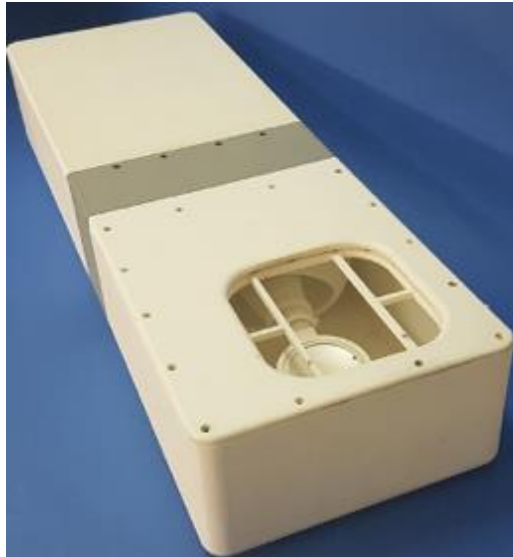


Figure 18: The 4 DOF SOUNDPET robotic device (version 1).

The robotic device was connected to the amplifier (AG1012, T & C Power Conversion Inc.) and signal generator (HP33120A, Agilent Technologies). A specially designed software (first version) fully described in Deliverable 5.1, was incorporated to control the sonication parameters and the motion of the robotic device. The developed software provided the ability of varying the frequency, voltage, sonication time, time between each step, space between each step and the grid pattern so as to create discrete or overlapping lesions on the excised tissue. Figure 19 shows a photo of the complete experimental set-up.

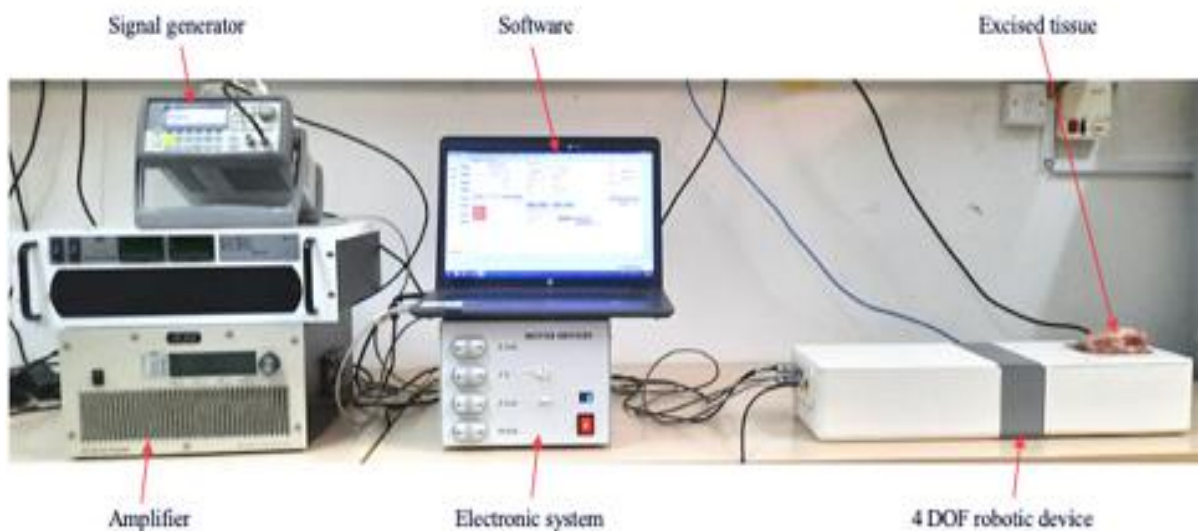


Figure 19: Experimental set-up used for ablation of excised pork tissue using the 4 DOF robotic device (version 1).

Ablation of small tumour-like excised tissue using movement of the robotic device (version 1)

The motors and encoders of the robotic system (version 1) were connected through the electronic system (Deliverable 3.3) to the software (Deliverable 5.1). The 2.6 MHz (D=38 mm, ROC=61 mm) focused transducer was connected to the RF amplifier (AG1012, T & C Power Conversion Inc.) which was controlled by the software. Small pieces of excised tissue were cut

with a height of approximately 20 mm, in order to replicate the dimensions of tumours having a diameter of 20 mm. A plastic structure (Figure 20, left) was used to support the excised tissue on the acoustic window of the robot, with its bottom surface immersed in degassed water. A metallic material (Figure 20, right) was placed at the top surface of the tissue to reduce reflections from the sample/air interface. The software provided the ability to vary the frequency, sonication time, delay and space between each step and the selection of the grid pattern. The experimental set-up used for the tissue ablations is shown in Figure 21.

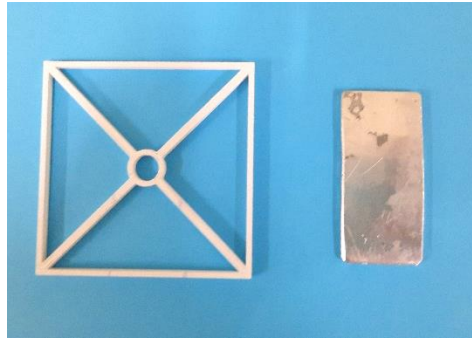


Figure 20: Plastic structure (left) and metallic material (right) used for the experiment.

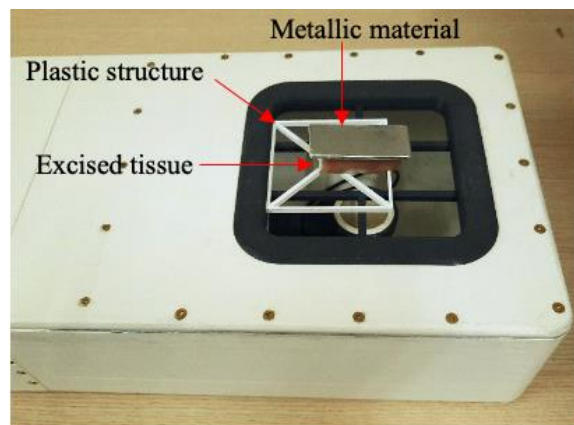


Figure 21: Experimental set-up used for ablations of excised tissue with the robotic system (version 1).

The distance between the transducer and the bottom surface of the excised tissue was 50 mm (the excised tissue was placed on a 3 mm plastic structure). The transducer was navigated along the X (forward and backward) and Y (left and right) axes, for grid sonications on the excised tissue. Sonications were performed in a 3×3 grid pattern using varying sonication time and acoustic power. A 3 mm grid step was chosen for all cases to create overlapping lesions. The 3×3 ablation pattern is shown in Figure 22.

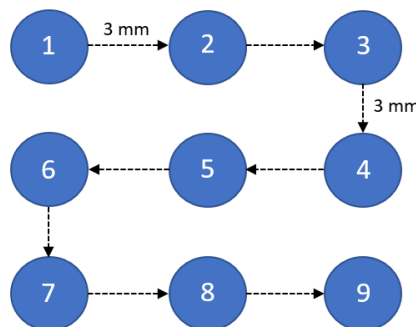


Figure 22: The 3×3 grid with a 3 mm step followed for excised tissue ablations.

Ablation of excised tissue using movement of the robotic device (version 2)

Ablations on excised porcine tissue were performed with varying acoustic power and sonication time in order to evaluate the ability of the 4-DOF robotic system (version 2) in producing multiple discrete and overlapping lesions. This version of the SOUNDPET robotic device includes a thin membrane embedded on the acoustic window as shown in Figure 23 to eliminate issues regarding the water level change. The water container was designed to operate as a vacuum, resulting in a stable water level during motion of the transducer. The membrane was added to allow unaffected transmission of the ultrasound beam from the water container to the testing material. In this regard, the creation of lesions with accommodation of a thin membrane between the water container of the robot and the tissue was investigated. Figure 24 shows a photo of the experimental set-up used for grid sonications in excised tissues. Water was added between the top part of the membrane and the excised tissue for coupling purposes. A plastic glove filled with water was placed on top of the tissue to minimize reflections from the tissue/air interface with ultrasound gel placed between the tissue and the glove.

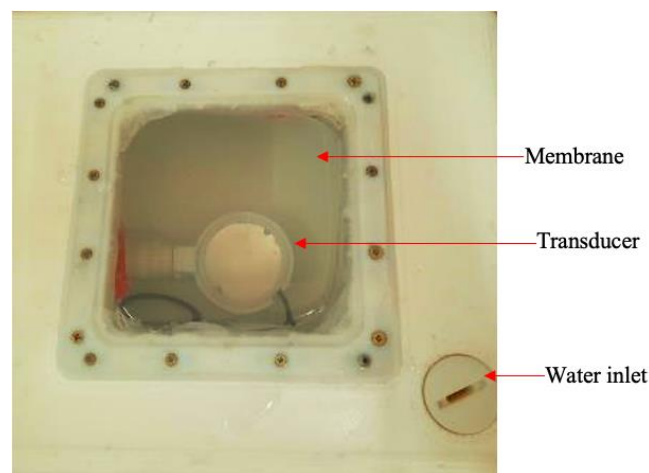


Figure 23: Membrane attached on the acoustic window of the robotic device (version 2).

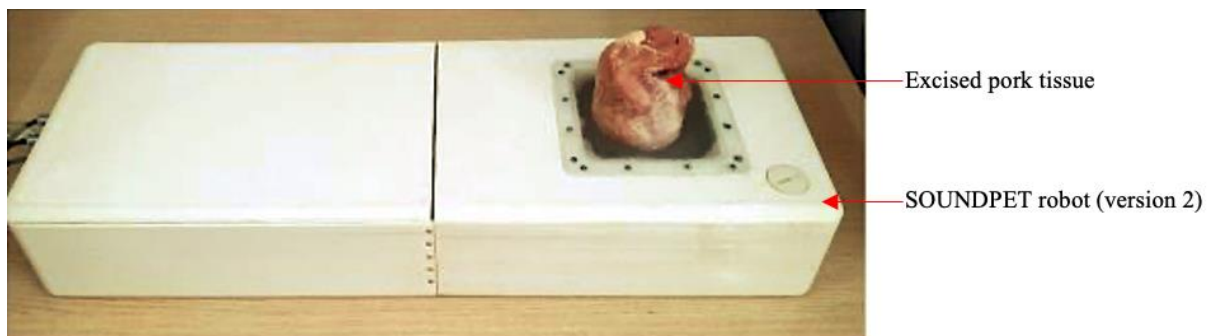


Figure 24: Photos of the experimental set-up used for ablations of excised pork tissue with the robotic device (version 2).

Sonications were executed using both the 1.1 MHz transducer (D=60 mm, ROC=70 mm) and the 2.75 MHz transducer (D=50 mm, ROC=65 mm). The transducers were navigated along the X (forward and backward) and Y (left and right) axes, to create discrete and overlapping lesions in excised tissue. Discrete lesions were formed for sonications performed in 3×2 grid patterns with a 10 mm step using varied acoustic power for sonication times of 5 s and 10 s. The 3×2 ablation protocols followed for discrete lesions are shown in Figure 25.

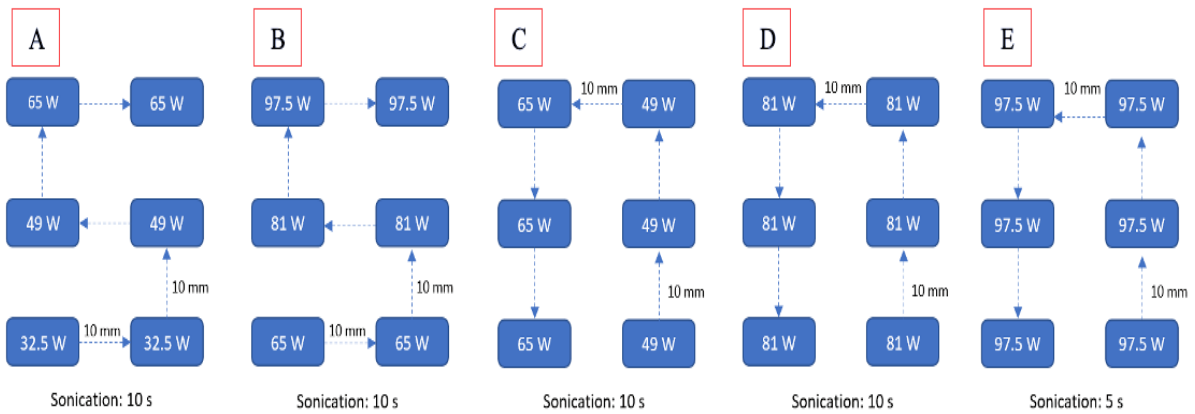


Figure 25: Sonications in 3x2 grids with a 10 mm step followed for excised tissue ablation using varying acoustic power (32.5–97.5 W) for sonication times of 10 s (A-D), and 5 s (E).

Ablation of excised tissue using movement of the robotic device (version 3)

The ability of the robot version 3 and the 2.75 MHz transducer (D=50 mm, ROC=65 mm) to create discrete and overlapping lesions was evaluated by ablating excised pork loin tissue using varying acoustic power and sonication times. The differentiation of this version of the robot compared to previous versions is the position of the transducer. In this version of the robot, the transducer is located above the sample resulting in top-to-bottom propagation ultrasound. Figure 26 shows the experimental set-up used for tissue ablation. The excised pork tissue was positioned under the acoustic window of the robotic device. Ultrasound gel was added between the tissue and the membrane that covers the acoustic window of the robot to minimize air and serve as a coupling medium.

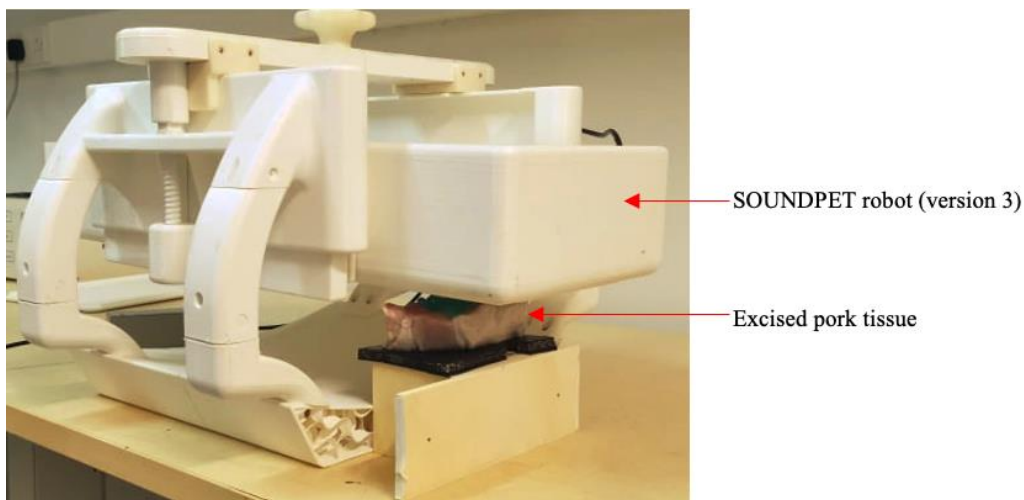


Figure 26: Experimental set-up used for ablations of excised tissue using the robotic device (version 3).

Ablation of excised tissue using movement of the robotic device (version 4)

Sonications were executed on excised pork tissue to investigate the ability of the robot version 4 and the 2.75 MHz transducer (D=50 mm, ROC=65 mm) in creating lesions. Compared to previous versions, this robotic system does not include a bellow. Therefore, stable water level is maintained during transducer motion. Figure 27 shows the experimental set-up used for tissue ablation. Excised pork tissue was placed on the acoustic window of the device and was

immersed in water above the transducer. Transducer movement was performed in various grid patterns with varied steps for the creation of discrete and overlapping lesions. Sonications were performed at varied acoustical power and sonication times at a focal depth of 25 mm.

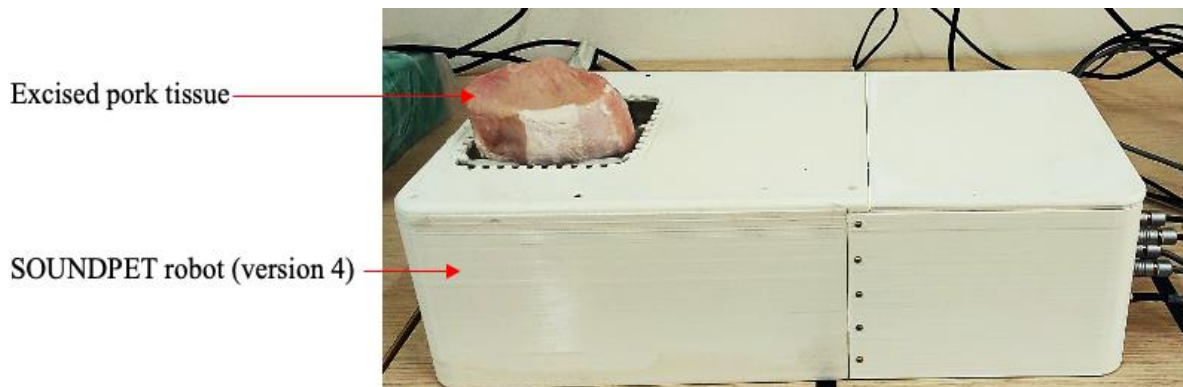


Figure 27: Experimental set-up used for ablations of excised tissue using the robotic device (version 4).

SOUNDPET system evaluation using a thermal imaging camera

A thermal camera (Fluke TiS55, Fluke Corporation, Everett, Washington, USA) was used to evaluate the SOUNDPET robotic system (version 1 and version 2). Initially the robotic system (version 1) was connected, via cables, to an amplifier (AG1016, T & C Power Conversion) and the electronic driving system (Deliverable 3.3). The thermal camera was positioned on top of the robotic system for temperature measurements. Figure 29 shows photos of the experimental set-up.

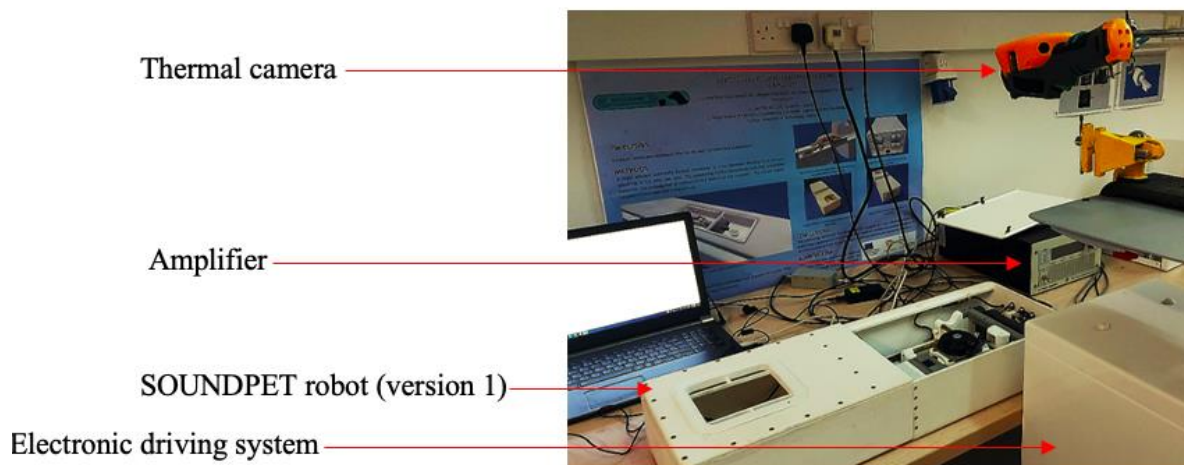


Figure 28: Experimental set-up used for SOUNDPET system evaluation using a thermal camera.

Initially, movement of the robotic device (version 1) was initiated in a 10×10 grid pattern with a 2 mm step for evaluating the temperature increase of the X-axis motor (USR60-S3N, Shinsei Kogyo Corporation, Tokyo, Japan) during robotic motion. The camera was positioned on top of the X-axis motor of the SOUNDPET system (version 1) as shown in Figure 29 for temperature measurements. Motion was initiated in the same grid pattern for evaluation of the temperature increase of the X-axis driver (D6060, Shinsei Kogyo Corporation) during motion. In this regard, the thermal camera was positioned on top of the X-axis driver (D6060, Shinsei Kogyo Corporation), as set in the electronic driving system.

Thermal camera



X-axis motor

Figure 29: Experimental set-up used for evaluation of the temperature increase of the X-axis motor of the robotic system (version 1).

The temperature increase during sonications with the 2.75 MHz transducer (D=50 mm, ROC=65 mm) was assessed on thin plastic films (0.7 mm thickness, Fortus FDM400mc print plate, Stratasys). A plastic film was placed on the acoustic window of the robotic device (version 1) with the thermal camera positioned on top for temperature measurements. Temperature increase was measured during 3×3 grid sonications with a 10 mm step executed using an acoustic power of 3 W for a sonication time of 9 s and a delay of 9 s.

The temperature increase during sonications with the 2.75 MHz transducer (D=50 mm, ROC=65 mm) and the robotic device (version 2) was assessed on excised pork tissue. A piece of excised tissue was placed on the membrane of the robot (version 2) with the thermal camera positioned on top of the tissue for temperature measurements as shown in Figure 30. Water was placed between the tissue and the top part of the membrane for coupling purposes. The gradual increase in temperature was recorded during sonications at an acoustical power of 45 W for a sonication time of 90 s at a 20 mm focal depth using movement of the transducer in a 3×3 grid with a 10 mm step.

Thermal camera

Excised pork tissue

SOUNDPET robot (version 2)

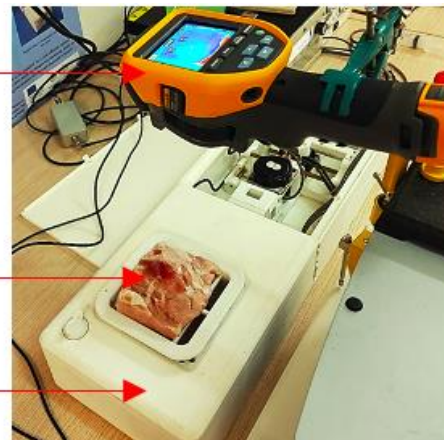


Figure 30: Experimental set-up used for evaluation of the temperature increase within excised tissue during sonications executed with the robotic system (version 2).

Results

Degassing of water

Table 1 shows a comparison of the oxygen content measurements between the degassed water using the aluminum vacuum chamber for 1 hour and the non-degassed water.

Table 1: Oxygen content measurements for degassed and non-degassed water.

Degassing process	Degassing process duration (hours)	Oxygen content (mg/L)
Degassed water (Aluminum Vacuum chamber @ -0.94 bar)	1	2.74
Non-degassed water	0	8.21

Table 2 shows the oxygen content measurements for degassed water after degassing for 0–120 minutes (20 minutes steps) using the aluminum vacuum chamber. Figure 32 shows a graph of the oxygen content measurements for degassed water versus the degassing duration.

Table 2: Oxygen content measurements after degassing the water for 0 – 120 min using the aluminum vacuum chamber @ -0.94 bar.

Degassing duration (min)	Oxygen content (mg/L)
0	8.21
20	3.92
40	3.12
60	2.74
80	2.45
100	2.40
120	2.38

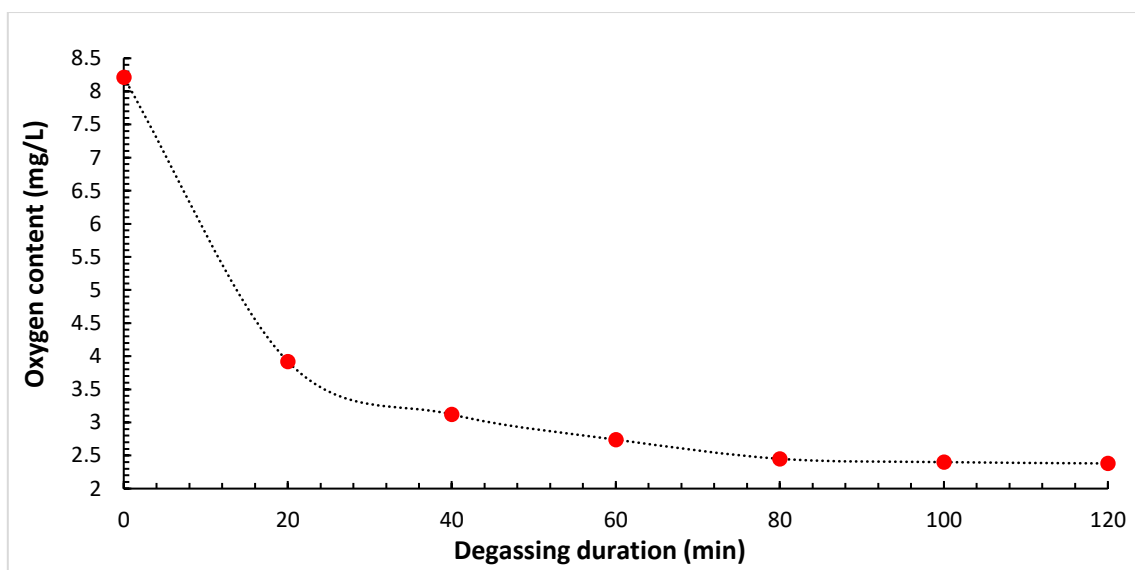


Figure 31: Oxygen level of the water sample for 0 – 120 min of degasification using the aluminum vacuum chamber @ -0.94 bar.

Table 3 shows the oxygen content of the water after it was degassed for 1.2 hours in the aluminum vacuum chamber (@ -0.94 bar). Table 3 also shows the oxygen content of the water sample as recorded every 30 minutes of a 3-hour period after degasification, so as to observe the rate at which oxygen levels increase at atmospheric pressure. Figure 33 shows a graph of the oxygen content of the degassed water as a function of time, for a 3-hour period of exposure to atmospheric pressure.

Table 3: Oxygen content measurements of water degassed for 1.2 hours in the aluminum vacuum chamber (@ -0.94 bar) as recorded at specific time intervals after degasification for a 3 hour exposure to atmospheric pressure.

Time after degasification (hours)	Oxygen content (mg/L)
0	2.09
0.5	2.79
1	3.48
1.5	4.25
2	4.81
2.5	5.42
3	5.89

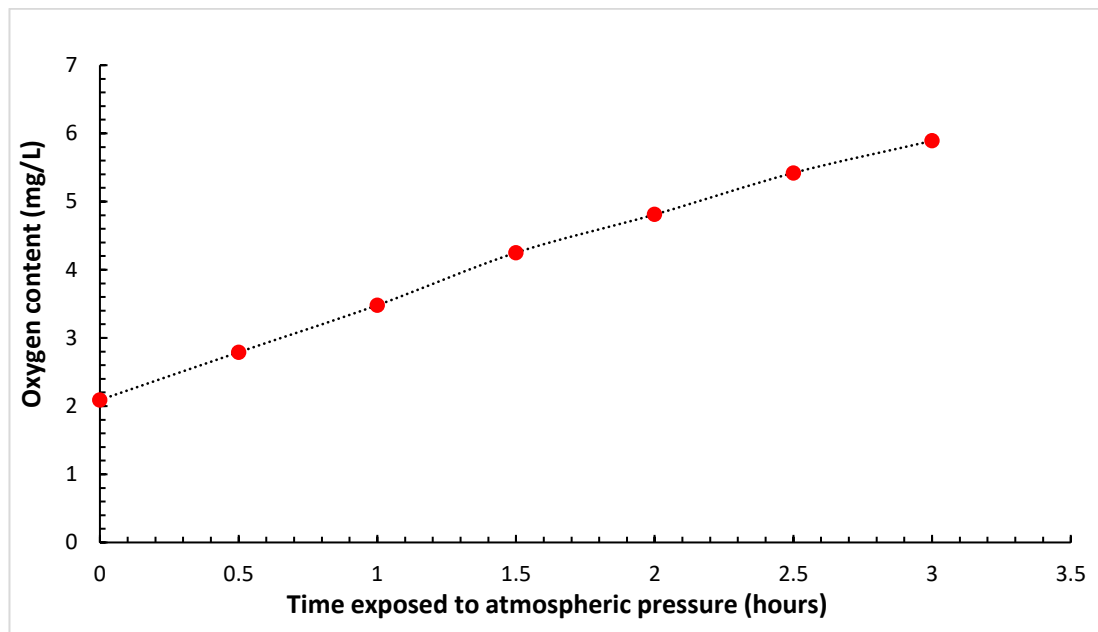


Figure 32: Oxygen content measurements as a function of time for a 3-hour period of degassed water exposure to atmospheric pressure.

Table 4 shows the oxygen content measurements of water after it was degassed for 40 minutes in the aluminum vacuum chamber (@ -0.94 bar). Table 4 also shows the oxygen content of the degassed water sample as recorded every 30 minutes of a 1.5-hour period of exposure to atmospheric pressure so as to observe the rate at which oxygen levels increase. Figure 34 shows a graph of the oxygen content of the degassed water as a function of time for a 1.5-hour period of exposure to atmospheric pressure.

Table 4: Oxygen content of water degassed for 40 minutes in the aluminum vacuum chamber (@ -0.94 bar) as recorded at specific time intervals after degasification for a 1.5 hour exposure to atmospheric pressure.

Time after degasification (hours)	Oxygen content (mg/L)
0	3.37
0.5	4.31
1	5.27
1.5	5.84

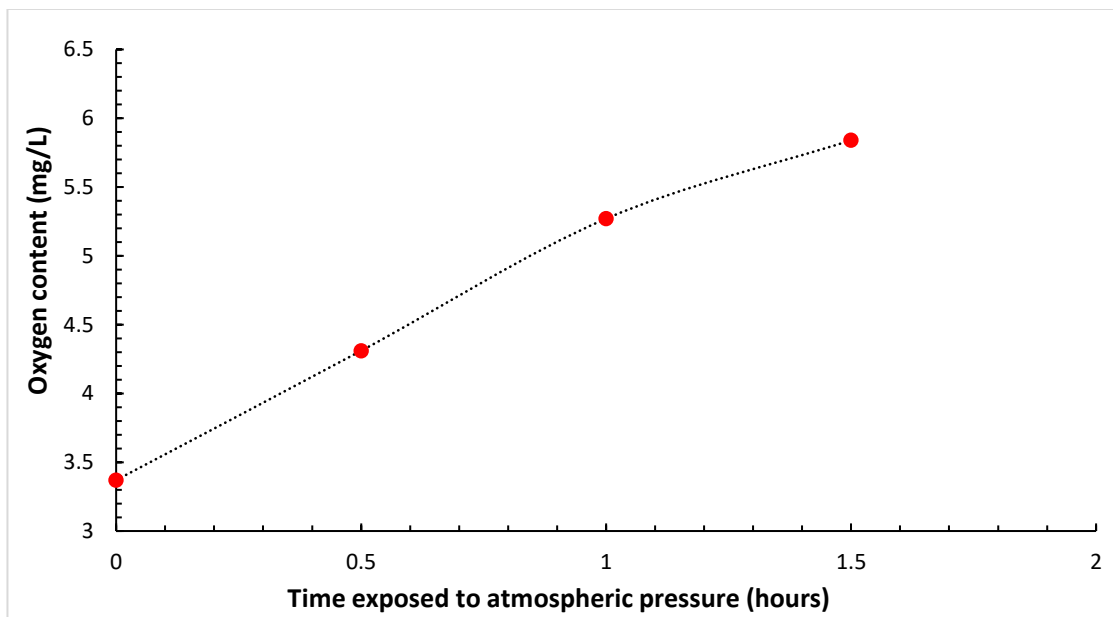


Figure 33: Oxygen content as a function of time for a 1-5-hour period of degassed water exposure to atmospheric pressure.

Table 5 shows the oxygen content of water after it was degassed for 20 minutes in the aluminum vacuum chamber (@ -0.94 bar). Table 5 also shows the oxygen content of the degassed water sample as recorded every 30 minutes of a 1.5-hour period of exposure to atmospheric pressure so as to observe the rate at which oxygen increases. Figure 35 shows a graph of the oxygen content of the degassed water as a function of time for a 1.5-hour period of exposure to atmospheric pressure.

Table 5: Oxygen content of water degassed for 20 minutes in the aluminum vacuum chamber (@ -0.94 bar) as recorded at specific time intervals after degasification for a 1.5 hour exposure to atmospheric pressure.

Time after degasification (hours)	Oxygen content (mg/L)
0	4.45
0.5	5.68
1	6.52
1.5	7.04

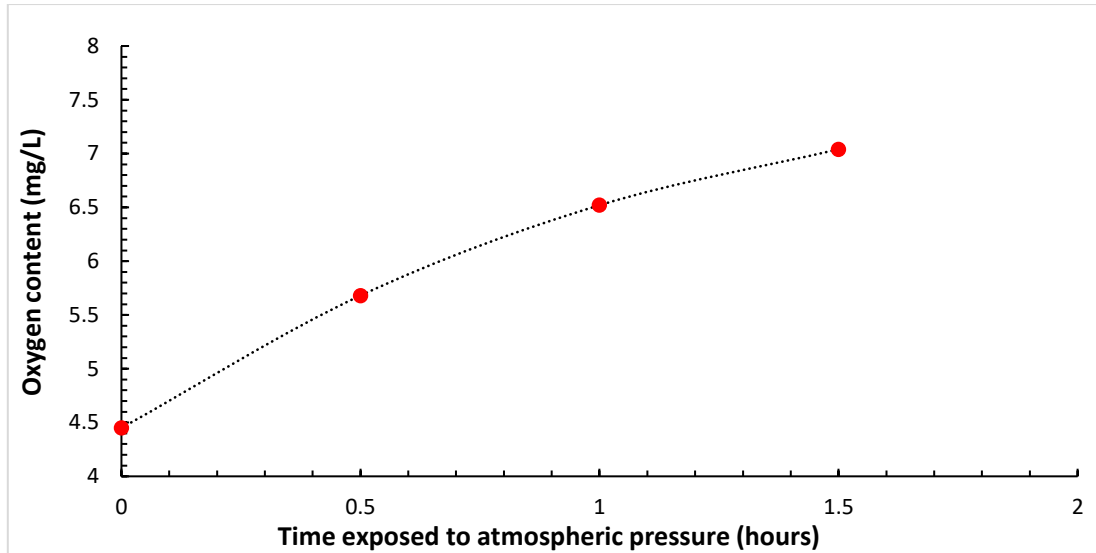


Figure 34: Oxygen content as a function of time for a 1.5-hour period of degassed water exposure to atmospheric pressure.

Temperature increase in phantom using thermocouple

The 1.1 MHz (D=60 mm, ROC=70 mm) transducer was used, and the transducer-phantom distance was set to 50 mm, resulting in an expected focal depth of 20 mm within the agar/wood powder-based phantom. The thermocouple was inserted at different locations within the phantom at 5 mm steps. A constant acoustical power of 11 W and a sonication time of 60 s were used for low power sonication at each 5 mm depth. Table 6 shows the sonication parameters used and the temperature change achieved at the different distances along the phantom. Figure 35 shows the temperature change versus distance of the thermocouple within the agar/wood powder-based phantom.

Table 6: Temperature change recorded at varied thermocouple distances within the agar/wood powder-based phantom during sonications with the 1.1 MHz transducer (D=60 mm, ROC=70 mm) at acoustic power of 11 W for a sonication time of 60 s at 20 mm focal depth for estimating the focal point of the transducer within the phantom.

Acoustical power (W)	Sonication time (s)	Energy (J)	Thermocouple distance within phantom (mm)	ΔT (°C)
11	60	660	5	6.6
			10	6.8
			15	8.2
			20 (expected focal point)	10.3
			25	8.1
			30	8.6
			35	2.9
			40	11.9
			45	5.7
			50	8.2

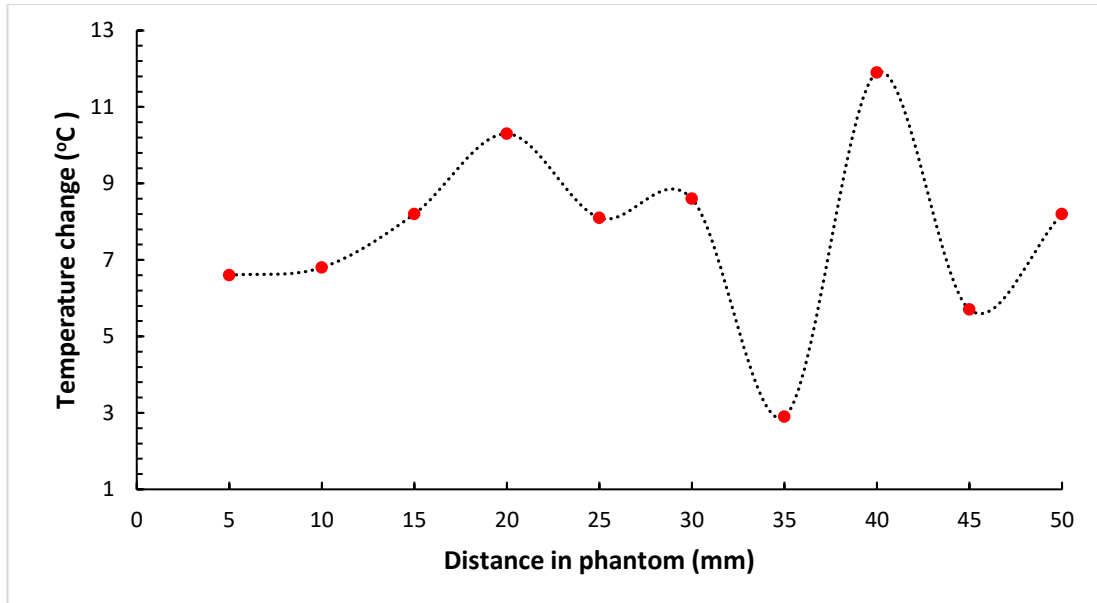


Figure 35: Temperature change versus distance of the thermocouple in the agar/wood powder-based phantom recorded during sonications with the 1.1 MHz transducer ($D=60$ mm, $ROC=70$ mm) using acoustical power of 11 W for a sonication time of 60 s at a focal depth of 20 mm.

The transducer-phantom distance was changed to 60 mm, thus shifting the focal depth of the transducer to 10 mm within the phantom. The thermocouple was again inserted at the same 5 mm set distance steps. At each depth, the acoustical power of 11 W was again used for a sonication time of 60 s. Table 7 shows the sonication parameters used and the temperature change achieved at the different distances along the phantom. Figure 36 shows the temperature change versus distance of the thermocouple within the agar/wood powder-based phantom at the new focal depth.

Table 7: Temperature change recorded at varied thermocouple distances within the agar/wood powder-based phantom during sonications with the 1.1 MHz transducer ($D=60$ mm, $ROC=70$ mm) at acoustic power of 11 W for a sonication time of 60 s at 10 mm focal depth for estimating the focal point of the transducer within the phantom.

Acoustical power (W)	Sonication time (s)	Energy (J)	Thermocouple distance within phantom (mm)	ΔT (°C)
11	60	660	5	8
			10 (expected focal point)	10.9
			15	11.6
			20	12.6
			25	11.1
			30	8.2
			35	9.4
			40	6.4

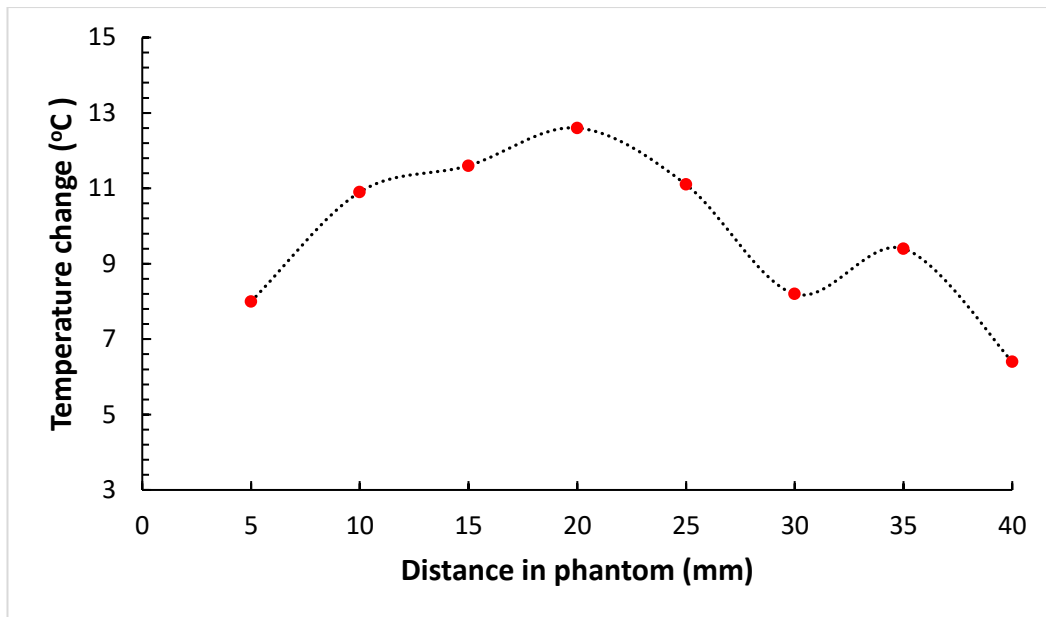


Figure 36: Temperature change versus distance of the thermocouple in the agar/wood powder-based phantom recorded during sonications with the 1.1 MHz transducer ($D=60$ mm, $ROC=70$ mm) using acoustical power of 11 W for a sonication time of 60 s at a focal depth of 10 mm.

The focal point of the transducer was situated between a 10 mm and 20 mm depth within the phantom. Hence, two thermocouples were inserted within the phantom, one at 10 mm depth and one at 20 mm depth. Acoustical powers of 18.5 W, 29.6 W, 37 W, 55.5 W and 66.6 W were used for a sonication time of 30 s. Figure 37 shows the rate of change of temperature during sonications as recorded at the 20 mm depth, while Figure 38 shows the recorded rate of temperature change at the 10 mm depth.

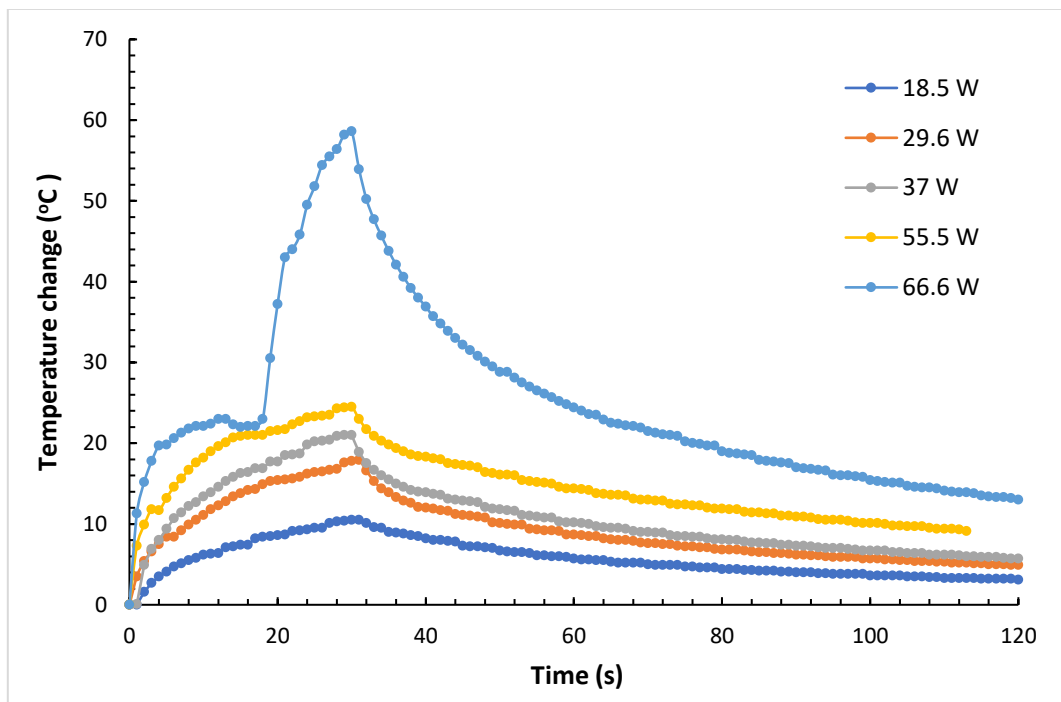


Figure 37: Temperature change versus time recorded for thermocouple location at 20 mm depth within the phantom during sonications with the 1.1 MHz transducer ($D=60$ mm, $ROC=70$ mm) using varied acoustical powers (18.5, 29.6, 37, 55.5 and 66.6 W) for a sonication time of 30 s at 10 mm focal depth.

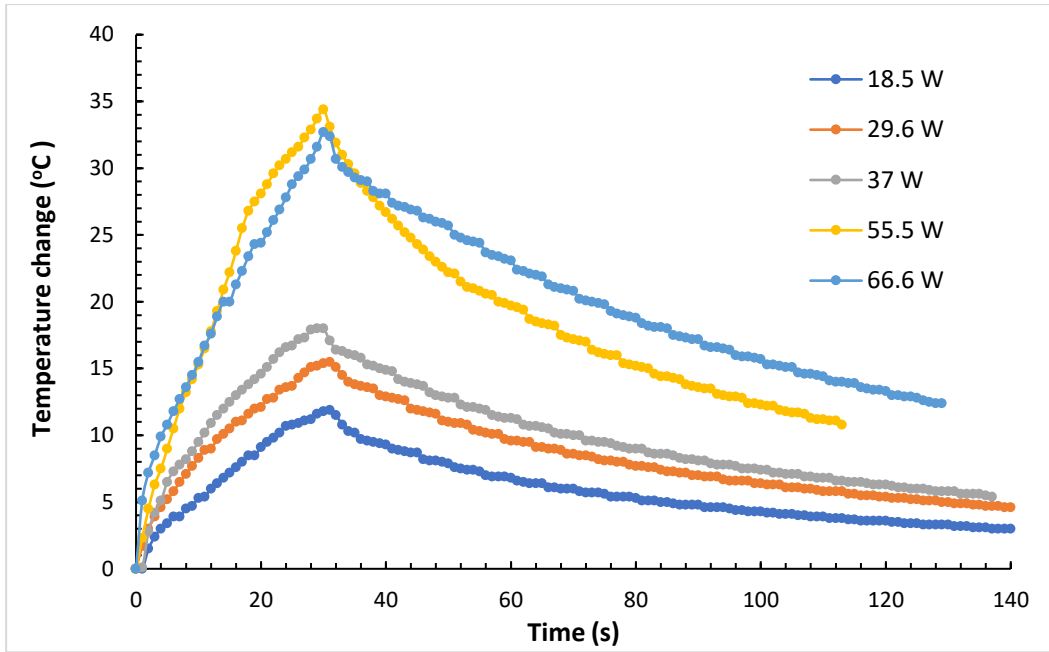


Figure 38: Temperature change versus time obtained for thermocouple location at 10 mm depth within the phantom during sonications with the 1.1 MHz transducer ($D=60$ mm, $ROC=70$ mm) using varied acoustical powers (18.5, 29.6, 37, 55.5 and 66.6 W) for a sonication time of 30 s at 10 mm focal depth.

The acoustical power of 66.6 W resulted in a temperature increase of 58.6 °C. This temperature increase resulted in the formation of a lesion (gel melting) in the agar/wood powder-based phantom. Figure 39A shows the lesion formed on a plane perpendicular to the beam, while Figure 39B shows the lesion formed on a plane parallel to the beam. The formed lesion had a 6.27 mm diameter and a length of 8.86 mm.

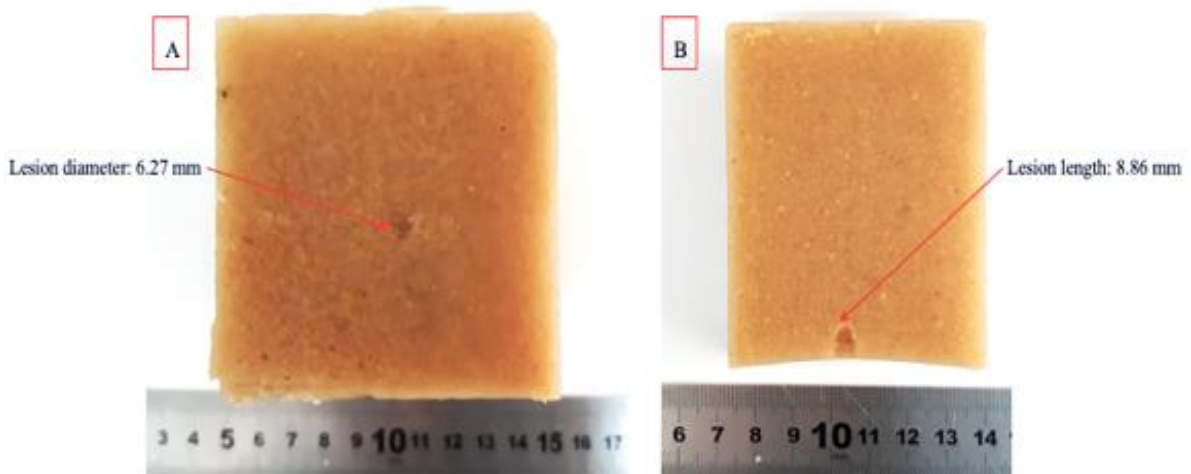


Figure 39: Lesion formed on the agar/wood powder-based phantom after exposure with the 1.1 MHz transducer ($D=60$ mm, $ROC=70$ mm) at acoustical power of 66.6 W for a sonication time of 30 s at 10 mm focal depth. A) Lesion formed on plane perpendicular to the beam, and B) Lesion formed on plane parallel to the beam.

Temperature increase in excised tissue using thermocouple

The 1.1 MHz transducer ($D=60$ mm, $ROC=70$ mm) was employed for sonications. The transducer-tissue distance was set at 60 mm, resulting in an expected focal depth of 10 mm

within the tissue. The thermocouple was inserted at different set locations within the tissue at 5 mm steps. At each depth, an acoustical power of 11 W was used for a sonication time of 60 s. Table 8 shows the sonication parameters used and the temperature change recorded at the different distances along the tissue. Figure 40 shows the temperature change versus distance of the thermocouple within the excised tissue.

Table 8: Temperature change recorded at varied thermocouple distances within the excised tissue during sonications with the 1.1 MHz transducer ($D=60$ mm, $ROC=70$ mm) using acoustic power of 11 W for a sonication time of 60 s at 10 mm focal depth for estimating the focal point of the transducer within the excised tissue.

Acoustical power (W)	Sonication time (s)	Energy (J)	Thermocouple distance within phantom (mm)	ΔT ($^{\circ}C$)
11	60	660	5	7.3
			10 (expected focal point)	11.4
			15	9.2
			20	8.2
			25	6.1
			30	2.7
			35	1.6
			40	2.8

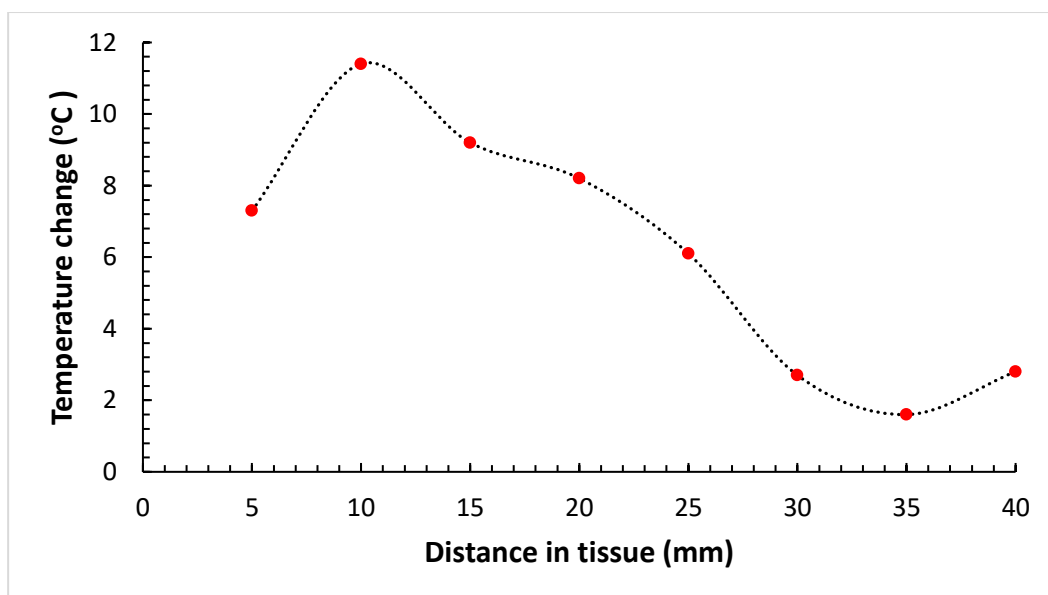


Figure 40: Temperature change versus distance of the thermocouple in the excised tissue recorded during sonications with the 1.1 MHz transducer ($D=60$ mm, $ROC=70$ mm) using acoustical power of 11 W for a sonication time of 60 s at a focal depth of 10 mm.

The increase of temperature at the distance of 10 mm was the greatest, confirming focal depth at 10 mm. The thermocouple was then inserted within the tissue at the focal point (10 mm), and varying acoustical power was used for a constant sonication time, so as to record the rate

of change of temperature during sonications. Acoustical power of 18.5 W, 29.6 W, 37 W and 74 W were used for a sonication time of 30 s. Figure 41 shows **Error! Reference source not found.** the rate of change of temperature recorded during sonications at the 10 mm focal depth using varying acoustical power.

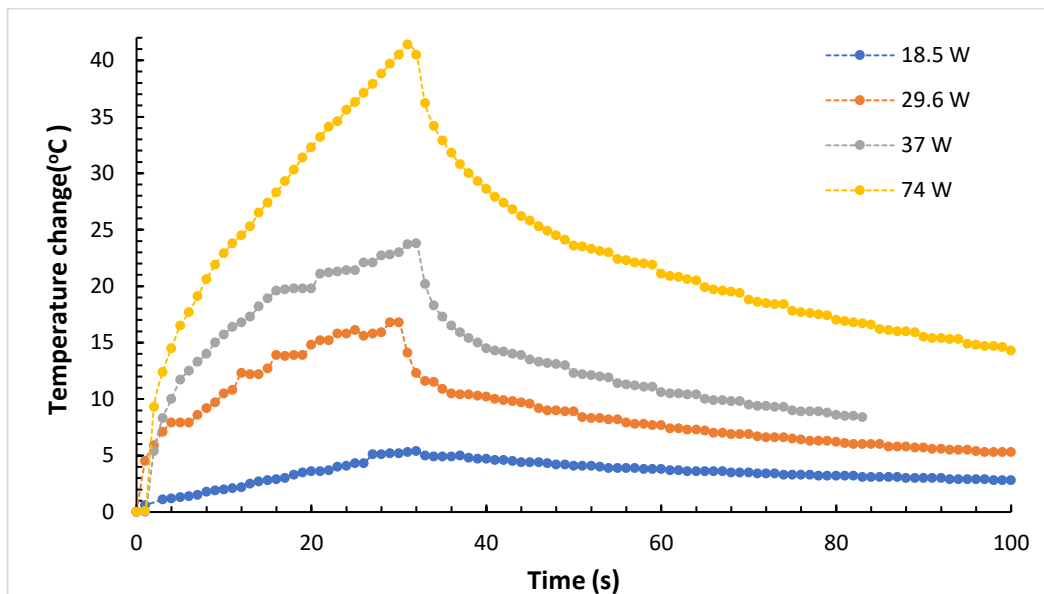


Figure 41: Temperature change versus time obtained for sonications performed on excised tissue with the 1.1 MHz transducer ($D=60$ mm, $ROC=70$ mm) using varied acoustical powers (18.5, 29.6, 37 and 74 W) for a sonication time of 30 s at 10 mm focal depth.

The acoustical power of 74 W induced a temperature change of 40.5 °C. This temperature increase would probably result in the formation of a lesion; thus, the tissue was sliced at 10 mm to examine the lesion and measure its dimensions. Figure 42A shows **Error! Reference source not found.** the lesion formed on a plane perpendicular to the beam, while Figure 42B shows the lesion formed on a plane parallel to the beam. The formed lesion had a 5.94 mm diameter and a 16.27 mm length.



Figure 42: Lesion formed on excised pork tissue after exposure with the 1.1 MHz transducer ($D=60$ mm, $ROC=70$ mm) at acoustical power of 74 W for a sonication time of 30 s at 10 mm focal depth. A)

Lesion formed on a plane perpendicular to the beam. Slice of the tissue at 10 mm and its mirror (from left to right), and B) Lesion formed on a plane parallel to the beam.

Temperature increase in phantom using the robotic device (version 1)

The 2.6 MHz transducer (D=38 mm, ROC=61 mm) was employed with the transducer-phantom distance set at 50 mm, resulting in an expected focal depth of 10 mm within the agar-based phantom. Temperature change was recorded during sonications of 10 s and 60 s performed using varying acoustical power in the range of 11.5-46 W. Figure 43 and Figure 44 show the temperature change versus time for sonications performed using acoustical power of 46 W for a sonication time of 10 s and acoustical power of 23 W for a sonication time of 60 s, respectively.

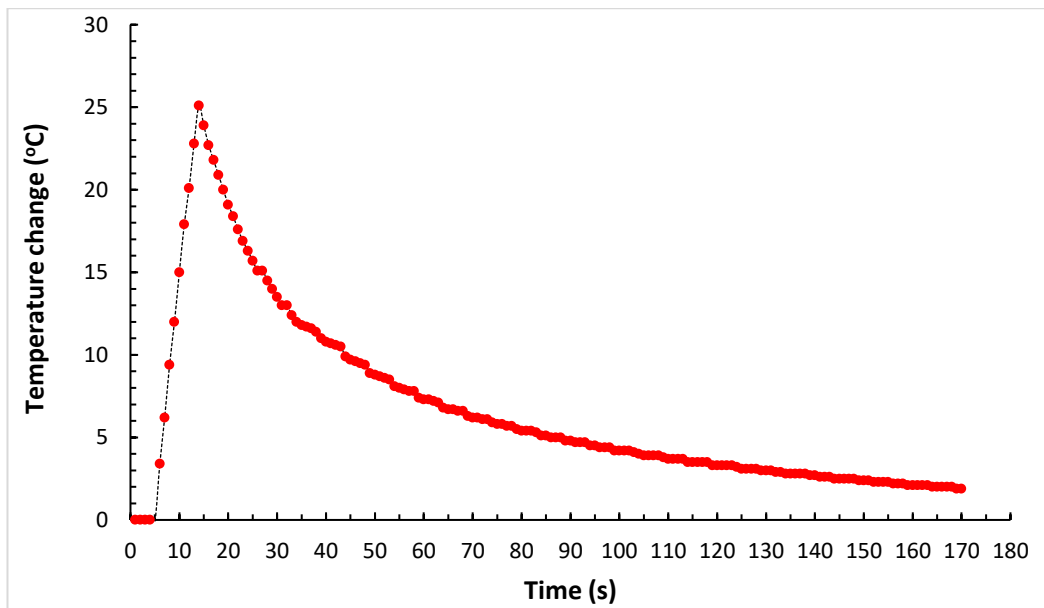


Figure 43: Temperature change as a function of time induced during sonications on agar-based phantom with a 2.6 MHz transducer (D=38 mm, ROC=61 mm) at acoustic power of 46 W for a sonication time of 10 s at 10 mm focal depth.

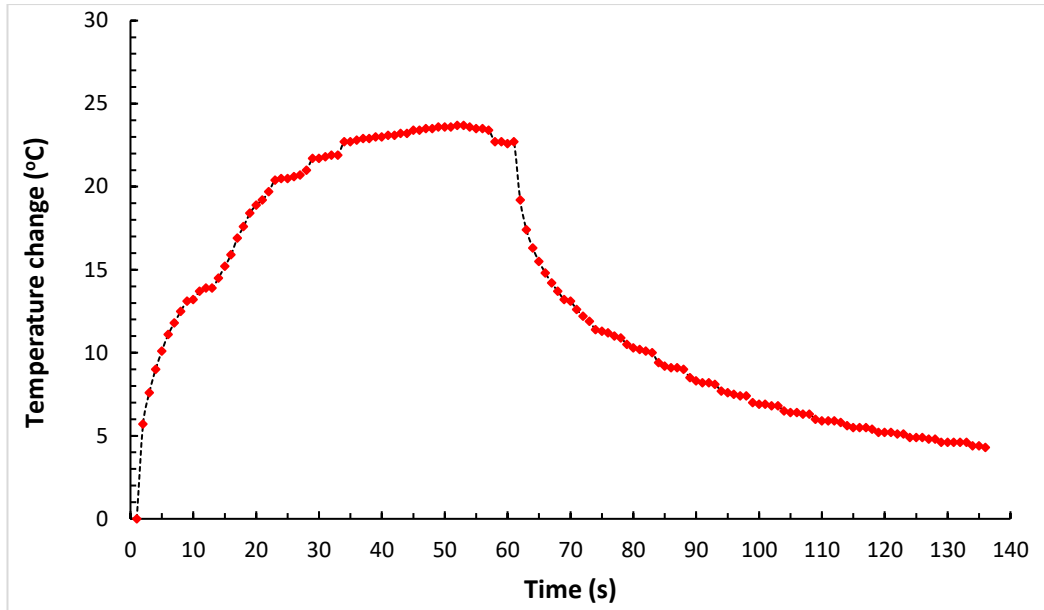


Figure 44: Temperature change as a function of time induced during sonications on agar-based phantom with a 2.6 MHz transducer ($D=38$ mm, $ROC=61$ mm) at acoustic power of 23 W for a sonication time of 60 s at 10 mm focal depth.

Table 9 summarizes the sonication parameters used in the experiments as well as the temperature change recorded and the total thermal dose induced for the different sonication protocols using the robotic device version 1.

Table 9: Temperature change and total dose induced for sonications executed on agar-based phantom using the 2.6 MHz transducer ($D=38$ mm, $ROC=61$ mm) and the robotic device (version 1) at varying acoustical power and sonication time at 10 mm focal depth.

Acoustic power (W)	Sonication time (s)	Energy (J)	Temperature change (°C)	Total dose (CEM at 43 °C)
11.5	10	115	5.2	0.116
23	10	230	12.4	15.29
23	60	1380	23.7	3548.8
34.5	10	345	18.7	838.5
46	10	460	25.1	39233.2
46	60	2760	60.2	1.38E+15

The near-field heating was estimated during 5×5 grid sonications with a 3 mm step executed with an acoustical power of 23 W for a sonication time of 10 s and a time delay of 60 s. The temperature change was measured simultaneously at 2 depths (5 and 20 mm) in the phantom, with the focal depth adjusted at 20 mm. Figure 45 shows the temperature change versus time as recorded at these two locations. The temperatures have been shifted so that the initial starting temperature is set at 37 °C in order to simulate the temperature of human body.

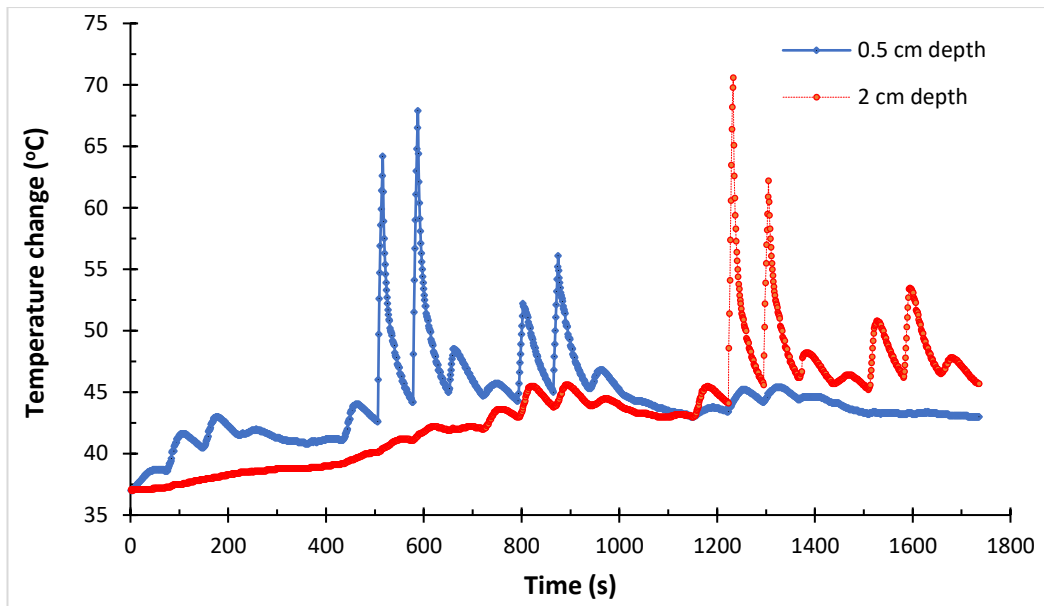


Figure 45: Temperature change versus time at near-field (0.5 cm depth) and focus (2 cm depth) for sonications on agar-based phantom with the 2.6 MHz transducer ($D=38$ mm, $ROC=61$ mm) and robotic device (version 1) in a 5×5 grid with a 3 mm step using acoustical power of 23 W, sonication time of 10 s and time delay of 60 s at 20 mm focal depth.

Table 10 summarizes the peak and average temperature changes (ΔT) as well as the induced thermal dose recorded at each depth (5 mm or 20 mm) for the 5×5 grid pattern sonications.

Table 10: Peak and average temperature change and total dose at 5 mm and 20 mm depths within the agar-based phantom for sonications with the 2.6 MHz transducer ($D=38$ mm, $ROC=61$ mm) in a 5×5 grid with a 3 mm step using acoustical power of 23 W for sonication time of 10 s and 60 s delay at 20 mm focal depth.

Depth (mm)	Peak ΔT ($^{\circ}C$)	Average ΔT ($^{\circ}C$)	Total dose (CEM43 $^{\circ}C$)
5	30.9	7.24	1870180
2	33.6	6.45	11777267

Temperature increase in excised tissue using the robotic device (version 1)

Sonications were executed on excised tissue using the robotic device version 1 and the 2.6 MHz transducer ($D=38$ mm, $ROC=61$ mm). The increase of temperature at the focal point (10 mm focal depth) within the excised tissue was recorded using a thermocouple, during sonications executed with varying acoustical power and sonication time at 10 mm focal depth. Initially, acoustical power of 2.3 to 20.7 W was used for a sonication time of 10 s. Table 11 summarizes the sonication parameters used in the experiment as well as the temperature change recorded in the excised tissue and the total thermal dose induced for sonications performed using varied acoustical powers. The temperatures have been shifted so that the initial starting temperature is set at 37 $^{\circ}C$ in order to simulate the temperature of human body.

Table 11: Temperature changes and total dose induced for sonications executed on excised tissue using the 2.6 MHz transducer ($D=38$ mm, $ROC=61$ mm) and the robotic device (version 1) at varying acoustical power for a sonication time of 10 s at 10 mm focal depth.

Acoustic power (W)	Energy (J)	Temperature change (°C)	Total dose CEM at 43 °C
2.3	23	0.2	0.00055
4.6	46	1.5	0.001
6.9	69	2.7	0.0027
9.2	92	4	0.011
11.5	115	6.4	0.13
13.8	138	8.1	0.46
16.1	161	10.5	2.06
18.4	184	11.8	5.5
20.7	207	12.6	13.78

Figure 46 and Figure 47 show the rate of change of temperature recorded during sonications at acoustical power of 2.3 W and 4.6 W using an increased sonication time of 40 s, respectively. Sonications at acoustical power of 2.3 W and 4.6 W for a sonication time of 40 s resulted in a temperature increase of 5.3 °C and 9.6 °C, respectively.

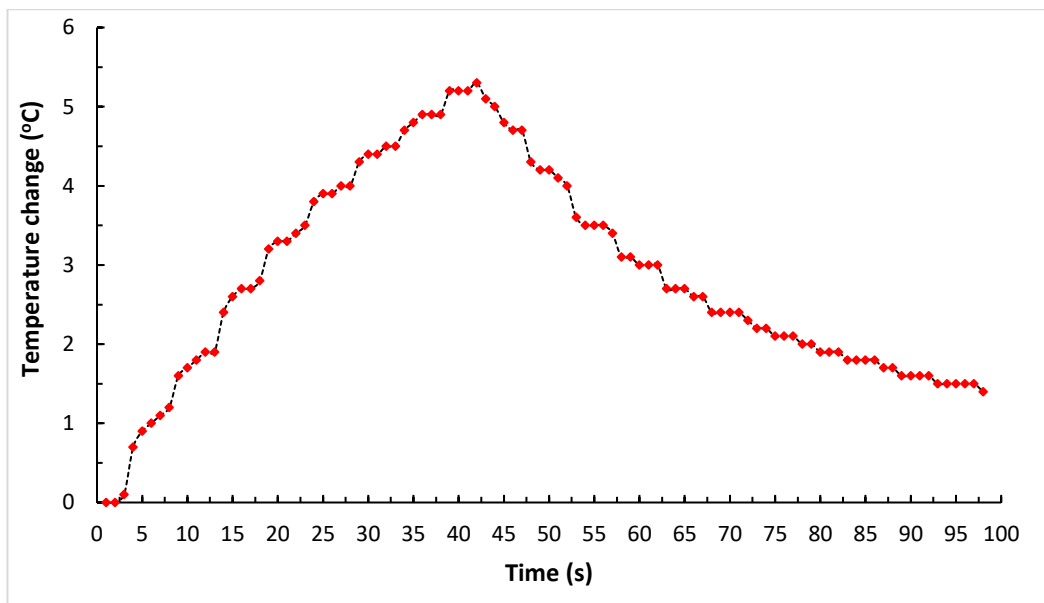


Figure 46: Temperature change as a function of time recorded for sonications on excised tissue with the 2.6 MHz transducer ($D=38$ mm, $ROC=61$ mm) and robotic device (version 1) using acoustic power of 2.3 W for a sonication time of 40 s at 10 mm focal depth.

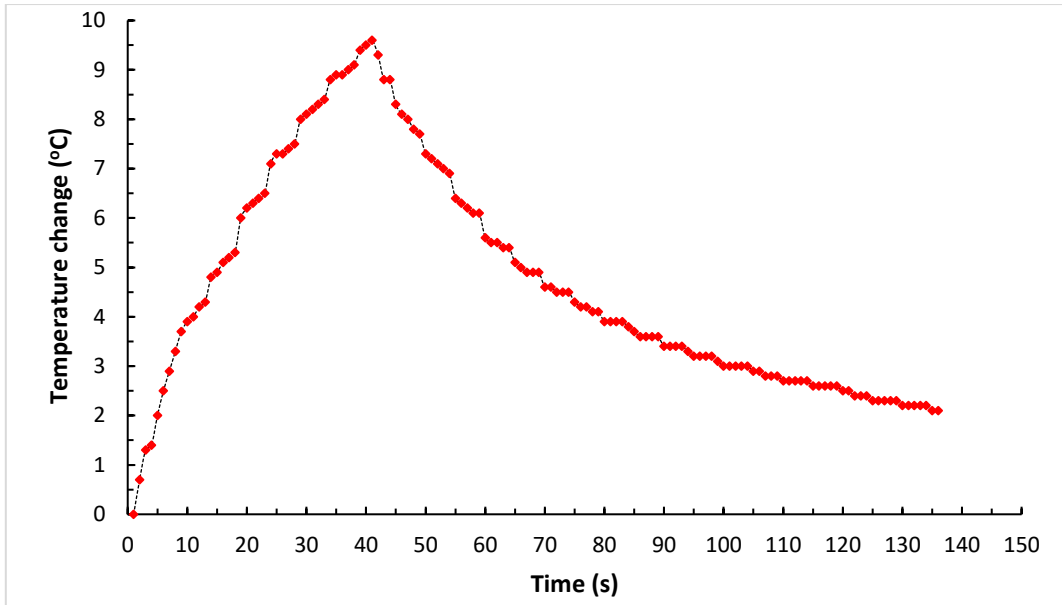


Figure 47: Temperature change as a function of time recorded for sonications on excised tissue with the 2.6 MHz transducer ($D=38$ mm, $ROC=61$ mm) and robotic device (version 1) at acoustic power of 4.6 W for a sonication time of 40 s at 10 mm focal depth.

Temperature increase in phantom using the robotic device (version 2)

Sonications were also performed using the 1.1 MHz transducer ($D=50$ mm, $ROC=80$ mm) and the robotic device (version 2) that includes a membrane on the acoustic window. Sonications were executed using varying acoustical power for a sonication time of 60 s at 20 mm focal depth, with the temperature change within the agar-based phantom recorded. Figure 48 shows the temperature change versus time for sonications executed using acoustical power of 65 W for a sonication time of 60 s.

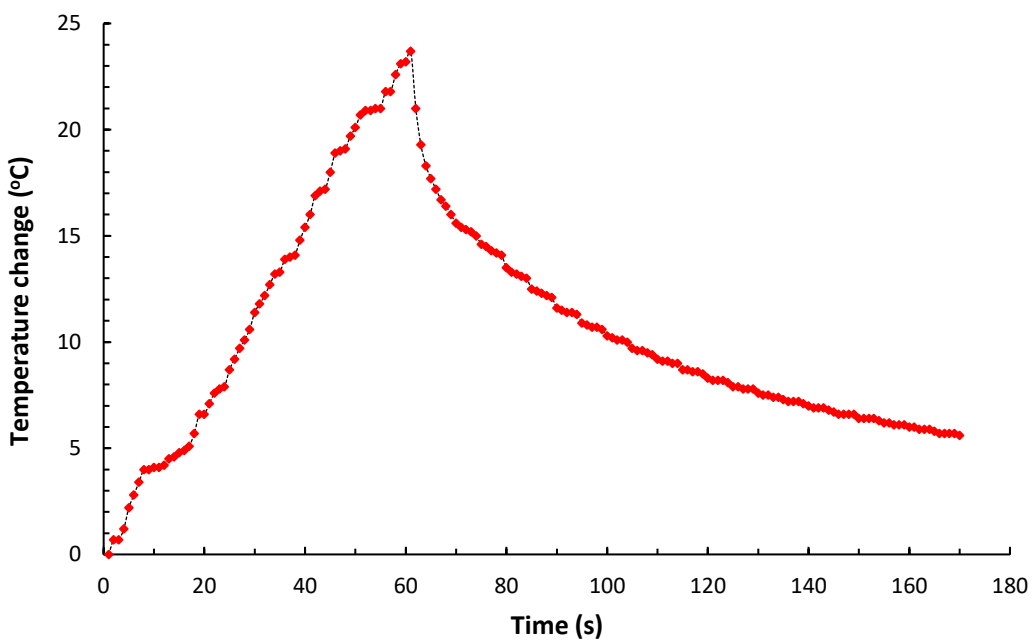


Figure 48: Temperature change as a function of time for sonications executed on agar-based phantom using a 1.1 MHz transducer ($D=50$ mm, $ROC=80$ mm) at acoustic power of 65 W for a sonication time of 60 s at 20 mm focal depth.

Table 12 summarizes the sonication parameters used in the experiments as well as the temperature change recorded for the different sonication protocols performed using the robotic device version 2 and the 1.1 MHz transducer (D=50 mm, ROC=80 mm).

Table 12: Temperature changes recorded for sonications executed on agar-based phantom using the 1.1 MHz transducer (D=50 mm, ROC=80 mm) and the robotic device (version 2) at varying acoustical power for a sonication time of 60 s at 20 mm focal depth.

Acoustic power (W)	Sonication (s)	Energy (J)	Temperature change (°C)
32.5	60	1950	3.1
65		3900	23.7
97.5		5850	47.8

The robotic device with the membrane (version 2) was also used with the 2.75 MHz transducer (D=50 mm, ROC=65 mm) employed for sonications. Temperature changes within the agar-based phantom were recorded for sonications performed at varying acoustical power of 16-60 W (15 W steps) for a sonication time of 120 s at 20 mm focal depth. Figure 50 shows the temperature change as a function of time induced by sonications at varying acoustical power.

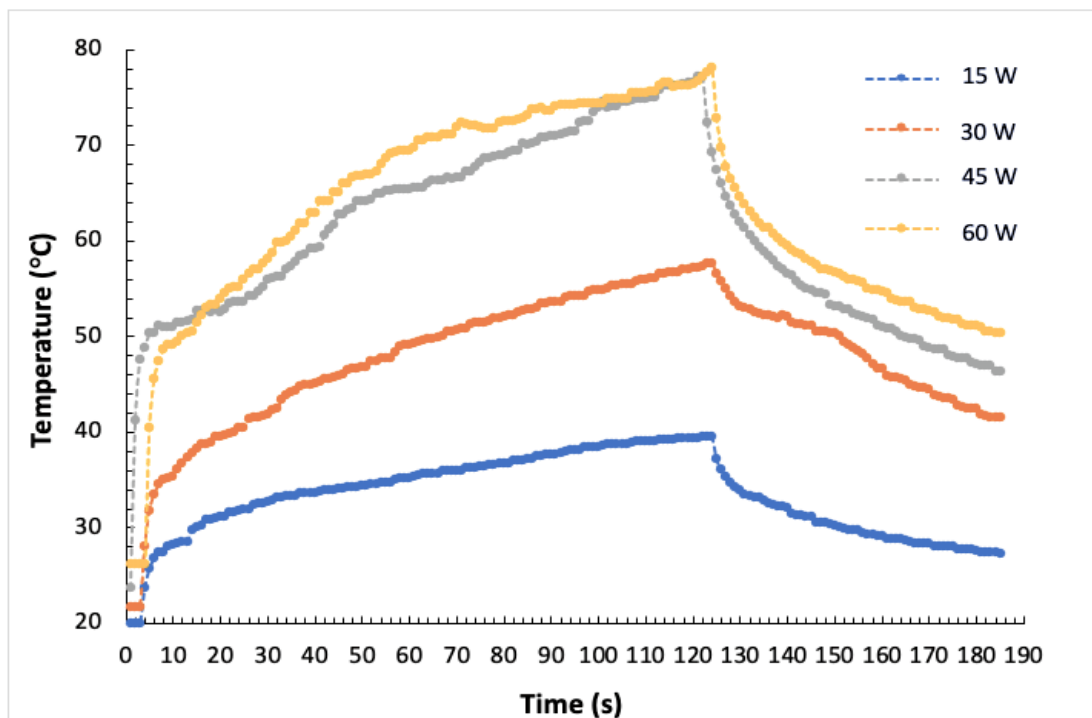


Figure 49: Temperature change as a function of time induced during sonications executed on agar-based phantom using the 2.75 MHz transducer (D=50 mm, ROC=65 mm) at acoustic power of 15 W, 30 W, 45 W and 60 W for a sonication time of 120 s at 20 mm focal depth.

Table 13 summarizes the sonication parameters used in the experiments as well as the temperature change recorded for the different sonications executed at varying acoustical power using the robotic device version 2 and the 2.75 MHz transducer (D=50 mm, ROC=65 mm).

Table 13: Temperature changes recorded for sonications executed on an agar-based phantom using the 2.75 MHz transducer (D=50 mm, ROC=65 mm) and the robotic device (version 2) at varying acoustical power for a sonication time of 120 s at 20 mm focal depth.

Acoustic power (W)	Sonication (s)	Energy (J)	Temperature change (°C)
15	120	1800	39.6
30		3600	57.7
45		5400	77.2
60		7200	78.1

Temperature increase in excised tissue using the robotic device (version 2)

Sonications were executed on excised tissue using the robotic device (version 2) with the membrane and the 2.75 MHz transducer (D=50 mm, ROC=65 mm) at 20 mm focal depth, so as to record the temperature increase during sonications. The thermocouple was inserted at a depth of 20 mm within the excised tissue to record the temperature increase at the focal point during sonications executed at varying acoustical power (15 W, 30 W and 45 W) for a constant sonication time of 60 s. Figure 51 shows the rate of change of temperature recorded during sonications performed using varying acoustical power.

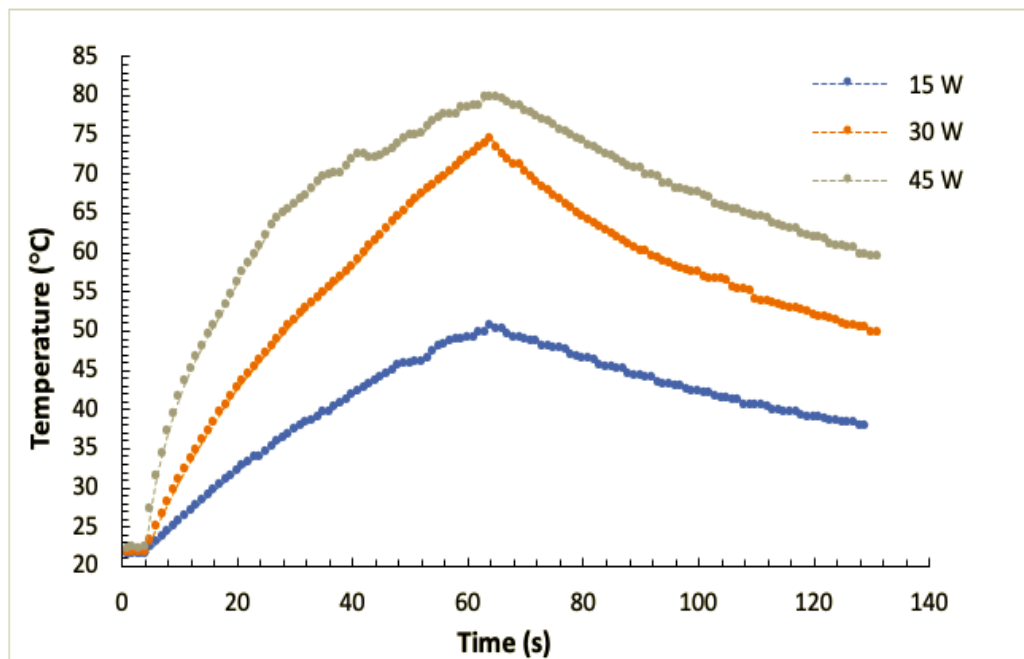


Figure 50: Temperature change versus time recorded for sonications on excised pork tissue with the 2.75 MHz transducer ($D=50$ mm, $ROC=65$ mm) and robotic device (version 2) using varied acoustic power (15 W, 30 W and 45 W) for a sonication time of 60 s at 20 mm focal depth.

Sonications at acoustical power of 15 W, 30 W and 45 W induced a temperature change of 50.7 °C, 74.4 °C and 79.9 °C, respectively. These temperature increases would probably result in the formation of lesions. Therefore, the tissue was sliced to examine the lesions formed as a result of the sonications executed at each power (15, 30, and 45 W). Figure 52A, Figure 52B and Figure 52C show the lesions formed on plane parallel to the beam after sonications using acoustic power of 15 W, 30 W and 45 W, respectively.

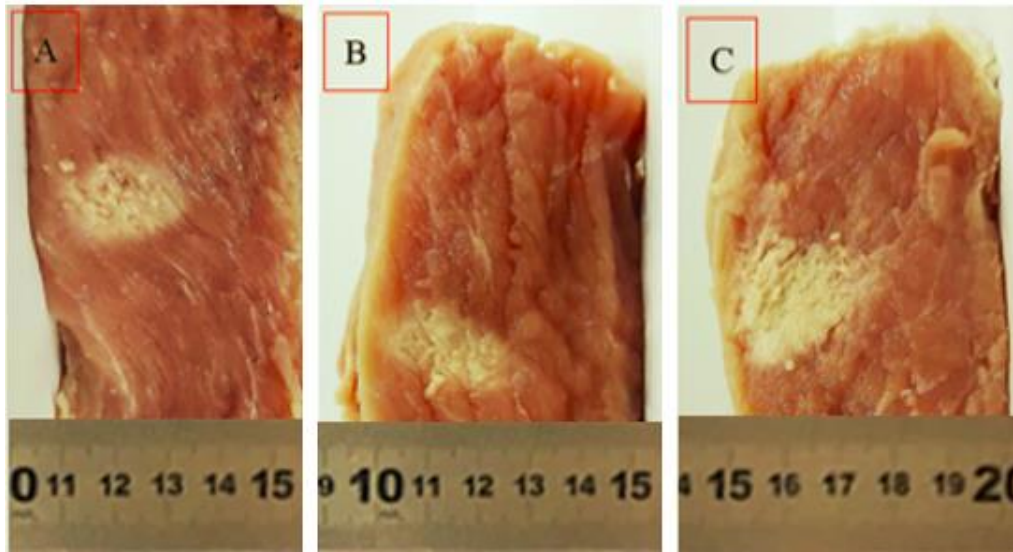


Figure 51: Lesions formed on excised pork tissue on a plane parallel to the beam after sonications executed with the 2.75 MHz transducer ($D=50$ mm, $ROC=65$ mm) and robotic device (version 2) at varied acoustical power for a sonication time of 60 s at 20 mm focal depth. Lesions formed using an acoustic power of A) 15 W, B) 30 W, and C) 45 W.

Multiple ablations on excised tissue using manual movement of the transducer

The effect of lesion formation on the tissue was examined by movement of the 1.1 MHz transducer ($D=60$ mm, $ROC=70$ mm) in various grid patterns (depending on the shape of the tissue) and sonications executed at varied acoustical powers and sonication times at different focal depths. The transducer-tissue distance was set at 70 mm, therefore resulting at an interfacial focal point. An acoustical power of 78 W was applied for a sonication time of 30 s. Manual movement of the transducer was performed in a 3×3 grid with a 15 mm space between each step for the formation of discrete lesions. Figure 52A shows the lesions formed on a plane perpendicular to the beam, while Figure 52B shows the lesions formed on a plane parallel to the ultrasonic beam. Table 14 summarizes the individual dimensions of the lesions. The formed lesions had an average diameter of 7.8 mm and an average length of 20.85 mm.

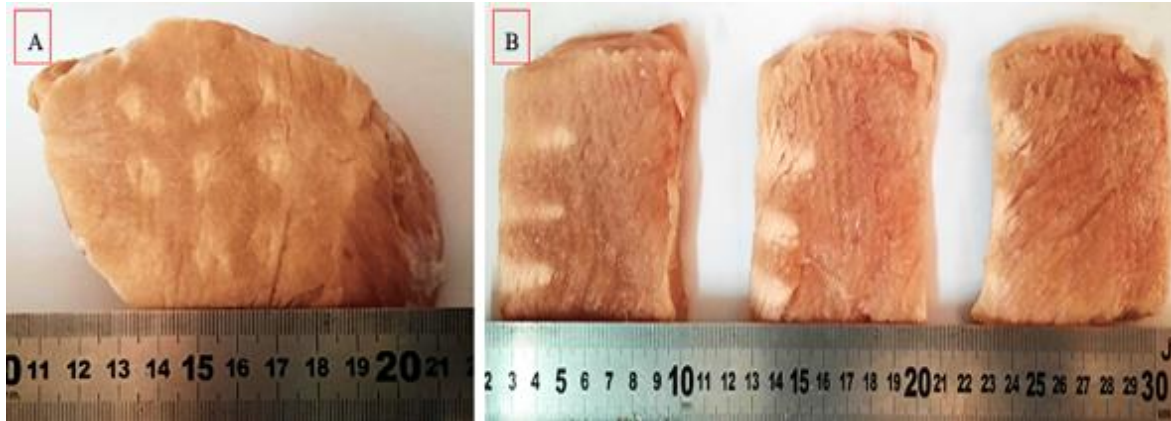


Figure 52: Lesions formed on excised tissue after exposure at acoustical power of 78 W for a sonication time of 30 s, with manual movement of the 1.1 MHz transducer ($D=60$ mm, $ROC=70$ mm) in a 3×3 grid with a 15 mm step, with the focal point located at the tissue interface. A) Lesions formed on plane perpendicular to the beam, and B) Lesions formed on plane parallel to the beam.

Table 14: Dimensions of lesions formed resulting exposure at acoustical power of 78 W for a sonication time of 30 s, with manual movement of the 1.1 MHz transducer ($D=60$ mm, $ROC=70$ mm) in a 3×3 grid with a 15 mm step, with the focal point located at the tissue interface.

Acoustical Power (W)	Sonication Time (s)	Energy (J)	Lesion Diameter (mm)	Lesion Length (mm)
78	30	2340	7.9	24.74
			9.2	28.78
			7	31.35
			7.17	21.63
			8.35	20.68
			8.18	24.55
			8.13	11.25
			7.7	9.69
			6.58	15
Average			7.8	20.85

The acoustical power of 78 W was used for a decreased sonication time of 20 s. Manual movement of the transducer was performed in a 2×4 grid with a 15 mm step for the formation of discrete lesions. Figure 53 shows the formed lesions. Two of the formed lesions were superficial with no significant length, probably due to air bubbles existing in the tissue. Table 15 summarizes the individual dimensions of the lesions. The formed lesions had an average diameter of 6 mm and an average length of 16.68 mm.



Figure 53: Lesions formed on excised tissue after exposure at acoustical power of 78 W for a sonication time of 20 s, with manual movement of the 1.1 MHz transducer ($D=60$ mm, $ROC=70$ mm) in a 2×4 grid with a 15 mm step, with the focal point located at the tissue interface. A) Lesions formed on plane perpendicular to the beam, and B) Lesions formed on plane parallel to the beam.

Table 15: Dimensions of lesions formed resulting exposure at acoustical power of 78 W for a sonication time of 20 s, with manual movement of the 1.1 MHz transducer ($D=60$ mm, $ROC=70$ mm) in a 2×4 grid with a 15 mm step, with the focal point located at the tissue interface.

Acoustical power (W)	Sonication time (s)	Energy (J)	Lesion Diameter (mm)	Lesion Length (mm)
78	20	1560	6.11	14.41
			8.94	10.78
			5.65	7.87
			2.6	-
			5.36	21.26
			6.18	25.32
			4.9	20.42
			8.27	-
Average			6	16.68

The acoustical power of 78 W was then used for a decreased sonication time of 10 s, with movement in a 3×3 grid with a 15 mm step. Figure 54 shows the lesions formed on a plane parallel to the beam. Only 5 lesions were formed with an average diameter of 5.17 mm and an average length of 11.27 mm. Table 16 summarizes the individual dimensions of the formed lesions.

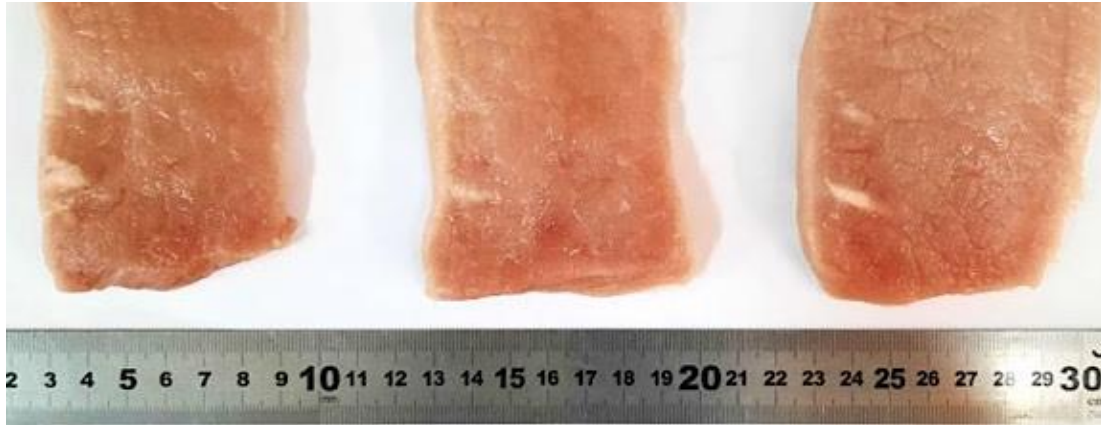


Figure 54: Lesions formed on a plane parallel to the beam after exposure at acoustical power of 78 W for a sonication time of 10 s, with manual movement of the 1.1 MHz transducer ($D=60$ mm, $ROC=70$ mm) in a 3×3 grid with a 15 mm step, with the focal point located at the tissue interface.

Table 16: Dimensions of lesions formed resulting exposure at acoustical power of 78 W for a sonication time of 10 s, with manual movement of the 1.1 MHz transducer ($D=60$ mm, $ROC=70$ mm) in a 3×3 grid with a 15 mm step, with the focal point located at the tissue interface.

Acoustical power (W)	Sonication time (s)	Energy (J)	Lesion Diameter (mm)	Lesion Length (mm)
78	10	780	4.25	10.59
			8.27	12.21
			4.3	10.48
			3.56	9.93
			5.45	13.12
Average			5.17	11.27

The transducer-tissue distance was changed to 60 mm, thus shifting the focal depth of the transducer at 10 mm within the tissue. An acoustical power of 62 W was used for a sonication time of 30 s to examine the formation of discrete lesions in a 3×3 grid with a 15 mm step. Figure 55 shows the formed lesions having an average diameter of 11.1 mm and an average length of 9.19 mm. Table 17 summarizes the individual dimensions of the formed lesions.

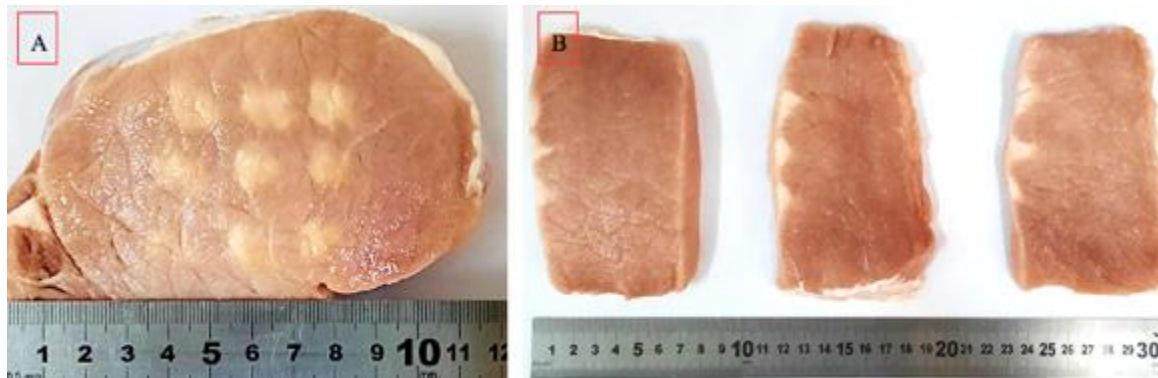


Figure 55: Lesions formed after exposure at acoustical power of 62 W for a sonication time of 30 s, with manual movement of the 1.1 MHz transducer ($D=60$ mm, $ROC=70$ mm) in a 3×3 grid with a 15 mm step, at 10 mm focal depth. A) Lesions formed on a plane perpendicular to the beam, and B) Lesions formed on a plane parallel to the beam.

Table 17: Dimensions of lesions formed resulting exposure at acoustical power of 62 W for a sonication time of 30 s, with manual movement of the 1.1 MHz transducer ($D=60$ mm, $ROC=70$ mm) in a 3×3 grid with a 15 mm step at 10 mm focal depth.

Acoustical power (W)	Sonication time (s)	Energy (J)	Lesion Diameter (mm)	Lesion Length (mm)
62	30	1860	11.19	11.64
			11.51	11.89
			11.42	5.73
			12.25	6.5
			11.64	7.34
			10.94	10.81
			10.42	6
			10.49	13.14
			10.09	9.66
<i>Average</i>			<i>11.1</i>	<i>9.19</i>

Thermal and cavitation lesions

The lesions shown on the first slice of tissue (from left) in Figure 54 were formed using an acoustical power of 78 W for a sonication time of 10 s, with the focal depth of the transducer located at the tissue interface. Although the same sonication parameters were used for the formation of both lesions, one was a normal ‘cigar’ shaped lesion indicating formation due to thermal mechanisms, while the other was a tadpole shaped lesion indicating formation due to cavitation mechanisms.

Since the lesions were formed on the same piece of excised tissue using the same parameters, a scanning electron microscope (SEM) (Quanta 200, FEI, Hillsboro, Oregon, USA) was used to examine the morphology of the surface of the two lesions and observe any differences that could result in the presence of cavitation mechanisms. Figure 56 shows again the photo of the lesions as formed on the excised tissue, with the thermal and cavitation lesions indicated.

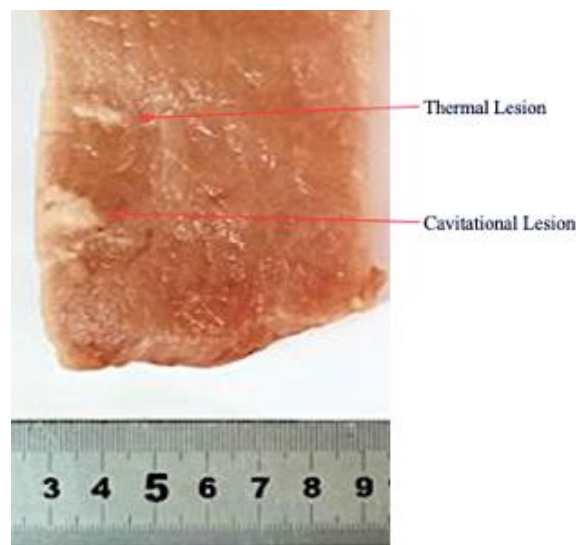


Figure 56: Thermal and cavitation lesions used for the acquisition of SEM images.

Prior to the SEM investigation, all samples were coated with a thin (<10 nm) silver layer in order to reduce electron charging effects. SEM images were collected at 20 kV accelerating voltage using different magnifications and working distances (distance between sample surface and electron pole). The same voltage (20 kV) was used for acquisition of all images, as a high voltage provides higher resolution. Figure 57 shows a low magnification (36×) SEM image of the surface of the thermal lesion. Orange boundary represents the lesion.

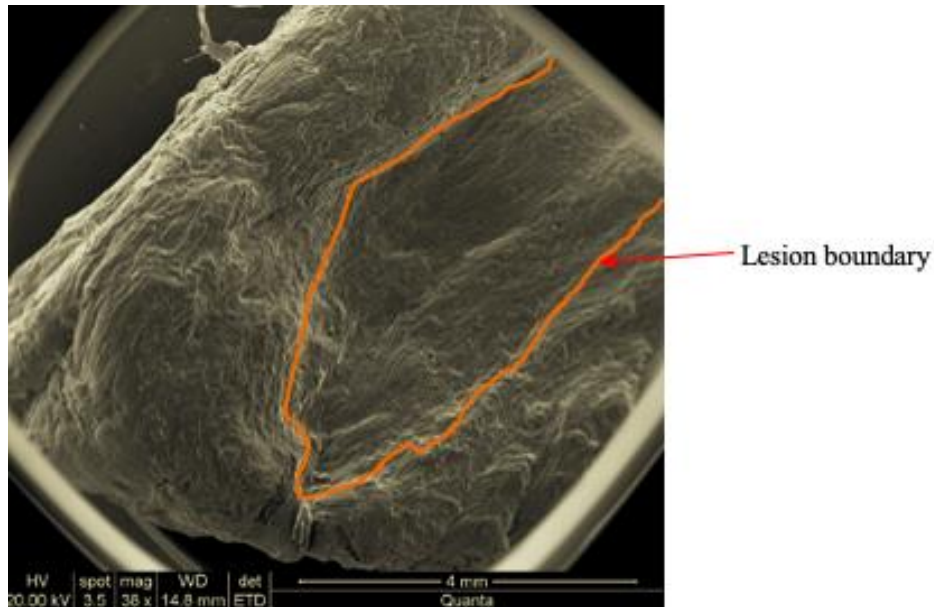


Figure 57: Low magnification (36×) SEM image of the thermal lesion.

Figure 58 shows a high-magnification (500×) SEM image acquired on the tissue outside the lesion boundary. Figure 59A shows a high-magnification (500×) SEM image acquired on the tissue within the lesion boundary. Figure 59B shows a high magnification (256×) SEM image of the thermal lesion, acquired on a smaller working distance, thus providing higher resolution. It is observed that some voids of the order of 250 μm exist within the lesion. Some morphological differences are observed between the ablated and non-ablated regions, with the ablated regions having a more sharply defined surface. Figure 60 shows a low magnification (50×) SEM image of the cavitation lesion.

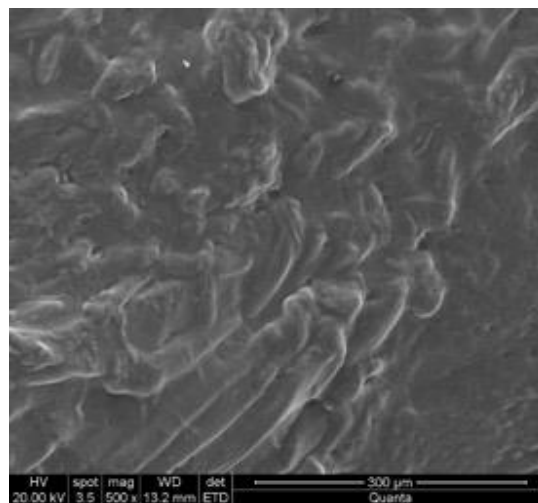


Figure 58: High magnification (500×) SEM image of tissue obtained outside the boundary of the thermal lesion.

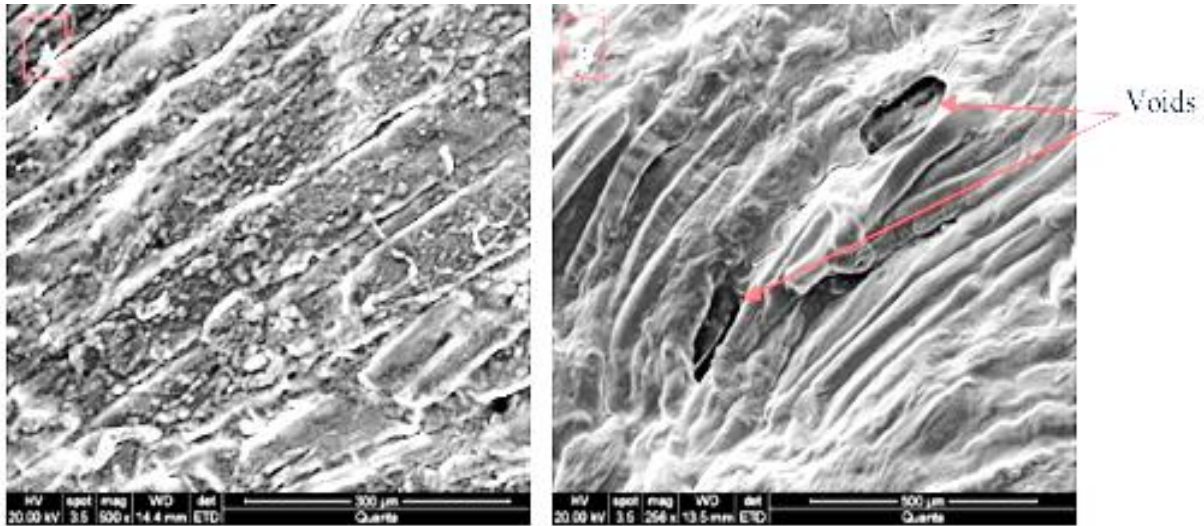


Figure 59: High magnification SEM images obtained inside the boundary of the thermal lesion. A) Image obtained with 500× magnification, and B) Image obtained with 256× magnification and decreased working distance indicating void inside the thermal lesion.

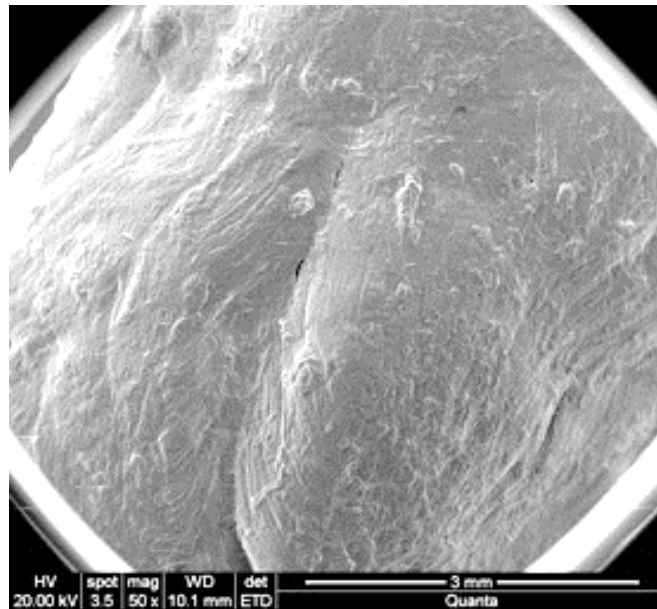


Figure 60: Low magnification (50×) SEM image of the cavitation lesion.

Back scattered electron (BSE) microscopy images were also obtained from the SEM system (Quanta 200, FEI). These images give a poorer spatial resolution compared to normal SEM images. However, because scattered electrons used for production of BSE images have larger energies than secondary electrons used for acquisition of SEM images, BSE images show higher contrast among regions with different phases/densities. Figure 61 shows the low magnification (39×) BSE image of the thermal lesion. The voids already presented in the respective SEM image (Figure 59B) can be seen. Figure 62 shows the low magnification (45×) BSE image of the cavitation lesion. The orange boundary represents the ablated area. Figure 63 shows an acquired high magnification (202×) BSE image of the tissue interface outside the boundary of the cavitation lesion. Some voids of an order greater than 500 μm are observed on the interface surface.

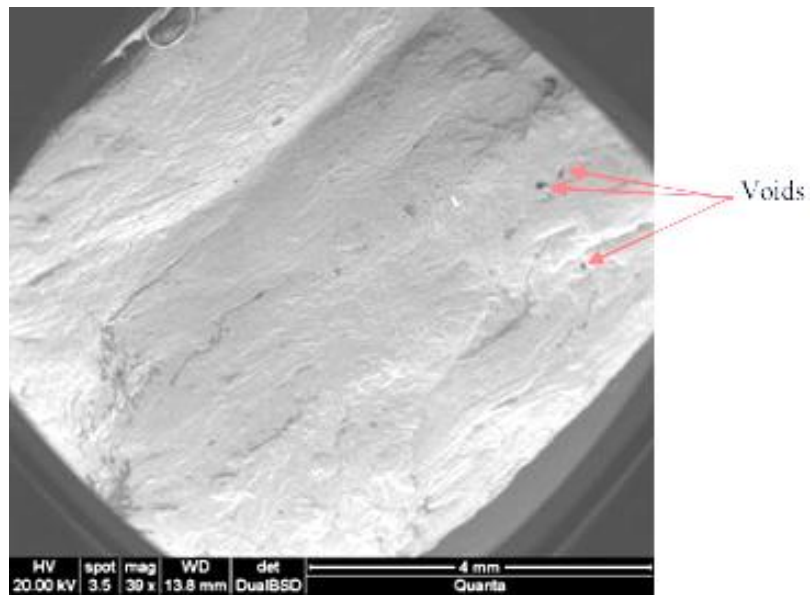


Figure 61: Low magnification (39 \times) BSE image of the thermal lesion.

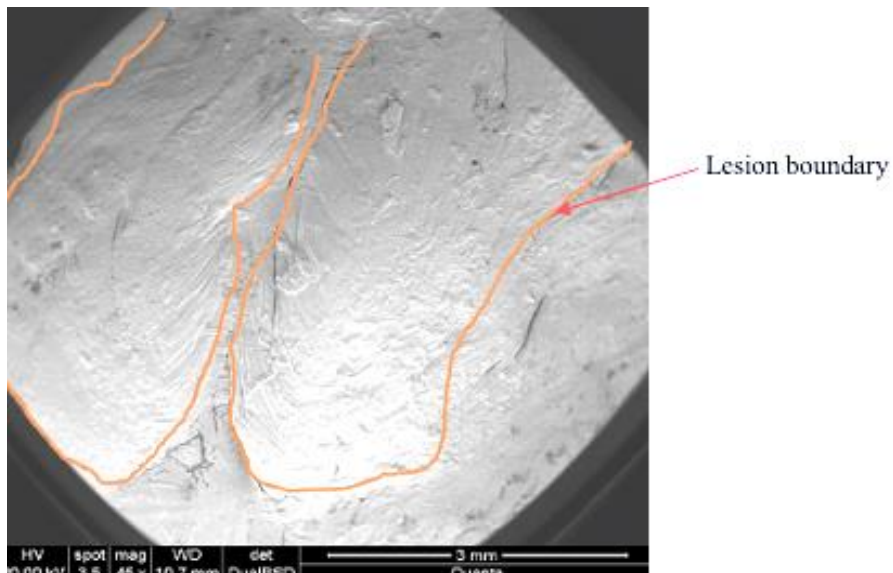


Figure 62: Low magnification (45 \times) BSE image of the cavitation lesion.

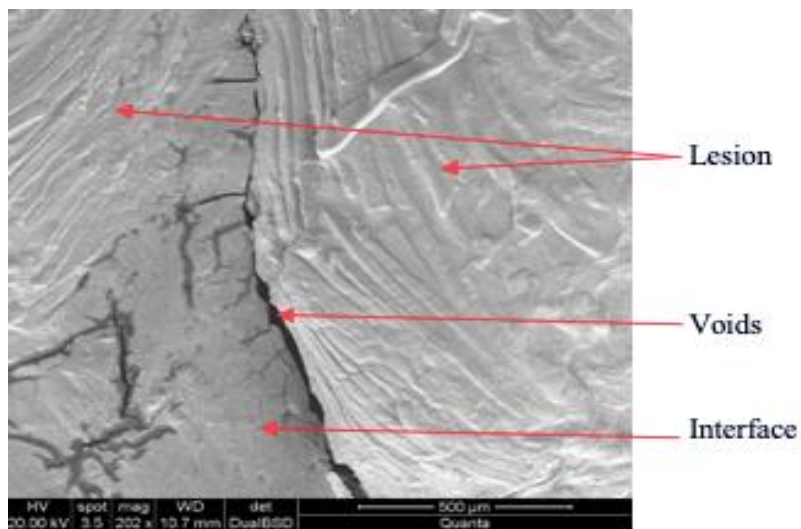


Figure 63: High magnification (202 \times) BSE image of the tissue interface outside the cavitation lesion boundary.

Ablation of excised tissue using movement of the robotic device (version 1)

Movement of the robotic device (version 1) in various grid patterns with different step sizes was used for the formation of discrete and overlapping lesions using the 1.1 MHz transducer (D=60 mm, ROC=70 mm). Different acoustical powers were used for varied sonication times for the ablation of seventeen (17) pieces of excised tissue at various focal depths. Below a selection of data is presented, while the results of all 17 pieces are listed in Table 38 and Table 39 in the conclusions section, for discrete and overlapping lesions respectively.

Formation of discrete lesions

Movement of the robotic device was used for the formation of discrete lesions using varied acoustical power and sonication time at various focal depths. The transducer-tissue distance was first set at 70 mm, thus shifting the focal point of the transducer on the tissue interface. An acoustical power of 55 W was used for a sonication time of 15 s with movement of the transducer in a 3×3 grid with a 10 mm step. Figure 64 shows the formed lesions. Only 4 lesions were formed, one of them superficial with no significant length. The lesions formed had an average diameter of 4.67 mm and an average length of 20.89 mm.



Figure 64: Lesions formed on excised tissue after exposure at acoustical power of 55 W for a sonication time of 15 s with movement of the 1.1 MHz transducer (D=60 mm, ROC=70 mm) using the robotic device (version 1) in a 3×3 grid with a 10 mm step, with the focal point located at the tissue interface. A) Slice of the tissue at 10 mm showing lesions formed on plane perpendicular to the beam, and B) Lesions formed on a plane parallel to the beam.

The transducer was moved in the Z axis to shift the focal depth to 10 mm within the tissue. Varied acoustical power was used for various sonication times. An acoustical power of 94 W was used for a sonication time of 20 s for the formation of discrete lesions in a 3×3 grid with a 15 mm step. After exposure, the tissue was sliced at 10 mm and the dimensions of the lesions were measured. Figure 65 shows the lesions formed on a plane perpendicular to the beam, while Figure 66 shows the lesions formed on a plane parallel to the beam. Table 18 lists the individual dimensions of the formed lesions. The lesions were formed with an average diameter of 6.59 mm and an average length of 30.6 mm.



Figure 65: Lesions formed on a plane perpendicular to the beam after exposure at acoustical power of 94 W for a sonication time of 20 s with movement of the 1.1 MHz transducer ($D=60$ mm, $ROC=70$ mm) using the robotic device (version 1) in a 3×3 grid with a 15 mm step at 10 mm focal depth. Slice of the tissue at 10 mm and its mirror (from left to right).



Figure 66: Lesions formed on a plane parallel to the beam after exposure at acoustical power of 94 W for a sonication time of 20 s with movement of the 1.1 MHz transducer ($D=60$ mm, $ROC=70$ mm) using the robotic device (version 1) in a 3×3 grid with a 15 mm step at 10 mm focal depth.

Table 18: Dimensions of lesions formed resulting exposure at acoustical power of 94 W for a sonication time of 20 s with movement of the 1.1 MHz transducer ($D=60$ mm, $ROC=70$ mm) using the robotic device (version 1) in a 3×3 grid with a 15 mm step at 10 mm focal depth.

Acoustical power (W)	Sonication time (s)	Energy (J)	Lesion Diameter (mm)	Lesion Length (mm)
94	20	1880	9.06	28.46
			6.32	31.85
			6.28	27.4
			4.09	9.62
			4.97	45.37
			8.62	38.79
			7.11	13.67
			7.11	35.97
			5.84	44.07
Average			6.59	30.6

An increased acoustical power of 109 W for a decreased sonication time of 10 s was used for the formation of discrete lesions in a 3×3 grid with a 15 mm step. After exposure, the tissue was sliced at 10 mm and the dimensions of the lesions were measured. Figure 67 shows the lesions formed on a plane perpendicular to the beam, while Figure 68 shows the lesions formed on a plane parallel to the beam. Only two lesions were formed with an average diameter of 5.21 mm and an average length of 18.9 mm. Table 19 lists the individual dimensions of the formed lesions.

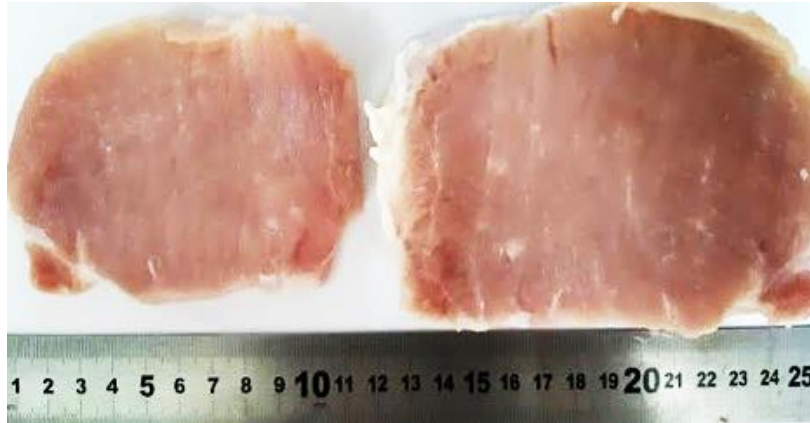


Figure 67: Lesions formed on a plane perpendicular to the beam after exposure at acoustical power of 109 W for a sonication time of 10 s with movement of the 1.1 MHz transducer ($D=60$ mm, $ROC=70$ mm) using the robotic device (version 1) in a 3×3 grid with a 15 mm step at 10 mm focal depth. Slice of the tissue at 10 mm and its mirror (from left to right).



Figure 68: Lesions formed on a plane parallel to the beam after exposure at acoustical power of 109 W for a sonication time of 10 s with movement of the 1.1 MHz transducer ($D=60$ mm, $ROC=70$ mm) using the robotic device (version 1) in a 3×3 grid with a 15 mm step at 10 mm focal depth.

Table 19: Dimensions of lesions formed resulting exposure at acoustical power of 109 W for a sonication time of 10 s with movement of the 1.1 MHz transducer ($D=60$ mm, $ROC=70$ mm) using the robotic device (version 1) in a 3×3 grid with a 15 mm step at 10 mm focal depth.

Acoustical power (W)	Sonication time (s)	Energy (J)	Lesion Diameter (mm)	Lesion Length (mm)
109	10	1090	4.83	14.57
			5.59	23.23
Average			5.21	18.9

The acoustical power of 109 W was then used for an increased sonication time of 15 s to examine the formation of lesions in a 3×3 grid with a 15 mm step. After sonication, the tissue was sliced at 10 mm and the dimensions of the formed discrete lesions were measured. Figure 69 shows the lesions formed on a plane perpendicular to the beam, while Figure 70 shows the lesions formed on a plane parallel to the beam. Table 20 lists the individual dimensions of the formed lesions. The formed lesions had an average diameter of 7.57 mm and an average length of 41.67 mm.



Figure 69: Lesions formed on a plane perpendicular to the beam after exposure at acoustical power of 109 W for a sonication time of 15 s with movement of the 1.1 MHz transducer ($D=60$ mm, $ROC=70$ mm) using the robotic device (version 1) in a 3×3 grid with a 15 mm step at 10 mm focal depth. Slice of the tissue at 10 mm and its mirror (from left to right).

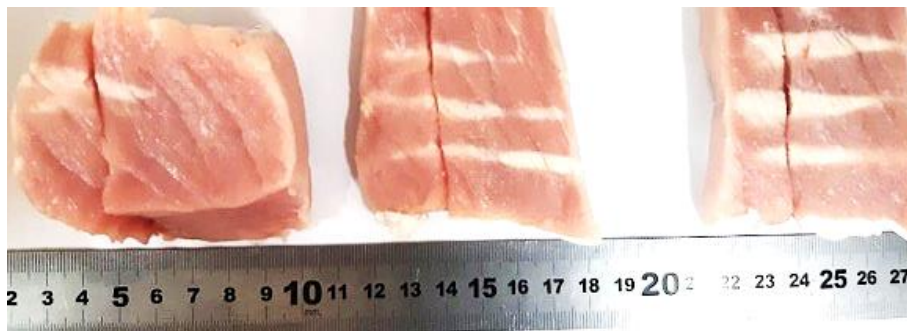


Figure 70: Lesions formed on a plane parallel to the beam after exposure at acoustical power of 109 W for a sonication time of 15 s with movement of the 1.1 MHz transducer ($D=60$ mm, $ROC=70$ mm) using the robotic device (version 1) in a 3×3 grid with a 15 mm step at 10 mm focal depth.

Table 20: Dimensions of lesions formed resulting exposure at acoustical power of 109 W for a sonication time of 15 s with movement of the 1.1 MHz transducer ($D=60$ mm, $ROC=70$ mm) using the robotic device (version 1) in a 3×3 grid with a 15 mm step at 10 mm focal depth.

Acoustical power (W)	Sonication time (s)	Energy (J)	Lesion Diameter (mm)	Lesion Length (mm)
109	15	1635	6.64	28.98
			5.16	34.38
			9.96	44.74
			8.28	52.19
			9.63	41.72
			6.2	48.8
			7.13	40.86
Average			7.57	41.67

Formation of overlapping lesions

Movement of the robotic device was used for the formation of overlapping lesions, using varied acoustical power and sonication time at various focal depths. The transducer-tissue distance was first set at 70 mm, thus shifting the focal point of the transducer at the tissue interface. An acoustical power of 55 W was used for a sonication time of 30 s with movement of the 1.1 MHz transducer (D=60 mm, ROC=70 mm) in a 3×3 grid with a 10 mm step. Figure 71A shows the formed lesions on a plane perpendicular to the beam, while Figure 71B shows the formed lesions on a plane parallel to the beam. The formed lesion had a surface area of 20.16×20.16 mm² and a 12.68 mm length.

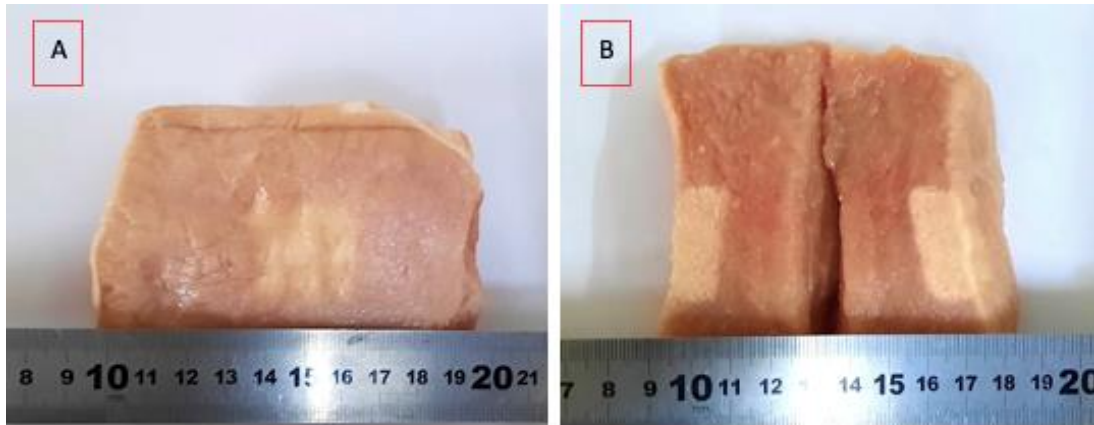


Figure 71: Overlapping lesions formed after exposure at acoustical power of 55 W for a sonication time of 30 s with movement of the 1.1 MHz transducer (D=60 mm, ROC=70 mm) using the robotic device (version 1) in a 3×3 grid with a 10 mm step, with the focal point located at the tissue interface. A) Lesions formed on plane perpendicular to the beam, and B) Lesions formed on plane parallel to the beam (mirror view).

The transducer-tissue distance was changed to 60 mm, thus shifting the focal point of the transducer to 10 mm within the excised tissue. An acoustical power of 74 W was used for a sonication time of 20 s for the formation of overlapping lesions in a 3×3 grid with a 10 mm step. After exposure, the tissue was sliced at 10 mm. Figure 72 shows the formed overlapping lesions. The formed lesions had a surface area of 31.06×29.23 mm² and a length of 29.96 mm.



Figure 72: Overlapping lesions formed after exposure at acoustical power of 74 W for a sonication time of 20 s with movement of the 1.1 MHz transducer (D=60 mm, ROC=70 mm) using the robotic device (version 1) in a 3×3 grid with a 10 mm step at 10 mm focal depth. A) Slice of the tissue at 10 mm and its mirror (from left to right) showing lesions formed on a plane perpendicular to the beam, and B) Lesions formed on a plane parallel to the beam.

Movement of the transducer was performed in a 4×4 grid with a 6 mm step for the ablation of tissue at a focal depth of 10 mm using varying ultrasonic energies (acoustical power × sonication time). An acoustical power of 94 W was used for a sonication time of 20 s. Figure 73 shows the formed overlapping lesions having a surface area of 23.5×24.05 mm² and a length of 21.27 mm. An increased acoustical power of 109 W was then used for a decreased sonication time of 15 s. Figure 74 shows the formed overlapping lesions having a surface area of 22.63×22.11 mm² and a 38.79 mm length.

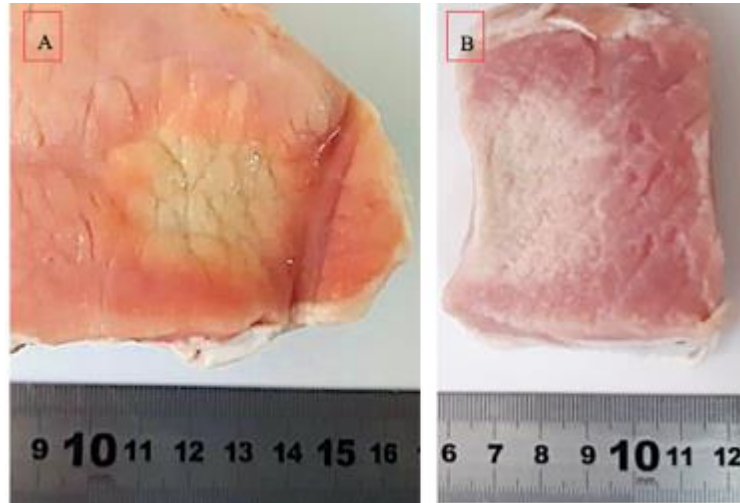


Figure 73: Overlapping lesions formed after exposure at acoustical power of 94 W for a sonication time of 20 s with movement of the 1.1 MHz transducer (D=60 mm, ROC=70 mm) using the robotic device (version 1) in a 4×4 grid with a 6 mm step at 10 mm focal depth. A) Lesions formed on a plane perpendicular to the beam, and B) Lesions formed on a plane parallel to the beam.

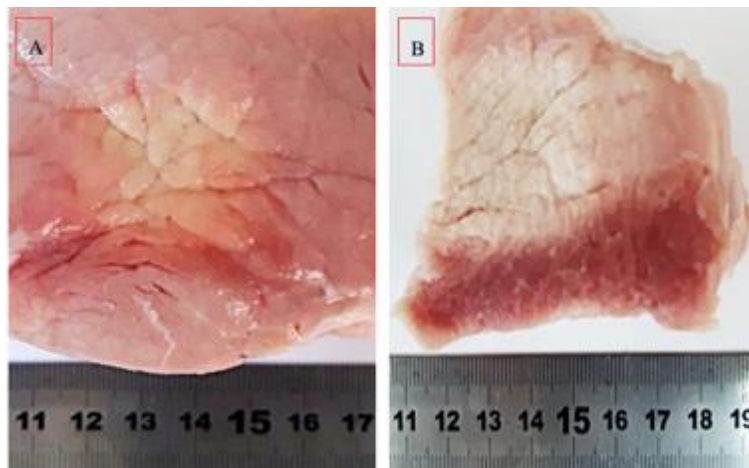


Figure 74: Overlapping lesions formed after exposure at acoustical power of 109 W for a sonication time of 15 s with movement of the 1.1 MHz transducer (D=60 mm, ROC=70 mm) using the robotic device (version 1) in a 4×4 grid with a 6 mm step at 10 mm focal depth. A) Lesions formed on a plane perpendicular to the beam, and B) Lesions formed on a plane parallel to the beam.

Ablation of small tumour-like excised tissue using movement of the robotic device (version 1)

Overlapping lesions were observed on the tissue after the 3×3 grid sonications with a 3 mm step executed with the robotic device (version 1) and the 2.6 MHz transducer (D=38 mm, ROC=61 mm) using an acoustic power of 46 W for a sonication time of 10 s at 10 mm focal

depth. The lesions formed in a plane perpendicular to the ultrasound beam are shown in Figure 75A. The tissue was vertically sliced so that the length of the overlapping lesions could be measured, as shown in Figure 75B. The ultrasonic energy (460 J) created overlapping lesions with a surface area of $14.6 \times 14 \text{ mm}^2$ and a length of 11 mm.

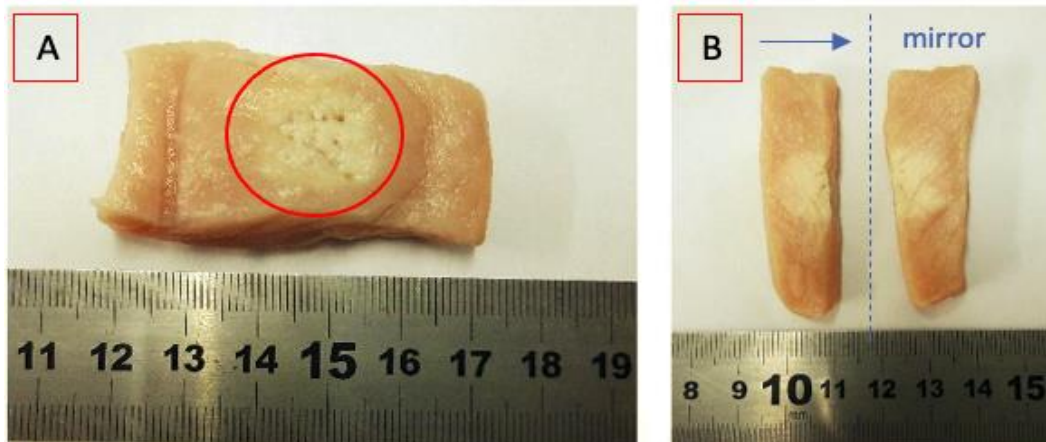


Figure 75: Overlapping lesions formed on excised tissue after 3×3 grid sonications with a 3 mm step executed with the 2.6 MHz transducer ($D=38 \text{ mm}$, $ROC=61 \text{ mm}$) and robotic device (version 1) using acoustic power of 46 W for a sonication time of 10 s at 10 mm focal depth. A) Lesions (red circle) as formed at the interface (from the sonicated side) of the tissue on a plane perpendicular to the beam, and B) Vertical cross-section (mirror view) of the ablated area showing lesions formed on plane parallel to the ultrasound beam. Blue arrow indicates the beam direction.

Sonications were executed using an increased acoustic power of 57.5 W for a sonication time of 15 s. A 3×3 grid pattern with a 3 mm step was performed and the overlapping lesions formed in a plane perpendicular to the ultrasound beam are shown in Figure 76A. The tissue was vertically sliced so that the length of the formed overlapping lesions could be measured as shown in Figure 76B. The ultrasonic energy (862.5 J) formed overlapping lesions with a surface area of $16.2 \times 15.45 \text{ mm}^2$ and a length of 17.5 mm.

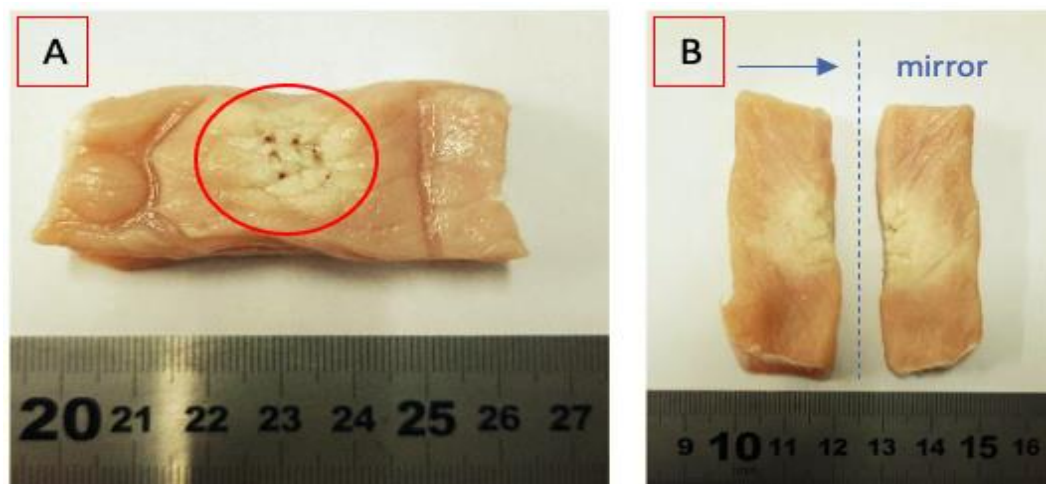


Figure 76: Overlapping lesions formed on excised tissue after 3×3 grid sonications with a 3 mm step, executed with the 2.6 MHz transducer ($D=38 \text{ mm}$, $ROC=61 \text{ mm}$) and robotic device (version 1) using acoustic power of 57.5 W for a sonication time of 15 s at 10 mm focal depth. A) Lesions (red circle) as formed at the interface (from the sonicated side) of the tissue on a plane perpendicular to the beam, and B) Vertical cross-section (mirror view) of the ablated area showing lesions formed on plane parallel to the ultrasound beam. Blue arrow indicates the beam direction.

The dimensions of the overlapping lesions formed after 3×3 grid sonications executed on 4 pieces of excised tissues using varied ultrasonic protocols are summarized in Table 21.

Table 21: Dimensions of overlapping lesions formed on excised tissue after 3×3 grid sonications with a 3 mm step executed with the 2.6 MHz transducer (D=38 mm, ROC=61 mm) and robotic device (version 1) using varied acoustic power and sonication time at 10 mm focal depth.

Acoustic power (W)	Sonication time (s)	Energy (J)	Lesion surface area (mm ²)	Lesion Length (mm)
46	10	460	14.6 × 14	11
57.5	10	575	15.25 × 14.2	11.65
57.5	15	862.5	16.2 × 15.45	17.5
57.5	15	862.5	15.26 × 15.18	10.5

Ablation of excised tissue using movement of the robotic device (version 2)

Formation of discrete lesions

A piece of excised pork tissue was sonicated in a 3×2 grid with a 10 mm step using acoustic power of 32.5, 49, and 65 W for a sonication time of 10 s at a focal depth of 20 mm. The interface of the tissue from the sonicated side after exposure is shown in Figure 77. Only one lesion formed with acoustic power of 49 W was barely visible on the interface.

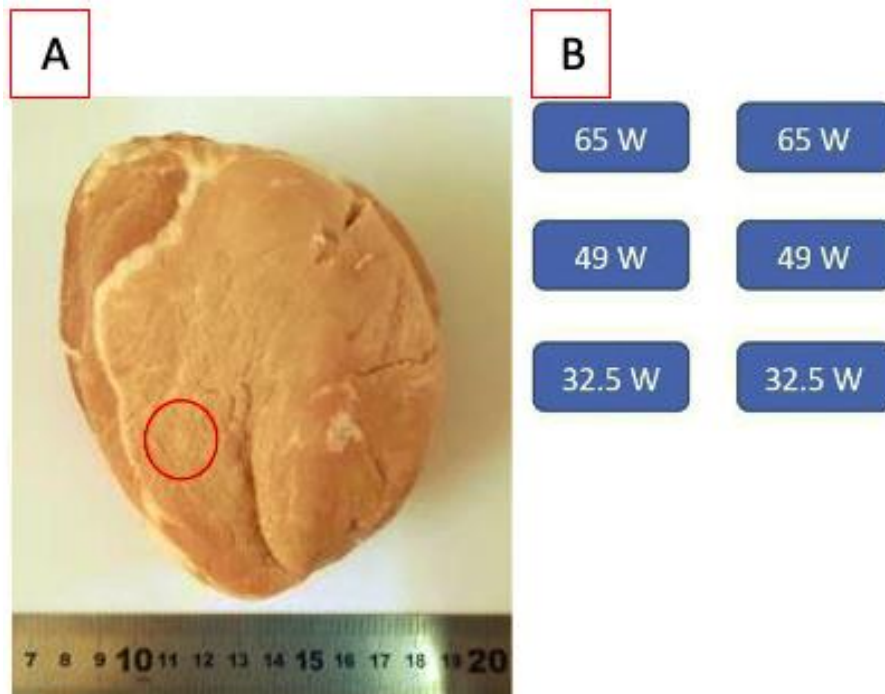


Figure 77: A) The interface of the excised tissue after 3×2 grid sonications with a 10 mm step executed with a 1.1 MHz transducer (D=60 mm, ROC=70 mm) and robotic device (version 2) using varied acoustic power (32.5, 49, and 65 W), for a sonication time of 10 s at a focal depth of 20 mm, showing one faint lesion (red circle) formed with acoustic power of 49 W, and B) Acoustic power used for each sonication of the 3×2 grid.

The tissue was vertically sliced so that the length of the induced lesions could be measured, as shown in Figure 78. The acoustic power of 32.5 W was not sufficient to induce lesions, while the acoustic power of 49 W and 65 W created faint lesions. There was a poor penetration of the ultrasound beam possibly due to inhomogeneity of the tissue and appearance of air bubbles in the tissue. The diameter and length of the formed lesions are shown in Table 22.

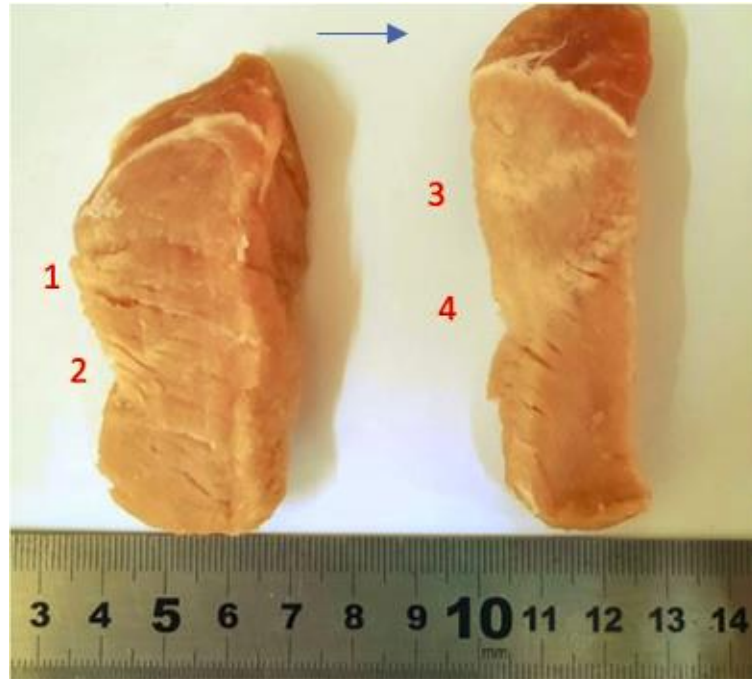


Figure 78: A) Lesions formed on excised tissue on a plane parallel to the beam after 3×2 grid sonications with a 10 mm step executed with a 1.1 MHz transducer ($D=60$ mm, $ROC=70$ mm) and robotic device (version 2) using varied acoustic power (32.5, 49, and 65 W), for a sonication time of 10 s at a focal depth of 20 mm. The blue arrow indicates the beam direction, and B) Diameter and length of the 4 lesions formed with acoustic power of 49 W and 65 W.

Table 22: Dimensions of lesions formed resulting exposure at varied acoustical power for a sonication time of 10 s with movement of the 1.1 MHz transducer ($D=60$ mm, $ROC=70$ mm) using the robotic device (version 2) in a 3×2 grid with a 10 mm step at 20 mm focal depth.

Lesion	Acoustical power (W)	Sonication time (s)	Lesion Diameter (mm)	Lesion Length (mm)
1	49	10	6.87	7.34
2			7.42	10.21
3	65		6.51	21.49
4			8.92	17.59

An acoustic power of 81 W was then applied for a sonication time of 10 s for 3×2 grid sonications at six different locations with a 10 mm step. After sonications, one lesion appeared on the tissue interface as shown in Figure 79.



Figure 79: The interface of the excised tissue after the 3×2 grid sonications with a 10 mm step executed with a 1.1 MHz transducer ($D=60$ mm, $ROC=70$ mm) and robotic device (version 2) using acoustic power of 81 W for a sonication time of 10 s at a focal depth of 20 mm, showing one lesion formed (red arrow).

The tissue was vertically cut so that the length of the induced lesions could be measured, as shown in Figure 80A and Figure 80B. Six lesions were formed at a distance of 10 mm from the tissue interface with an average diameter of 3.75 mm and an average length of 17.53 mm. The individual diameters and lengths of the 6 lesions are shown in Table 23.

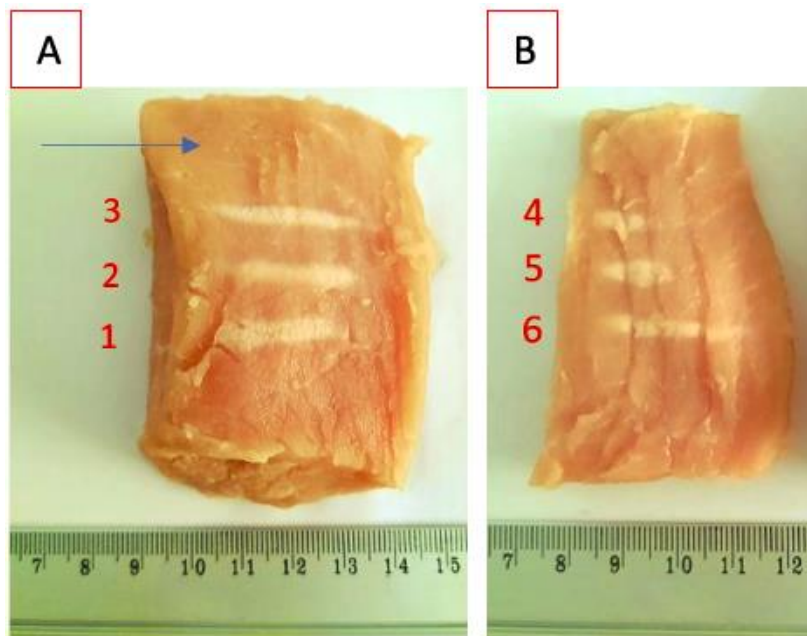


Figure 80: Lesions formed on excised tissue on a plane parallel to the beam after 3×2 grid sonications with a 10 mm step executed with a 1.1 MHz transducer ($D=60$ mm, $ROC=70$ mm) and robotic device (version 2) using acoustic power of 81 W for a sonication time of 10 s at a focal depth of 20 mm. A) Lesions 1, 2 and 3. The blue arrow indicates the beam direction, and B) Lesions 4, 5 and 6.

Table 23: Dimensions of lesions formed resulting exposure at acoustical power of 81 W for a sonication time of 10 s with movement of the 1.1 MHz transducer ($D=60$ mm, $ROC=70$ mm) using the robotic device (version 2) in a 3×2 grid with a 10 mm step at 20 mm focal depth.

Lesion	Acoustical power (W)	Sonication time (s)	Energy (J)	Lesion Diameter (mm)	Lesion Length (mm)
1	81	10	810	3.73	18.47
2				2.82	18.29
3				3.3	22.3
4				3.91	10.72
5				4.87	13.22
6				3.86	22.17
Average				3.75	17.53

Grid sonications were also executed using the 2.75 MHz transducer ($D=50$ mm, $ROC=65$ mm). Initially, 3×2 grid sonications with a 10 mm step were performed with an acoustic power of 45 W applied for sonication times of 30 s, 60 s and 120 s. The lesions created on the sonicated interface of the tissue after exposure on a plane perpendicular to the beam are shown in Figure 81.

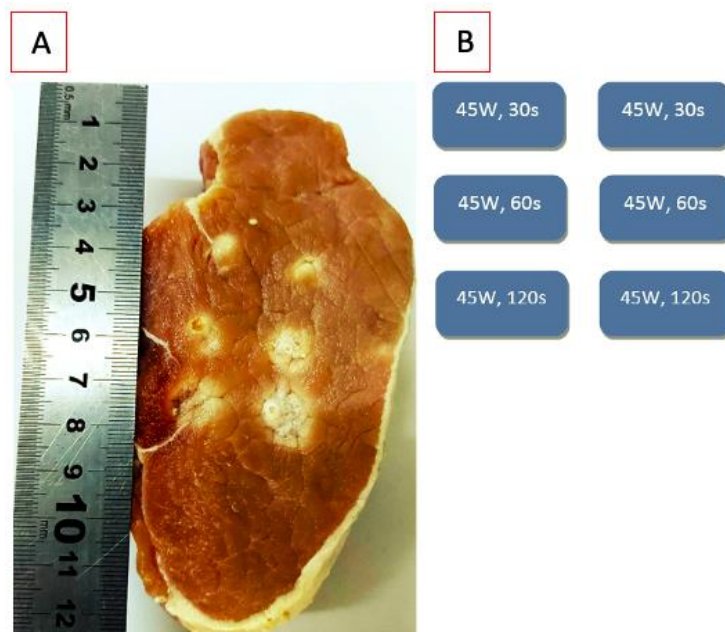


Figure 81: A) Lesions formed on the interface of the excised tissue on a plane perpendicular to the beam after 3×2 grid sonications with a 10 mm step executed with a 2.75 MHz transducer ($D=50$ mm, $ROC=65$ mm) and robotic device (version 2) using acoustic power of 45 W for sonication times of 30 s, 60 s and 120 s at a focal depth of 25 mm, and B) Sonication parameters used for each sonication of the 3×2 grid.

The tissue was vertically sliced so that the length of the induced lesions could be measured, as shown in Figure 84. Six lesions were created, with the diameter and length of the 6 lesions shown in Table 24.

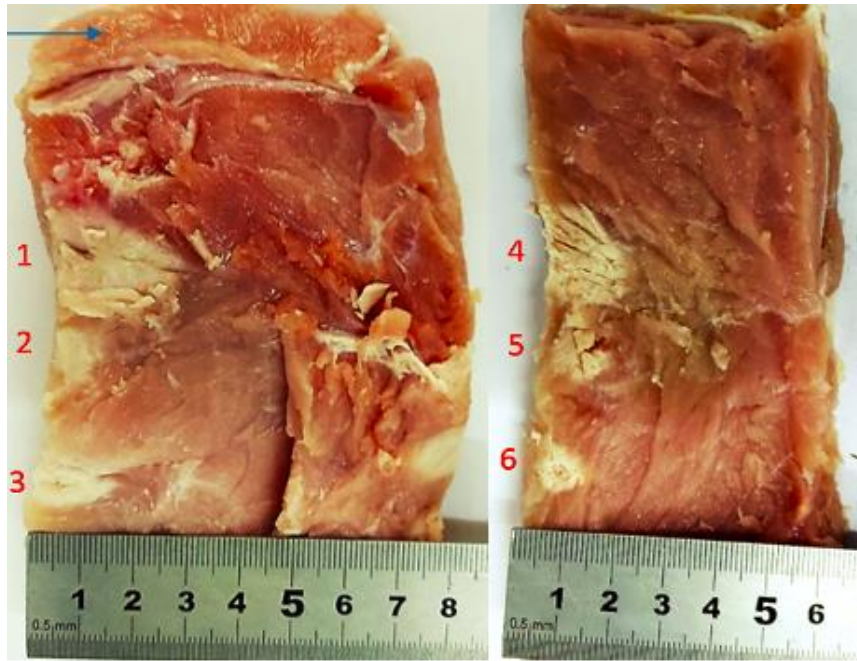


Figure 82: Lesions formed on excised tissue on a plane parallel to the beam after 3×2 grid sonications with a 10 mm step executed with a 2.75 MHz transducer ($D=50$ mm, $ROC=65$ mm) and robotic device (version 2) using acoustical power of 45 W for sonication times of 30 s, 60 s and 120 s at 25 mm focal depth. The blue arrow indicates the beam direction.

Table 24: Dimensions of lesions formed resulting exposure at acoustical power of 45 W for sonication times of 30 s, 60 s and 120 s with movement of the 2.75 MHz transducer ($D=50$ mm, $ROC=65$ mm) using the robotic device (version 2) in a 3×2 grid with a 10 mm step at 25 mm focal depth.

Lesion	Acoustical power (W)	Sonication time (s)	Energy (J)	Lesion Diameter (mm)	Lesion Length (mm)
3	45	30	1350	7	18
6				8	10
2		60	2700	10	10
5				10	13
1		120	5400	18	25
4				18	20

An acoustic power of 60 W was then applied for a sonication time of 30 s for 1×3 grid sonications with a 15 mm step. The lesions created on the sonicated surface of the tissue on a plane perpendicular to the beam are shown in Figure 85.



Figure 83: Lesions formed on the interface of the excised tissue on a plane perpendicular to the beam after 1×3 grid sonications with a 15 mm step executed with a 2.75 MHz transducer ($D=50$ mm, $ROC=65$ mm) and robotic device (version 2) using acoustic power of 60 W for a sonication time of 30 s at a focal depth of 25 mm.

The tissue was vertically sliced so that the length of the induced lesions could be measured, as shown in Figure 86. Three lesions were created, with an average diameter of 8 mm and an average length of 13 mm. The diameters and lengths of the 3 lesions are shown in Table 25.

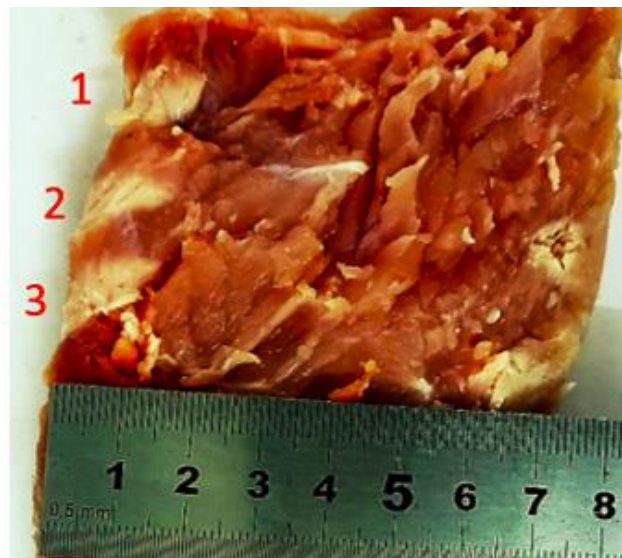


Figure 84: Lesions formed on excised tissue on a plane parallel to the beam after 1×3 grid sonications with a 15 mm step executed with a 2.75 MHz transducer ($D=50$ mm, $ROC=65$ mm) and robotic device (version 2) using acoustic power of 60 W for a sonication time of 30 s at a focal depth of 25 mm.

Table 25: Dimensions of lesions formed resulting exposure at acoustical power of 60 W for a sonication time of 30 s with movement of the 2.75 MHz transducer ($D=50$ mm, $ROC=65$ mm) using the robotic device (version 2) in a 1×3 grid with a 15 mm step at 25 mm focal depth.

Lesion	Acoustical power (W)	Sonation time (s)	Energy (J)	Lesion Diameter (mm)	Lesion Length (mm)
1	60	30	1800	8	13
2				8	13
3				8	13
Average				8	13

Formation of overlapping lesions

Overlapping lesions were formed after grid sonications with the 1.1 MHz transducer (D=60 mm, ROC=70 mm) executed with varied acoustical power and sonication time at various focal depths. Initially, the focal depth of the transducer was set at 20 mm within the tissue. An acoustical power of 81 W was used for a sonication time of 10 s with movement of the 1.1 MHz transducer (D=60 mm, ROC=70 mm) in a 5×5 grid with a 3 mm step. Figure 85A and Figure 85B show the formed overlapping lesions on planes perpendicular and parallel to the beam, respectively. The formed lesion had a width of 21.2 mm and a 21.7 mm length.

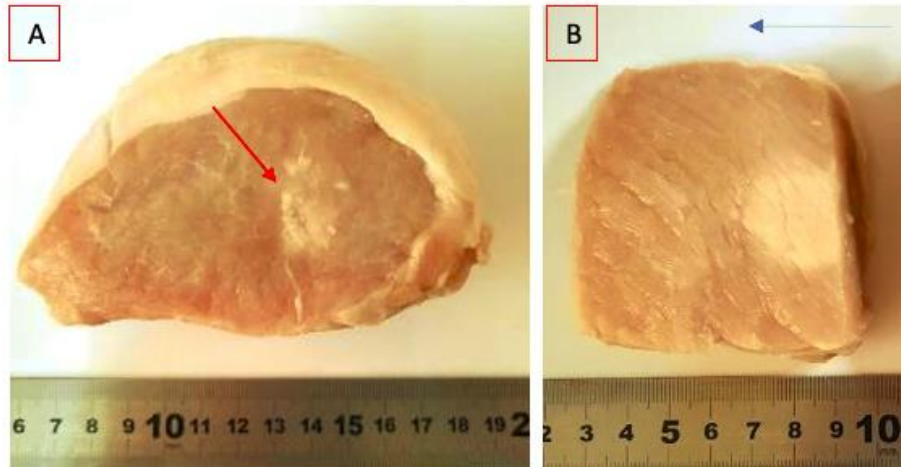


Figure 85: Overlapping lesions formed after exposure at acoustical power of 81 W for a sonication time of 10 s with movement of the 1.1 MHz transducer (D=60 mm, ROC=70 mm) using the robotic device (version 2) in a 5×5 grid with a 3 mm step at a focal depth of 20 mm. A) Lesions (red arrow) formed on tissue interface on plane perpendicular to the beam, and B) Lesions formed on plane parallel to the beam. The blue arrow indicates the beam direction.

The focal depth was changed to 30 mm within the excised tissue. An acoustical power of 81 W was used for a sonication time of 10 s for the formation of overlapping lesions in a 5×5 grid with a 3 mm step. Figure 86A shows the overlapping lesions as formed on the tissue interface on a plane perpendicular to the beam. Figure 86B shows the formed overlapping lesions in a plane parallel to the ultrasound beam. The width and length of the ablated area was 23.90 mm and 17.90 mm, respectively.

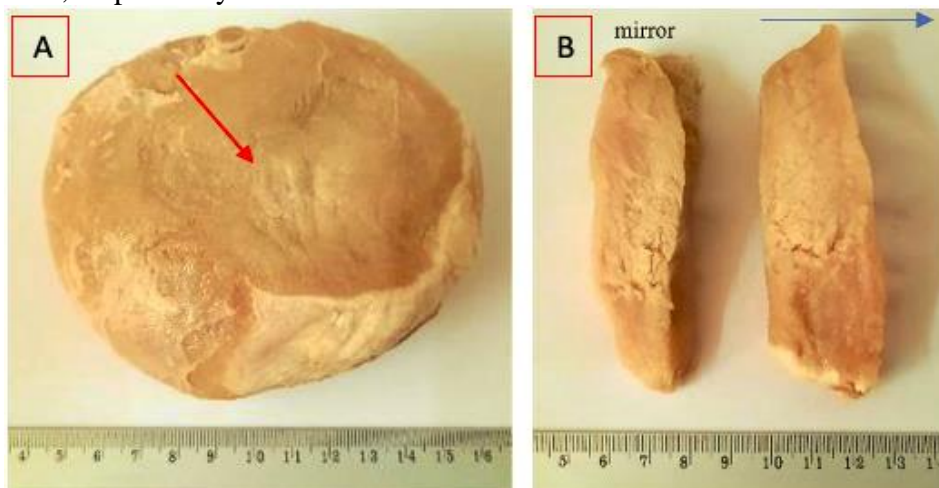


Figure 86: Overlapping lesions formed after exposure at acoustical power of 81 W for a sonication time of 10 s with movement of the 1.1 MHz transducer (D=60 mm, ROC=70 mm) using the robotic device (version 2) in a 5×5 grid with a 3 mm step at a focal depth of 30 mm. A) Lesions (red arrow) formed on tissue interface on plane perpendicular to the beam, and B) Lesions formed on plane parallel to the beam. The blue arrow indicates the beam direction.

Movement of the transducer was then performed in an 8×8 grid with a 3 mm step for the ablation of tissue at 30 mm focal depth using acoustic power of 97.5 W for a sonication time of 10 s. Figure 87A shows the overlapping lesions as formed on the interface of the tissue on a plane perpendicular to the beam. Figure 87B shows the overlapping lesions as formed in a plane parallel to the ultrasound beam. The width and length of the ablated area was 31.46 mm and 29.37 mm, respectively.

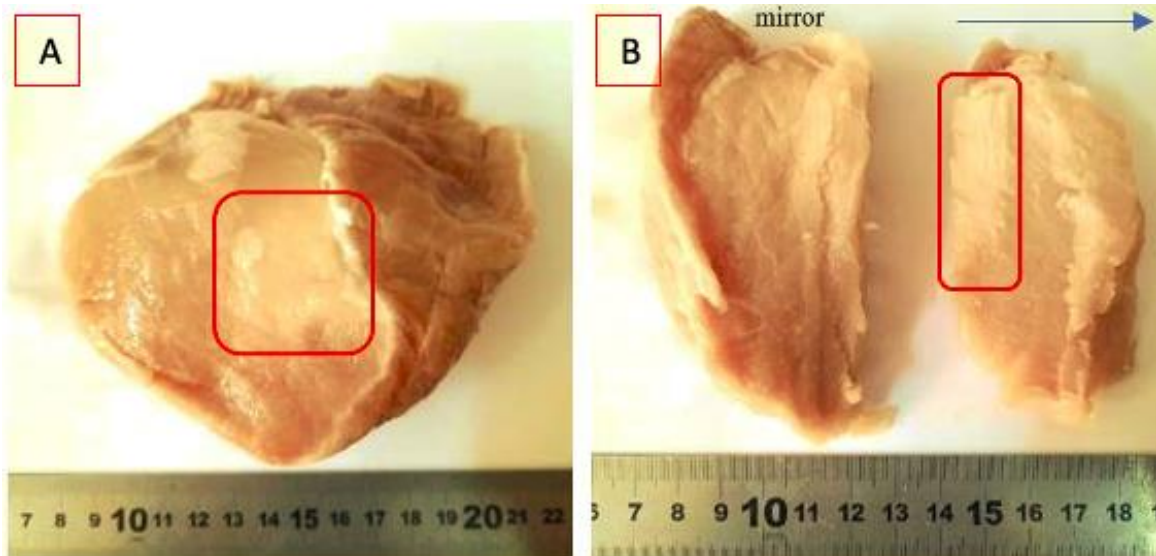


Figure 87: Overlapping lesions formed after exposure at acoustical power of 97.5 W for a sonication time of 10 s with movement of the 1.1 MHz transducer ($D=60$ mm, $ROC=70$ mm) using the robotic device (version 2) in an 8×8 grid with a 3 mm step at a focal depth of 30 mm. A) Lesions formed on plane perpendicular to the beam, and B) Lesions formed on plane parallel to the beam. The red squares indicate the ablated area and the blue arrow indicates the beam direction.

A piece of excised tissue was sonicated at acoustical power of 81 W for a sonication time of 8 s at a focal depth of 30 mm, using movement of the transducer in a 10×10 grid pattern with a 3 mm space between each step. Figure 88A shows the interface of the excised tissue after sonications. A small ablated area was observed on the interface. Figure 88B shows the overlapping lesions as formed in a plane parallel to the ultrasound beam. The width and length of the ablated area was 29.8 mm and 37.4 mm, respectively.

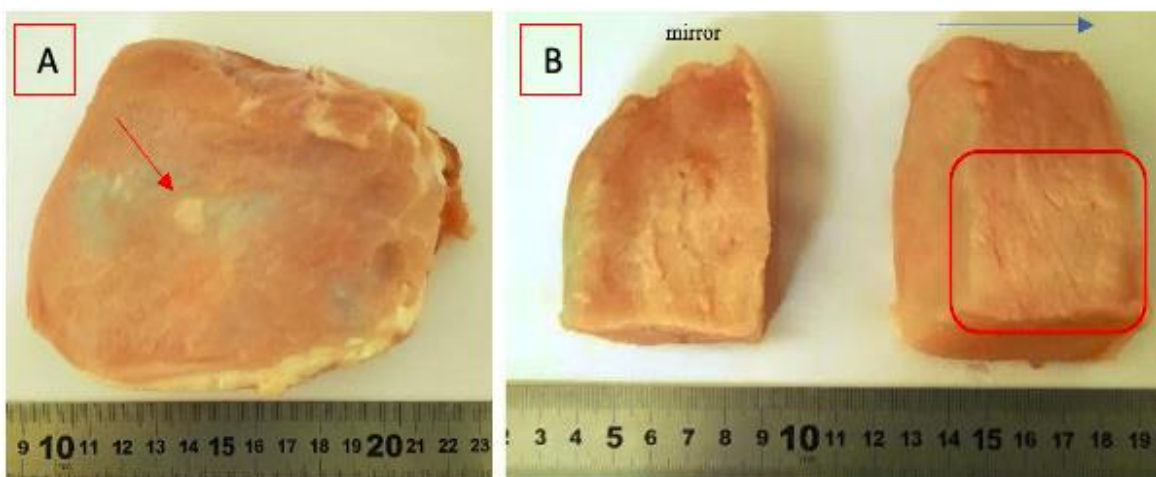


Figure 88: Overlapping lesions formed after exposure at acoustical power of 81 W for a sonication time of 8 s with movement of the 1.1 MHz transducer ($D=60$ mm, $ROC=70$ mm) using the robotic device (version 2) in a 10×10 grid with a 3 mm step at a focal depth of 30 mm. A) Lesions (red arrow) formed on plane perpendicular to the beam, and B) Lesions (red square) formed on plane parallel to the beam. The blue arrow indicates the beam direction.

An increased acoustic power of 97.5 W for a sonication time of 6 s was used for sonications at a focal depth of 30 mm using movement of the transducer in a 10×10 grid pattern with a 4 mm space between each step. Figure 89A shows the interface of the excised tissue after sonications. Some lesions were observed on the interface. Figure 89B shows the overlapping lesions as formed in a plane parallel to the ultrasound beam. The width and length of the ablated area was 38 mm and 28 mm, respectively.

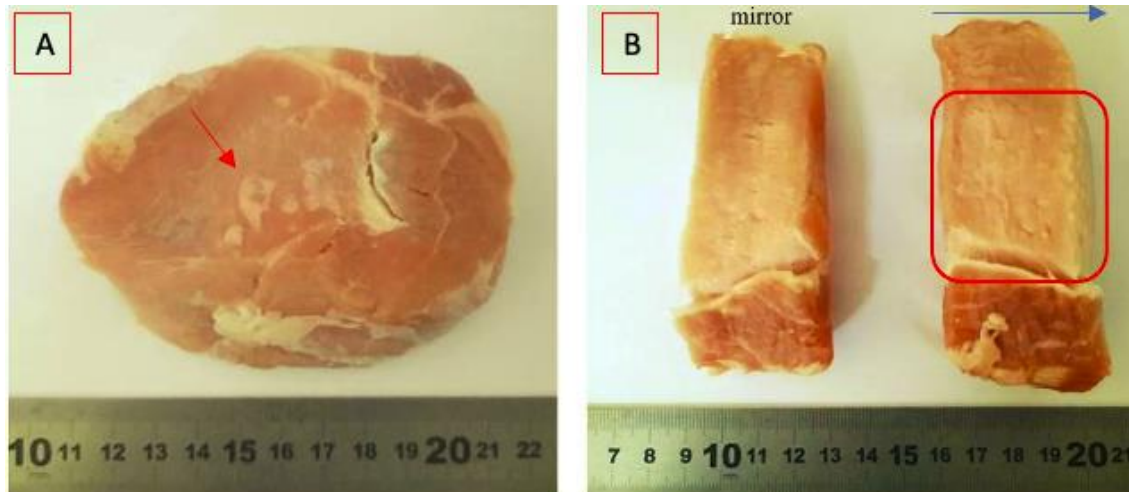


Figure 89: Overlapping lesions formed after exposure at acoustical power of 97.5 W for a sonication time of 6 s with movement of the 1.1 MHz transducer ($D=60$ mm, $ROC=70$ mm) using the robotic device (version 2) in a 10×10 grid with a 4 mm step at a focal depth of 30 mm. A) Lesions (red arrow) formed on plane perpendicular to the beam, and B) Lesions (red square) formed on plane parallel to the beam. The blue arrow indicates the beam direction.

Ablation of excised tissue using movement of the robotic device (version 3)

Formation of discrete lesions

Initially, an acoustical power of 45 W was used for a sonication time of 20 s for the formation of three discrete lesions at a focal depth of 20 mm. Figure 93 shows the lesions formed after sonications on a plane perpendicular to the beam. Only one superficial lesion with no significant length was formed on the tissue. Two out of the three sonications did not create any lesions, probably due to the air bubbles existing in the tissue.



Figure 90: The interface of the excised tissue showing only one lesion (red arrow) formed on a plane perpendicular to the beam after sonications at 3 locations with the 2.75 MHz transducer ($D=50$ mm, $ROC=65$ mm) and robotic device (version 3) using acoustic power of 45 W for a sonication time of 20 s at a focal depth of 20 mm.

The focal depth was increased to 30 mm and four sonications were performed on the tissue using an acoustic power of 45 W for a sonication time of 20 s. Two sonications were consecutively performed at a single location on the tissue, while two sonications were performed at different locations on the tissue for the creation of three discrete lesions. After exposure, the tissue was sliced at 10 mm and the dimensions of the three lesions were measured. Figure 94 shows the three lesions formed on a plane perpendicular to the beam, while Figure 95, Figure 96 and Figure 97 shows the lesions formed on a plane parallel to the beam. Table 26 lists the individual dimensions of the formed lesions.

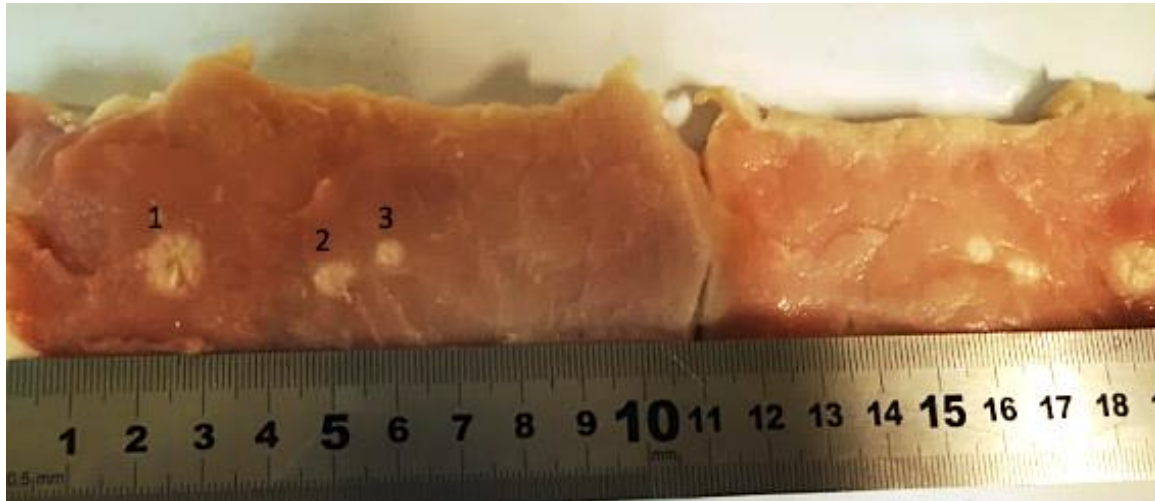


Figure 91: Lesions (numbers) formed on excised tissue on a plane perpendicular to the beam after double (number 1) and single (numbers 2 and 3) exposures at acoustical power of 45 W for a sonication time of 20 s with the 2.75 MHz transducer ($D=50$ mm, $ROC=65$ mm) and robotic device (version 3) at a 30 mm focal depth. Slice of the tissue at 10 mm and its mirror (from left to right).

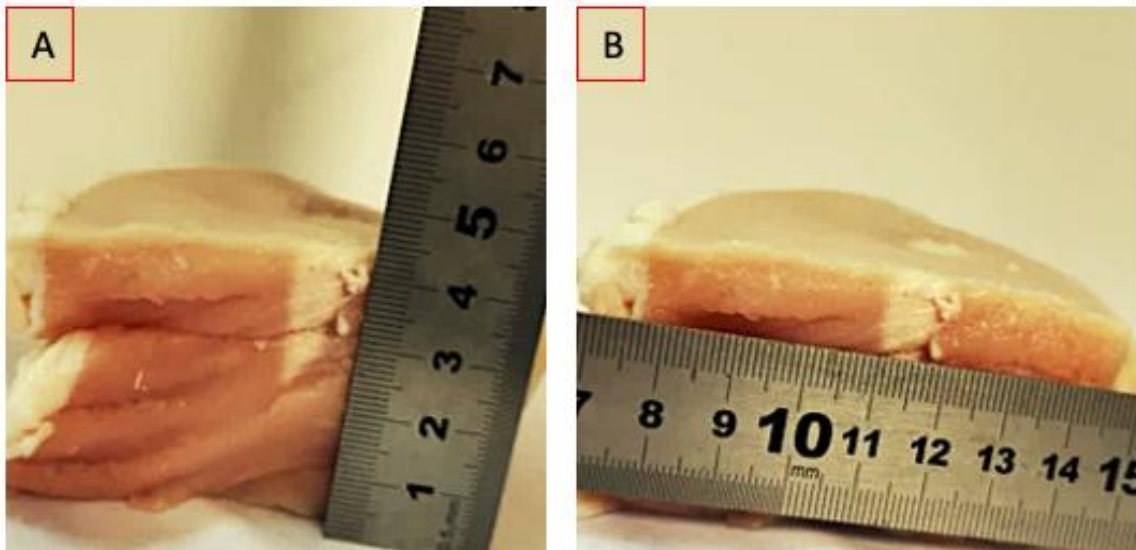


Figure 92: First lesion formed on excised tissue on a plane parallel to the beam after double exposure at acoustical power of 45 W for a sonication time of 20 s with the 2.75 MHz transducer ($D=50$ mm, $ROC=65$ mm) and robotic device (version 3) at a 30 mm focal depth. A) Measurements for length, and B) Measurements for diameter.

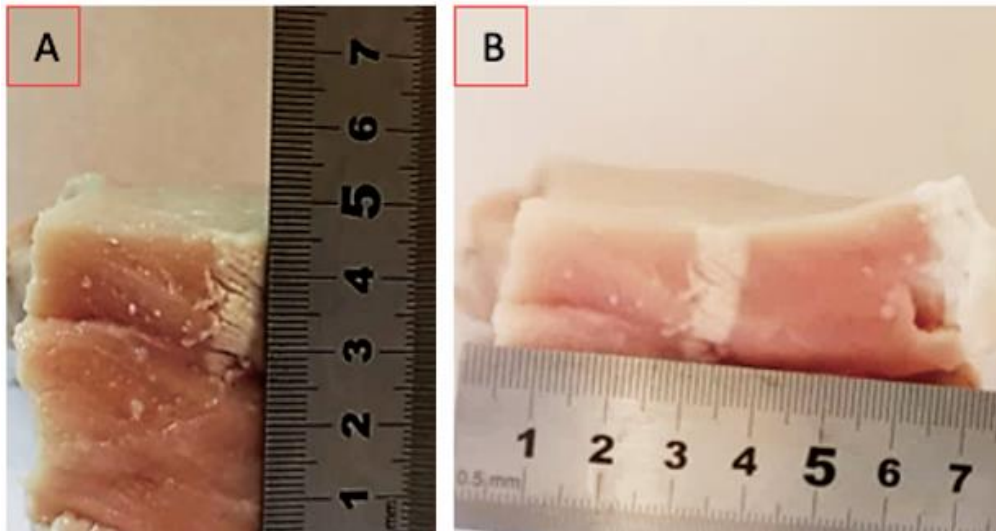


Figure 93: Second lesion formed on excised tissue on a plane parallel to the beam after single exposure at acoustical power of 45 W for a sonication time of 20 s with the 2.75 MHz transducer ($D=50$ mm, $ROC=65$ mm) and robotic device (version 3) at a 30 mm focal depth. A) Measurements for length, and B) Measurements for diameter.

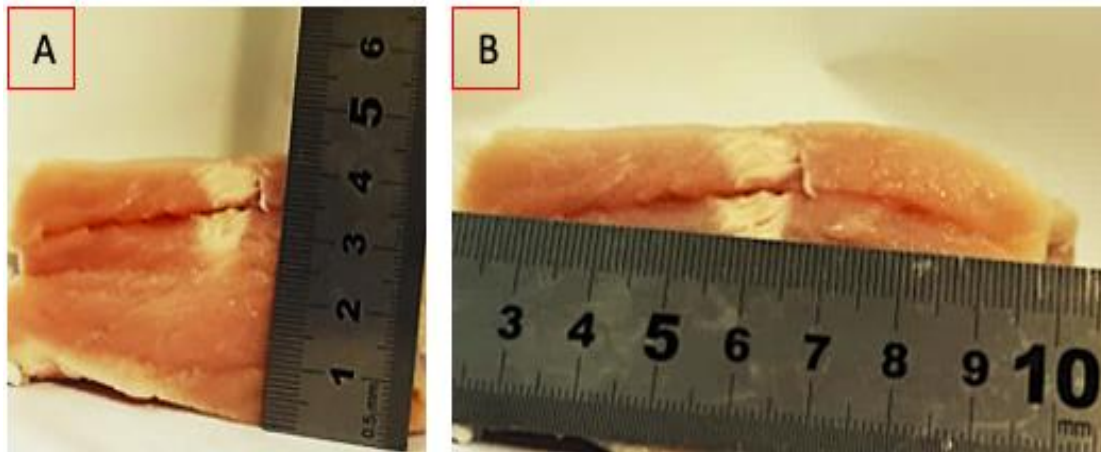


Figure 94: Third lesion formed on excised tissue on a plane parallel to the beam after single exposure at acoustical power of 45 W for a sonication time of 20 s with the 2.75 MHz transducer ($D=50$ mm, $ROC=65$ mm) and robotic device (version 3) at a 30 mm focal depth. A) Measurements for length, and B) Measurements for diameter.

Table 26: Dimensions of three lesions formed on excised tissue after four sonications executed at acoustical power of 45 W for a sonication time of 20 s with the 2.75 MHz transducer ($D=50$ mm, $ROC=65$ mm) and robotic device (version 3) at 30 mm focal depth.

Sonication	Lesion	Acoustical power (W)	Sonication time (s)	Energy (J)	Lesion Diameter (mm)	Lesion Length (mm)
1	1	45	20	900	11	21
2						19
3	2				8	19
4	3				7	21
Average					8.66	20.33

The acoustical power of 45 W was then used for a sonication time of 10 s to examine the formation of lesions in a 3×3 grid pattern with a 15 mm step. Sonications were executed at a focal depth of 25 mm. After exposure, the tissue was sliced at 10 mm and the dimensions of the lesions were measured. Figure 98 shows the lesions formed on a plane perpendicular to the beam after the horizontal tissue dissection.

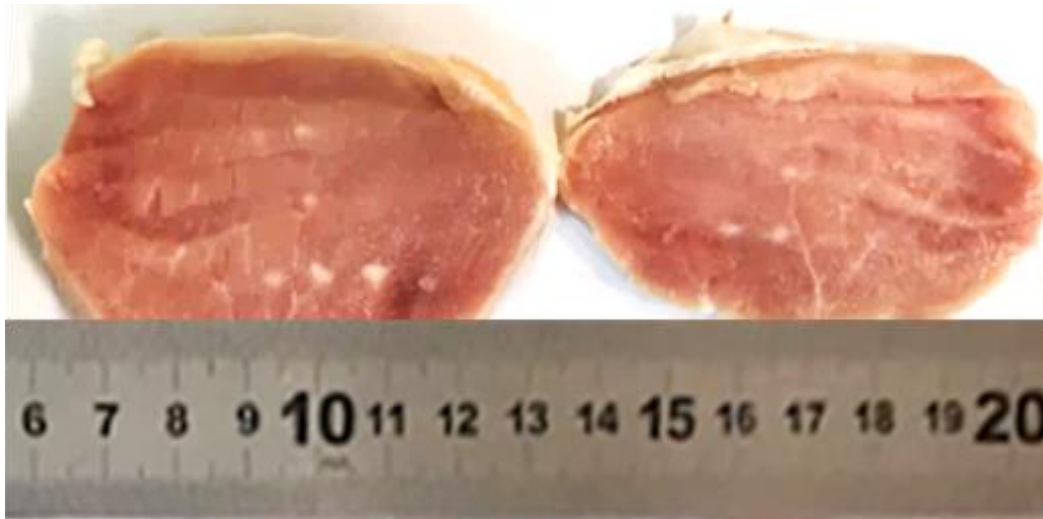


Figure 95: Lesions formed on excised tissue on a plane perpendicular to the beam after exposure at acoustical power of 45 W for a sonication time of 10 s with movement of the 2.75 MHz transducer ($D=50$ mm, $ROC=65$ mm) using the robotic device (version 3) in a 3×3 grid with a 15 mm step at a focal depth of 25 mm. Slice of the tissue at 10 mm and its mirror (from left to right).

The tissue was vertically sliced so that the length of the induced lesions could be measured. Figure 99 shows the 9 lesions formed on the excised tissue on a plane parallel to the beam. Table 27 lists the individual dimensions of the 9 lesions formed with an average diameter of 2.44 mm and an average length of 22.22 mm.

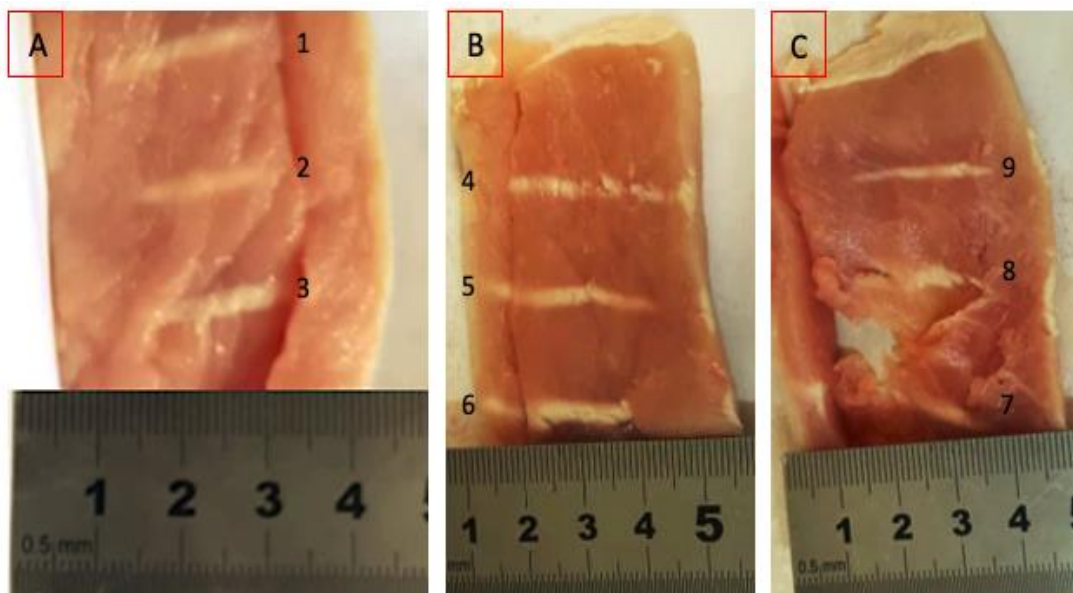


Figure 96: Lesions formed on excised tissue on a plane parallel to the beam after exposure at acoustical power of 45 W for a sonication time of 10 s with movement of the 2.75 MHz transducer ($D=50$ mm, $ROC=65$ mm) using the robotic device (version 3) in a 3×3 grid with a 15 mm step at a 25 mm focal depth. A) Lesions 1, 2 and 3, B) Lesions 4, 5 and 6, and C) Lesions 7, 8 and 9.

Table 27: Dimensions of lesions formed on excised tissue resulting exposure at acoustical power of 45 W for a sonication time of 10 s with movement of the 2.75 MHz transducer ($D=50$ mm, $ROC=65$ mm) using the robotic device (version 3) in a 3×3 grid with a 15 mm step at a 25 mm focal depth.

Lesion	Acoustical power (W)	Sonication time (s)	Energy (J)	Lesion Diameter (mm)	Lesion Length (mm)
1	45	10	450	2	18
2				2	15
3				3	18
4				2	25
5				2	28
6				3	26
7				3	28
8				3	19
9				2	23
Average				2.44	22.22

An acoustical power of 45 W was also used for an increased sonication time of 20 s for the formation of discrete lesions in a 3×3 grid with a 15 mm step at a 25 mm focal depth. After exposure, the tissue was sliced at 10 mm and the dimensions of the lesions were measured. Figure 100 shows the lesions formed on a plane perpendicular to the beam, while Figure 101 shows the lesions formed on a plane parallel to the beam. Table 28 lists the individual dimensions of the 9 formed lesions.



Figure 97: Lesions formed on excised tissue on a plane perpendicular to the beam after exposure at acoustical power of 45 W for a sonication time of 20 s with movement of the 2.75 MHz transducer ($D=50$ mm, $ROC=65$ mm) using the robotic device (version 3) in a 3×3 grid with a 15 mm step at a 25 mm focal depth. Slice of the tissue at 10 mm and its mirror (from left to right).

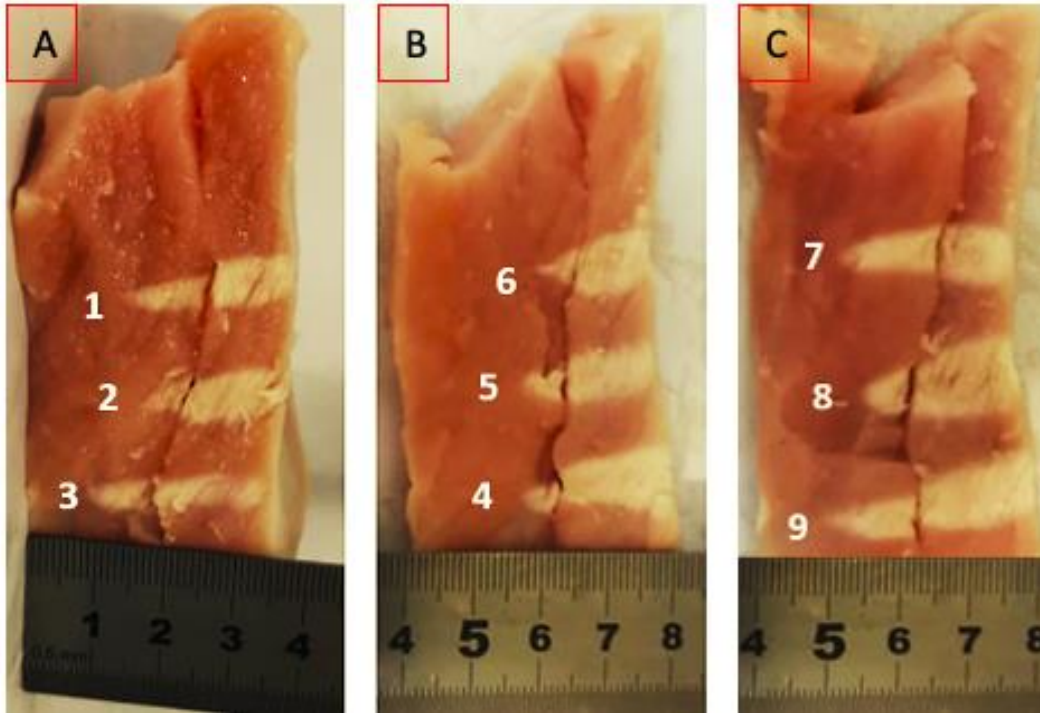


Figure 98: Lesions formed on excised tissue on a plane parallel to the beam after exposure at acoustical power of 45 W for a sonication time of 20 s with movement of the 2.75 MHz transducer ($D=50$ mm, $ROC=65$ mm) using the robotic device (version 3) in a 3×3 grid with a 15 mm step at a 25 mm focal depth. A) Lesions 1, 2 and 3, B) Lesions 4, 5 and 6, and C) Lesions 7, 8 and 9.

Table 28: Dimensions of lesions formed on excised tissue resulting exposure at acoustical power of 45 W for a sonication time of 20 s with movement of the 2.75 MHz transducer ($D=50$ mm, $ROC=65$ mm) using the robotic device (version 3) in a 3×3 grid with a 15 mm step at a 25 mm focal depth.

Lesion	Acoustical power (W)	Sonication time (s)	Energy (J)	Lesion Diameter (mm)	Lesion Length (mm)
1	45	20	900	7	25
2				8	20
3				4	25
4				8	24
5				7	23
6				9	19
7				6	19
8				10	17
9				8	20
Average				7.44	21.33

Formation of overlapping lesions

Sonications at varied acoustical power and sonication time were executed at a 25 mm focal depth for the creation of overlapping lesions using movement of the transducer in a 3×3 grid

with a 5 mm step. Initially, an acoustical power of 45 W was used for a sonication time of 10 s. After exposure, the tissue was horizontally sliced at 15 mm. Figure 102A and Figure 102B show the formed overlapping lesions in planes perpendicular and parallel to the beam, respectively. The width and length of the ablated area was 14 mm and 24 mm, respectively.



Figure 99: Overlapping lesions formed on excised tissue after exposure at acoustical power of 45 W for a sonication time of 10 s with movement of the 2.75MHz transducer ($D=50$ mm, $ROC=65$ mm) in a 3×3 grid with a 5 mm step at a 25 mm focal depth. A) Lesions formed on plane perpendicular to the beam. Slice of the tissue at 15 mm and its mirror (from left to right), and B) Lesions formed on plane parallel to the beam.

Sonifications in a 3×3 grid pattern with a 5 mm step were executed at the 25 mm focal depth using the acoustical power of 45 W for an increased sonication time of 20 s. Figure 103A shows the overlapping lesions formed in a plane perpendicular to the beam after horizontal tissue dissection at 15 mm. Figure 103B shows the overlapping lesions formed on a plane parallel to the beam. The width and length of the overlapping lesions was 21 mm and 24 mm, respectively.



Figure 100: Overlapping lesions formed on excised tissue after exposure at acoustical power of 45 W for a sonication time of 20 s with movement of the 2.75MHz transducer ($D=50$ mm, $ROC=65$ mm) using the robotic device (version 3) in a 3×3 grid with a 5 mm step a) Lesions formed on plane perpendicular to the beam. Slice of the tissue at 15 mm and its mirror (from left to right), b) Lesions formed on plane parallel to the beam.

An increased acoustical power of 60 W was used for a sonication time of 10 s for the formation of overlapping lesions in a 3×3 grid pattern with a 5 mm step at 25 mm focal depth. Figure 102A and Figure 102B show the formed overlapping lesions in planes perpendicular and parallel to the beam, respectively. The overlapping lesions were formed with an average width of 17 mm and an average length of 18 mm.

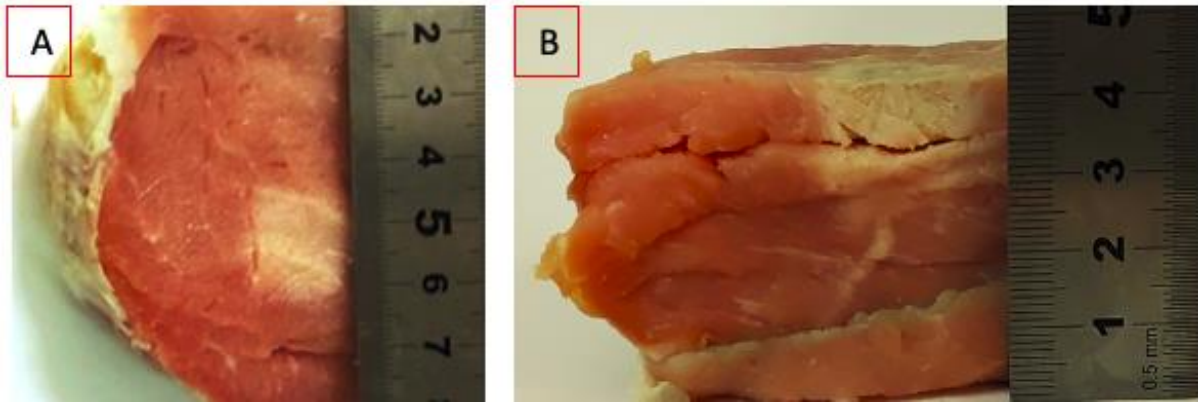


Figure 101: Overlapping lesions formed on excised tissue after exposure at acoustical power of 60 W for a sonication time of 10 s with movement of the 2.75 MHz transducer ($D=50$ mm, $ROC=65$ mm) using the robotic device (version 3) in a 3×3 grid with a 5 mm step at a 25 mm focal depth. A) Slice of the tissue at 10 mm showing lesions formed on plane perpendicular to the beam, and B) Lesions formed on plane parallel to the beam.

Ablation of excised tissue using movement of the robotic device (version 4)

Formation of discrete lesions

Sonications were performed with movement of the robotic device (version 4) for the creation of discrete lesions using varied acoustical power and sonication time at a 25 mm focal depth. Initially, an acoustic power of 45 W was used for sonication times of 10 s and 15 s. The transducer was moved manually in a 3×2 grid with a 15 mm step for the formation of 6 lesions. The first three sonications were executed with a sonication time of 10 s and the remaining three with the 15 s sonication time. Figure 105 shows the formed lesions after sonications on a plane parallel to the beam. The diameters and lengths of the 6 lesions are shown in Table 29.

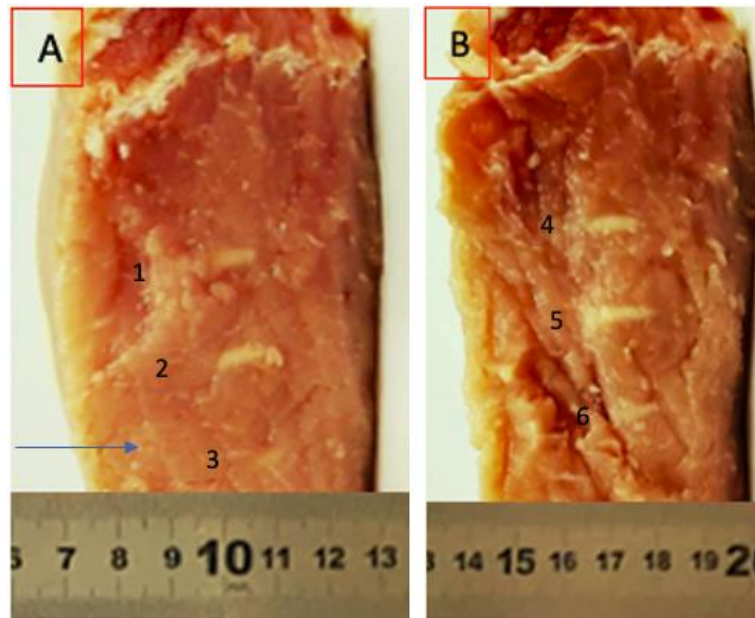


Figure 102: Lesions (black numbers) formed on excised tissue on a plane parallel to the beam after exposure at acoustical power of 45 W for sonication times of 10 s and 15 s with movement of the 2.75 MHz transducer ($D=50$ mm, $ROC=65$ mm) using the robotic device (version 4) in a 3×2 grid with a 15 mm step at a 25 mm focal depth. The blue arrow indicates the beam direction. A) Lesions 1, 2 and 3 formed with sonication time of 10 s, and B) Lesions 4, 5 and 6 formed with sonication time of 15 s.

Table 29: Dimensions of lesions formed on excised tissue resulting exposure at acoustical power of 45 W for sonication times of 10 s and 15 s with movement of the 2.75 MHz transducer ($D=50$ mm, $ROC=65$ mm) using the robotic device (version 4) in a 3×2 grid with a 15 mm step at a 25 mm focal depth.

Lesion	Acoustical power (W)	Sonication time (s)	Energy (J)	Lesion Diameter (mm)	Lesion Length (mm)
1	45	10	450	2	7
2				3	10
3				2	4
4		15	675	3	10
5				3	15
6				3	10

Sonications were performed using the same pulse durations of 10 s and 15 s for an increased acoustic power of 60 W at 25 mm focal depth. Manual movement of the transducer was performed in a 3×2 grid with a 15 mm step for the formation of 6 discrete lesions. Figure 106 shows the 6 lesions formed on a plane parallel to the ultrasonic beam. The diameters and lengths of the 6 lesions are shown in Table 30.

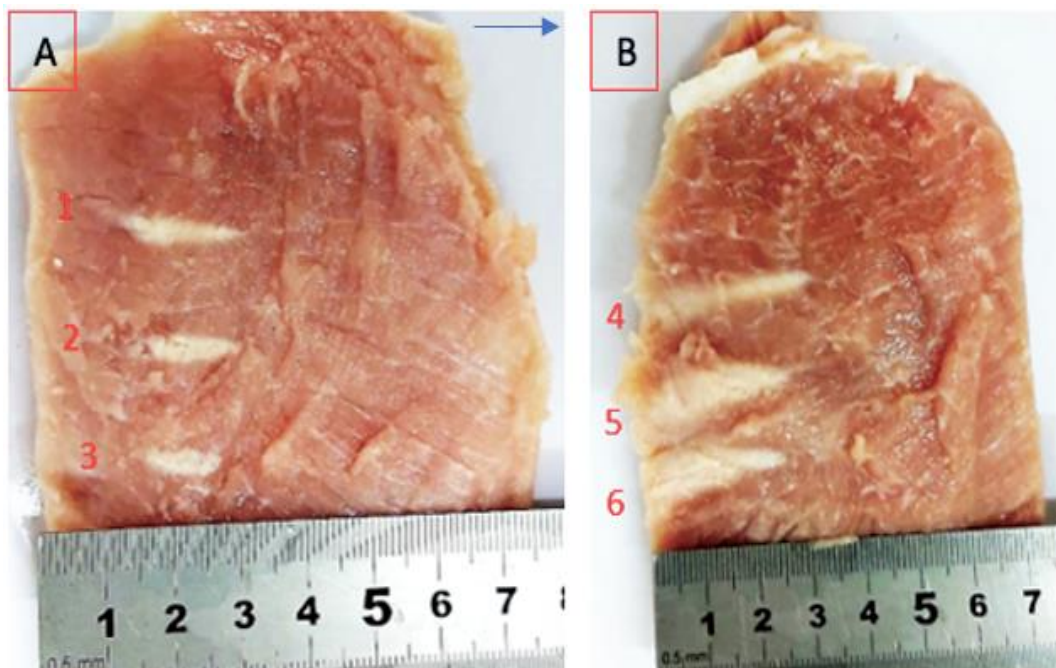


Figure 103: Lesions (red numbers) formed on excised tissue on a plane parallel to the beam after exposure at acoustic power of 60 W for sonication times of 10 s and 15 s using movement of the 2.75 MHz transducer ($D=50$ mm, $ROC=65$ mm) with the robotic device (version 4) in a 3×2 grid with a 15 mm step at a 25 mm focal depth. The blue arrow indicates the beam direction. A) Lesions 1, 2 and 3 formed with sonication time of 10 s, and B) Lesions 4, 5 and 6 formed with sonication time of 15 s.

Table 30: Dimensions of lesions formed on excised tissue resulting exposure at acoustical power of 60 W for sonication times of 10 s and 15 s with movement of the 2.75 MHz transducer ($D=50$ mm, $ROC=65$ mm) using the robotic device (version 4) in a 3×2 grid with a 15 mm step at a 25 mm focal depth.

Lesion	Acoustical power (W)	Sonication time (s)	Energy (J)	Lesion Diameter (mm)	Lesion Length (mm)
1	60	10	600	3	13
2				3	13
3				3	10
4		15	900	3	25
5				8	25
6				8	25

Sonications were executed using the acoustical power of 60 W for increased sonication times of 20 s and 30 s at 25 mm focal depth using movement of the transducer in a 3×2 grid with a 15 mm step. Figure 107 shows 6 lesions formed on the tissue after sonications on a plane parallel to the beam. The diameters and lengths of the 6 lesions is shown in Table 31.

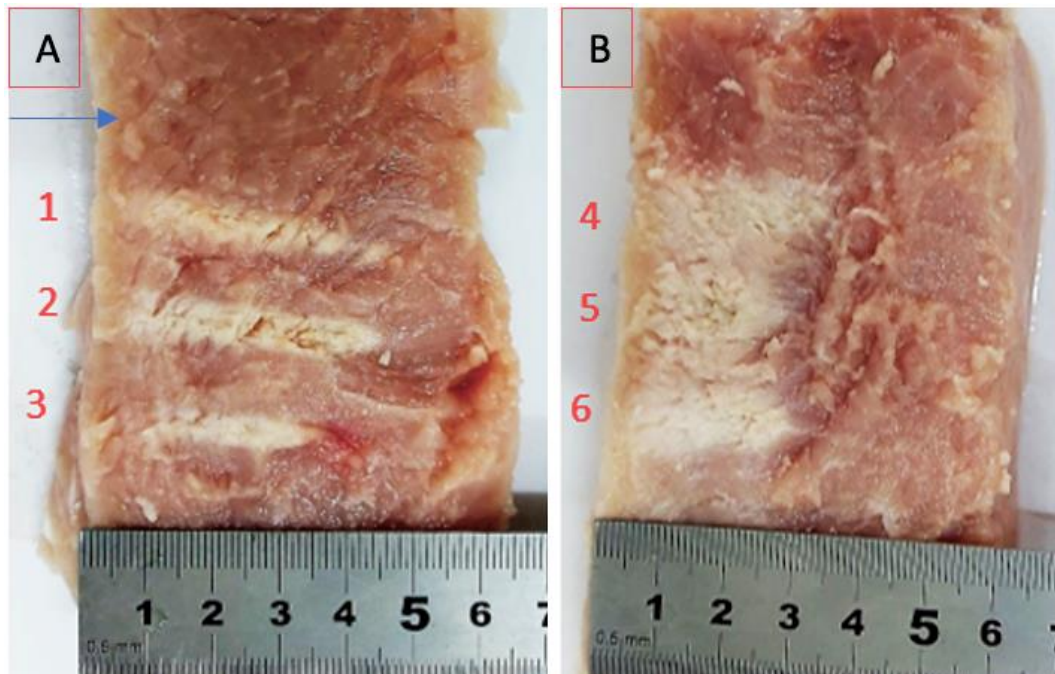


Figure 104: Lesions (red numbers) formed on excised tissue on a plane parallel to the beam after exposure at acoustic power of 60 W for sonication times of 20 s and 30 s using movement of the 2.75 MHz transducer ($D=50$ mm, $ROC=65$ mm) with the robotic device (version 4) in a 3×2 grid with a 15 mm step at a 25 mm focal depth. The blue arrow indicates the beam direction. A) Lesions 1, 2 and 3 formed with sonication time of 20 s, and B) Lesions 4, 5 and 6 formed with sonication time of 30 s.

Table 31: Dimensions of lesions formed on excised tissue resulting exposure at acoustical power of 60 W for sonication times of 20 s and 30 s using movement of the 2.75 MHz transducer ($D=50$ mm, $ROC=65$ mm) with the robotic device (version 4) in a 3×2 grid with a 15 mm step at a 25 mm focal depth.

Lesion	Acoustical power (W)	Sonication time (s)	Energy (J)	Lesion Diameter (mm)	Lesion Length (mm)
1	60	20	1200	5	45
2				5	45
3				5	25
4		30	1800	13	30
5				13	25
6				13	25

Furthermore, an acoustic power of 75 W was applied to the tissue for sonication times of 10 s, 20 s and 30 s for sonications in a 3×1 grid with a 10 mm step at 25 mm focal depth. The lesions created on the surface of the tissue after sonications are shown in Figure 108.

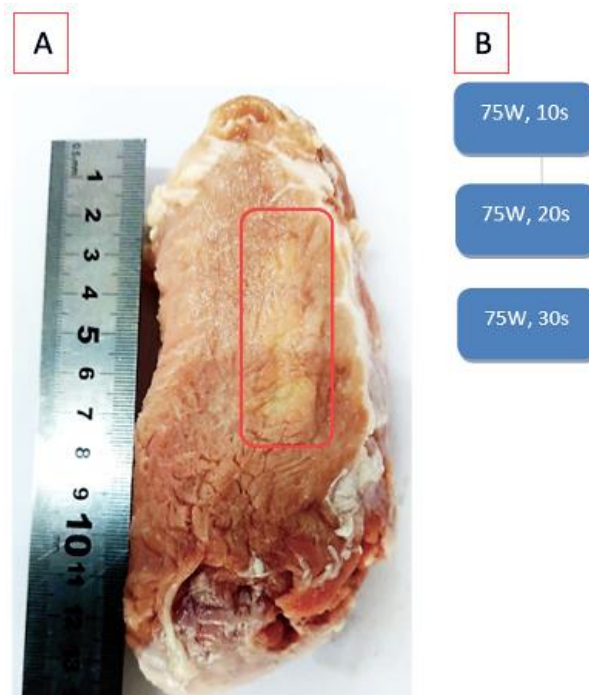


Figure 105: A) Lesions formed (red rectangle) on the interface of excised tissue on a plane perpendicular to the beam after 3×1 grid sonications with a 10 mm step executed with a 2.75 MHz transducer ($D=50$ mm, $ROC=65$ mm) and robotic device (version 4) at acoustic power of 75 W for sonication times of 10 s, 20 s and 30 s at a focal depth of 25 mm, and B) Sonication parameters used for each sonication of the 3×1 grid.

The tissue was vertically sliced so that the length of the induced lesions could be measured, as shown in Figure 109. Three lesions were created, with the diameters and lengths of the 3 lesions shown in Table 32.

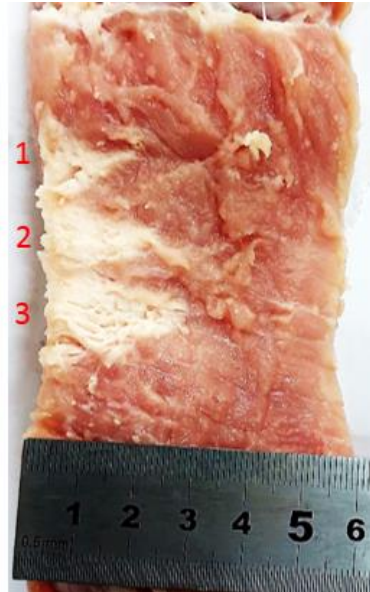


Figure 106: Lesions formed (red numbers) on excised tissue on a plane parallel to the beam after 3×1 grid sonications with a 10 mm step executed with a 2.75 MHz transducer ($D=50$ mm, $ROC=65$ mm) and robotic device (version 4) at acoustical power of 75 W for sonication times of 10 s (lesion 1), 20 s (lesion 2) and 30 s (lesion 3) at a focal depth of 25 mm.

Table 32: Dimensions of lesions formed on excised tissue resulting exposure at acoustical power of 75 W for sonication times of 10 s, 20 s and 30 s using movement of the 2.75 MHz transducer ($D=50$ mm, $ROC=65$ mm) with the robotic device (version 4) in a 3×1 grid with a 10 mm step at a 25 mm focal depth.

Lesion	Acoustical power (W)	Sonication time (s)	Energy (J)	Lesion Diameter (mm)	Lesion Length (mm)
1	75	10	750	10	20
2		20	1500	14	25
3		30	2250	16	30

Formation of overlapping lesions

Overlapping lesions were formed using movement of the transducer with the robotic device (version 4) in various grid patterns with sonications executed at varying acoustical powers and sonication times at a 25 mm focal depth. Initially, an acoustical power of 60 W was used for a sonication time of 30 s for the formation of overlapping lesions in a 4×4 grid pattern with a 4 mm step. The overlapping lesions as formed in a plane perpendicular to the ultrasound beam on the tissue interface and after horizontally slicing the tissue at 10 mm are shown in Figure 111A and Figure 111B, respectively. Figure 112 shows the formed lesions on a plane parallel to the beam. The lesions were formed with a width of 36 mm and a length of 36 mm.

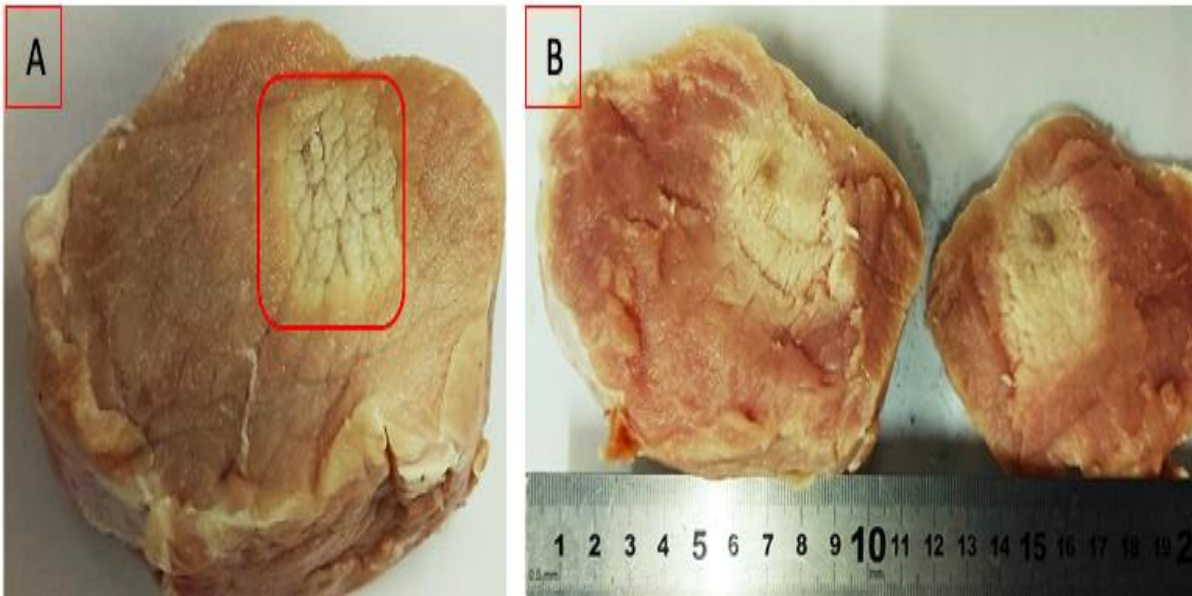


Figure 107: Overlapping lesions formed on excised tissue on plane perpendicular to the beam after exposure at acoustical power of 60 W for a sonication time of 30 s using movement of the 2.75 MHz transducer ($D=50$ mm, $ROC=65$ mm) with the robotic device (version 4) in a 4×4 grid with a 4 mm step at a 25 mm focal depth. A) Lesions (red square) formed on the surface of the tissue, and B Slice of the tissue at 10 mm and its mirror (from right to left) showing formed lesions.

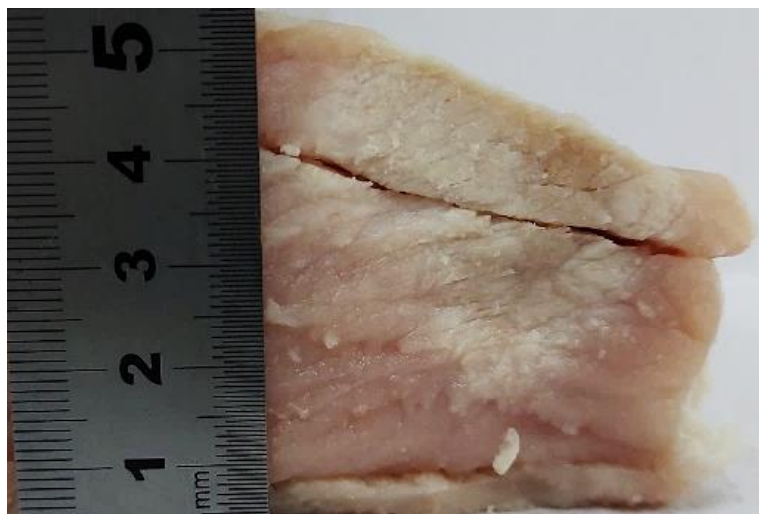


Figure 108: Overlapping lesions formed on excised tissue on plane parallel to the beam after exposure at acoustical power of 60 W for a sonication time of 30 s using movement of the 2.75 MHz transducer ($D=50$ mm, $ROC=65$ mm) with the robotic device (version 4) in a 4×4 grid with a 4 mm step at 25 mm focal depth.

Sonifications were performed using the acoustical power of 60 W for the sonication time of 30 s at the 25 mm focal depth, with the grid pattern changed to 3×3 with a 4 mm step. The overlapping lesions as formed in a plane perpendicular to the ultrasound beam on the tissue interface and after horizontally slicing the tissue at 10 mm are shown in Figure 114A and Figure 114B, respectively. Figure 115 shows the formed lesions on a plane parallel to the beam. The overlapping lesions were formed with a width of 31 mm and a 34 mm length.

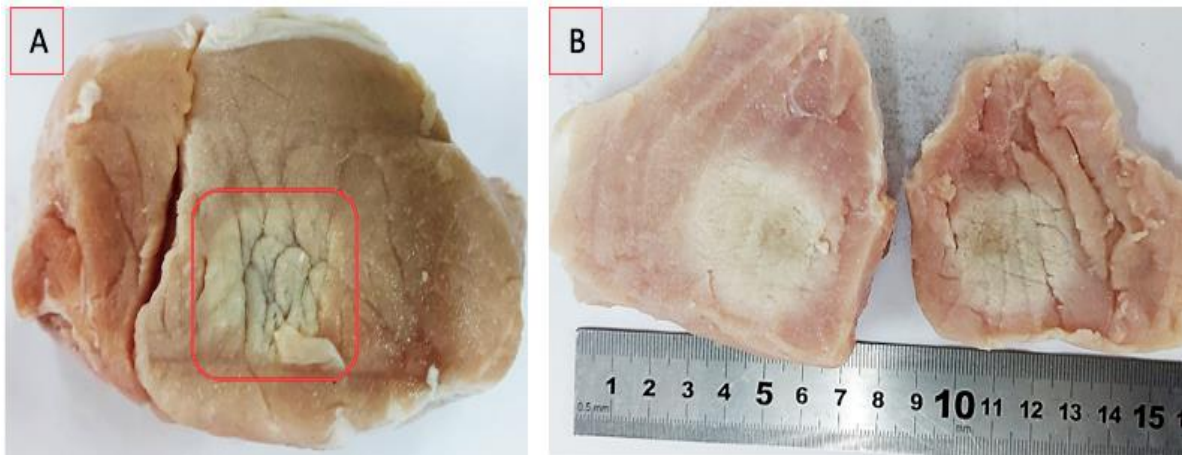


Figure 109: Overlapping lesions formed on excised tissue on plane perpendicular to the beam after exposure at acoustical power of 60 W for a sonication time of 30 s using movement of the 2.75 MHz transducer ($D=50$ mm, $ROC=65$ mm) with the robotic device (version 4) in a 3×3 grid with a 4 mm step at a 25 mm focal depth. A) Lesions (red square) formed on the surface of the tissue, and B) Slice of the tissue at 10 mm and its mirror (from right to left) showing formed lesions.

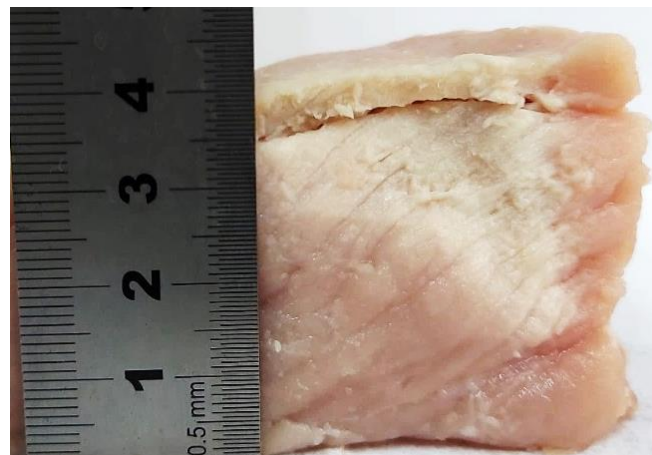


Figure 110: Overlapping lesions formed on excised tissue on plane parallel to the beam after exposure at acoustical power of 60 W for a sonication time of 30 s using movement of the 2.75 MHz transducer ($D=50$ mm, $ROC=65$ mm) with the robotic device (version 4) in a 3×3 grid with a 4 mm step at 25 mm focal depth.

SOUNDPET system evaluation using a thermal imaging camera

Temperature increase of the X-axis motor during movement of the robotic device (version 1)

Movement of the robot (version 1) was performed in a 10×10 grid with a 2 mm step to study the temperature increase of the X-axis motor (USR60-S3N, Shinsei Kogyo Corporation) during motion using the thermal camera (Fluke TiS55, Fluke Corporation). The thermal camera was set to take a photo every 3 s. Figure 116A shows the thermal image acquired before robotic movement showing the initial temperature of the motor, while Figure 116B shows the thermal image acquired at the end of the grid movement, showing the maximum temperature of the motor. Table 33 summarizes the temperatures of the X-axis motor as recorded before and after robotic motion. Robotic movement in a 10×10 grid pattern induced a temperature change of 2.10 °C.

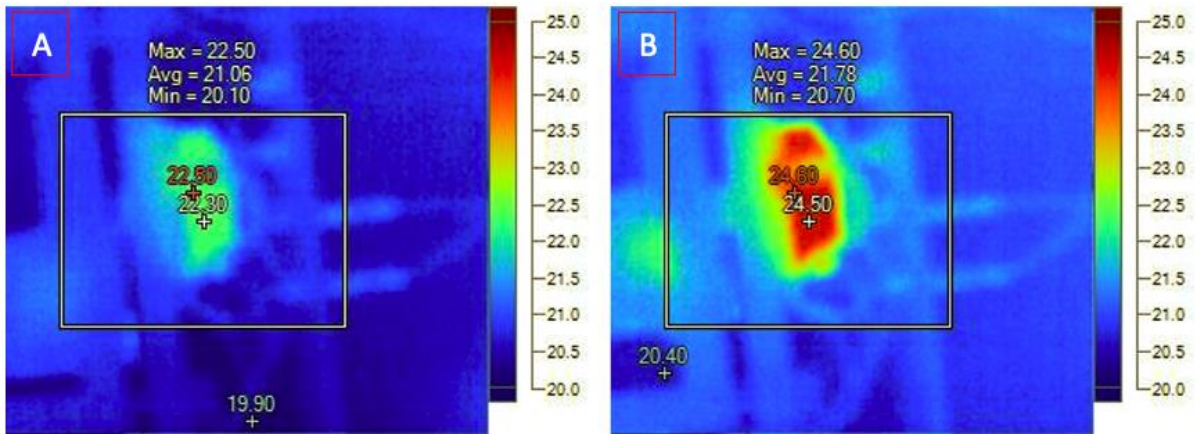


Figure 111: Thermal images acquired with the thermal camera showing the temperature of the X-axis motor of the robot (version 1). A) Image acquired before robotic motion, and B) Image acquired after robotic motion in a 10×10 grid with a 2 mm step.

Table 33: Temperatures of the X-axis motor as measured with the thermal camera before and after movement of the robot (version 1) in a 10×10 grid pattern with a 2 mm step.

X-Motor state	Temperature (°C)	Temperature change (°C)
Before robotic motion	22.50	2.1
After robotic motion	24.60	

Temperature increase of the X-axis driver during movement of the robotic device (version 1)

Movement of the robot (version 1) was performed in a 10×10 grid pattern with a 2 mm step to examine the temperature increase of the X-axis driver (D6060, Shinsei Kogyo Corporation) during motion using the thermal camera. The thermal camera was set to take a photo every 3 seconds. Figure 117A the thermal image acquired before robotic movement showing the initial temperature of the driver, while Figure 117B shows the thermal image acquired at the end of the grid movement, showing the maximum temperature obtained by the driver.

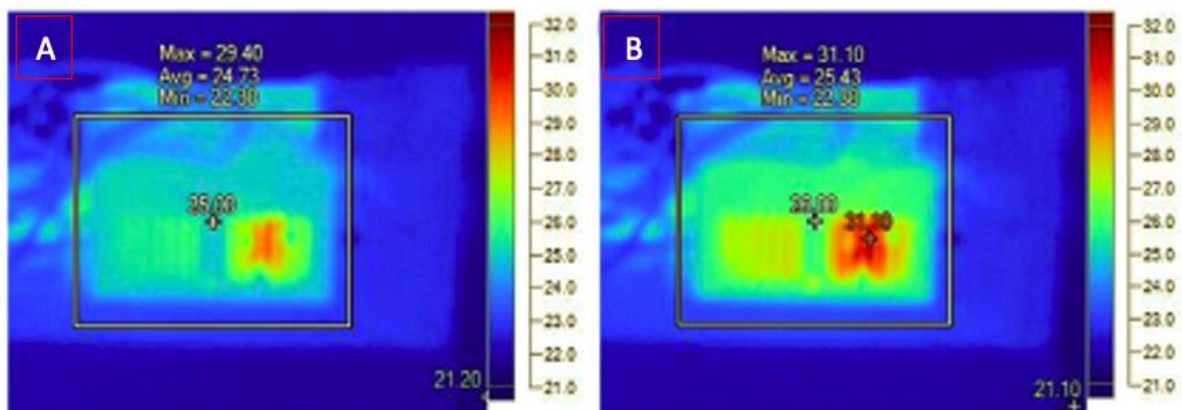


Figure 112: Thermal images acquired with the thermal camera showing the temperature of the X-axis driver. A) Image acquired before robotic motion, and B) Image acquired after robotic motion in a 10×10 grid with a 2 mm step.

Table 34 shows **Error! Reference source not found.** the temperatures of the X-axis driver as recorded before and after robotic movement in the 10×10 grid. Robotic movement in a 10×10 grid pattern induced a temperature change of 1.70 °C.

Table 34: Temperatures of the X-axis driver as measured with the thermal camera before and after movement of the robot (version 1) in a 10×10 grid pattern with 2 mm step.

X-Driver state	Temperature (°C)	Temperature change (°C)
Before robotic motion	29.40	1.7
After robotic motion	31.10	

Temperature increase in plastic films during sonications using movement of the robotic device (version 1)

Temperature increase in plastic films was assessed during grid sonications executed with the 2.75 MHz transducer (D=50 mm, ROC=65 mm) at an acoustical power of 3 W for a sonication time of 9 s. The transducer was moved using the robotic device (version 1) in a 3×3 grid with a 10 mm step. A delay of 9 s was used between sonications. The camera was set to take automatic shots every 3 s, with a total number of 60 photos. Figure 119 shows the 3×3 grid movement (sonication path) followed for sonications as planned with the software (Deliverable 5.1).

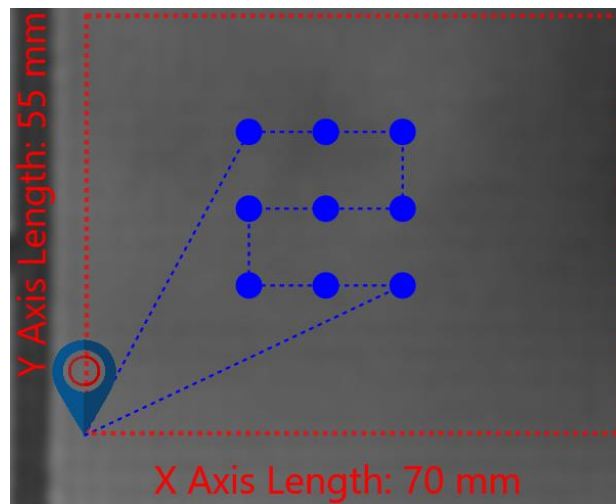


Figure 113: Screenshot of the software showing the 3×3 grid sonication path followed for sonications on plastic films.

Figure 120 shows the thermal images acquired with the thermal camera during the 3×3 grid sonications, showing the temperature recorded at each of the 9 sonication points. From the 60 images, those that show the maximum temperature for each of the 9 sonication points are presented. Table 35 shows the maximum temperature at the grid point and the reference temperature at the central point of the thermal image for the 9 sonications.

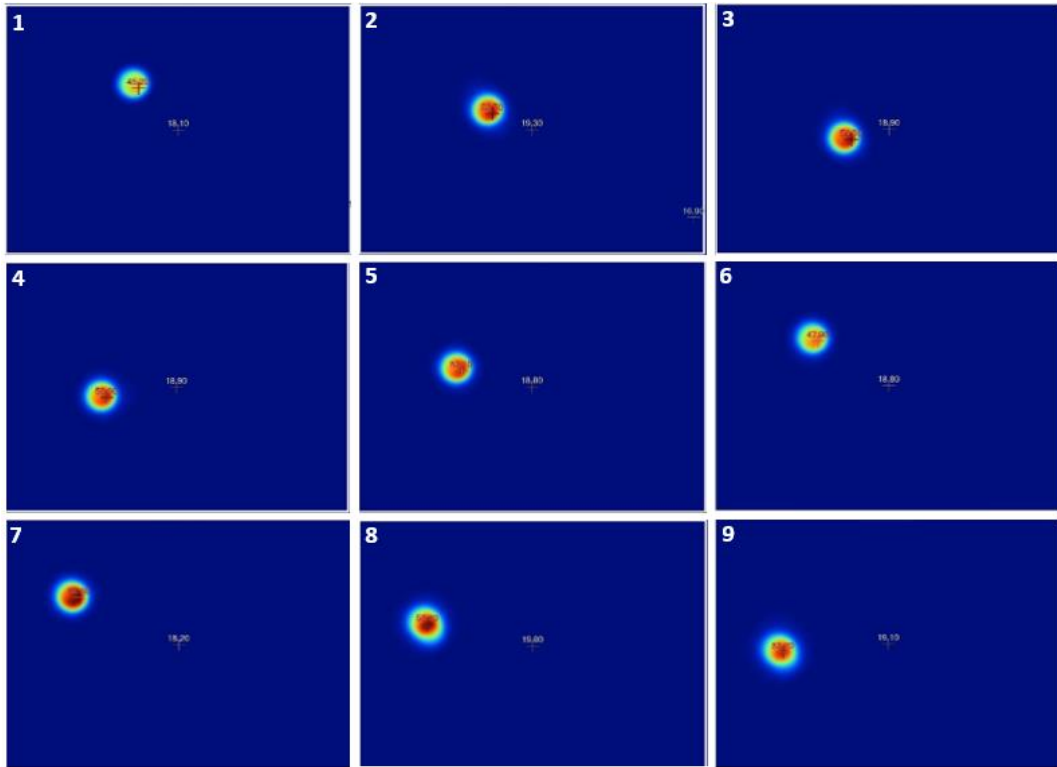


Figure 114: Thermal images acquired with the thermal camera showing the maximum temperature at 9 locations during sonications on plastic films at acoustic power of 10 W for a sonication time of 9 s with movement of the 2.75 MHz transducer ($D=50$ mm, $ROC=65$ mm) using the robotic device (version 1) in a 3×3 grid pattern with a 10 mm step.

Table 35: Temperatures as recorded at 9 locations with the thermal camera during sonications on plastic films at acoustic power of 3 W for a sonication time of 9 s, with movement of the 2.75 MHz transducer ($D=50$ mm, $ROC=65$ mm) using the robotic device (version 1) in a 3×3 grid with a 10 mm step.

Sonication point	Maximum Sonication Point Temperature ($^{\circ}\text{C}$)	Centerpoint Temperature ($^{\circ}\text{C}$)
1	45.20	18.10
2	53.70	19.30
3	54.30	18.90
4	53.00	18.90
5	53.10	18.80
6	47.90	18.80
7	58.30	18.20
8	56.60	19.00
9	53.20	19.10

Temperature increase in excised tissue during sonications using movement of the robotic device (version 2)

The thermal camera was used to evaluate the robotic device (version 2) during sonications executed on excised pork tissue. The 2.75 MHz transducer ($D=50$ mm, $ROC=65$ mm) was

moved in a 3×3 grid with a 10 mm step with sonications executed using an acoustic power of 45 W for a sonication time of 90 s at a 20 mm focal depth. The gradual temperature increase of pork tissue during the sonications was recorded with the thermal camera set to take a photo every 10 s. Figure 115A shows the thermal image acquired after the first sonication, Figure 115B shows the thermal image acquired after the fifth sonication, while Figure 115C shows the thermal image acquired after the last sonication.

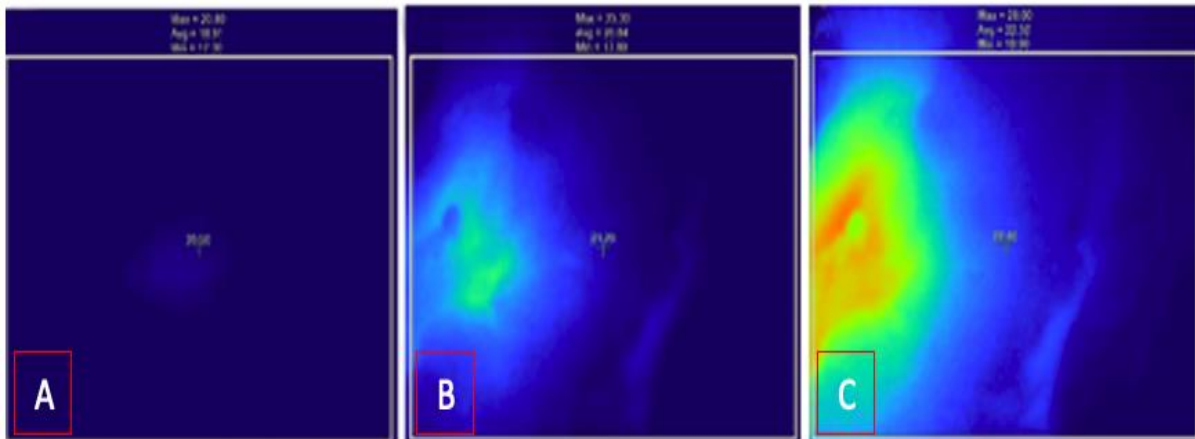


Figure 115: Thermal images acquired with the thermal camera showing the maximum temperature increase within excised pork tissue during sonications at acoustical power of 45 W for a sonication time of 90 s with movement of the 2.75 MHz transducer ($D=50$ mm, $ROC=65$ mm) using the robotic device (version 2) in a 3×3 grid with a 10 mm step at a 20 mm focal depth. Images acquired after A) the first sonication, B) the fifth sonication, and C) the last sonication.

Table 36 summarizes the temperatures recorded in the excised pork tissue for the three different sonications of the 3×3 grid pattern (first, fifth and last sonication). A temperature change of 8.10 °C was recorded between sonications executed at the first and last sonication points of the 3×3 grid. The tissue was sliced to examine whether lesions were formed in the tissue. Figure 127A and Figure 127B show the formed overlapping lesions in planes perpendicular and parallel to the beam, respectively.

Table 36: Temperatures as recorded at 3 locations with the thermal camera during sonications on excised pork tissue at acoustic power of 45 W for a sonication time of 90 s, with movement of the 2.75 MHz transducer ($D=50$ mm, $ROC=65$ mm) using the robotic device (version 2) in a 3×3 grid with a 10 mm step at a 20 mm focal depth.

Sonication point	Temperature (°C)	Temperature change (°C)
1	20.80	-
5	25.30	4.5
9	28.90	8.1

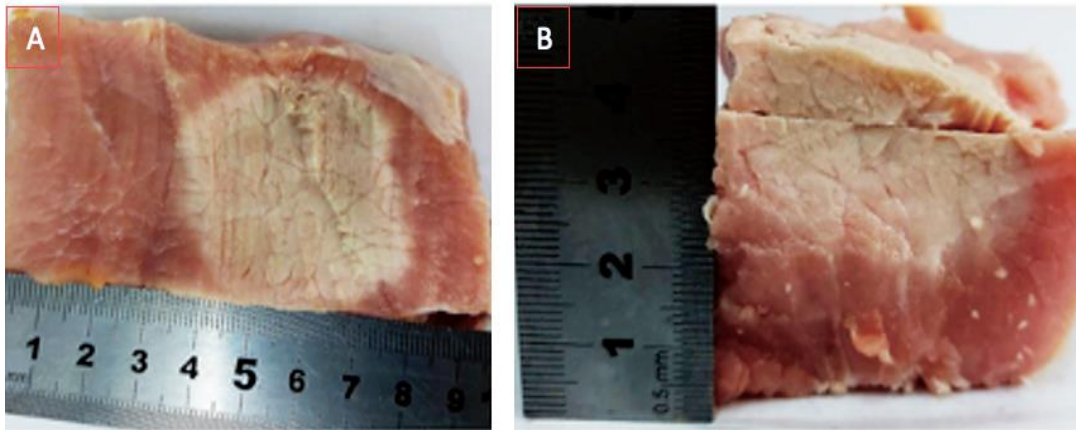


Figure 116: Overlapping lesions formed on excised tissue after exposure at acoustic power of 45 W for a sonication time of 90 s with movement of the 2.75 MHz transducer ($D=50$ mm, $ROC=65$ mm) using the robotic device (version 2) in a 3×3 grid with a 10 mm step at a 20 mm focal depth. A) Slice of the tissue at 10 mm showing lesions formed on plane perpendicular to the beam, and B) Lesions formed on plane parallel to the beam.

Discussion

In this deliverable, the evaluation of the thermal heating of the transducer used in the SOUNDPET project is presented. The transducer initially proposed, operates at 1.1 MHz, has a diameter of 60 mm and focuses beam at 70 mm. The evaluation of the 1.1 MHz transducer ($D=60$ mm, $ROC=70$ mm) was performed in an agar/wood powder-based phantom and in freshly excised porcine tissue. Nevertheless, more transducers were progressively introduced throughout the project. Specifically, another 1.1 MHz transducer ($D=50$ mm, $ROC=80$ mm), a 2.6 MHz transducer ($D=38$ mm, $ROC=61$ mm) and a 2.75 MHz transducer ($D=50$ mm, $ROC=65$ mm) were evaluated in agar-based phantoms doped with silica and in excised pork tissues. Phantoms provided the ability to imitate human tissue, thus measuring the temperature increase using different sonication parameters. Additionally, since a standard procedure is used for their development (Deliverable 4.1), phantoms provide the ability of data reproducibility. On the other hand, when excised tissue is ablated using high acoustical energies, the ability of lesion formation is provided.

Initially, an oxygen meter was used to assess the degassing process of water. An aluminum vacuum chamber was used for degasification with the oxygen content of water measured for different degassing times. Measurements were also performed for the rate of increase of oxygen levels when degassed water is exposed to atmospheric pressure after a certain degassing time. The oxygen content was first measured for degassed (for 1 hour) and non-degassed water with values of 2.74 mg/L and 8.21 mg/L found, respectively. Water was degassed for durations ranging from 0 to 120 minutes, with the oxygen content levels measured for each degassing duration. An exponential decay of the oxygen levels with the degassing duration was observed. Oxygen in water after 20, 40 and 60 minutes of degassing decreased at high rate, taking the values of 3.92 mg/L, 3.12 mg/L and 2.74 mg/L, respectively. In contrast, for degassing durations greater than 80 minutes, the oxygen content in water seems to stabilize to approximately 2.40 mg/L. Moreover, a water sample that was degassed for 1.2 hours was exposed to atmospheric pressure and the rate of oxygen increase was measured. The oxygen content of the water increased by a 3-fold after a 3-hour exposure (5.89 mg/L) compared to the initial measurement (2.09 mg/L). The data demonstrate that after a 3-hour exposure, water maintains some of its degassing properties, since the oxygen level in non-degassed water was measured at 8.21 mg/L compared to 5.89 mg/L recorded 3 hours after degassing. Additionally,

the oxygen content of water that was degassed for 40 minutes was recorded every 30 minutes of exposure to atmospheric pressure with the rate of increase of oxygen observed for a total period of 1.5 hours. The average rate of oxygen increase was 0.823 mg/L for every half hour, reaching a value of 5.84 mg/L after 1.5 hours.

An experimental set-up for measurement of temperature elevation, was designed to provide localisation of the focal point of the 1.1 MHz transducer (D=60 mm, ROC=70 mm) within the phantom and the excised tissue. The mechanical design used provided the ability of modifying the transducer-phantom/tissue distance, thus shifting the focal depth within the specimen, as well as the placement of a thermocouple at set distances of 5 mm within the phantom/tissue, for measurement of the temperature increase during low and high power sonications. The experimental set up was first used with the agar/wood powder-based phantom for localisation of the focal point of the transducer within the phantom, with the transducer-phantom distance set at 50 mm (i.e. expected focal point at 20 mm). The focal point was estimated with insertion of the thermocouple along the phantom at distances of every 5 mm. By applying an acoustical power of 11 W for a sonication time of 60 s in each 5 mm set distance, the effect of temperature change was measured. There was a high temperature increase at 20 mm (i.e. proving the focal point of the transducer). However, the highest temperature increase was recorded at 40 mm within the phantom, probably due to high reflection of the ultrasonic beam on the top surface of the phantom (the ultrasonic beam was visible on the top surface during sonications). Therefore, the transducer-phantom distance was changed to 60 mm, shifting the expected focal point of the transducer to 10 mm within the phantom. The acoustical power of 11 W was used again for measurement of the temperature change at the set distances along the phantom. Low power sonications showed high temperature increase between 10 mm and 20 mm within the phantom, resulting in a possible shift of the focal depth within that range.

Thus, two thermocouples were inserted in the phantom, one at 10 mm depth and one at 20 mm depth. Sonications at different acoustical powers were performed to measure the induced temperature increase at the different depths within the agar/wood powder-based phantom. Low and high acoustical power (18.5-66.6 W) were used for measurement of the induced temperature change. At the various low acoustical powers, higher temperatures were recorded at either depth, while at the highest acoustical power (66.6 W), higher temperatures were recorded at the 20 mm depth. A low acoustical power of 18.5 W and an energy of 555 J resulted in a higher temperature change of 11.5 °C recorded at 10 mm depth compared to a 9.6 °C temperature change recorded at 20 mm depth using the same energy. Application of an acoustical power of 29.6 W and an energy of 888 J resulted in approximately constant temperature changes recorded at the two depths. The acoustical power of 37 W resulted in a higher temperature change recorded at the 20 mm depth, while a higher temperature was recorded at the 10 mm depth using an acoustical power of 55.5 W. The acoustical power of 66.6 W and an energy of 1998 J induced a 58.6 °C temperature change at the 20 mm depth, which resulted in the formation of a lesion (in the form of gel melting) on the agar/wood powder-based phantom. The ability of the phantom in creating lesions at high acoustical powers was already confirmed in Deliverable 4.1. As seen from the experiments, the expected focal depth of the transducer was between 10 mm and 20 mm.

The experimental design with the 1.1 MHz transducer (D=60 mm, ROC=70 mm) was then used with excised porcine tissue. The transducer-tissue distance was set at 60 mm, indicating a 10 mm focal depth within the tissue. The thermocouple was inserted at the set locations of every 5 mm within the tissue for measurement of the temperature change after application of an acoustical power of 11 W for a sonication time of 60 s. The highest temperature change was recorded at 10 mm within the tissue, proving the 10 mm focal depth of the transducer. After confirmation of the focal point, the thermocouple was inserted at the 10 mm depth and

sonications were performed using different acoustical powers (18.5-74 W). Acoustical powers of 18.5 W (energy 555 J), 29.6 W (energy 888 J) and 37 W (energy 1110 J) resulted in a recorded temperature change of 5.4 °C, 16.8 °C and 23.8 °C, respectively. A high acoustical power of 74 W (energy 2220 J) resulted in a recorded temperature increase of 40.5 °C. The applied energy of 2220 J was sufficient for the formation of a lesion with a 5.94 mm diameter and 16.27 mm length.

Temperature measurements for different acoustical power were recorded in an agar-based phantom for sonications executed with the 2.6 MHz transducer (D=38 mm, ROC=61 mm) and the robotic device (version 1). The temperature change varied from 5.2 °C (11.5 W acoustical) to 25.1 °C (46 W acoustical) for a sonication time of 10 s. The temperature increase was higher for an increased sonication time of 60 s; 23.7 °C at acoustic power of 23 W and 60.2 °C at acoustic power of 46 W. The temperature was also recorded with a thermocouple in porcine excised tissue during sonications with low acoustical power (2.3-20.7 W), since there is a need to apply low power to detect the focal spot of the ultrasound beam during the initial stage of MR thermometry experiments. Thermal dose calculations performed for the low power sonications confirmed that the induced thermal dose is safe without damaging the tissue at the focus.

The robotic device (version 2) with the membrane on the acoustic window was used to evaluate the temperature increase within agar-based phantoms during sonications. Initially, temperature elevations in an agar-based phantom were measured at the focus for sonications executed with the 1.1 MHz transducer (D=50 mm, ROC=80 mm) using varied acoustical power (32.5-97.5 W) and constant sonication time (60 s). The temperature change was 3.1 °C at acoustical power of 32.5 W and dramatically increased to 47.8 °C at acoustic power of 97.5 W. Temperature elevations were also assessed during sonications executed with the 2.75 MHz transducer (D=50 mm, ROC=65 mm) at varied acoustical power (15-60 W) for a constant sonication time of 120 s at 20 mm focal depth. Temperature increase was recorded at the focal point with a thermocouple where a gradual increase in temperature was observed with increasing power. Temperature changes of 39.6°C - 78.1°C were observed for acoustic power of 15-60 W, with higher temperatures recorded at increased power.

The 2.75 MHz transducer (D=50 mm, ROC=65 mm) and the robot (version 2) were also used to measure temperature increase in excised pork tissue. Sonications were executed at the centre of the excised tissue using varied acoustical power (15-45 W) for a fixed sonication time of 60 s at 20 mm focal depth. The thermocouple was placed at a distance of 20 mm within the tissue for temperature measurements. Acoustical powers of 15 W (energy 900 J), 30 W (energy 1800 J) and 45 W (energy 2700 J) resulted in a recorded temperature change of 50.7 °C, 74.4 °C and 79.9 °C, respectively. The applied powers resulted in the formation of three lesions on the excised pork tissue.

The multiple ablations set-up was used for the formation of discrete lesions. The 1.1 MHz transducer (D=60 mm, ROC=70 mm) was manually moved in either 3×3 or 2×4 grids, depending on the shape of the excised tissue, with a 15 mm step at various focal depths. Initially, sonications were performed at a constant acoustical power of 78 W for sonication times of 10 s, 20 s, and 30 s, with the focal point of the transducer located on the tissue interface (transducer-tissue distance was 70 mm). Figure 117 shows the average lesion diameter versus sonication time, while Figure 118 shows the average lesion length versus sonication time. The average lesion diameter and length increased with increasing sonication time. Additionally, the formation of more lesions, closer to the number of intended (grid pattern), was observed at higher sonication times.

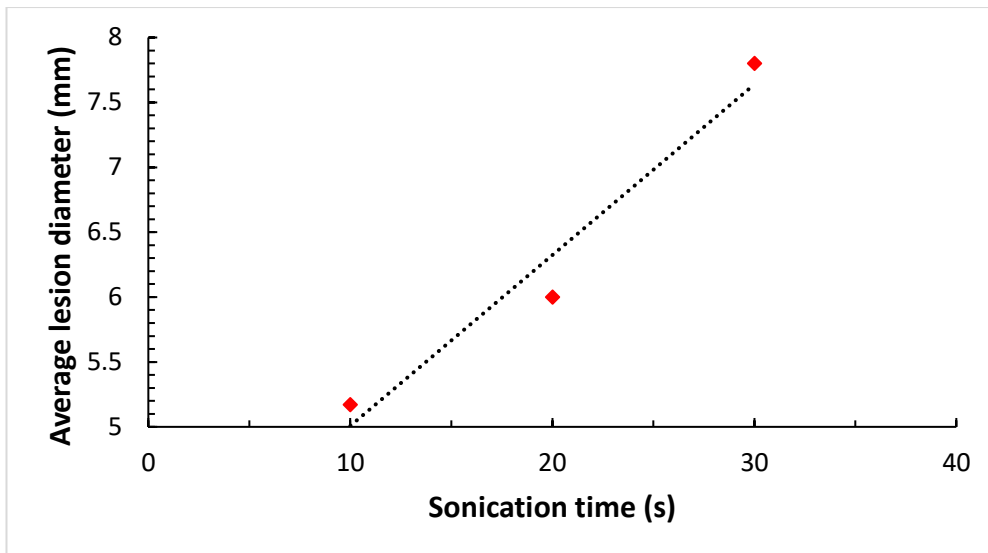


Figure 117: Average lesion diameter versus sonication time for discrete lesions formed on excised tissue after exposure at constant acoustical power of 78 W using manual movement of the 1.1 MHz transducer ($D=60$ mm, $ROC=70$ mm) in various grid patterns with a 15 mm step with the focal point located on the tissue interface.

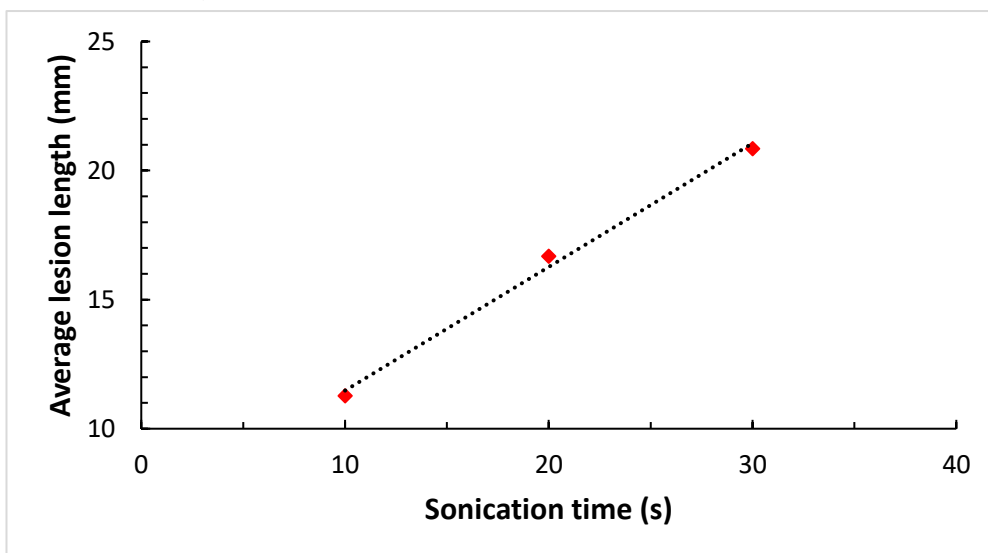


Figure 118: Average lesion length versus sonication time for discrete lesions formed on excised tissue after exposure at constant acoustical power of 78 W using manual movement of the 1.1 MHz transducer ($D=60$ mm, $ROC=70$ mm) in various grid patterns with a 15 mm step with the focal point located on the tissue interface.

The transducer-tissue distance was then changed to 60 mm, thus shifting the focal point of the transducer to 10 mm within the tissue. An acoustical power of 62 W for a sonication time of 30 s resulted in the formation of all intended lesions with an average diameter of 11.1 mm and an average length of 9.19 mm. Table 37 summarizes the dimensions of the formed lesions when the tissue was sonicated with manual movement of the transducer.

Two lesions formed using an acoustical power of 78 W for a sonication time of 10 s were analysed with a SEM to observe any morphological differences in the tissue that were related to the presence of cavitation mechanisms during lesion formation. While the lesions were formed on the same piece of tissue, one was of normal cigar shape indicating thermal formation, while the other was a tadpole shaped indicating cavitational formation. Low and

high magnification images of the surface of the lesions were taken. The SEM images of the thermal lesion showed some voids of the order of 250 μm presented within the ablated area. Additionally, it was observed that in the ablated areas the microstructure of the fibres presented in the tissue was damaged. The surface of the ablated area had sharply defined parts that were not perceptible in the non-ablated area. BSE images of both thermal and cavitation lesions were also taken providing a greater contrast between the ablated and non-ablated regions. The BSE images of the thermal lesion showed a smoother surface than the cavitation lesion. Additionally, the BSE image of the interface around the cavitation lesion boundary, indicated voids and surface defects greater than 500 μm . This could be a possible explanation in the formation of the cavitation lesion, since those defects indicate the presence of air bubbles and minimise the transmission of the ultrasonic beam.

The 1.1 MHz transducer ($D=60$ mm, $ROC=70$ mm) was then moved by the robotic device (version 1) for the formation of discrete and overlapping lesions in a grid pattern. Different acoustical power, sonication time and focal depths were used for the formation of lesions in various grid patterns and steps sizes. Discrete lesions were created using a 3×3 grid with a 10 mm or 15 mm space between each step. The transducer-tissue distance was set at 70 mm, thus resulting on location of the focal point of the transducer on the tissue interface. An acoustical power of 55 W for sonication times of 15 s and 20 s with a 10 s space between each step was used for ablation. Higher sonication time resulted in larger average lesion diameter and average lesion length. Additionally, the increased sonication time resulted in a higher number of formed lesions (8/9), while the sonication time of 10 s resulted in the formation of only 3 lesions with significant length. The focal depth was then changed to 10 mm and different ultrasonic energies were applied on the excised tissue for the formation of lesions in a 3×3 grid with a 15 mm space between each step. The application of an acoustical power of 74 W for a 10 s sonication time (740 J energy) resulted in no lesion formation. Acoustical powers of 90 W (900 J energy) and 109 W (1090 J energy) for sonication time of 10 s resulted in the formation of two lesions. The application of higher values of ultrasonic energy resulted in a greater number of formed lesions, with the application of 1830 J (94 W for 20 s) and 2180 J (109 W for 20 s) resulting in the formation of all nine intended lesions.

Table 38 shows the average dimensions of all lesions formed at different focal depths using various energies. The number of formed lesions after each sonication is also presented with the font colour indicating the formation of a good number of lesions (orange: for less than half, yellow: half, green: more than half). Generally, average lesion diameter and average lesion length increased with increasing application of energy. There were cases where among the formed lesions there was a large variation in length, probably due to presence of air bubbles or defects in the excised tissue. This can also be supported from the fact that not all lesions were formed in the grid pattern in cases where the application of energy was sufficient for the creation of lesions. However, most of the formed lesions were of normal 'cigar' shape indicating their formation only due to thermal mechanisms. When an acoustical power of 94 W was applied for sonication times of 10 s (940 J energy) and 15 s (1410 J) at the 20 mm focal depth, it resulted in no lesion formation and in the formation of a single lesion of 3.67 mm diameter but no significant length, respectively.

Overlapping lesions were then formed using movement of the 1.1 MHz transducer ($D=60$ mm, $ROC=70$ mm) with the robotic device (version 1) in a 3×3 or 4×4 grid pattern, with a 6 mm, 10 mm or 15 mm space between each step. Different acoustical power was used for tissue ablation with the focal point located on the tissue interface and at 10 mm and 20 mm deep within the tissue. Table 39 shows the dimensions of all overlapping lesions formed at different focal depths using various energies. It was observed that the use of an acoustical power of 94 W for a sonication time of 20 s (1880 J energy) at 10 mm focal depth formed an overlapping

lesion. Overlapping lesions as formed on a plane perpendicular to the beam at 10 mm focal depth using a 4×4 grid with a 6 mm space between each step were of square shape, indicating the spatial accuracy of the robotic device. Additionally, it was observed that these overlapping lesions had an increased surface area and a decreased length with increasing amount of applied energy. This can be attributed to presence of air bubbles in the tissue and non-homogeneous beam propagation due to medium differences along the transmission path. As a result, there is presence of increased cavitation effects at the interface, resulting in lesions of greater surface area and smaller length. The use of an acoustical power of 74 W for the formation of overlapping lesions in a 3×3 grid with a 10 mm space between each step for sonication times of 10 s and 20 s resulted in increased lesion length and decreased lesion surface area with increasing sonication time. This also indicates the presence of cavitation during lesion formation, limiting the formation of lesions on a plane perpendicular to the beam.

Overlapping lesions in a small tumour-like excised tissue were performed using the robotic device (version 1) and the 2.6 MHz transducer (D=38 mm, ROC=61 mm). Sonications of varying acoustic power, sonication time, and delay between the grid points were applied. A 3×3 pattern was followed with a 3 mm step. The minimum applied ultrasonic energy of 460 J was adequate to create lesions. The 3×3 grid pattern ablated a minimum tissue area of 14.6×14 mm², while the increase of ultrasonic energy increased the coagulation area. This approach to ablate a small tissue tumor-like model at early stage in a laboratory setting (without MR feedback) is helpful for future small animal preclinical experiments.

Ablations of excised tissue were performed using the robotic device (version 2) with the membrane on the acoustic window and the 1.1 MHz transducer (D=60 mm, ROC=70 mm). The main purpose of these experiments was to test whether the focused ultrasound waves are transmitted unaffected from the thin membrane. The formation of lesions as well as the minimum ultrasonic energy required for lesion formation were investigated. Sonications in 3×2 grids were performed with varying acoustic power of 32.5 W to 97.5 W for sonication times of 5 s and 10 s. The focal depth and grid step remained constant at 20 mm and 10 mm, respectively. Table 40 lists **Error! Reference source not found.** the individual dimensions of the lesions that were formed using the robotic device (version 2) and the 1.1 MHz transducer (D=60 mm, ROC=70 mm). The acoustic power of 32.5 W was not adequate to create lesions. Faint lesions were observed by applying acoustic power of 49 W. Lesions of good length to diameter ratio were induced by applying a minimum acoustic power of 65 W (650 J). Cigar-shaped lesions were produced at acoustic power of 81 W for a sonication time of 10 s. Only one lesion was induced by applying acoustic power of 97.5 W for a sonication time of 5 s. Ultrasonic energy greater than 487.5 J was required to create lesions. The observed variation of the lesion length to diameter can be attributed to tissue inhomogeneities that possibly affected the ultrasonic beam propagation. Nevertheless, it seems that the transducer can induce lesions on excised tissue even with presence of a thin membrane along the propagation of the ultrasonic beam.

Overlapping lesions on excised tissues were also formed using the robotic device (version 2) and the 1.1 MHz transducer (D=60 mm, ROC=70 mm). Multiple sonications in 5×5, 8×8 and 10×10 grids were performed using varied acoustical power, sonication time and focal depth. Table 41 lists the ultrasonic protocols of each grid pattern and the size of the ablated area. The ultrasonic energy of 486 J (81 W acoustic power for 6 s sonication) and the 3 mm step between each grid point were adequate to ablate a tissue area with a 35.45 mm width and a 30 mm length. The energy of 405 J created discrete lesions. Despite the fact that the focal depth was set at 20 mm and 30 mm within the tissue, the majority of the lesions were shifted and were formed at the interface.

Moreover, the robotic device (version 3) was used with the 2.75 MHz transducer (D=50 mm, ROC=65 mm) for the formation of discrete lesions on excised pork tissue. Tissue lesions were formed using a constant acoustical power of 45 W for sonication times of 10 s and 20 s. The focal depth was initially set at 20 mm and then at 30 mm. The ultrasonic parameters used and the dimensions of the induced lesions are shown in Table 42. At a focal depth of 20 mm, no lesions of significant length were formed for a sonication time of 20 s. Lesions appeared by increasing the focal depth to 30 mm. For sonications executed in a 3×3 grid at a focal depth of 25 mm and a sonication time of 10 s, all lesions were successfully formed with a cigar shape. Similarly, for the same 3×3 grid sonications executed with an increased sonication time of 20 s, all lesions were successfully formed but with a cavitation shape.

Overlapping lesions were then formed using the 2.75 MHz transducer (D=50 mm, ROC=65 mm) and the robotic device (version 3). Sonications were executed in a 3×3 grid pattern with a 5 mm step at a focal depth of 25 mm using acoustic powers of 45 W and 60 W for sonication times of 10 s and 20 s. The ultrasonic parameters and the dimensions of the formed lesions are shown in Table 43. The acoustic power of 45 W successfully formed overlapping lesions with dimensions of 14 mm×24 mm and 21 mm×24 mm for sonication times of 10 s and 20 s, respectively. Despite a focal depth of 25 mm within the tissue used, the lesions were formed at the tissue interface.

Concluding, the robotic device (version 4) was used to perform ablation on excised tissue, with the focused transducer operating at 2.75 MHz (D=50 mm, ROC=65 mm). The ability of the transducer to create multiple discrete lesions was evaluated by performing sonications at acoustic powers of 45 W to 75 W for sonication times of 10 s, 15 s, 20 s and 30 s at a focal depth of 25 mm. Table 44 lists the individual dimensions of the discrete lesions formed using the robotic device version 4. The acoustic powers of 45 W and 60 W for sonication times of 10 s and 15 s successfully created 6 lesions, respectively. The acoustic power of 60 W was also used with increased sonication times of 20 s and 30 s where it was observed that the lesions became more cavitation. The 2.75 MHz transducer (D=50 mm, ROC=65 mm) with the robotic device version 4 was also examined for overlapping lesions. In this case a constant acoustic power of 60 W for a sonication time of 30 s was used for sonications in different grid patterns. The ultrasonic parameters used and the dimensions of the lesions are shown in Table 45. Robotic motion in 3×3 and 4×4 grid patterns with a 4 mm step was successful in forming overlapping lesions.

Finally, a thermal imaging camera (Fluke TiS55, Fluke Corporation) was used to evaluate the SOUNDPET system. Initially, the thermal camera was used to evaluate the temperature increase of the driver and the motor of the X-axis of the robotic device (version 1) during robotic movement. In this regard, the camera recorded thermal images of either the X-axis driver or the X-axis motor during movement of the robotic device in a 10×10 grid with a 2 mm step. The temperature change induced by robotic motion for the driver and the motor was 1.70 °C and 2.10 °C, respectively. This indicates that the axes of the robotic system can operate during large grid movements without overheating, thereby showcasing a smooth operation during treatment.

The camera was also used to evaluate the temperature increase during sonications. Initially, thermal images were acquired during sonications on plastic films executed with the 2.75 MHz transducer (D=50 mm, ROC=65 mm) and the robotic device (version 1). Sonications were performed using an acoustic power of 10 W for a sonication time of 9 s with motion in a 3×3 grid with a 10 mm step. The temperature increase of the 9 sonications was successfully shown in thermal images, with the maximum temperature ranging between 45.20 °C to 58.30 °C. The thermal camera was also used to evaluate sonications on excised pork tissue using the robotic

device (version 2) with the membrane. Thermal images were obtained during 3×3 grid sonications with a 3 mm step at an acoustic power of 45 W for a sonication time of 90 s at a focal depth of 20 mm. Thermal images showed a temperature change of 8.10 °C induced by the grid sonications. Sonications resulted in the formation of overlapping lesions on the excised pork tissue.

Overall, the transducers progressively used for integration in the various versions of the robotic device were able of inducing high temperatures in both excised pork tissue and agar-based phantoms, as well as creating lesions in both phantoms and excised tissue. Manual and robotic movement of all transducers for the creation of discrete lesions, generally resulted in the formation of lesions with increased diameter and length with increasing sonication time. Most of the lesions were cigar shaped, formed around the focal point of the transducer, indicating formation due to pure thermal mechanisms. In cases where the lesion diameter or length decreased with increased application of ultrasonic energy, this indicated the presence of air bubbles in the excised tissue and the formation of lesions due to cavitation mechanisms. Future *in-vivo* experiments will not have this problem since no presence of air bubbles is expected during sonication. The creation of overlapping lesions of square shape proves the spatial accuracy of the movement of the robotic device. The robotic device and the transducer will be used for the ablation of rabbits for *in-vivo* evaluation of the thermal heating of the system (Deliverable 6.5) as well as performing treatment in cats and dogs with mammary tumours (Deliverable 6.6). Since these will be *in-vivo* experiments, the intensity of the transducer must be increased to account for the conduction of heat due to blood perfusion. Larger lesions and small sonication times are desirable for *in-vivo* application of FUS. Since the system has been proven able to form larger lesions at increased amounts of energy, this will allow for the use of increased acoustical powers and small sonication times for the *in-vivo* creation of thermal lesions.

Table 37: List of average diameters and lengths of discrete lesions formed on excised tissue after sonications at different acoustical powers, sonication times and focal depths using manual movement of the 1.1 MHz transducer ($D=60$ mm, $ROC=70$ mm) in various grid patterns with a 15 mm step using the multiple ablations set-up.

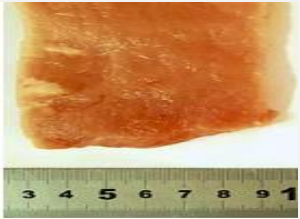
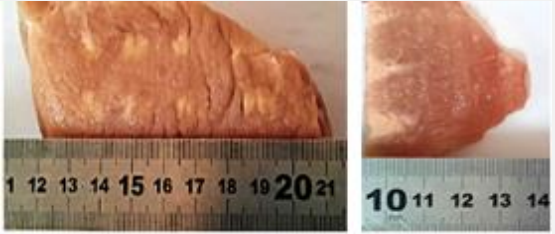
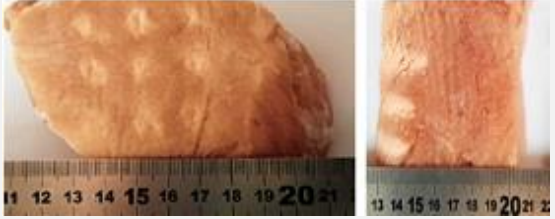
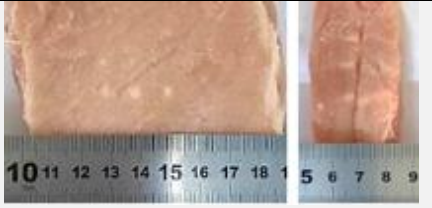
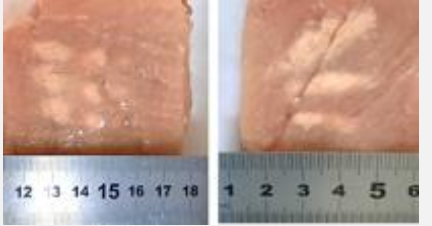
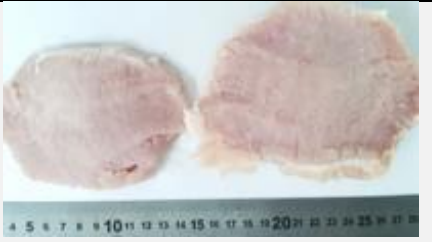
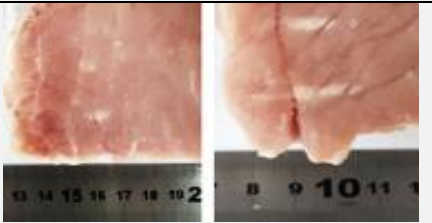
Acoustical Power (W)	Sonication Time (s)	Energy (J)	Focal Depth (mm)	Grid Pattern	Space between each step (mm)	Average Lesion Diameter (mm)	Average Lesion Length (mm)	Number of Formed Lesions	Indicative Photos of Formed Lesions
78	10	780	interface	3×3	15	5.17	11.27	5/9	
	20	1560		2×4		6	16.68	6/8	
	30	2340		3×3		7.8	20.85	9/9	
62	30	1860	10	3×3		11.1	9.19	9/9	

Table 38: List of average diameters and lengths of discrete lesions formed on excised tissue after sonications at different acoustical powers, sonication times and focal depths using movement of the 1.1 MHz transducer ($D=60$ mm, $ROC=70$ mm) with the robotic device (version 1) in various grid patterns with different steps.

Acoustical Power (W)	Sonication Time (s)	Energy (J)	Focal Depth (mm)	Grid Pattern	Space between each step (mm)	Average Lesion Diameter (mm)	Average Lesion Length (mm)	Number of Formed Lesions	Indicative Photo of Formed Lesions
55	15	825	interface	3×3	10	4.67	20.89	4/9	
	20	1100				7.94	24.65	8/9	
74	10	740	10	3×3	15	-	-	0/9	
90	10	900				7	4.3	2/9	
109	10	1090				5.21	18.9	2/9	

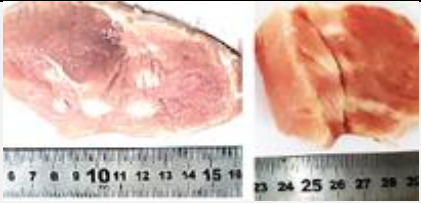
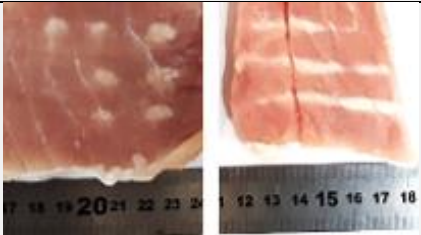
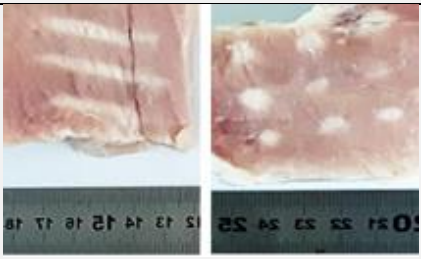
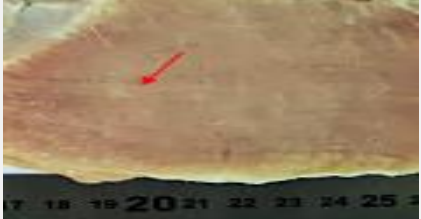
94	15	1410	10	3×3	15	8.54	21.59	7/9	
109	15	1635				7.57	41.67	7/9	
94	20	1880				6.59	30.6	9/9	
109	20	2180				8.3	32.1	9/9	
94	10	940	20	3×3	15	-	-	0/9	
94	15	1410				3.67	-	1/9	

Table 39: List of average diameters and lengths of overlapping lesions formed on excised tissue after sonications at different acoustical powers, sonication times and focal depths using movement of the 1.1 MHz transducer ($D=60$ mm, $ROC=70$ mm) with the robotic device (version 1) in various grid patterns with different steps.

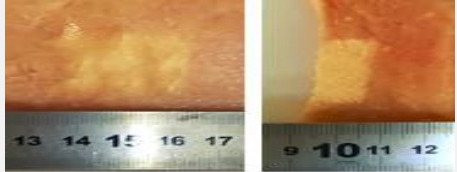
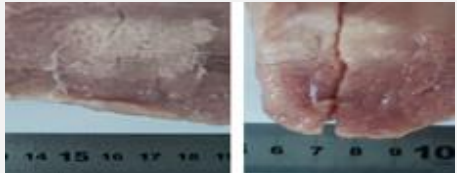
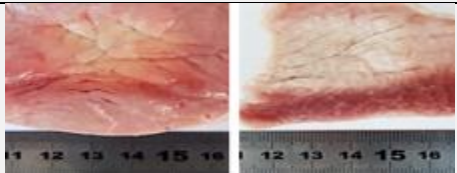
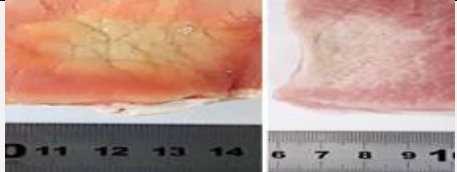
Acoustical Power (W)	Sonication Time (s)	Energy (J)	Focal Depth (mm)	Grid Pattern	Space between each step (mm)	Lesion Width (mm ²) {area}	Lesion Length (mm)	Indicative Photo of Formed Lesions
55	30	1650	interface	3×3	10	20.16×20.16{406.4}	12.68	
74	20	1480	10	3×3	10	31.06×29.23 {907.9}	29.96	
	30	2220				28.86×22.85 {659.5}	35.67	
109	15	1635		4×4	6	22.63×22.11 {500.4}	38.79	
94	20	1880				23.5×24.05 {565.2}	21.27	
94	20	1880	20	3×3	15	25.8×22.47 {579.7}	22.3	

Table 40: Dimensions of discrete lesions formed on excised tissue resulting exposure at different acoustical power for sonication times of 5 s and 10 s using movement of the 1.1 MHz transducer ($D=60$ mm, $ROC=70$ mm) with the robotic device (version 2) in a 3×2 grid pattern with a 10 mm step at 20 mm focal depth.

Acoustical power (W)	Sonication time (s)	Energy (J)	Formed lesion	Lesion Diameter (mm)	Lesion Length (mm)	Ratio length to diameter
32.5	10	325	no	-	-	-
			no	-	-	-
49		490	yes	6.87	7.34	1.07
			yes	7.42	10.21	1.38
65		650	yes	6.51	21.49	3.30
			yes	8.92	17.59	1.97
65	10	650	yes	5.01	-	-
			yes	5.11	-	-
81		810	yes	6.20	16	2.58
			yes	4.58	16.60	3.62
97.5		975	yes	5.88	21.31	3.62
			yes	7.07	23.59	3.34
65	10	650	no	-	-	-
			yes	4.58	12.82	2.79
81		810	yes	4.48	18.50	4.13
			yes	5.08	17.17	3.38
97.5		975	yes	6.29	22.18	3.53
			yes	6.68	19.81	2.97
49	10	490	yes	1.74	3.63	2.09
			no	-	-	-
			yes	3.62	8	2.21
65		650	yes	4.25	4.61	1.08
			no	-	-	-
			no	-	-	-
81	5	810	yes	3.73	18.47	4.95
			yes	2.82	18.29	6.49
			yes	3.30	22.30	6.76
			yes	3.91	10.72	2.74
			yes	4.87	13.22	2.71
			yes	3.86	22.17	5.74
97.5	5	487.5	yes	6	-	-
			yes	6	-	-
			yes	2.47	9.96	4.03
			no	-	-	-
			no	-	-	-
			no	-	-	-

Table 41: List of average diameters and lengths of overlapping lesions formed on excised tissue resulting exposure at varied acoustical powers, sonication times and focal depths using movement of the 1.1 MHz transducer ($D=60$ mm, $ROC=70$ mm) with the robotic device (version 2) in various grid patterns with different steps.

Acoustic power (W)	Sonication time (s)	Energy (J)	Grid pattern	Step (mm)	Focal depth (mm)	Ablated area - width×length (mm ²)
81	10	810	5×5	3	20	21.2 × 21.7
					30	23.9 × 17.9
14.8 × 17.9						
28 × 10						
26.13 × 18.88						
21.62 × 20.08						
31.46 × 29.37						
81	5	487.5	8×8			30
	6	585			35.45 × 30	
	8	780			29.8 × 37.4	
10	975	No lesions				
81	5	405	10×10	4	38 × 28	
	6	486			51 × 25	
	8	648				
97.5	5	487.5				
	6	585				
	8	780				

Table 42: List of average diameters and lengths of discrete lesions formed on excised tissue after sonications at acoustical power of 45 W for sonication times of 10 s and 20 s at a 25 mm focal depth using movement of the 2.75 MHz transducer ($D=50$ mm, $ROC=65$ mm) with the robotic device (version 3) in a 3×3 grid pattern with a 15 mm step.

Acoustical Power (W)	Sonication Time (s)	Energy (J)	Focal Depth (mm)	Grid Pattern	Space between each step (mm)	Average Lesion Diameter (mm)	Average Lesion Length (mm)	Number of Formed Lesions	Indicative Photo of Formed Lesions
45	10	450	25	3×3	15	2.44	22.22	9/9	
	20	900				7.44	21.33	9/9	

Table 43: List of average diameters and lengths of overlapping lesions formed on excised tissue after sonications at different acoustical powers for sonication times of 10 s and 20 s at a 25 mm focal depth using movement of the 2.75 MHz transducer ($D=50$ mm, $ROC=65$ mm) with the robotic device (version 3) in a 3×3 grid pattern with a 5 mm step.

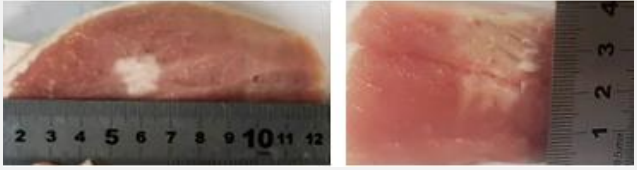
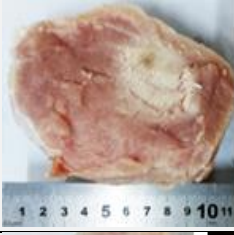
Acoustical Power (W)	Sonication Time (s)	Energy (J)	Focal Depth (mm)	Grid Pattern	Space between each step (mm)	Lesion Diameter (mm ²) {area}	Lesion Length (mm)	Indicative Photo of Formed Lesions
45	10	450	25	3×3	5	14×14 {196}	24	
45	20	900				21×19 {399}	24	
60	10	600				17×16 {272}	18	

Table 44: List of average diameters and lengths of discrete lesions formed on excised tissue after sonications at varied acoustical power and sonication times at a 25 mm focal depth using movement of the 2.75 MHz transducer ($D=50$ mm, $ROC=65$ mm) with the robotic device (version 4) in various grid patterns with different steps.

Acoustical Power (W)	Sonication Time (s)	Energy (J)	Focal Depth (mm)	Grid Pattern	Space between each step (mm)	Average Lesion Diameter (mm)	Average Lesion Length (mm)	Number of Formed Lesions	Indicative Photo of Formed Lesions
45	10	450	25	3×2	15	2.33	7	3/3	
	15	675				3	11.67	3/3	
60	10	600		3×2	15	3	12	3/3	
	15	900				6.33	25	3/3	
	20	1200				5	36.67	3/3	

	30	1800				13	26.67	3/3	
75	10	750	3x1	10	10	20	1/1		
	20	1500			14	25	1/1		
	30	2250			16	30	1/1		

Table 45: List of average diameters and lengths of overlapping lesions formed on excised tissue after sonications at acoustical power of 60 W for a sonication time of 30 s and 20 s at a 25 mm focal depth using movement of the 2.75 MHz transducer ($D=50$ mm, $ROC=65$ mm) with the robotic device (version 4) in various grid patterns with a 4 mm step.

Acoustical Power (W)	Sonication Time (s)	Energy (J)	Focal Depth (mm)	Grid Pattern	Space between each step (mm)	Lesion Diameter (mm ²) {area}	Lesion Length (mm)	Indicative Photo of Formed Lesions
60	30	1800	25	4x4	4	36x36 {1296}	33	
				3x3		34x31 {1054}	28	

MRI Experiments

Assessment of lesion detection using a 1.5 T MRI scanner

The movement of the SOUNDPET robotic device was assessed initially with 3×3 grid sonications performed inside the MRI environment. Specifically, linear motion was assessed in the X and Y axes. The SOUNDPET robot (version 1) was placed on the table of a 1.5 T MRI scanner (Signa HD16, GE Healthcare, Chicago, Illinois, USA). A piece of excised pork tissue was positioned on the acoustic window of the robotic system. On the top surface of the tissue, a general-purpose flex (GPFLEX) surface coil (Signa 1.5 T Receiver only, GE Healthcare) was positioned, with rectangular cushions placed next to the robot for supporting the coil as shown in Figure 119. The 2.6 MHz ultrasonic transducer (D=38 mm, ROC=61 mm) that was integrated in the robot (version 1) was connected to an amplifier (AG1016, T & C Power Conversion, Inc.) for powering purposes.



Figure 119: Experimental set-up inside the 1.5 T MRI scanner with the SOUNDPET robot (version 1) (i) positioned on the MRI table and a piece of excised pork tissue placed on the acoustic window of the robot. Rectangular cushions were placed next to the robot (ii) for supporting the GPFLEX surface coil (iii) that was placed on top for MR image acquisition.

The robotic system was connected through cables, with the electronic driving system (Deliverable 3.3) that controls large motors (USR60-S3N, Shinsei Kogyo Corporation) shown in Figure 120. Following a 3×3 grid pattern, the piece of excised tissue was initially sonicated at 9 locations with low acoustic power (20 W for 10 s) at 10 mm focal depth. The grid process was also repeated with high acoustic power (66 W for 20 s) for creating a 3×3 lesion grid. In both grid sonications, a step size of 10 mm was used between successive points.

During the sonications the excised tissue was scanned, with MR images acquired using a T1-Weighted (T1-W) Fast Spin Echo (FSE) sequence (Repetition time (TR)=300 ms, Echo time

(TE)=7 ms, Field of View (FOV)=280×280 mm², Slice thickness=10 mm, Matrix =128×128, Echo train length (ETL)=3, Number of Averages (NEX)=0.5, Flip angle=90°, Pixel bandwidth=75 Hz/pixel) as well as a T1-W high resolution Fast Spin Echo (FSE HR) sequence (TR=200ms, TE=9 ms, FOV=260×260 mm², Slice thickness=4 mm, Matrix=224×192, ETL=3, NEX=4, Flip angle=90°, Pixel bandwidth=75 Hz/pixel) and a T2-Weighted (T2-W) FSE HR sequence (TR=2000 ms, TE=18 ms, FOV=260×260 mm², Slice thickness=4 mm, Matrix=224×192, ETL=3, NEX=4, Flip angle=90°, Pixel bandwidth=75 Hz/pixel).



Figure 120: Electronic system for controlling the large USR60-S3N (Shinsei Corporation) motors.

Results

Figure 121 shows the T1-W FSE images acquired on a coronal plane during the 3×3 grid sonications executed with a high acoustic power (66 W for 20 s). The acquired MR images show the actual movement of the SOUNDPET robot version 1 in the X and Y axes compared to the schematic diagram of the intended 3×3 grid.

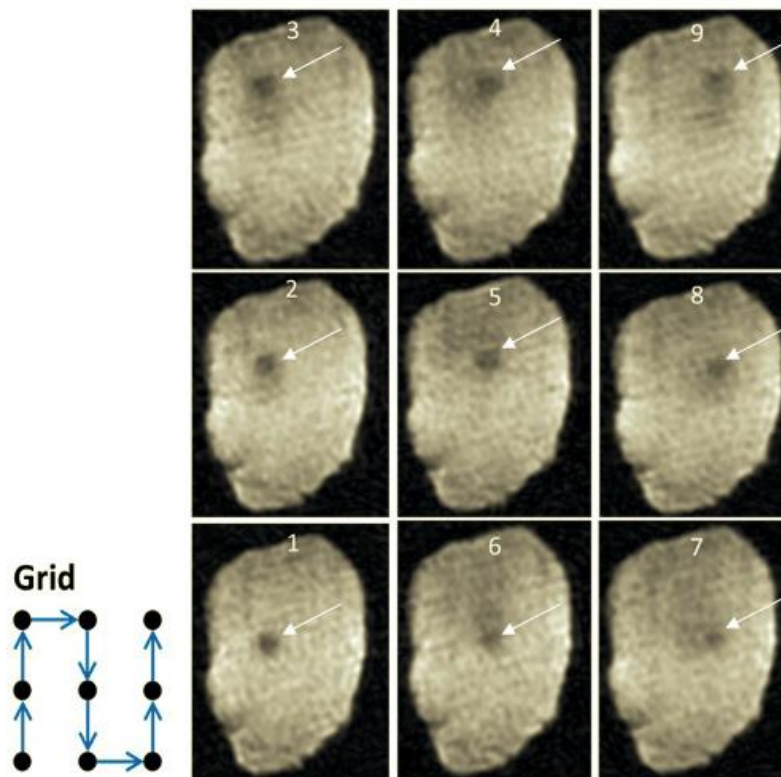


Figure 121: Coronal images (right) acquired using a T1-W FSE sequence showing thermal heating at 9 locations during 3×3 grid sonications with a 10 mm step (left) on excised pork tissue using a 2.6 MHz transducer (D=38 mm, ROC=61 mm) at acoustic power of 66 W for a sonication time of 20 s at 10 mm focal depth. Arrows indicate thermal heating.

The ultrasonic protocol (66 W for 20 s) was sufficient for the formation of 9 lesions on the excised tissue as shown in Figure 122A. The formed lesions were visualized on a plane perpendicular to the beam with T1-W and T2-W FSE HR images of the excised tissue as shown in Figure 122B and Figure 122C respectively. Correspondingly, sagittal T1-W (Figure 123) and T2-W (Figure 124) FSE HR images showed the formed lesions on a plane parallel to the beam.

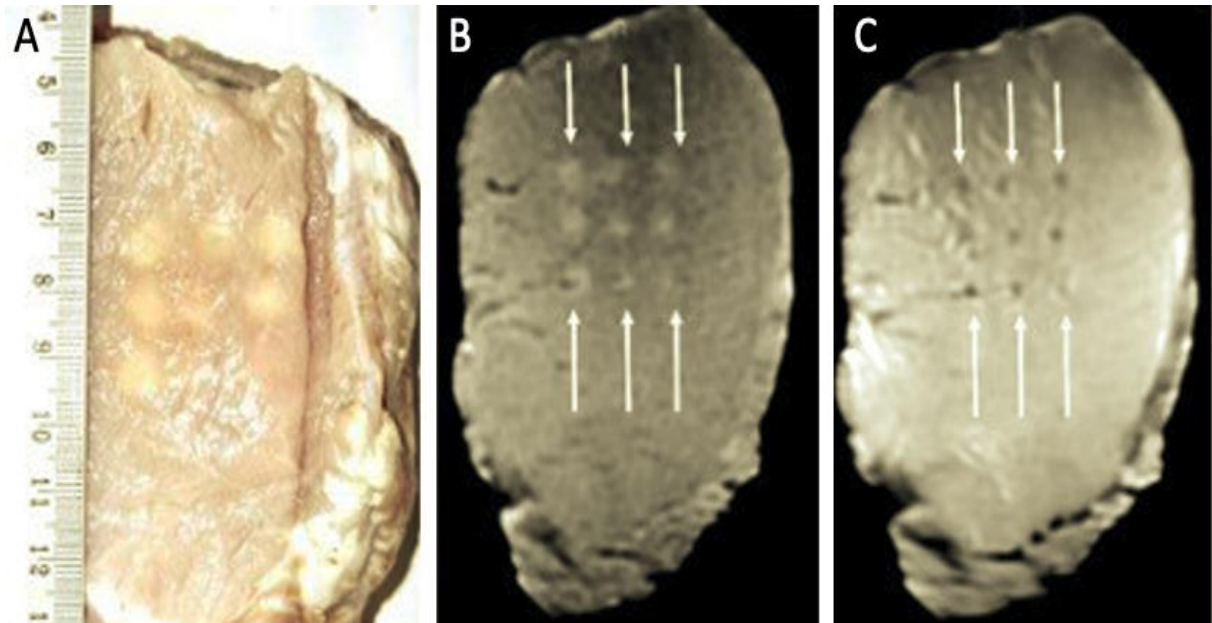


Figure 122: A) Photo of lesions formed on excised tissue on a plane perpendicular to the beam after sonications with a 2.6 MHz transducer ($D=38$ mm, $ROC=61$ mm) in a 3×3 grid with a 10 mm step using acoustic power of 66 W for a sonication time of 20 s at 10 mm focal depth, B) T1-W FSE High Resolution, and C) T2-W FSE High Resolution images of the 9 lesions acquired in coronal plane after sonications.

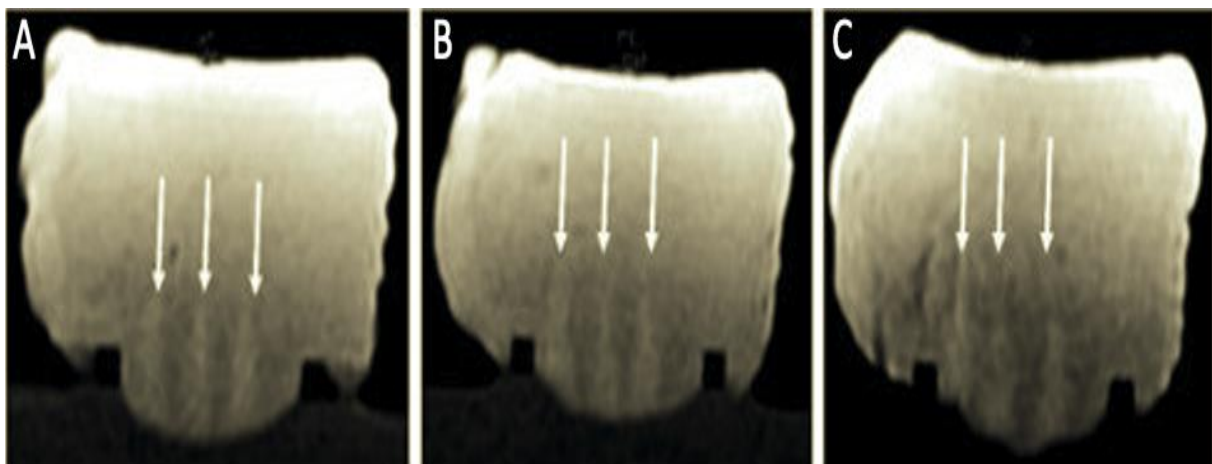


Figure 123: Sagittal images acquired using the T1-W FSE HR sequence after sonications with the 2.6 MHz transducer ($D=38$ mm, $ROC=61$ mm) in a 3×3 grid with a 10 mm step using acoustic power of 66 W for a sonication time of 20 s at 10 mm focal depth. A) Lesions 1, 6, and 7, B) Lesions 2, 5, and 8, and C) Lesions 3, 4, and 9.

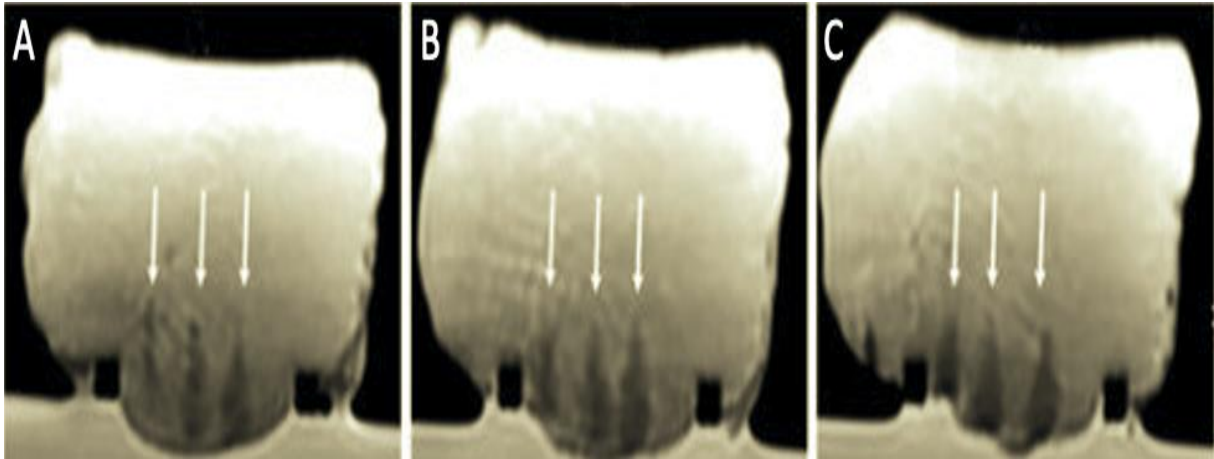


Figure 124: Sagittal images acquired using the T2-W FSE HR sequence after sonications with the 2.6 MHz transducer ($D=38$ mm, $ROC=61$ mm) in a 3×3 grid with a 10 mm step using acoustic power of 66 W for a sonication time of 20 s at 10 mm focal depth. A) Lesions 1, 6, and 7, B) Lesions 2, 5, and 8, and C) Lesions 3, 4, and 9.

The excised tissue was sliced at 10 mm (distance of focal spot) and the dimensions of the formed lesions were measured. The width and length of the 3×3 lesion grid was measured with a ruler as shown in Figure 125. Additionally, from the formed lesions, a slight displacement of the transducer to the right was observed between the 5th and 6th lesion (Figure 125).

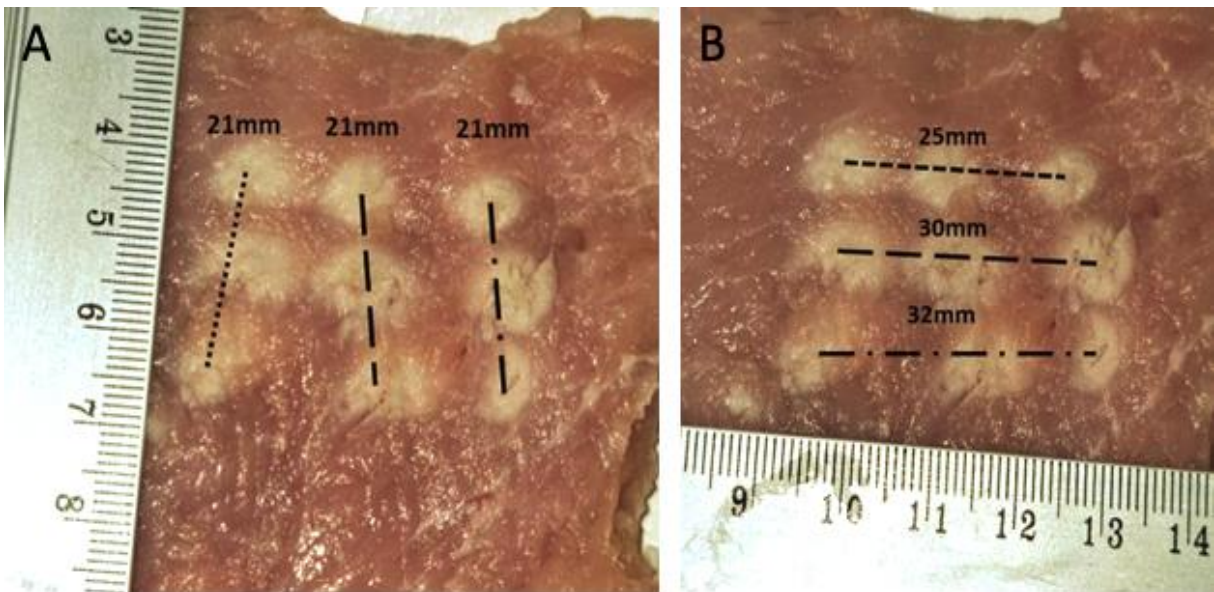


Figure 125: Photos of the 3×3 lesion grid formed on excised tissue on a plane perpendicular to the beam after sonications with a 2.6 MHz transducer ($D=38$ mm, $ROC=61$ mm) using acoustic power of 66 W for a sonication time of 20 s at 10 mm focal depth. A) Measurements for lesion length, and B) Measurements for lesion width.

Additionally, distances between the formed lesions were measured from the acquired MRI images as well as using a ruler on the sliced excised tissue as shown in Table 46. Similar measurements using the MRI images and the ruler were performed for the dimensions (diameter and length) of the formed lesions as shown in Table 47.

Table 46: Distances between lesions formed on excised tissue after sonications in a 3×3 grid with a 2.6 MHz transducer (D=38 mm, ROC=61 mm) using acoustic power of 66 W for a sonication time of 20 s at 10 mm focal depth as measured from T1-W FSE, T1-W FSE HR and T2-W FSE HR images as well as using a ruler.

Lesion	T1-W FSE (mm)	T1-W FSE HR (mm)	T2-W FSE HR (mm)	Ruler (mm)
1 to 2	9.3	8.9	9.3	12
2 to 3	10	9.2	10.5	10
3 to 4	9.3	9.3	8.5	11
4 to 5	8.5	9.9	9.7	10.5
5 to 6	11	9.8	9.7	10.5
6 to 7	10.5	9.2	9.4	12
7 to 8	8.3	9.7	10	10.5
8 to 9	10.8	9.8	10	10

Table 47: Dimensions of lesions formed on excised tissue after sonications in a 3×3 grid with a 2.6 MHz transducer (D=38 mm, ROC=61 mm) at acoustic power of 66 W for a sonication time of 20 s at 10 mm focal depth as measured from T1-W FSE HR and T2-W FSE HR images as well as using a ruler.

Lesion	Diameter			Length		
	T1-W FSE HR (mm)	T2-W FSE HR (mm)	Ruler (mm)	T1-W FSE HR (mm)	T2-W FSE HR (mm)	Ruler (mm)
1	9.5	-	9	18.8	19.6	-
2	8.8	-	9	18.9	13.1	-
3	9.2	-	9	13.6	10	-
4	10.5	-	8	17	14.9	-
5	9.8	-	11	18.2	17.7	-
6	9.8	-	10	18.2	18.2	-
7	7.6	-	7	18.2	16.2	-
8	9.7	-	9	18.6	17.4	-
9	10.5	-	8	15.4	13.9	-

Subsection Conclusions

As seen from Figure 121 and Figure 122, the lesions formed in a 3×3 grid were clearly visible in the coronal plane in both T1-W and T2-W images. Moreover, the lesions were also visible in sagittal images of both sequences (Figure 123 and Figure 124). A main objective of this experiment was to assess the accuracy of transducer displacement as a result of robotic motion during the 3×3 grid sonications. In this regard, distances between the formed lesions were measured using the acquired MR images and were compared with actual distances measured using a ruler. Distance measurements between lesions as quantified from T2-W images were closer to the actual values compared to distances measured from T1-W images (Table 46). Additionally, it was concluded that the T2-W high-resolution sequence offers higher contrast to noise ratio (CNR) between the lesion and normal tissue than the T1-W image. The distance between lesion 3 and lesion 4 as measured with T1-W and T2-W imaging was found lower than the actual value of 10 mm (Table 46). This discretion may have been caused by diversion of the beam due to the excised tissue structure (presence of internal fibres). Moreover, a displacement of the transducer to the right was observed between lesion 5 to lesion 6 (Figure 125) which was probably due to the presence of fibres in the excised tissue. Additionally, the diameter measurements of the 9 lesions as measured from T1-W images were close to the actual values (Table 47). In contrast, length measurements for lesions 1, 2 and 3 were not very accurate (Table 47) because image quality and contrast were affected by the presence of a nearby grid.

Assessment of the effect of the imaging coil in thermal heating detection

The purpose of the experiment was to assess the effect of the type of the imaging coil on the detection of thermal heating. The SOUNDPET robot (version 2) was placed on the table of a 1.5 T MRI scanner (Signa HD16, GE Healthcare). An agar-based phantom (6 % w/v agar) was positioned on the acoustic window of the robotic system. A GPFLEX surface coil (Signa 1.5 T Receiver only, GE Healthcare) and a lumbar spine coil (Signa 1.5 T 12 Channel, GE Healthcare) were either positioned on top of the agar-based phantom as shown in Figure 126 for MR image acquisition. The transducer ($f=1.1$ MHz, $D=50$ mm, $ROC=80$ mm) integrated within the robotic system was connected to an amplifier (AG1016, T & C Power Conversion) for powering purposes.

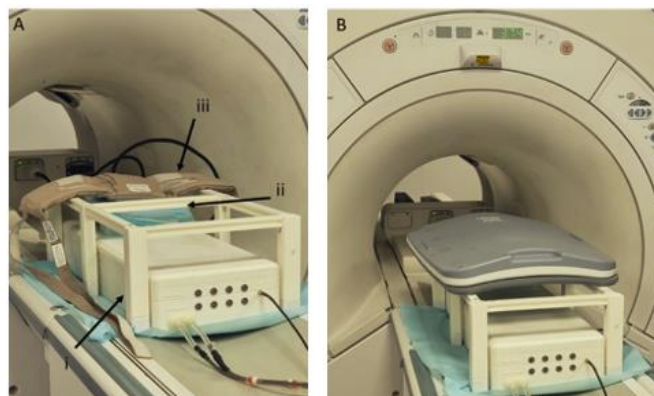


Figure 126: Experimental set-up inside the 1.5 T MRI scanner with the SOUNDPET robot (version 2) (i) positioned on the MRI table and an agar-based (6 % w/v agar) phantom (ii) placed on the acoustic window. A) A GPFLEX surface (iii) coil, and B) a lumbar spine coil were positioned on top for MR image acquisition.

A series of sonications were executed on the agar-based phantom using an acoustic power in the range of 65-81 W for a sonication time between 30-60 s at a focal depth of 40 mm. The GPFLEX surface coil was used for MR image acquisition during the first five sonications, while the lumbar spine coil was used for image acquisition during one sonication. During the six sonications, MR image acquisition of the agar phantom was performed using a Spoiled Gradient Echo (SPGR) sequence with the following parameters: TR=29 ms, TE=13 ms, FOV=280×280 mm², Slice thickness=10 mm, Matrix=160×160, ETL=1, NEX=1, Flip angle=30°, Pixel bandwidth=31 Hz/pixel.

Results

Coronal SPGR images acquired during sonications (65 W for 30 s) using the GPFLEX surface coil are shown in Figure 127. Figure 128 shows coronal SPGR images acquired with the GPFLEX surface coil at different timepoints after the end of sonications executed at acoustic power of 73 W for a sonication time of 60 s. Figure 129 and Figure 130 show sagittal images acquired during sonications (75 W for 60 s) using the GPFLEX surface and lumbar spine coils, respectively.

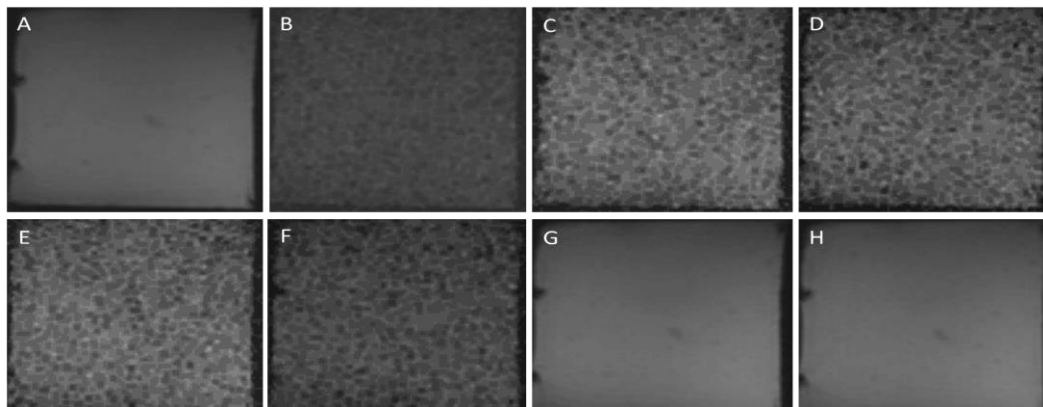


Figure 127: Coronal SPGR images of an agar-based phantom acquired with the GPFLEX surface coil during sonications with a 1.1 MHz transducer (D=50 mm, ROC=80 mm) at acoustic power of 65 W for a sonication time of 30 s at 40 mm focal depth. Images acquired A) before the sonication, B) at 5 s of sonication, C) at 10 s of sonication, D) at 15 s of sonication, E) at 20 s of sonication, F) at 25 s of sonication, G) at 30 s of sonication, and H) at 5 s after sonication.

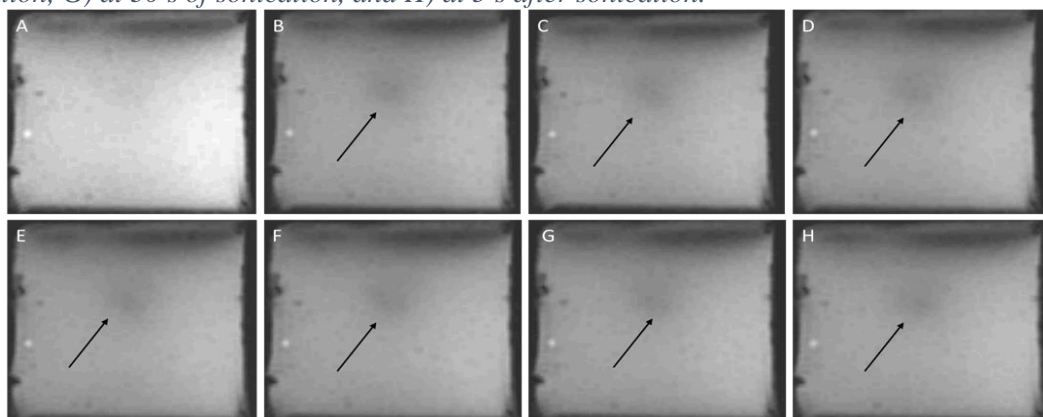


Figure 128: Coronal SPGR images of an agar-based phantom acquired with the GPFLEX surface coil at different timepoints after sonications with a 1.1 MHz transducer (D=50 mm, ROC=80 mm) at acoustic power of 73 W for a sonication time of 60 s at 40 mm focal depth. Images acquired A) before sonication, B) at 5 s after sonication, C) at 10 s after sonication, D) at 15 s after sonication, E) at 20 s after sonication, F) at 25 s after sonication, G) at 30 s after sonication, and H) at 35 s after sonication. Arrows indicate thermal heating.

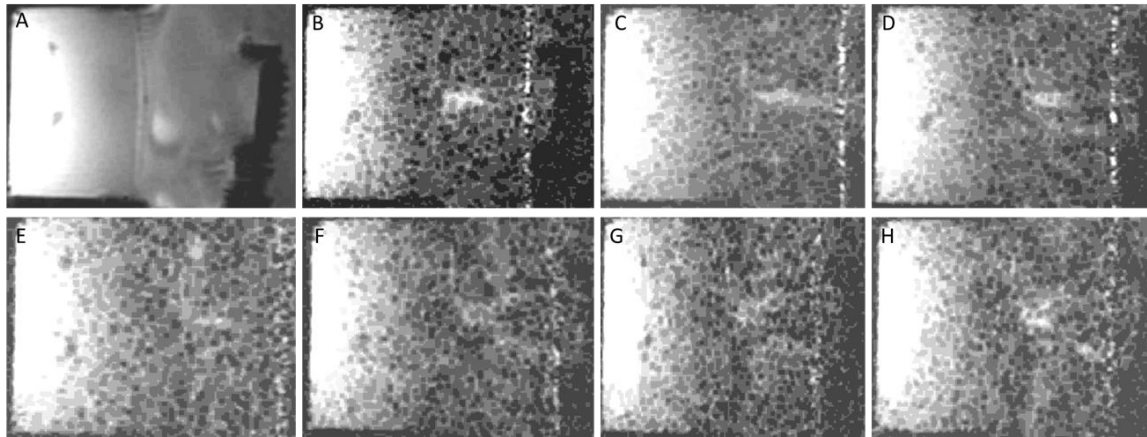


Figure 129: Sagittal SPGR images of an agar-based phantom acquired with the GPFLEX surface coil during sonications with a 1.1 MHz transducer ($D=50$ mm, $ROC=80$ mm) at acoustic power of 81 W for a sonication time of 60 s at 40 mm focal depth. Images acquired A) before sonication, B) at 5 s of sonication, C) at 10 s of sonication, D) at 15 s of sonication, E) at 20 s of sonication, F) at 25 s of sonication, G) at 30 s of sonication, and H) at 35 s of sonication.

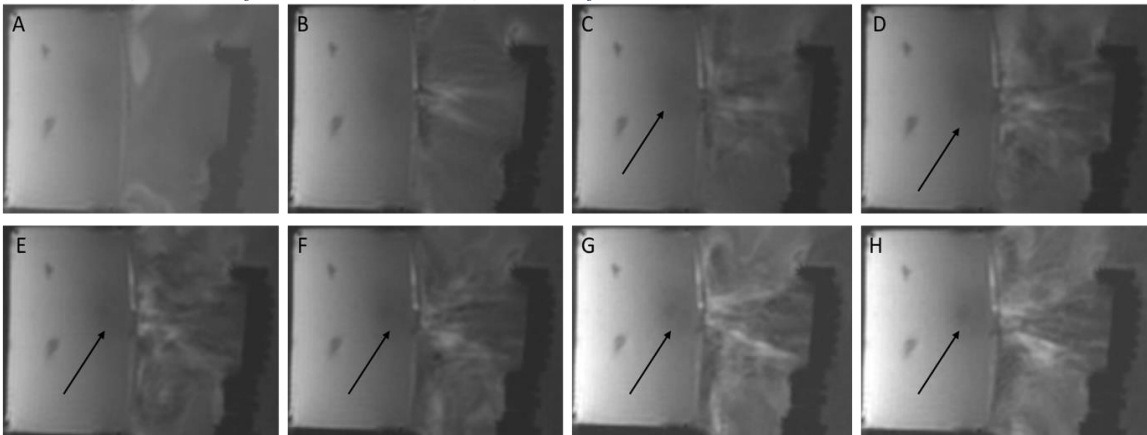


Figure 130: Sagittal SPGR images of an agar-based phantom acquired with the lumbar spine coil during sonications with a 1.1 MHz transducer ($D=50$ mm, $ROC=80$ mm) at acoustic power of 81 W for a sonication time of 60 s at 40 mm focal depth. Images acquired A) before sonication, B) at 5 s of sonication, C) at 10 s of sonication, D) at 15 s of sonication, E) at 20 s of sonication, F) at 25 s of sonication, G) at 30 s of sonication, and H) at 35 s of sonication. Arrows indicate thermal heating.

Table 48 shows the maximum temperature recorded with MR thermometry (Deliverable 4.2) during sonications with the GPFLEX surface and the lumbar spine coils.

Table 48: Maximum temperature recorded with MR thermometry within the agar-based phantom during sonications with a 1.1 MHz transducer ($D=50$ mm, $ROC=80$ mm) at 40 mm focal depth as calculated from images acquired with different imaging coils.

Acoustic power (W)	Sonication time (s)	Imaging coil	Imaging plane	Maximum temperature (°C)
65	30	Surface	Coronal	66.57
81	60	Surface	Sagittal	29.55
		Lumbar	Sagittal	2.69

Subsection Conclusions

The purpose of this experiment was to assess the effect of the type of the imaging coil (surface or lumbar) on the detection of thermal heating during sonications executed within the MRI environment. Sonications (81 W for 60 s) imaged with the surface coil resulted in increased temperatures compared to the lumbar spine coil (Table 48). Nevertheless, with the surface coil image quality was poor during activation of the transducer (Figure 127 and Figure 129). In this regard, thermal heating at the focal spot was not visible on acquired SPGR images (Figure 127 and Figure 129). However, heating at the focal spot was clearly visible as a black spot on such images acquired with the surface coil at varied timepoints after the sonications (Figure 128). Contrary, employment of the lumbar spine coil resulted in clear visualization of the thermal heating at the focal point during the sonications, with minimal artifacts on the images. Nevertheless, the lumbar spine coil generated significantly lower temperatures compared to the surface coil. Therefore, judicious selection of the coil type is required prior to experiments, to result in accurate MR imaging of the sonications and ultimately correct evaluation of the thermal heating of the transducer.

Assessment of robotic movement of SOUNDPET version 1 during 3×3 grid sonications

The purpose of this experiment was to assess the movement of the robotic device with two 3×3 grid sonications; one with low power and one with high power. The motion was assessed for the X and Y axes. The SOUNDPET robot (version 1) was placed on the table of the 1.5 T MRI (Signa HD16, GE Healthcare) as shown in Figure 131A with an agar-based phantom (6 % w/v agar, 4 % w/v silica) (77.4 mm (w) × 91.8 mm (l) × 63 mm (h)) (Figure 131B) positioned on the acoustic window of the system. On top of the phantom a GPFLEX surface coil (Signa 1.5 T Receiver only, GE Healthcare) was positioned for MR image acquisition, with a plastic positioner (coil holder) used to avoid contact between the phantom and the MR coil (Figure 131A). The 2.6 MHz transducer (D=38 mm, ROC=61 mm) integrated in the robot was connected to an amplifier (AG1016, T & C Power Conversion).

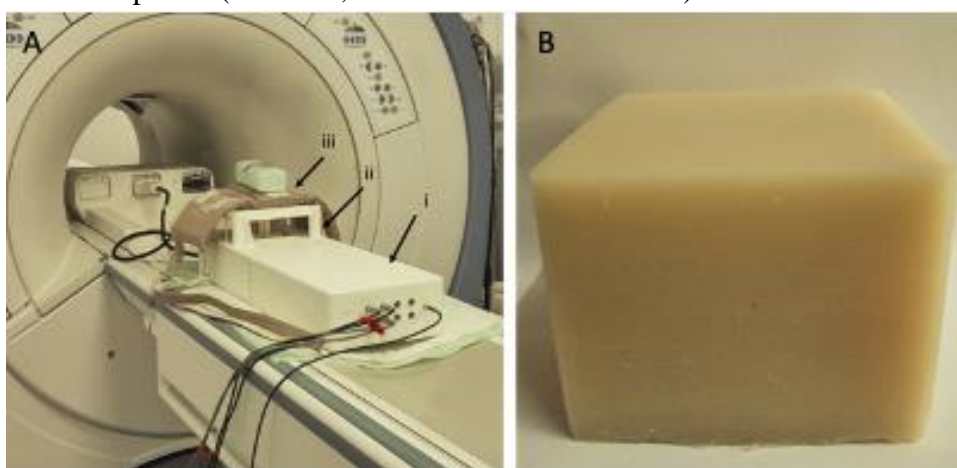


Figure 131: A) Experimental set-up inside the 1.5 T MRI scanner with the SOUNDPET robot (version 1) (i) positioned on the MRI table and an agar-based phantom (6 % w/v agar, 4 % w/v silica) placed on the acoustic window. A plastic positioner (ii) was used for supporting the GPFLEX surface coil (iii) that was placed on top for MR image acquisition, and B) Photo of the agar-based phantom (6 % w/v agar, 4 % w/v silica) used in the experiment.

Following a 3×3 grid pattern with a 10 mm step, the agar-based phantom was initially sonicated at 9 locations with low acoustic power (20 W) for a sonication time of 10 s at 10 mm focal depth (Grid 1). The grid process was repeated for sonications at the same 9 locations using high acoustic power (66 W) for a sonication time of 20 s at 10 mm focal depth (Grid 2). During the two 3×3 grid sonications, a T1-W FSE sequence (TR=300 ms, TE=7 ms, FOV=280×280 mm², Slice thickness=10 mm, Matrix=128×128, ETL=3, NEX=0.5, Flip angle=90°, Pixel bandwidth=75 Hz/pixel) was used for MR image acquisition. The T1-W FSE images were used for visualizing the thermal heating at the 9 sonication points and assessing the accuracy of robotic movement during the grid operation.

Results

Figure 132 and Figure 133 show the T1-W FSE images acquired during the low power (20 W for 10 s), and high power (66 W for 20 s) sonications respectively, showing the thermal heating as a black spot at each sonication point. Table 49 shows the distances between the sonication points as measured from T1-W FSE images acquired during execution of the two grids.

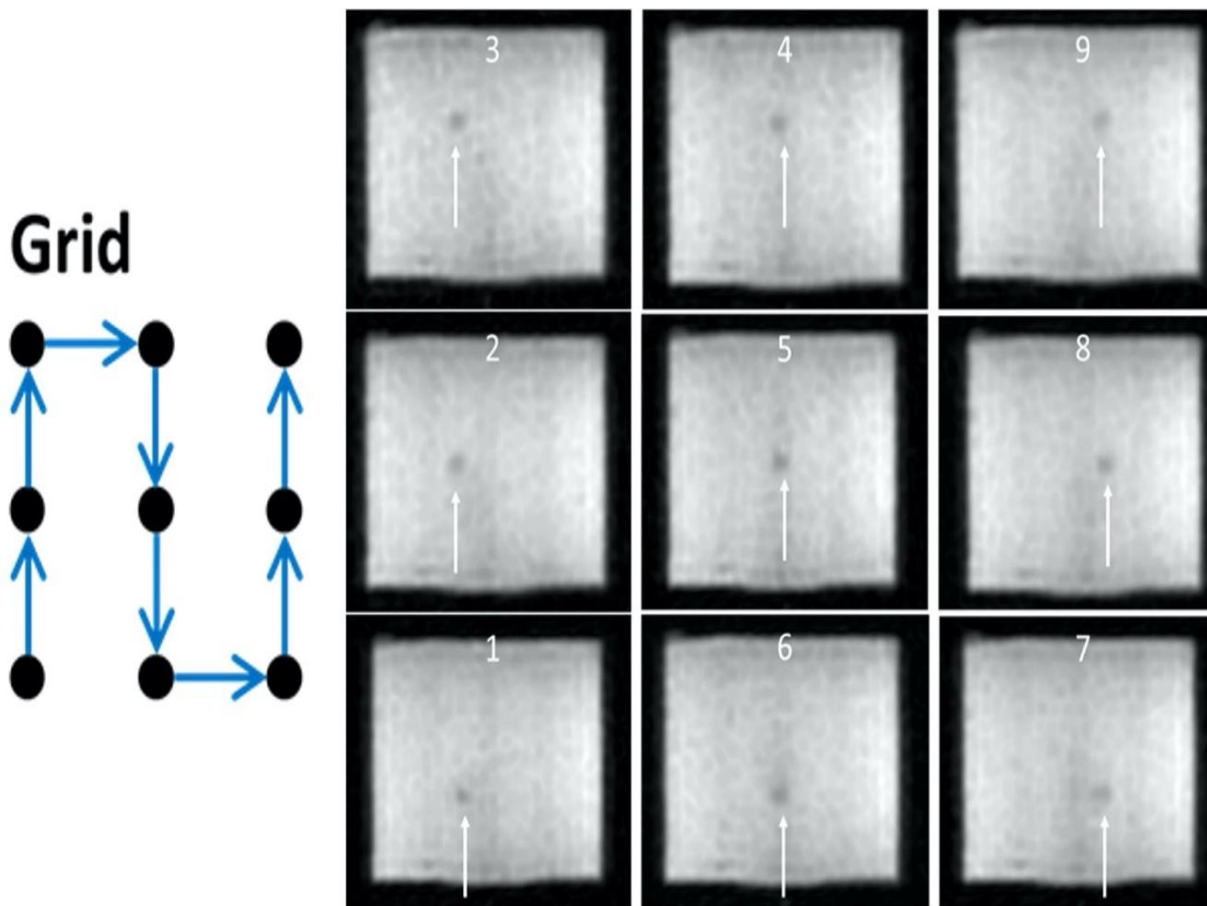


Figure 132: Coronal T1-W FSE images (right) showing thermal heating at 9 locations during 3×3 grid sonications with a 10 mm step (left) on an agar-based phantom (6 % w/v agar, 4 % w/v silica) using a 2.6 MHz transducer (D=38 mm, ROC=61 mm) at acoustic power of 20 W for a sonication time of 10 s at 10 mm focal depth. Arrows indicate thermal heating.

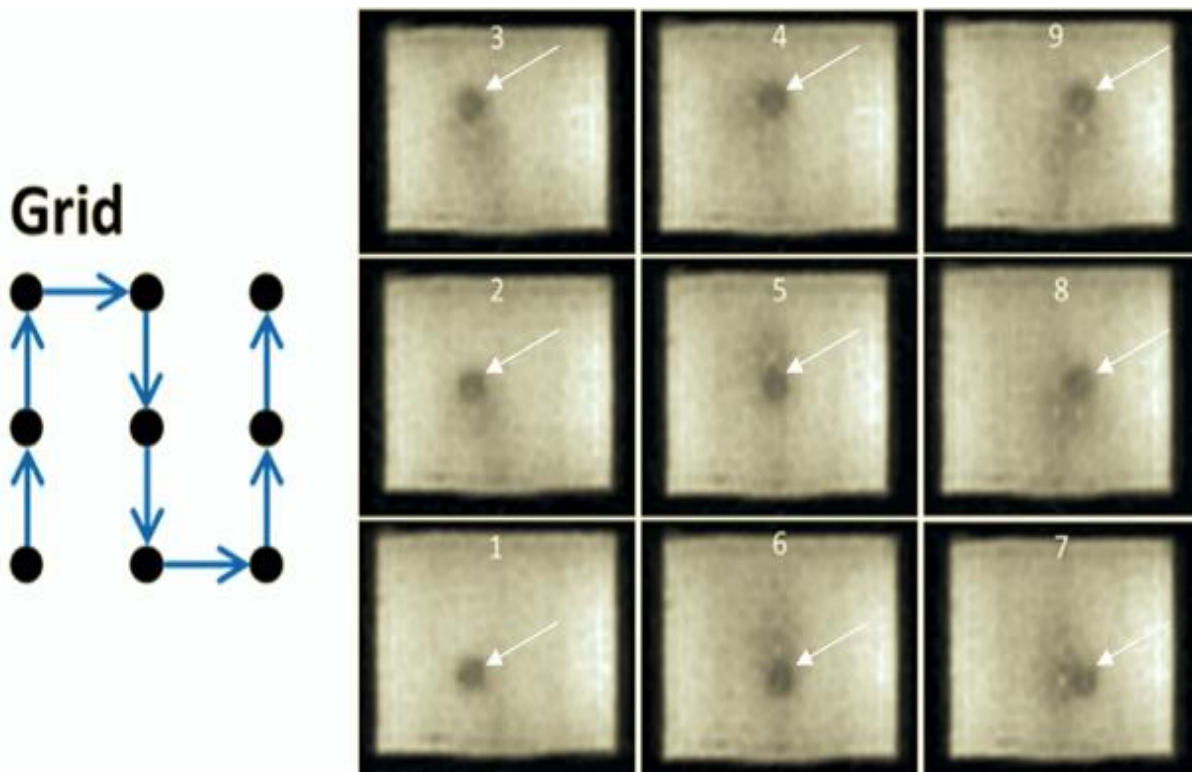


Figure 133: Coronal T1-W FSE images (right) showing thermal heating at 9 locations during 3×3 grid sonications with a 10 mm step (left) on an agar-based phantom (6 % w/v agar, 4 % w/v silicon dioxide) using a 2.6 MHz transducer ($D=38$ mm, $ROC=61$ mm) at acoustic power of 66 W for a sonication time of 20 s at 10 mm focal depth. Arrows indicate thermal heating.

Table 49: Distances between sonication points as measured from T1-W FSE images acquired during sonications executed in 3×3 grids with a 10 mm step using a 2.6 MHz transducer ($D=38$ mm, $ROC=61$ mm) at acoustic power of 20 W for a sonication time of 10 s (Grid 1) and acoustic power of 66 W for a sonication time of 20 s (Grid 2) at 10 mm focal depth.

Sonication point	Grid 1	Grid 2
	T1-W FSE (mm)	T1-W FSE (mm)
1 to 2	10.4	9.4
2 to 3	9.5	10.2
3 to 4	8.8	9.1
4 to 5	10.3	9.8
5 to 6	10.4	9.8
6 to 7	10.1	9.2
7 to 8	9.9	8.7
8 to 9	10	10.3

Subsection Conclusions

Thermal heating induced by the two 3×3 grid sonications was clearly visible on T1-W images acquired for both the low (20 W for 10 s) and high (66 W for 20 s) power grid sonications as shown in Figure 132 and Figure 133. Measuring distances between sonication points from T1-W images resulted in accurate displacement of the robot between successive sonication points, with the measured distances being in close agreement to the intended distance (10 mm) for both grids (Table 49). Moreover, T1-W images acquired during the high power (66 W) grid were of poor quality (Figure 133), while the quality of images acquired for the low power (20 W) grid was better.

Assessment of robotic movement of SOUNDPET version 2 during 6×6 grid sonications

The purpose of this experiment was to assess the movement of the robotic device with 6×6 grid sonications. The motion was assessed in the X and Y axes. The SOUNDPET robot (version 2) was placed on the table of the 1.5 T MRI (Signa HD16, GE Healthcare) as shown in Figure 134A. Two agar-based phantoms were individually positioned on the acoustic window of the robotic device for sonications; one agar-based phantom doped with silica (6 % w/v agar, 4 % w/v silica) (77.4 mm (w) × 91.8 mm (l) × 63 mm (h)) (Figure 131B), and a larger purely agar-based phantom (6 % w/v agar) (90 (w) × 160 mm (l) × 100 mm (h)). The large agar-based phantom (6 % w/v agar) was developed with a specific shape as shown in Figure 134B to allow support on the acoustic opening of the robot and achieve better coupling with the water. On top of either of the phantoms, a body coil (Signa 1.5 T 12 Channel, GE Healthcare) was positioned (Figure 134A) for MR image acquisition. The 2.75 MHz ultrasonic transducer (D=50 mm, ROC=65 mm) integrated in the robot was connected to an amplifier (AG1016, T & C Power Conversion).

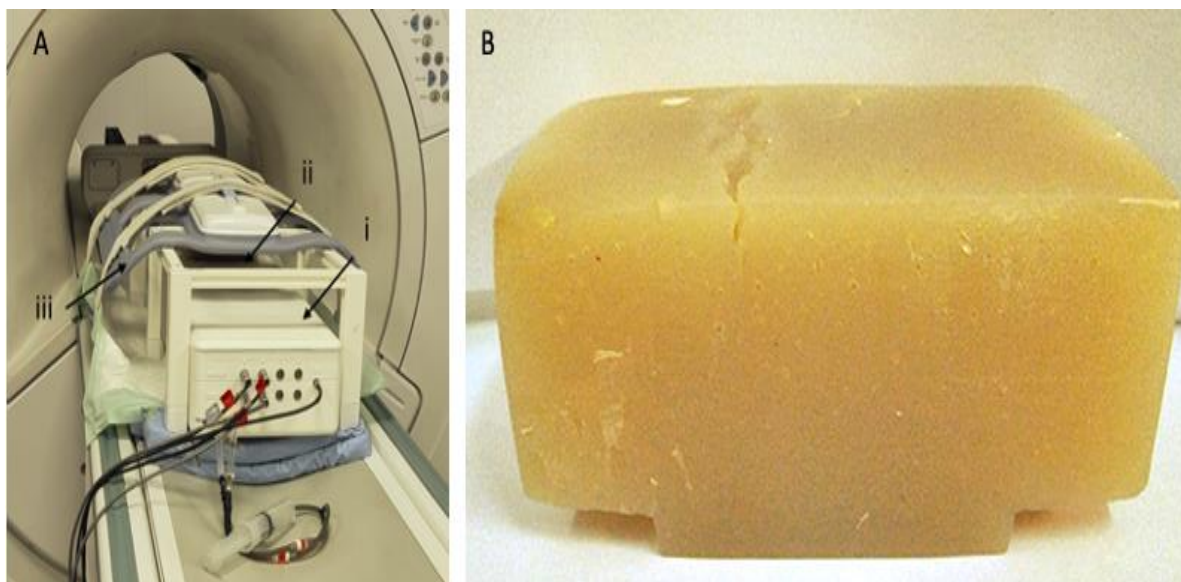


Figure 134: A) Experimental set-up inside the 1.5 T MRI scanner with the SOUNDPET robot (version 2) (i) positioned on the MRI table and an agar-based phantom (ii) placed on the acoustic window with a body coil placed on top for MR image acquisition, and B) Photo of the large agar-based phantom (6 % w/v agar) specifically developed to allow support on the acoustic opening of the robot.

Grid sonications were executed on either of the phantoms with robotic motion initiated in 6×6 grid patterns with a 3 mm step between successive points. The agar-based phantom doped with silica (6 % w/v agar, 4 % w/v silica) was sonicated using an acoustic power of 39 W for a sonication time of 30 s at 25 mm focal depth. The larger agar-based phantom (6 % w/v agar) was sonicated at the 36 locations using an acoustic power of 45 W for a sonication time of 18 s at 20 mm focal depth. Grid sonications on the two phantoms were imaged using a T1-W FSE sequence (TR=30 ms, TE=7 ms, FOV=280×280 mm², Slice thickness=10 mm, Matrix=128×128, ETL=3, NEX=0.5, Flip angle=90°, Pixel bandwidth=75 Hz/pixel).

Results

Figure 135 shows the T1-W images acquired during the 6×6 grid sonications (39 W for 30 s) executed on the agar-based phantom doped with silica (6 % w/v agar, 4 % w/v silica). However, acquired images were very noisy thus, the grid operation was terminated after 21 sonications. Figure 136 shows the 6×6 grid sonications (45 W for 18 s) executed on the larger agar-based phantom (6 % w/v agar). Image quality was better and thermal heating was successfully visualized at all 36 locations.

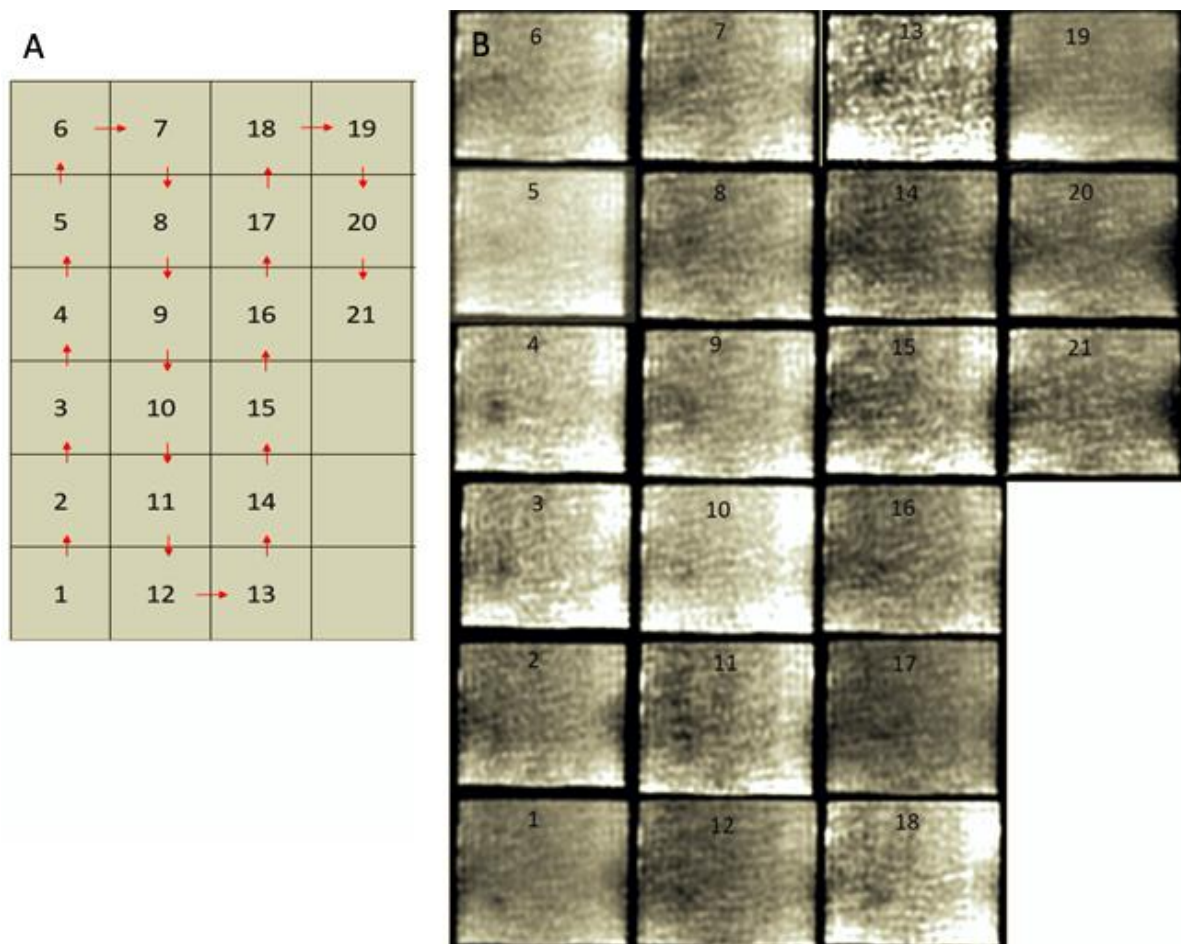


Figure 135: A) Direction of transducer motion for sonications at 21 locations of an intended 6×6 grid pattern with a 3 mm step, and B) Coronal T1-W FSE images acquired during the 21 sonications executed on an agar-based phantom doped with silica (6 % w/v agar, 4 % w/v silica) with a 2.75 MHz transducer (D=50 mm, ROC=65 mm) using an acoustic power of 39 W for a sonication time of 30 s at 25 mm focal depth.

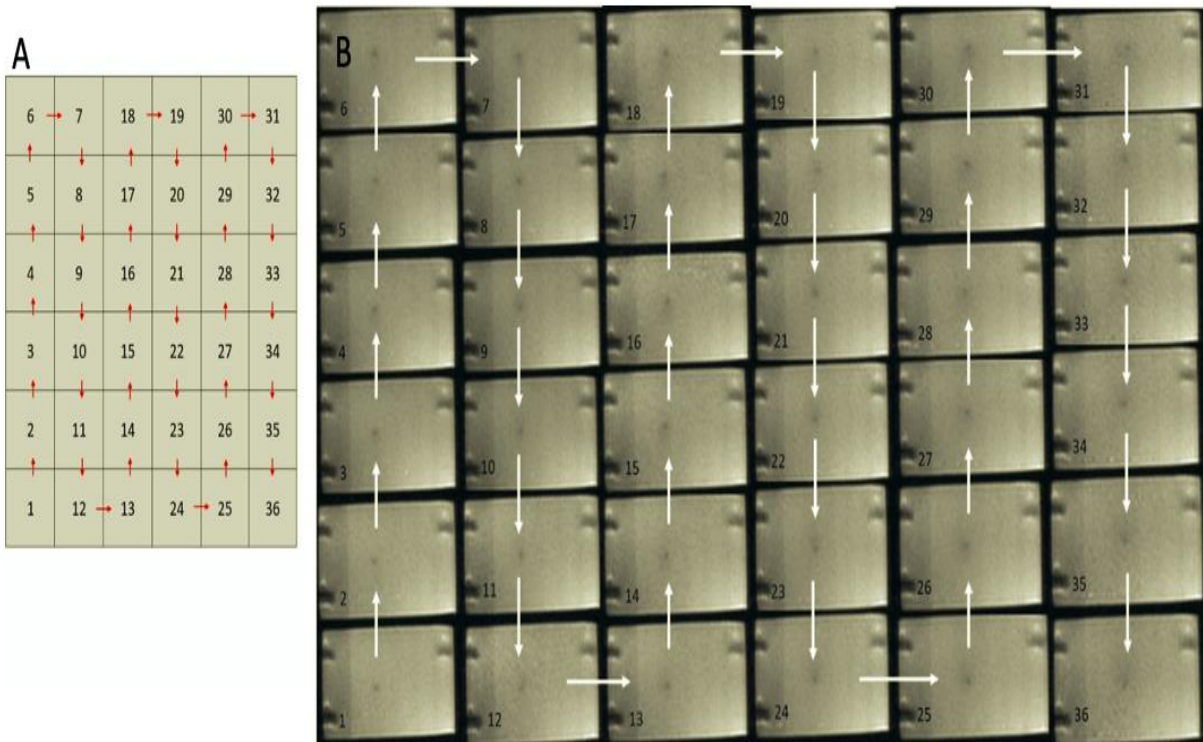


Figure 136: A) Direction of transducer motion for sonications in a 6×6 grid pattern with a 3 mm step, and B) Coronal T1-W FSE images showing thermal heating (black spot) at 36 locations during the 6×6 grid sonications executed on an agar-based phantom (6 % w/v agar) with a 2.75 MHz transducer ($D=50$ mm, $ROC=65$ mm) using an acoustic power of 45 W for a sonication time of 18 s at 20 mm focal depth.

Subsection Conclusions

MR images of the agar-based phantom doped with silica (6 % w/v agar, 4 % w/v silica) presented many black spots (Figure 135) probably due to the presence of silica particles. Another possibility for the low image quality was poor coupling between the water and the phantom. As the majority of thermal heating was not visible on T1-W FSE images, the accuracy of step movement of the robotic device could not be measured from the MR images.

To improve coupling, the 6×6 grid operation was repeated on a larger agar-based phantom (6 % w/v agar) lacking silica particles, that was specifically developed to fit on the opening of the device. In this regard, the phantom was more stable and achieved better coupling with the water during sonications, while the absence of silica ensured the non-appearance of image artifacts. The 6×6 grid sonications were followed, with the thermal heating clearly visible at all locations on the acquired T1-W images (Figure 136), presumably because of the larger and different phantom used compared to the first experiment. Moreover, with the larger phantom an improved image quality with increased Signal to Noise Ratio (SNR) was observed when the transducer was activated during the acquisition compared to the first experiment.

Optimizing the echo time (TE) and repetition time (TR) in T1-W and T2-W sequences for enhanced lesion detection

The purpose of this experiment was to determine the optimal values of TE and TR in T1-W and T2-W FSE sequences for optimal detection of lesions inflicted on excised pork tissue. The

SOUNDPET robot (version 2) was placed on the table of the 1.5 T MRI (Signa HD16, GE Healthcare) with a piece of excised pork tissue placed on the acoustic window as shown in Figure 137. On top of the excised tissue a GPFLEX surface coil (Signa 1.5 T Receiver only, GE Healthcare) was positioned for MR image acquisition, with a plastic positioner used to avoid contact between the tissue and the MR coil. The 2.75 MHz ultrasonic transducer (D=50 mm, ROC=65 mm) integrated within the robot was connected to an amplifier (AG1016, T & C Power Conversion).



Figure 137: Experimental set-up inside the 1.5 T MRI scanner with the SOUNDPET robot (version 2) (i) positioned on the MRI table and a piece of excised pork tissue (ii) placed on the acoustic window with a plastic positioner accommodated on top for supporting the GPFLEX coil (iii) used for MR image acquisition.

A series of single sonications were executed on the excised tissue using an acoustic power of 54 W for a sonication time of 30 s at 30 mm focal depth. The lesions inflicted by the sonications were imaged using a T1-W FSE and a T2-W FSE sequence with varied parameters as shown in Table 50, to examine the effect of the sequence parameters on the contrast between the lesion and the surrounding normal tissue.

Table 50: Parameters of the T1-W and T2-W FSE sequences used for MR image acquisition.

Sequence	TR (ms)	TE (ms)	ETL	FOV (mm ²)	Slice thickness (mm)	Matrix	NEX	Flip angle (°)	Pixel bandwidth (Hz/pixel)
T1-W FSE	300, 700, 1000, 1300, 1500	7	3	280×280	10	128×128	0.5	90	1.7
T2-W FSE	2500	10, 50, 90	14	260×260		192×128	2		0.5

Results

Figure 138 and Figure 139 show the T1-W FSE and T2-W FSE images acquired in axial plane using varied TR and TE respectively. Figure 140 and Figure 141 respectively show the coronal T1-W FSE and T2-W FSE images acquired with varied parameters.

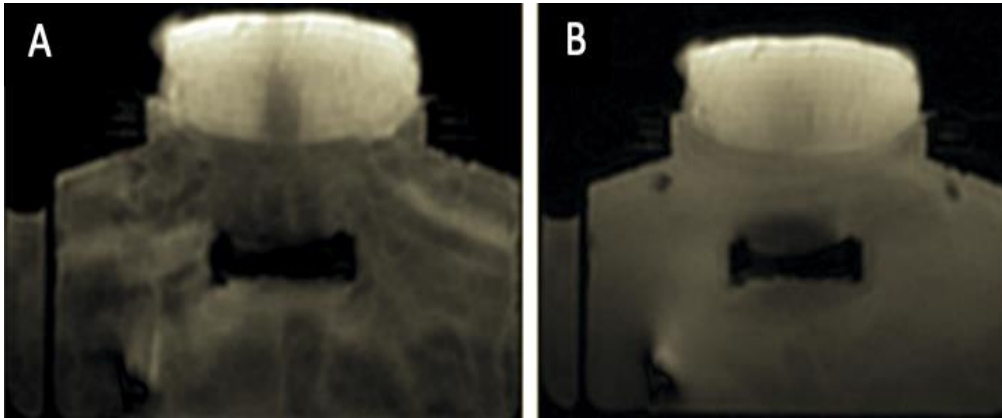


Figure 138: Axial T1-W FSE images of lesion inflicted on excised pork tissue after sonications with a 2.75 MHz transducer ($D=50$ mm, $ROC=65$ mm) using an acoustic power of 54 W for a sonication time of 30 s at 30 mm focal depth. Images acquired with A) $TR=300$ ms, and B) $TR=700$ ms.

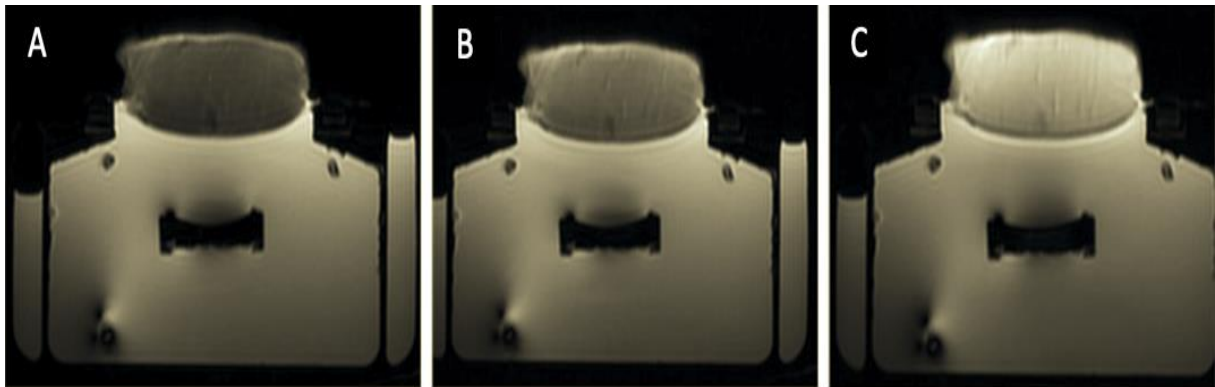


Figure 139: Axial T2-W FSE images of lesion inflicted on excised pork tissue after sonications with a 2.75 MHz transducer ($D=50$ mm, $ROC=65$ mm) using an acoustic power of 54 W for a sonication time of 30 s at 30 mm focal depth. Images acquired with A) $TE=90$ ms, B) $TE=50$ ms, and C) $TE=10$ ms.

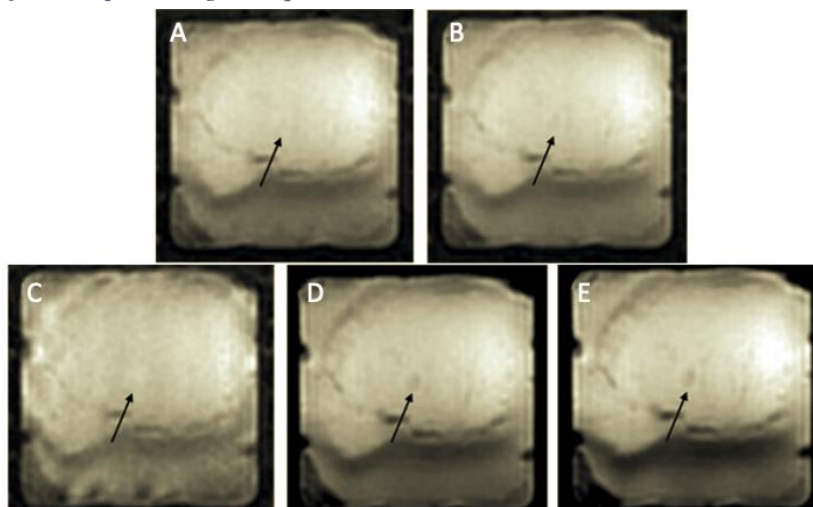


Figure 140: Coronal T1-W FSE images of lesion (black arrow) inflicted on excised pork tissue after sonications with a 2.75 MHz transducer ($D=50$ mm, $ROC=65$ mm) using an acoustic power of 54 W for a sonication time of 30 s at 30 mm focal depth. Images acquired with A) $TR=700$ ms, B) $TR=1000$ ms, C) $TR=300$ ms, D) $TR=1300$ ms, and E) $TR=1500$ ms.

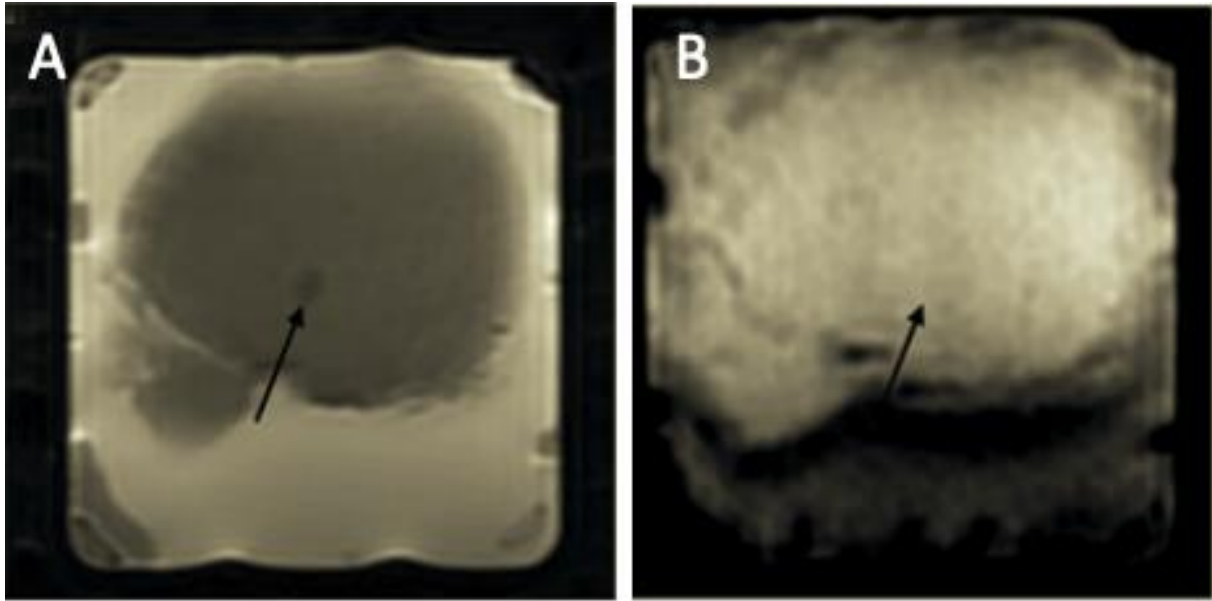


Figure 141: Coronal T2-W FSE images of lesion (black arrow) inflicted on excised pork tissue after sonications with a 2.75 MHz transducer ($D=50$ mm, $ROC=65$ mm) using an acoustic power of 54 W for a sonication time of 30 s at 30 mm focal depth. Images acquired with A) $TE=50$ ms, and B) $TE=10$ ms.

Subsection Conclusions

In this experiment, a very good coupling was achieved between the excised tissue and the membrane that covers the acoustic window of the robotic system. Based on the experimental results, a better CNR was achieved in T1-W FSE images acquired with TR at 300 ms (Figure 138A) and 1300 ms (Figure 140D) and in T2-W FSE images obtained with $TE=50$ ms (Figure 139B and Figure 141A). To assess the length of the lesion, a T1-W FSE sequence was used in axial plane with $TR=300$ ms (Figure 138A) to result in a short acquisition time. The diameter and length of the lesion were measured at 14 mm and 20 mm, respectively.

Optimizing the echo time (TE), repetition time (TR) and echo train length (ETL) of T1-W and T2-W sequences for lesion detection

The purpose of this experiment was to optimize the parameters of T1-W and T2-W FSE sequences for optimal detection of lesions inflicted on excised pork tissue resulting sonications. The SOUNDPET robot (version 2) was positioned on the table of the 1.5 T MRI scanner (Signa HD16, GE Healthcare). A piece of excised pork tissue was placed on the acoustic window of the robotic system and a GPFLEX coil (Signa 1.5 T Receiver only, GE Healthcare) was positioned on top for MR image acquisition as shown in Figure 142. The transducer ($f=1.1$ MHz, $D=50$ mm, $ROC=80$ mm) integrated within the robotic system was connected to an amplifier (AG1016, T & C Power Conversion) for powering purposes.

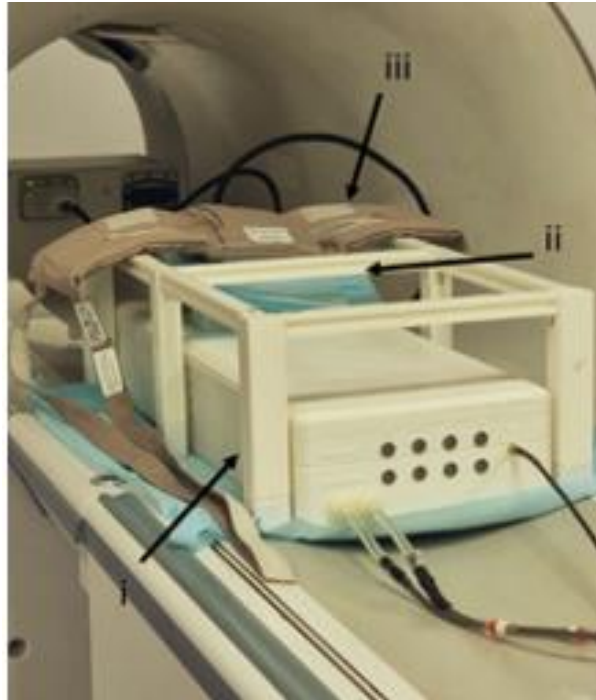


Figure 142: Experimental set-up inside the 1.5 T MRI scanner with the SOUNDPET robot (version 2) (i) positioned on the MRI table with a piece of excised pork tissue (ii) placed on the acoustic window and a GPFLEX coil (iii) placed on top for MR image acquisition.

Grid sonications were performed on the tissue using manual movement in a 2×3 pattern and acoustic power of 77.5 W for sonication times of 30 s and 60 s at 30 mm focal depth. After sonications, a series of T1-W and T2-W FSE sequences were used with varied parameters to assess their effect on the contrast between the lesions and the surrounding unaffected tissue. Specifically, varied ETL, TE and TR were examined for their effect on the image contrast. The parameters for the T1-W and T2-W FSE sequences are shown in Table 51. For each image, CNR calculations were performed by measuring Signal Intensities (SI) in Regions of Interest (ROIs) set for the lesion, the surrounding normal tissue and the background.

Table 51: Sequence parameters used for MR image acquisition for examining the effect of ETL, TE and TR on lesion contrast.

Sequence	TR (ms)	TE (ms)	ETL	FOV (mm ²)	Slice thickness (mm)	Matrix	NEX	Flip angle (°)	Pixel bandwidth (Hz/pixel)
T2-W FSE	2000	9, 26, 71, 89, 106	8, 12, 16	260×260	4	224×192	4	90	81
T1-W FSE	200, 300, 400, 600, 800, 1000	9	2, 3, 5				2		75

Results

T2-W FSE

Figure 143 shows the T2-W images (TE=53 ms, TR=2000 ms) acquired with varied ETL (8, 12 and 16). Following SI calculations for ROIs set for the lesion (white circle in Figure 143B), the surrounding unaffected tissue (black circle in Figure 143B) and the background (yellow circle in Figure 143B) in images acquired with varied ETL (Figure 144A), CNR analysis of the images was performed as shown in Figure 144B.

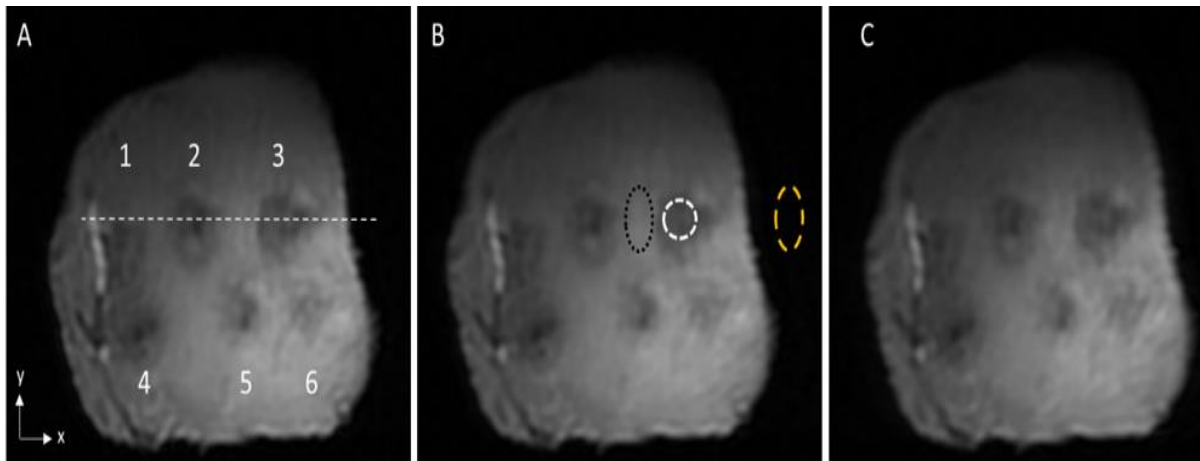


Figure 143: Axial T2-W FSE images (TE=53 ms, TR=2000 ms) of 6 lesions inflicted on excised pork tissue after sonications with a 1.1 MHz transducer (D=50 mm, ROC=80 mm) using acoustic power of 77.5 W for sonication times of 30 s and 60 s at 30 mm focal depth. Images acquired with varied ETL of A) 8, B) 12, and C) 16.

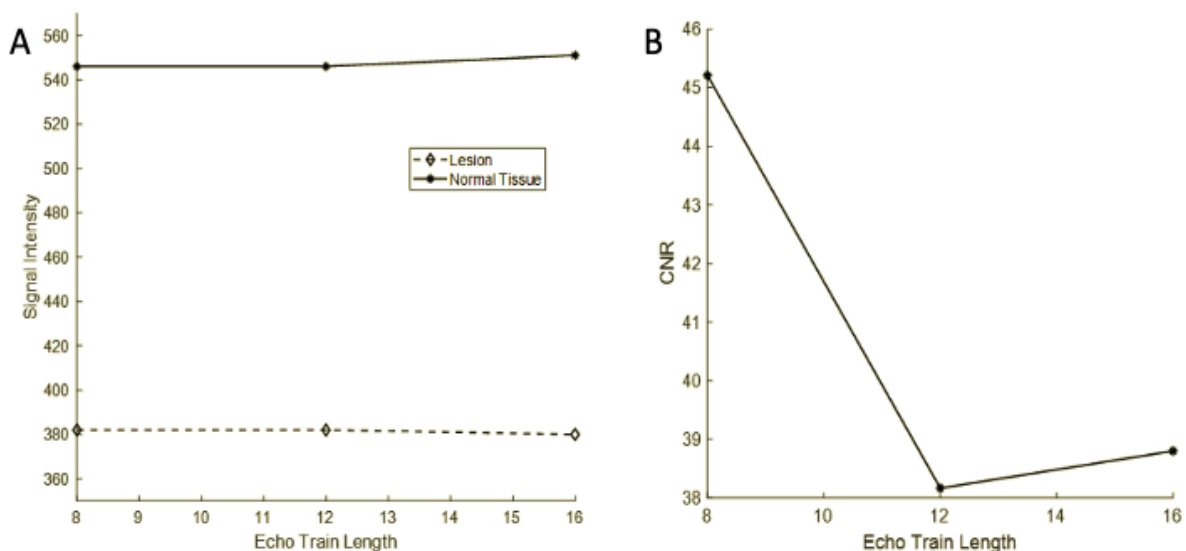


Figure 144: A) Signal intensity of lesion and surrounding normal tissue as measured from T2-W FSE (TE=53 ms, TR=2000 ms) images acquired with varied ETL (8, 12, and 16), and B) CNR between lesion and surrounding unaffected tissue against varied ETL (8, 12, and 16).

An ETL of 12 was chosen for subsequent experiments and T2-W images were acquired with varied TE values (9, 26, 71, 89, and 106 ms) as shown in Figure 145. SI calculations for the lesion and the surrounding unaffected tissue for images acquired with varied TE are shown in

Figure 146A with the corresponding CNR analysis between the two regions shown in Figure 146B.

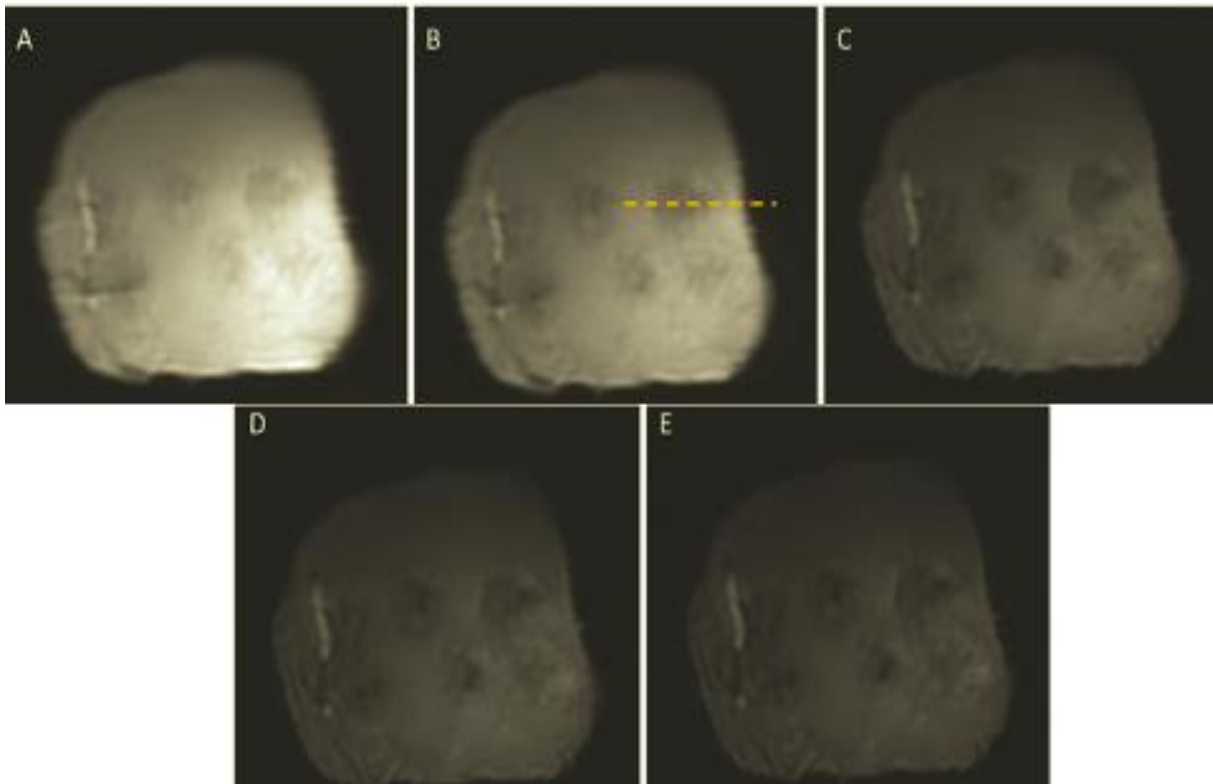


Figure 145: Axial T2-W FSE images ($ETL=12$, $TR=2000$ ms) of 6 lesions inflicted on excised pork tissue after sonications with a 1.1 MHz transducer ($D=50$ mm, $ROC=80$ mm) using acoustic power of 77.5 W for sonication times of 30 s and 60 s at 30 mm focal depth. Images acquired with varied TE of A) 9 ms, B) 26 ms, C) 71 ms, D) 89 ms, and E) 106 ms.

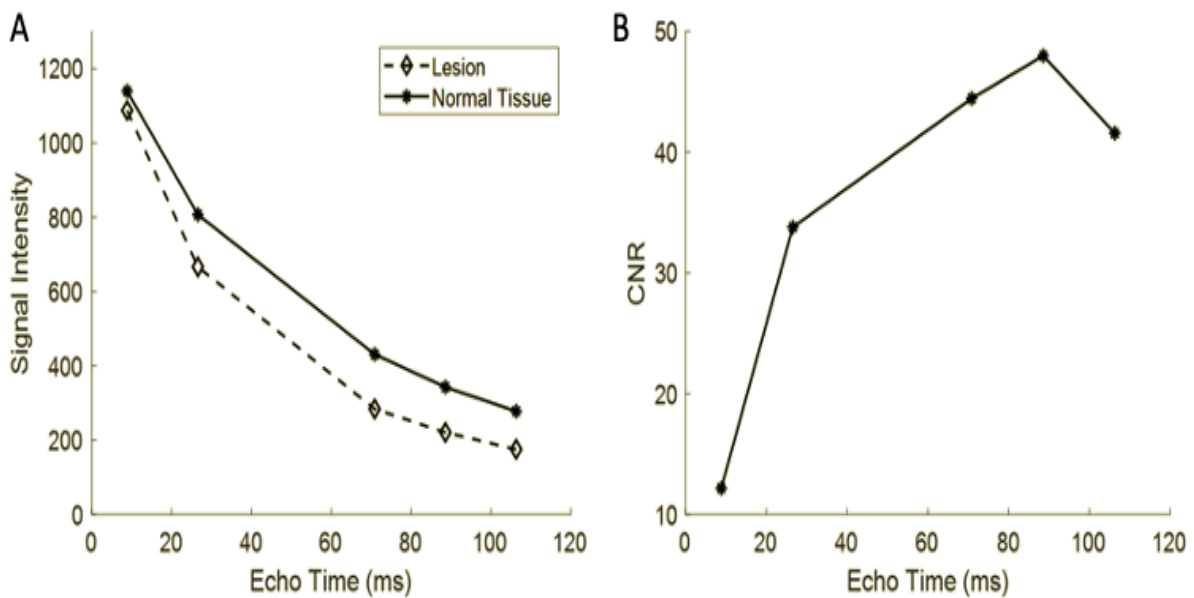


Figure 146: A) Signal intensity of lesion and surrounding normal tissue as measured from T2-W FSE ($ETL=12$, $TR=2000$ ms) images acquired with varied TE (9, 26, 71, 89, and 106 ms), and B) CNR between lesion and surrounding unaffected tissue against varied TE (9, 26, 71, 89, and 106 ms).

T1-W FSE

Figure 147 shows the T1-W images ($TE=9$ ms, $TR=200$ ms) acquired with varied ETL (2, 3 and 5). SI calculations for the lesion and the surrounding unaffected tissue for images acquired with varied ETL are shown in Figure 148A with the corresponding CNR analysis shown in Figure 148B.

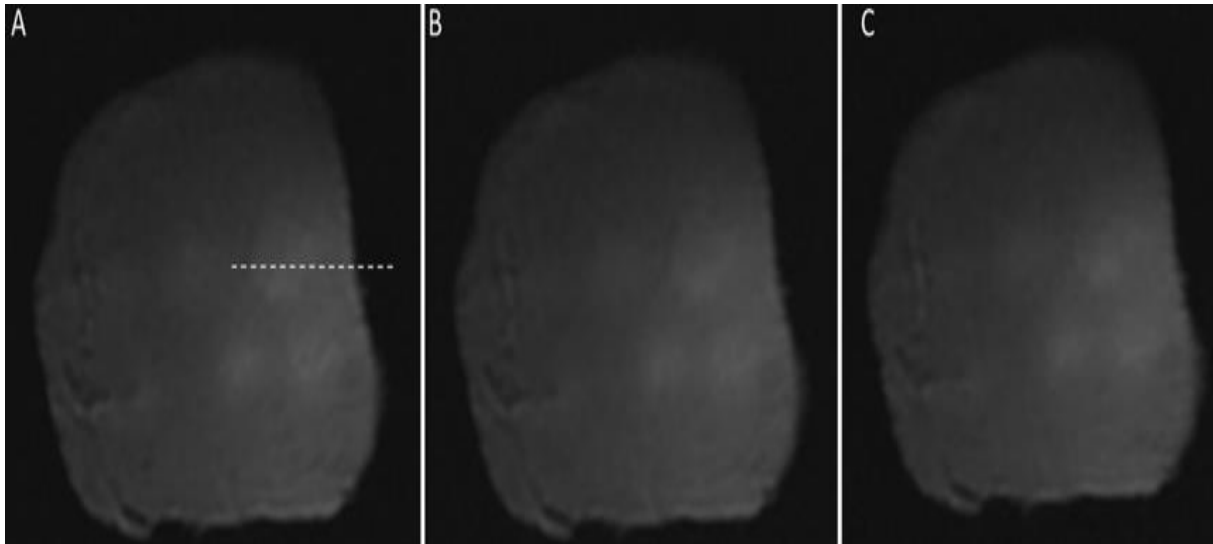


Figure 147: Axial T1-W FSE images ($TE=9$ ms, $TR=200$ ms) of 6 lesions inflicted on excised pork tissue after sonications with a 1.1 MHz transducer ($D=50$ mm, $ROC=80$ mm) using acoustic power of 77.5 W for sonication time of 30 s and 60 s at 30 mm focal depth. Images acquired with varied ETL of A) 2, B) 3, and C) 5.

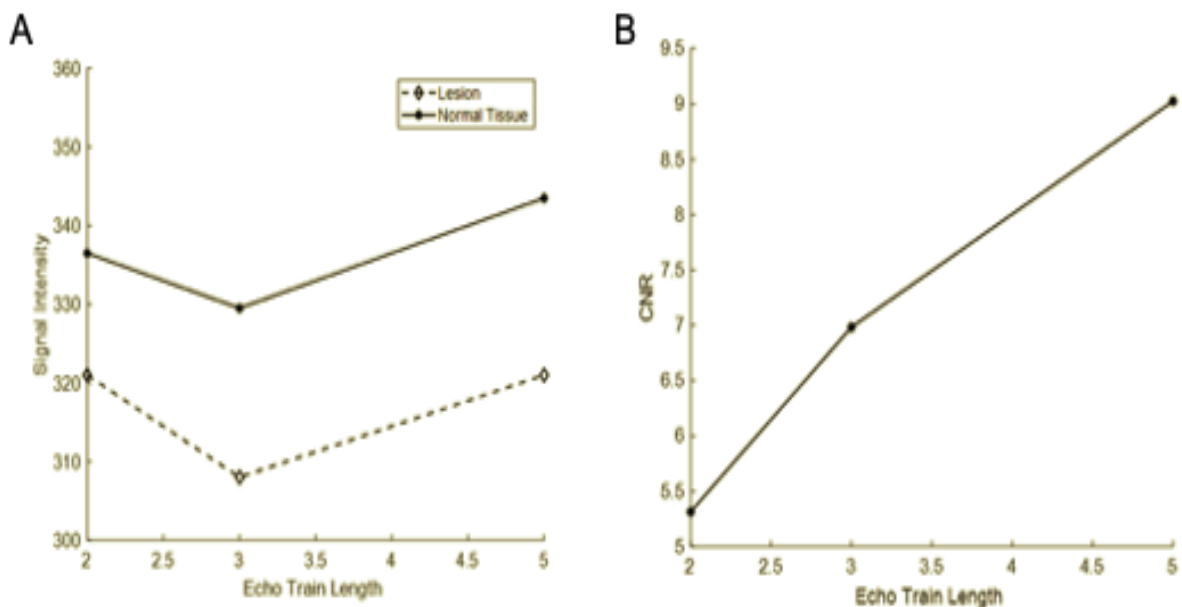


Figure 148: A) Signal intensity of lesion and surrounding normal tissue as measured from T1-W FSE ($TE=9$ ms, $TR=200$ ms) images acquired with varied ETL (2, 3, and 5), and B) CNR between lesion and surrounding unaffected tissue against varied ETL (2, 3, and 5).

An ETL of 2 was chosen for subsequent experiments and T1-W images were acquired with varied TR values (300, 400, 600, 800, and 1000 ms) as shown in Figure 149. SI calculations

for the lesion and the surrounding unaffected tissue for images acquired with varied TR are shown in Figure 150A with the corresponding CNR analysis between the two regions shown in Figure 150B.

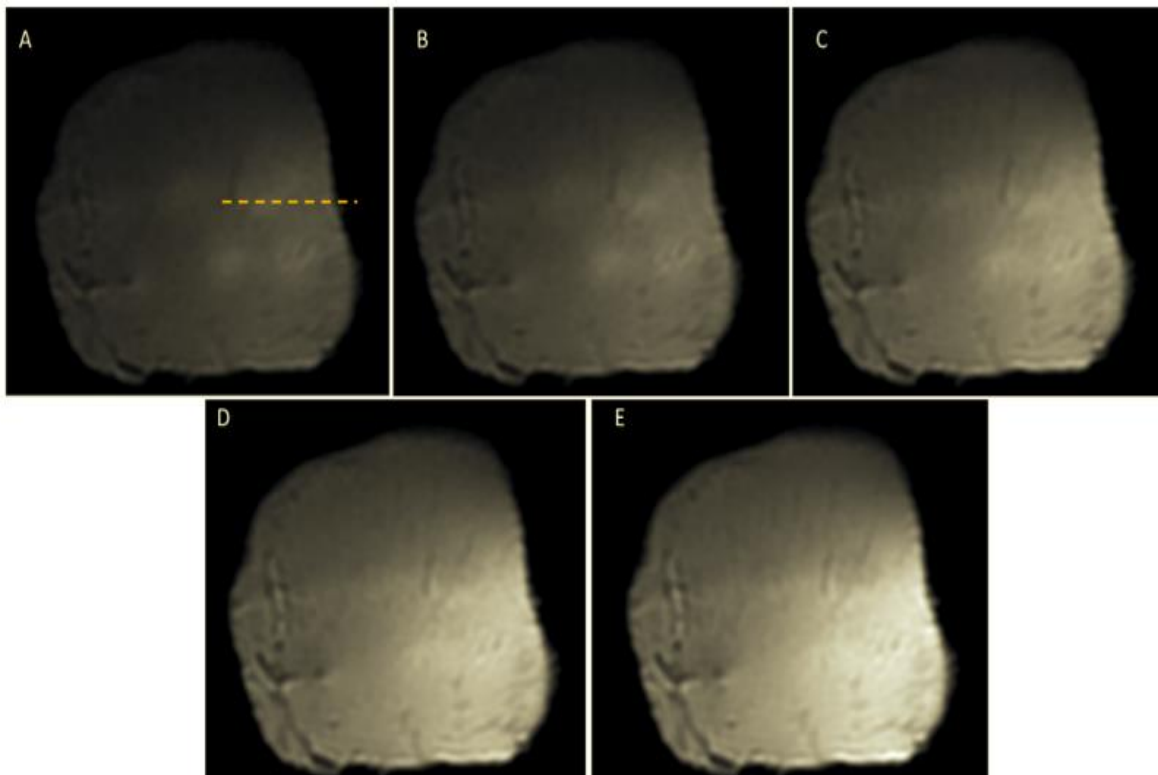


Figure 149: Axial T1-W FSE images (ETL=2, TE=200 ms) of 6 lesions inflicted on excised pork tissue after sonications with a 1.1 MHz transducer (D=50 mm, ROC=80 mm) using acoustic power of 77.5 W for sonication times of 30 s and 60 s at 30 mm focal depth. Images acquired with varied TR of A) 300 ms, B) 400 ms, C) 600 ms, D) 800 ms, and E) 1000 ms.

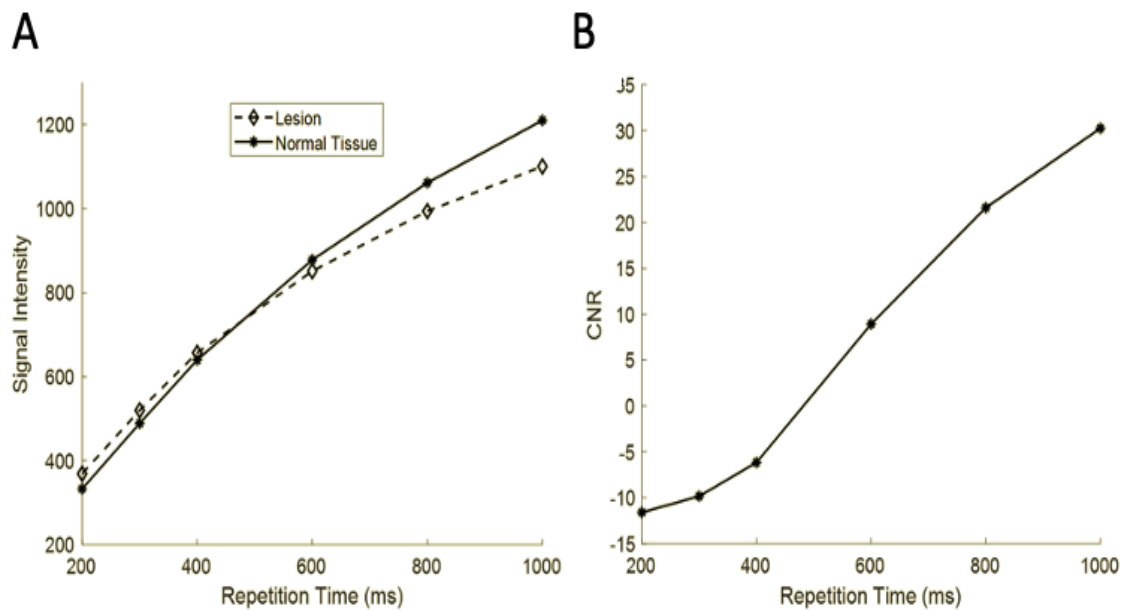


Figure 150: A) Signal intensity of lesion and surrounding normal tissue as measured from T1-W FSE images (ETL=2, TE=200 ms) acquired with varied TR (300, 400, 600, 800, and 1000 ms), and B) CNR between lesion and surrounding unaffected tissue against varied TR (300, 400, 600, 800, and 1000 ms).

The dimensions (diameter and length) of the formed lesions were measured with a ruler as shown in Figure 151. Additionally, dimensions of the lesions were also measured from the acquired T1-W and T2-W FSE images and compared to the dimensions measured with the ruler as shown in Table 52.

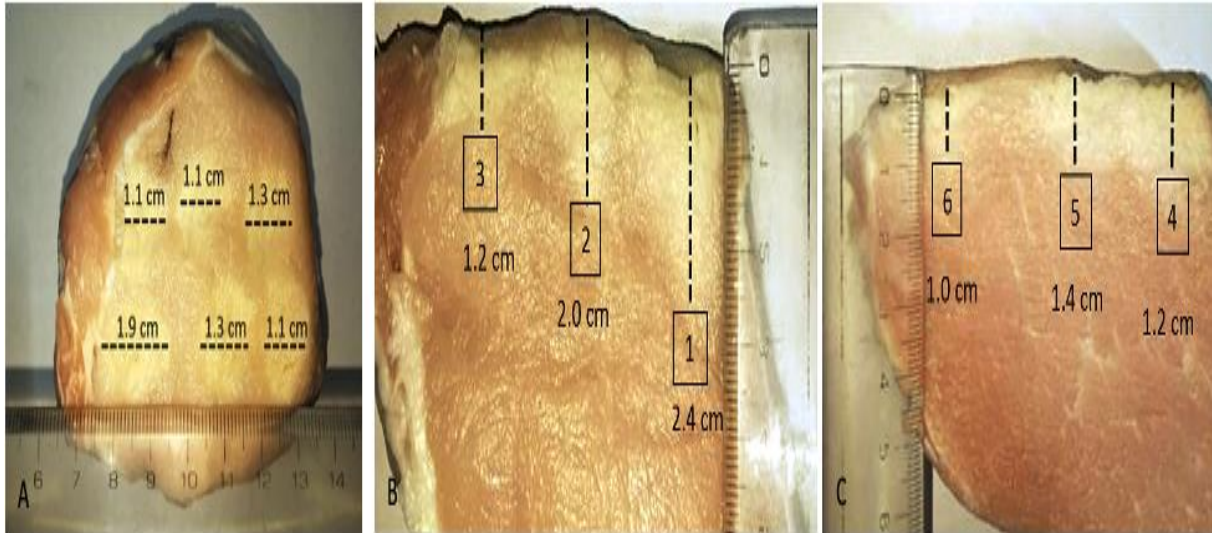


Figure 151: Photo of lesions formed on excised tissue after sonications with a 1.1 MHz transducer ($D=50$ mm, $ROC=80$ mm) in a 2×3 grid using acoustic power of 77.5 W for sonication times of 30 s and 60 s at 30 mm focal depth. A) Dimensions of lesions on a plane perpendicular to the beam, B) Dimensions of lesions 1, 2 and 3 on a plane parallel to the beam, and C) Dimensions of lesions 4, 5 and 6 on a plane parallel to the beam.

Table 52: Dimensions of lesions formed on excised tissue after sonications in a 2×3 grid with a 1.1 MHz transducer ($D=50$ mm, $ROC=80$ mm) at a 30 mm focal depth as measured with a ruler and from T1-W FSE and T2-W FSE images.

Lesion	Acoustic power (W)	Sonication time (s)	Diameter (mm)			Length (mm)		
			T1-W FSE	T2-W FSE	Ruler	T1-W FSE	T2-W FSE	Ruler
1	77.5	60	10	11	11	16	17	24
2			12	11	11	12	13	20
3			14	15	13	-	11	12
4		30	11	14	19	8	9	12
5			11	9	12	11	13	14
6			11	10	11	11	8	10

Subsection Conclusions

In this experiment two sequences, namely T1-W and T2-W FSE, were employed to generate high spatial resolution images of lesions inflicted on excised tissue after sonications. Following a series of image acquisitions, the sequence parameters were adjusted for optimal contrast between the lesion and the surrounding unaffected tissue. Regarding T2-W images, the ROI analysis for optimal ETL selection (Figure 143) suggested that the higher the ETL the lower the CNR (Figure 144). Moreover, SI measurements of lesions and normal tissue remained stable across varied ETL, however, with higher ETL resulting in image blurring. This suggests that a shorter ETL offers higher CNR, while longer ETL results in more T2-weighting. Based on these facts, an ETL of 12 was considered optimal. Correspondingly, higher TE resulted in higher CNR between the lesion and normal tissue (Figure 146), with a TE between 88-110 ms providing the optimal CNR. With respect to T1-W images acquired with varied ETL (Figure 147), longer ETL resulted in higher CNR (Figure 148). However, longer ETL resulted in increased image blurring (Figure 147), thus an ETL of 2 was considered optimal for maximum CNR. In this regard, T1-W images acquired with varied TR (Figure 149) showed that longer TR results in higher CNR (Figure 150). Nevertheless, at TR less than 600 ms the SI of the lesion was higher than normal tissue (Figure 150) but at TR>600 ms there was a signal swap that causes image weighting to move away from T1. In this regard, a TR between 200-300 ms should be optimal for adequate CNR on T1-W images. Additionally, a general underestimation of the dimensions of the formed lesions was observed in MR image measurements compared to the ruler-measured dimensions (Table 52). This might be attributed to the choice of slice within the imaging volume, sensitivity of the imaging technique, image quality, etc. Generally, the T2-W images achieved a higher CNR compared to T1-W images with maximum CNR of 48 and -11.6 respectively. The current parameters for both T1-W and T2-W protocols can be used and further optimized in the future for fine tuning the sequence in terms of contrast between the lesion and normal tissue. The respective values for TR and TE, should however remain within the range proposed, to maintain the desired T1 and T2 Weighting.

Assessment of the SOUNDPET version 2 robotic system during grid sonications on a tumor-like agar phantom

The purpose of this experiment was to assess the motion of the robotic system during grid sonications, as well as the quality of the MR images acquired during the sonications. The SOUNDPET robot (version 2) was positioned on the table of the 1.5 T MRI scanner (Signa HD16, GE Healthcare). An agar-based phantom (4 % w/v agar) with a tumor-like material (6 % w/v agar, 4 % w/v silica, 30 % v/v milk) in the centre was positioned on the acoustic window of the robotic system and a body coil (Signa 1.5 T 12 Channel, GE Healthcare) was placed on top for MR image acquisition as shown in Figure 152. The transducer ($f=1.1$ MHz, $D=50$ mm, $ROC=80$ mm) integrated within the robotic system was connected to an amplifier (AG1016, T & C Power Conversion) for powering purposes.



Figure 152: Experimental set-up inside the 1.5 T MRI scanner with the SOUNDPET robot (version 2) (i) positioned on the MRI table with a tumor-like (6 % w/v agar, 4 % w/v silica, 30 % v/v milk) agar-based (4 % w/v agar) phantom (ii) placed on the acoustic window and a body coil (iii) placed on top for MR image acquisition.

Movement of the robotic device was initiated in 5×4 and 2×2 patterns with a 5 mm step for grid sonications using an acoustic power of 81.25 W for a sonication time of 9 s at 30 mm focal depth. A T1-W FSE sequence was used with specific parameters (TR=200 ms, TE=17 ms, FOV=300×300 mm², Slice thickness=10 mm, Matrix=192×128, ETL=5, NEX=2, Flip angle=90°, Pixel bandwidth=27 Hz/pixel) for imaging the thermal heating at the focal spot during sonications.

Results

Figure 153 shows the T1-W FSE images acquired during the 5×4 grid sonications showing thermal heating as a black spot at the 20 points (white arrows). In 4 out of 20 sonications, thermal heating could not be detected. Correspondingly, Figure 154 shows the T1-W FSE images acquired during the 2×2 sonications. Notably, thermal heating could not be detected in the images due to the presence of noise.

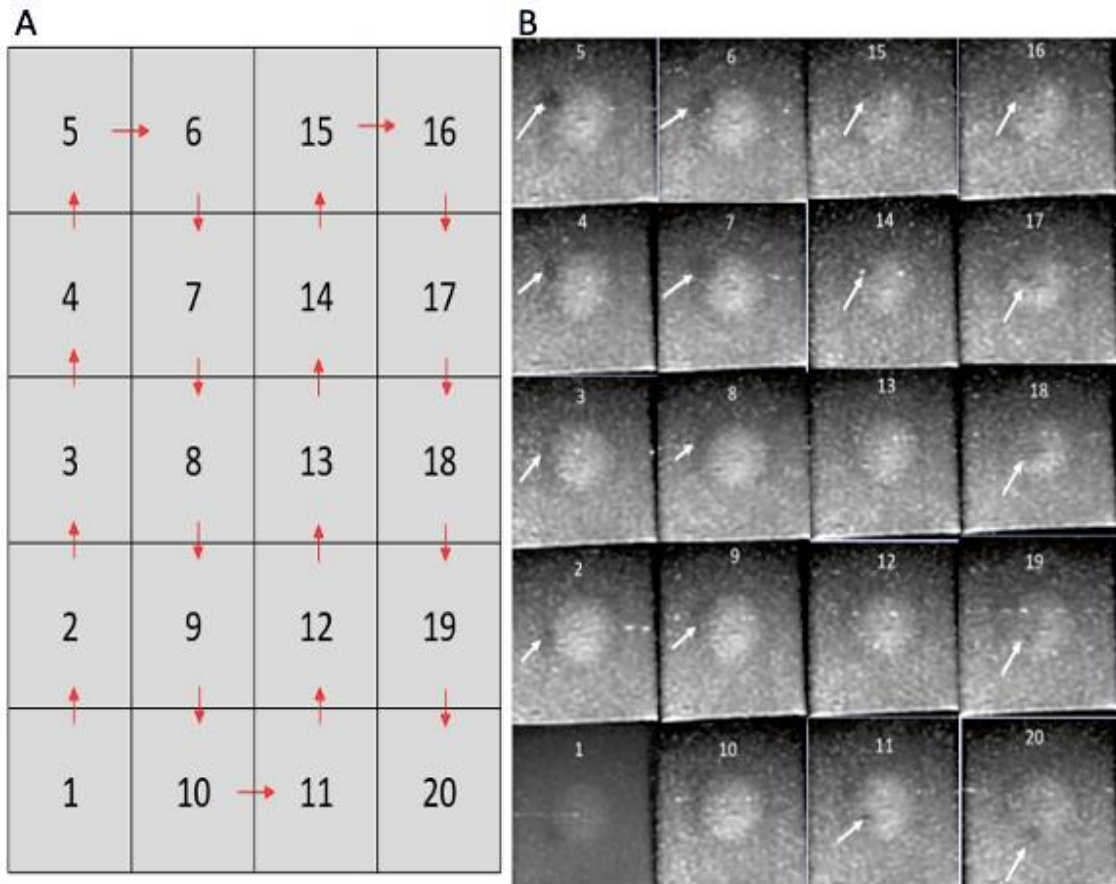


Figure 153: A) Direction of transducer motion for sonications in a 5×4 grid pattern with a 5 mm step, and B) Coronal T1-W FSE images showing thermal heating at the focal spot during the 5×4 grid sonications executed on a tumor-like (6 % w/v agar, 4 % w/v silica, 30 % v/v milk) agar-based phantom (4 % w/v agar) with a 1.1 MHz transducer ($D=50$ mm, $ROC=80$ mm) using an acoustic power of 81.25 W for a sonication time of 9 s at 30 mm focal depth. Arrows indicate thermal heating at the focal spot. Images without arrows indicate inability of heating localisation.

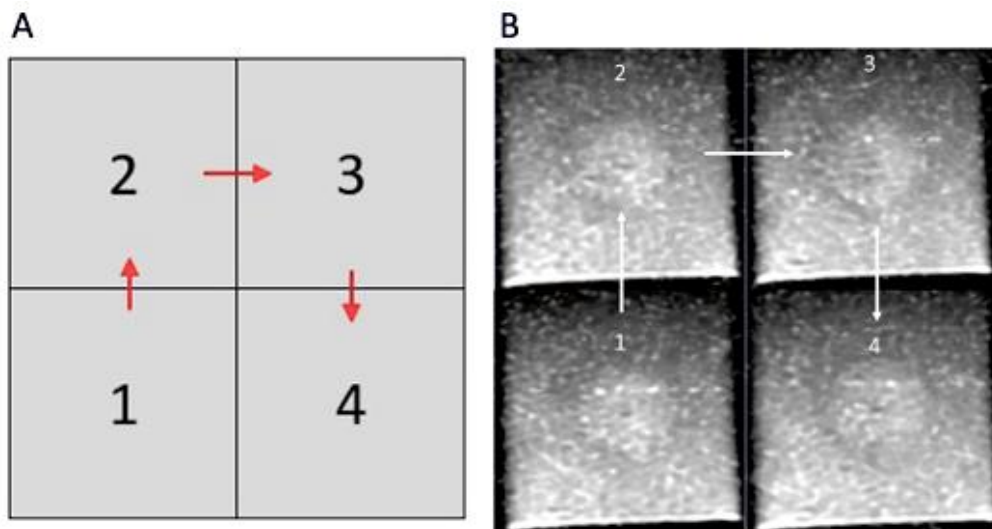


Figure 154: A) Direction of transducer motion for sonications in a 2×2 grid pattern with a 5 mm step, and B) Coronal T1-W FSE images acquired during the 2×2 grid sonications executed on a tumor-like (6 % w/v, 4 % w/v silica, 30 % v/v milk) agar-based phantom (4 % w/v agar) with a 1.1 MHz transducer ($D=50$ mm, $ROC=80$ mm) using an acoustic power of 81.25 W for a sonication time of 9 s at 30 mm focal depth.

Subsection Conclusions

The T1-W FSE MR images of the tumor-like phantom were characterized by low contrast between the tumor-like material and the agar-based background (Figure 153 and Figure 154). This might be attributed to selection of the imaging slice at the edge of the tumor-like material therefore causing partial volume effects. Nevertheless, increased contrast will be observed by modifying the scan parameters. Despite the low contrast, the transducer was accurately guided to the tumor-like material for execution of the grid sonications. The images acquired during sonications were characterised with noise artifacts and low quality, therefore making imaging of the thermal heating difficult. Specifically, heating could not be detected in 4 out of 20 sonications in the 5×4 grid (Figure 153), while heating was not detected in any of the 4 points of the 2×2 grid (Figure 154). Due to the low signal intensity in the images, sonication planning presented difficulties, with the grid not covering the entire tumor-like material. As a result, the step movement of the robotic motion could not be measured from MR images. Image artifacts could be attributed to vibrations of the phantom during sonications. Future experiments will entail the use of phantoms specifically developed to allow their support on the acoustic window, thus being less prone to vibrations during sonications (subsection: Assessing the performance of a software for MRI guided transducer navigation).

Assessing the performance of a software for MRI guided transducer navigation

The purpose of this experiment was to assess the movement of the robotic device using a software (Deliverable 5.1) developed for robotic motion and sonication parameters control. The SOUNDPET robot (version 2) was positioned on the table of the 1.5 T MRI scanner (Signa HD16, GE Healthcare) as shown in Figure 155A. An agar-based phantom (4 % w/v agar) with a tumor-like material (6 % w/v agar, 4 % w/v silica, 30 % v/v milk) in the centre was placed on the acoustic window of the robot. The phantom was developed with a specific shape as shown in Figure 156 to allow its support on the acoustic opening of the robotic system, thus reducing image artifacts caused by vibrations of the phantom during sonications. A body coil (Signa 1.5 T 12 Channel, GE Healthcare) was positioned on top of the phantom as shown in Figure 155A for MR image acquisition. Figure 155B shows a T1-W FSE image of the experimental set-up. The transducer ($f=2.75$ MHz, $D=50$ mm, $ROC=65$ mm) integrated within the robotic system was connected to an amplifier (AG1016, T & C Power Conversion) for powering purposes.

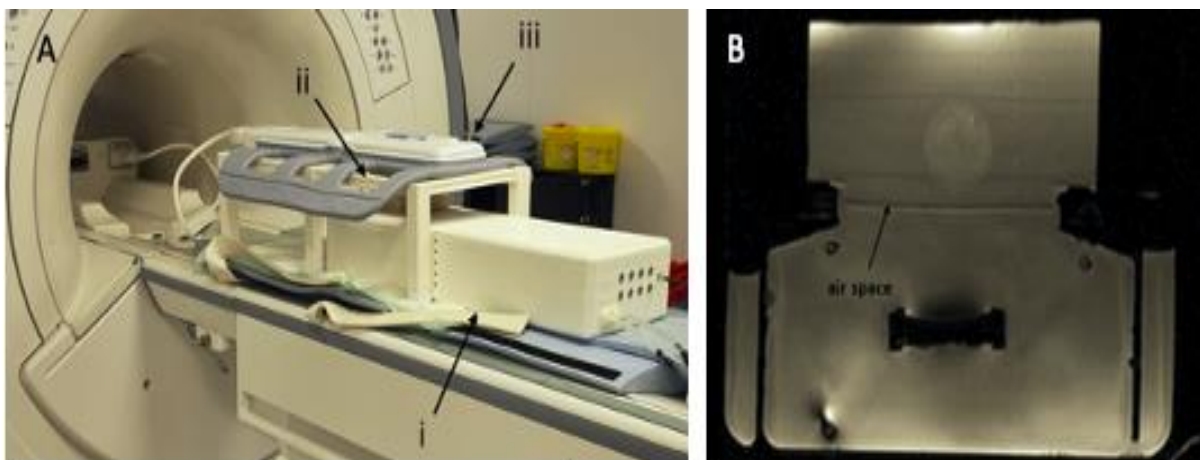


Figure 155: A) Experimental set-up inside the 1.5 T MRI scanner with the SOUNDPET robot (version 2) (i) positioned on the MRI table with a tumor-like (6 % w/v agar, 4 % w/v silica, 30 % v/v milk) agar-based (4 % w/v agar) phantom (ii) placed on the acoustic window and a body coil (iii) placed on top for MR image acquisition, and B) Axial T1-W FSE image of the experimental set-up.



Figure 156: Agar-based phantom (4 % w/v agar) featuring a tumor-like material (6 % w/v agar, 4 % w/v silica, 30 % v/v milk) in the centre developed with specific shape to allow its support on the acoustic opening of the robotic system.

The software was connected, through cables, to the robot and was used for robotic movement and ultrasonic parameters control. Specifically, it was used to assess navigation of the transducer to the target (tumor-like material of the agar-based phantom). The software was used for robotic movement in the X and Y axes with a T1-W FSE sequence (TR=400 ms, TE=15 ms, FOV=280×280 mm², Slice thickness=8 mm, Matrix=192×192, ETL=5, NEX=4, Flip angle=90°, Pixel bandwidth=6 Hz/pixel) used for image acquisition prior and after movement to assess the location of the transducer relative to the tumor-like material.

After robotic movement, sonications were executed on the phantom using acoustic power in the range of 45-60 W for sonication times of 20-120 s at 20 mm focal depth. During sonications an SPGR sequence (TR=22 ms, TE=8 ms, FOV=280×280 mm², Slice thickness=8 mm, Matrix=192×160, ETL=1, NEX=2, Flip angle=30°, Pixel bandwidth=12 Hz/pixel) was used to image the thermal heating at the focal spot.

Results

Initially, sonications were executed on the agar-based phantom using acoustic power of 45 W and 60 W for sonication times of 20 s and 30 s, respectively. Thermal heating during sonications was clearly visible on acquired SPGR images as shown in Figure 157.

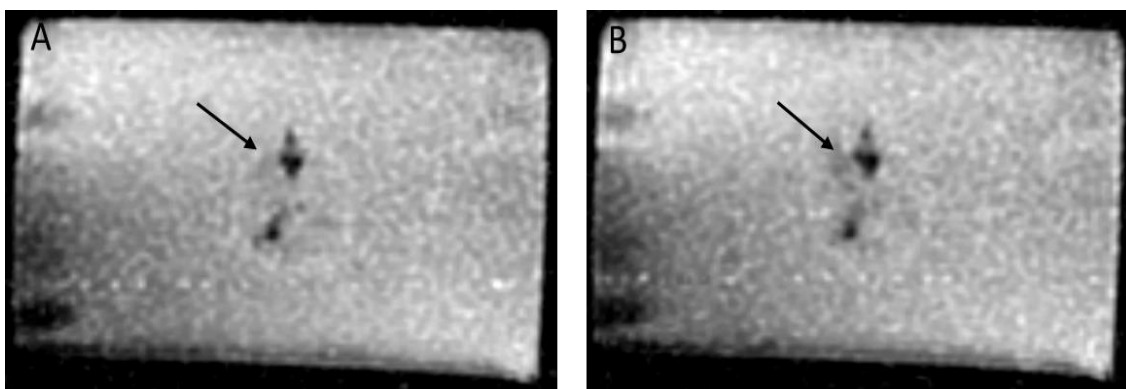


Figure 157: Coronal SPGR images of an agar-based phantom (4 % w/v agar) with a tumor-like material (6 % w/v agar, 4 % w/v silica, 30 % v/v milk) acquired during sonications with a 2.75 MHz transducer (D=50 mm, ROC=65 mm) at 20 mm focal depth using A) acoustic power of 45 W for a sonication time of 20 s, and B) acoustic power of 60 W for a sonication time of 30 s. Arrows indicate thermal heating.

The software was used to initiate motion of the transducer 8 mm forward in the X axis and 25 mm left in the Y axis. Figure 158 shows the T1-W FSE images acquired prior motion (Figure 158A) and after motion (Figure 158B). Moreover, Figure 158C shows the location of the transducer (green spot) after motion relative to the tumor-like material. After motion, sonications were executed at acoustic power of 54 W for a sonication time of 120 s with the thermal heating imaged on SPGR images as shown in Figure 159.

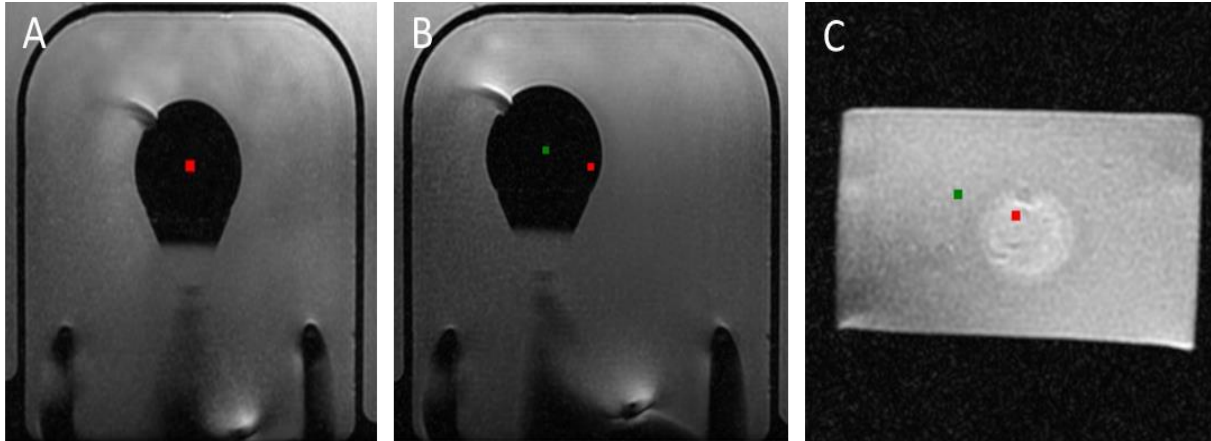


Figure 158: Coronal T1-W FSE images acquired at different transducer positions of the SOUNDPET robot version 2. A) Image acquired at initial position (red spot) of the transducer, B) Image acquired showing transducer position (green spot) relative to initial location (red spot) after motion (8 mm forward in X axis, 25 mm left in Y axis), and C) Image acquired showing transducer position (green spot) relative to its initial (red spot) location and the tumor-like material.

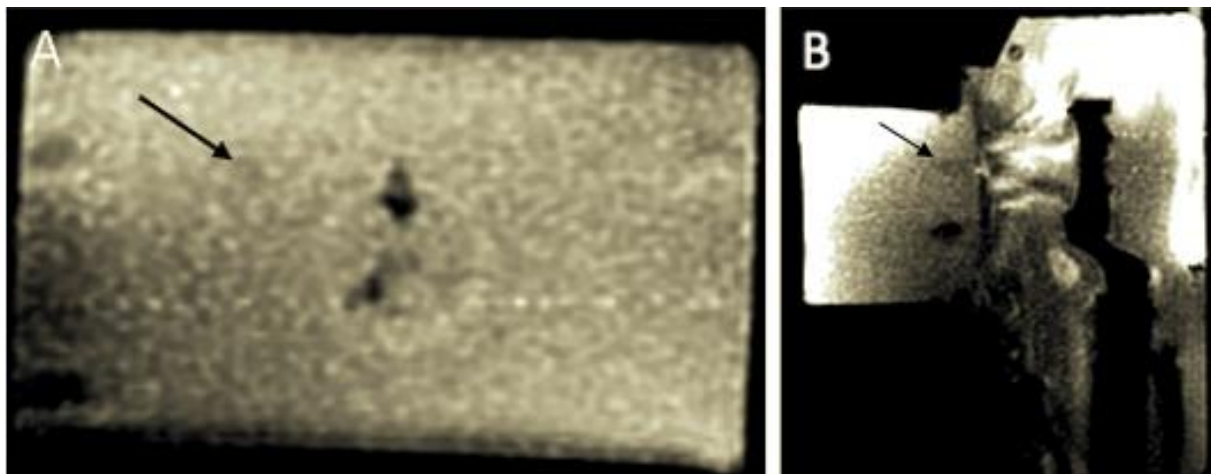


Figure 159: SPGR images of an agar-based phantom (4 % w/v agar) with a tumor-like material (6 % w/v agar, 4 % w/v silica, 30 % v/v milk) acquired during sonications with a 2.75 MHz transducer ($D=50$ mm, $ROC=65$ mm) using acoustic power of 54 W for a sonication time of 120 s at 20 mm focal depth. A) Coronal plane, and B) Sagittal plane. Arrows indicate thermal heating.

Robotic motion was also initiated 21 mm backwards in the X axis and 19 mm left in the Y axis. Figure 160 shows the T1-W FSE images acquired prior motion (Figure 160A) and after motion (Figure 160B), translating the location of the transducer relative to the tumor-like material (Figure 160C). After motion, the motion cables were disconnected from the robot and sonications were executed at acoustic power of 54 W for a sonication time of 120 s, with the thermal heating within the tumor-like material imaged on SPGR images as shown in Figure 161 and Figure 162.

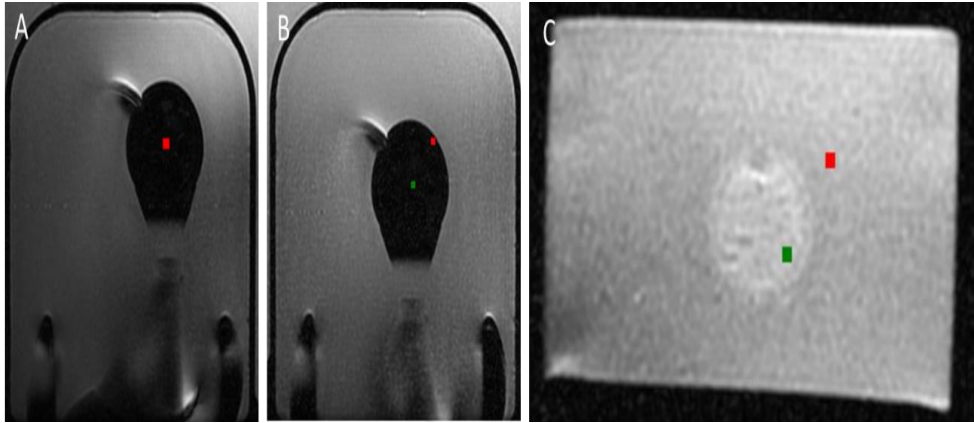


Figure 160: Coronal T1-W FSE images acquired at different transducer positions of the SOUNDPET robot version 2. A) Image acquired at initial position (red spot) of the transducer, B) Image acquired showing transducer position (green spot) relative to initial location (red spot) after motion (21 mm backwards in X axis, 19 mm left in Y axis), and C) Image acquired showing transducer position (green spot) relative to its initial (red spot) location and the tumor-like material.

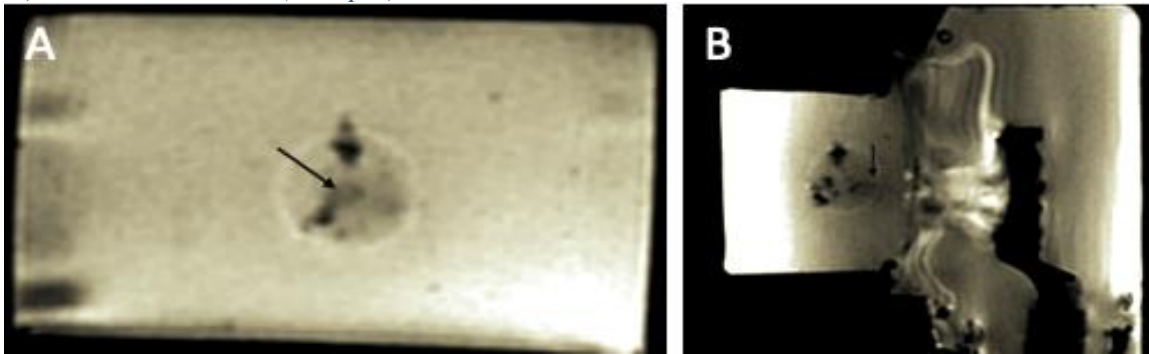


Figure 161: SPGR images of an agar-based phantom (4 % w/v agar) with a tumor-like material (6 % w/v agar, 4 % w/v silica, 30 % v/v milk) acquired with motion cables disconnected from the robot during sonications with a 2.75 MHz transducer ($D=50$ mm, $ROC=65$ mm) at acoustic power of 54 W for a sonication time of 120 s at 20 mm focal depth. A) Coronal plane, and B) Sagittal plane. Arrows indicate thermal heating.

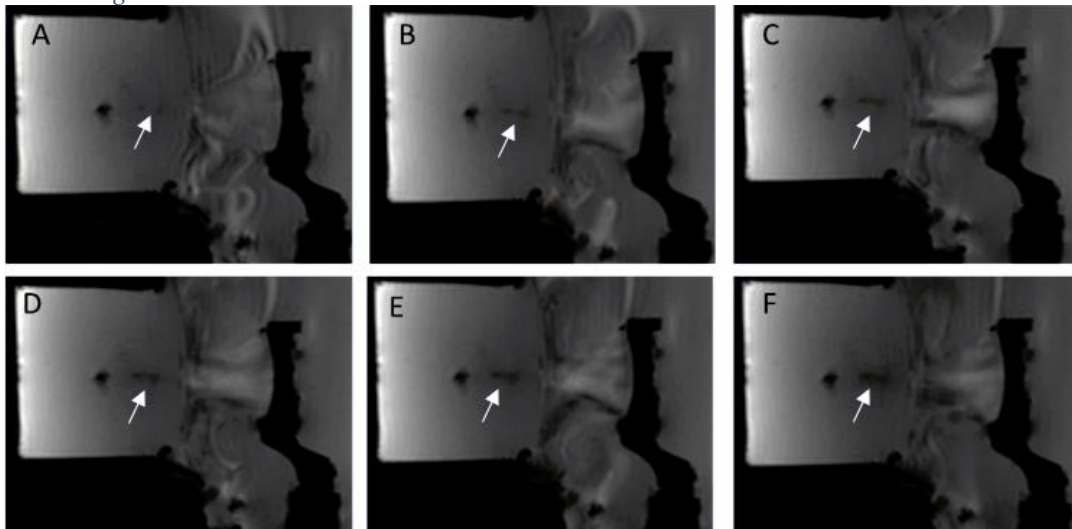


Figure 162: Sagittal SPGR images of an agar-based phantom (4 % w/v agar) with a tumor-like material (6 % w/v agar, 4 % w/v silica, 30 % v/v milk) acquired with motion cables disconnected from the robot at different timepoints during sonications with a 2.75 MHz transducer ($D=50$ mm, $ROC=65$ mm) at acoustic power of 54 W for a sonication time of 120 s at 20 mm focal depth showing the evolution of thermal heating (white arrows). Images acquired at A) 7 s of sonication, B) 14 s of sonication, C) 21 s of sonication, D) 28 s of sonication, E) 36 s of sonication, and F) 43 s of sonication.

Subsection Conclusions

Looking at Figure 158 and Figure 160, accurate transducer navigation to the target was achieved, with robotic motion initiated using the first version of the software. Moreover, thermal heating at the focal spot was clearly visible in both coronal (Figure 157, Figure 159 and Figure 161) and sagittal (Figure 159, Figure 161 and Figure 162) SPGR images acquired during sonications. Nevertheless, SPGR images acquired during sonications after disconnection of the robot motion cables (Figure 161 and Figure 162) resulted in increased SNR and less artifacts. Specifically, SNR was measured at 86 for images acquired with the cables disconnected compared to an SNR of 15.8 measured for images acquired with the motion cables connected. Additionally, employment of the body coil for MR image acquisition resulted in good quality images without any noticeable artifacts acquired during activation of the transducer, compared to artifacts present in such images acquired with other coil types during sonications (section: Assessment of the effect of the imaging coil in thermal heating detection).

Assessing the performance of a new software for MRI monitoring and planning

The purpose of the experiment was to assess the movement of the robotic device during two 3×3 grid operations performed with different ultrasonic parameters. The SOUNDPET robot (version 2) was placed on the table of the 1.5 T MRI scanner (Signa HD16, GE Healthcare) as shown in Figure 163. A piece of excised pork tissue was placed on the acoustic window of the robot with a body coil (Signa 1.5 T 12 channel, GE Healthcare) accommodated on top for MR image acquisition (Figure 163). The 2.75 MHz transducer (D=50 mm, ROC=65 mm) integrated within the robot was connected to an amplifier (AG1016, T & C Power Conversion).



Figure 163: Experimental set-up inside the 1.5 T MRI scanner with the SOUNDPET robot (version 2) positioned on the MRI table with a piece of excised pork tissue placed on the acoustic window and a body coil accommodated on top for MR image acquisition.

The HIFU software (Deliverable 5.1) was used to control the robotic motion and the ultrasonic parameters. The software allows treatment planning on MR images as shown in Figure 164 and initiates robotic motion according to the planned sonication area.



Figure 164: Screenshot of the software used in the experiment allowing treatment planning on MR images and execution of robotic motion based on the planned sonication area.

The software was used to initiate robotic motion and execute the grid sonications based on the treatment plan. Two 3×3 grid sonications were performed with a step movement of 10 mm between successive points. Sonications in the first 3×3 grid (Grid 1) were performed using an acoustic power of 45 W for a sonication time of 60 s at 20 mm focal depth. Sonications in the second 3×3 grid (Grid 2) were executed using an acoustic power of 60 W for a sonication time of 100 s at 20 mm focal depth. Both grid sonications were imaged using a T1-W FSE sequence (TR=300 ms, TE=11 ms, FOV=280×280 mm², Slice thickness=10 mm, Matrix=128×128, ETL=1, NEX=1, Flip angle=90°, Pixel bandwidth=32 Hz/pixel) and a T2-W FSE sequence (TR=2000 ms, TE=10, 30, 50, 60, or 70 ms, FOV=280×280 mm², Slice thickness=10 mm, Matrix=224×192, ETL=1, NEX=2, Flip angle=90°, Pixel bandwidth=27 Hz/pixel) for monitoring thermal heating within the tissue and visualizing the formed lesions.

Results

Initially, T2-W FSE images were acquired as shown in Figure 165 for localising the transducer relative to the excised tissue. The process of transducer localisation is fully explained in the software deliverable (Deliverable 5.1).

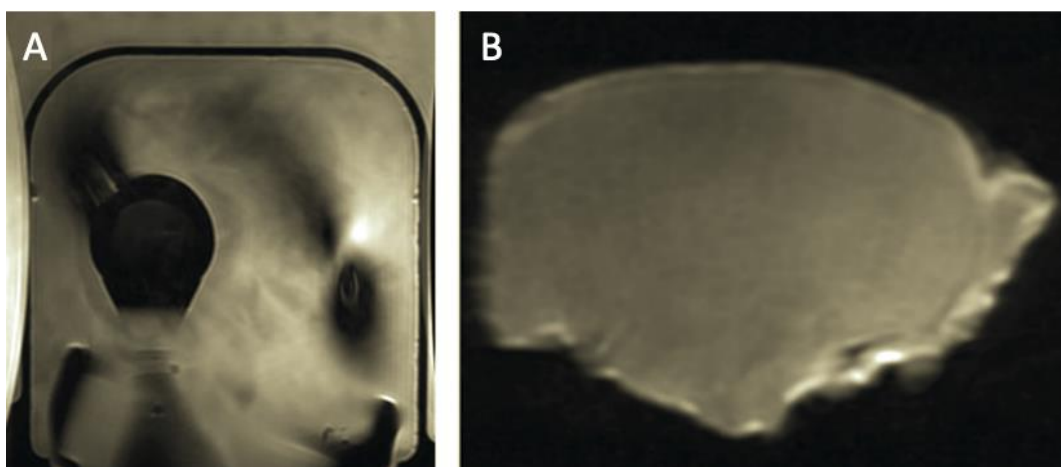


Figure 165: Coronal T2-W FSE images acquired for transducer positioning. Image acquired with A) the slice located at the surface of the transducer, and B) the slice located at 65 mm (focus) from the transducer.

After transducer localisation, treatment planning for the two 3×3 grid patterns was performed on the acquired MR images of the excised tissue as shown in Figure 166. The two 3×3 grid sonications were executed according to the planned paths and their corresponding ultrasonic parameters.

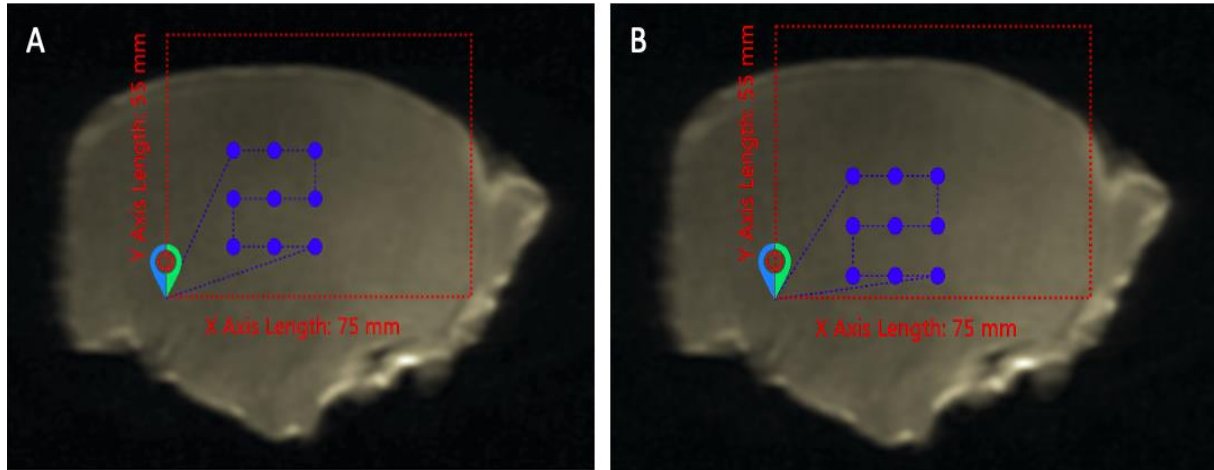


Figure 166: Sonication path for movement of the robot in a 3×3 grid pattern with a 10 mm step as planned on MR images of excised pork tissue using the second version of the software. A) Grid 1, and B) Grid 2.

Figure 167 and Figure 168 show the T1-W and T2-W FSE images acquired during Grid 1 (45 W for 60 s) and Grid 2 (60 W for 100 s) operations respectively, showing the thermal heating at the focal spots.

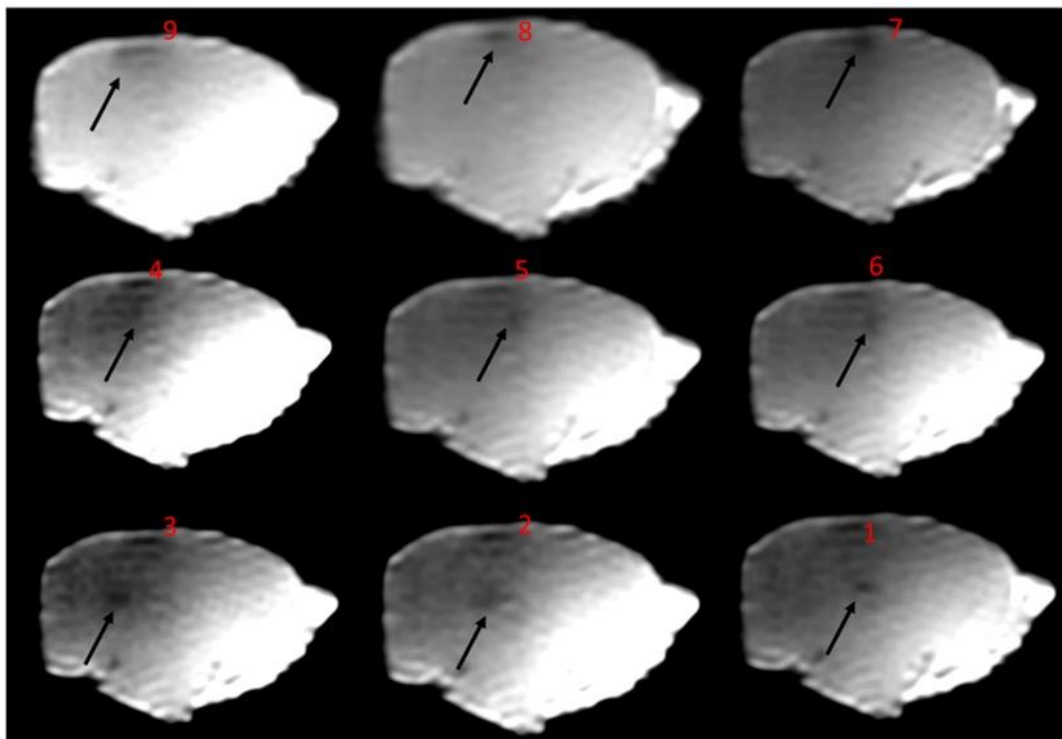


Figure 167: Coronal T1-W FSE images showing thermal heating at the focal spot (black arrows) during sonications on excised pork tissue in a 3×3 grid pattern with a 10 mm step using a 2.75 MHz transducer ($D=50$ mm, $ROC=65$ mm) at acoustic power of 45 W for a sonication time of 60 s at 20 mm focal depth (Grid 1).

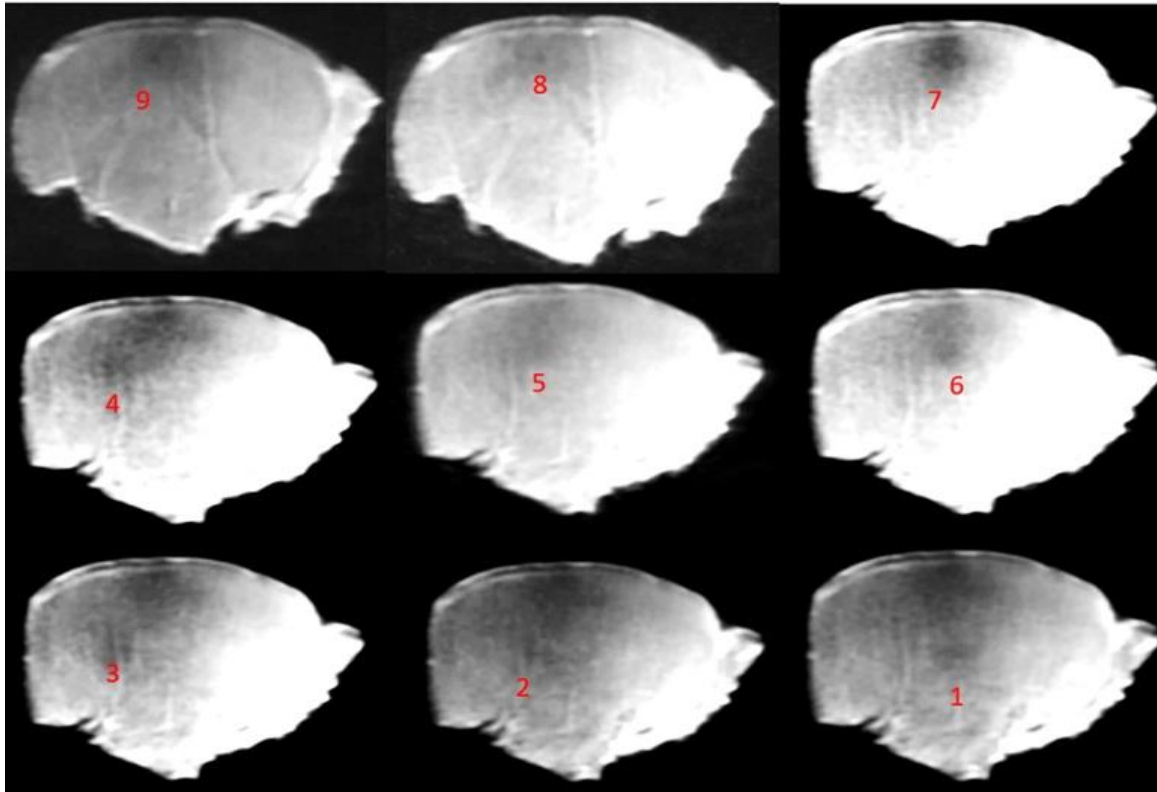


Figure 168: Coronal T2-W FSE images showing thermal heating at the focal spot (red numbers) during sonications on excised pork tissue in a 3×3 grid pattern with a 10 mm step using a 2.75 MHz transducer ($D=50$ mm, $ROC=65$ mm) at acoustic power of 60 W for a sonication time of 100 s at 20 mm focal depth (Grid 2).

After the two grid operations, a T2-W FSE axial image was acquired as shown in Figure 169 for imaging the lesions inflicted as a result of the sonications. Additionally, several T1-W and T2-W images were acquired in coronal plane using varied parameters as shown in Figure 170. After the experiments, the excised tissue was sliced at 20 mm (focal depth) and the formed lesions were measured in planes perpendicular and parallel to the beam as shown in Figure 171.

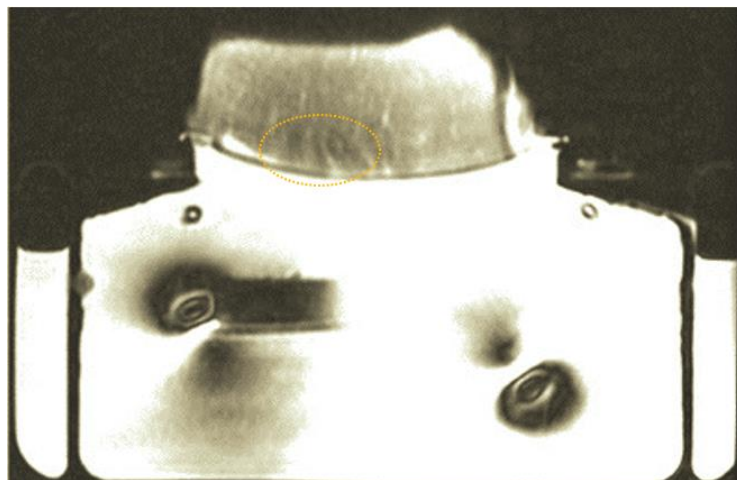


Figure 169: Axial T2-W FSE image of excised pork tissue acquired with $TE=50$ ms to visualize lesions formed after sonications in a 3×3 grid pattern with a 10 mm step using a 2.75 MHz transducer ($D=50$ mm, $ROC=65$ mm) at acoustic power of 45 W and 60 W for sonication times of 60 s (Grid 1) and 100 s (Grid 2) respectively, at 20 mm focal depth. Yellow circle indicates lesions.

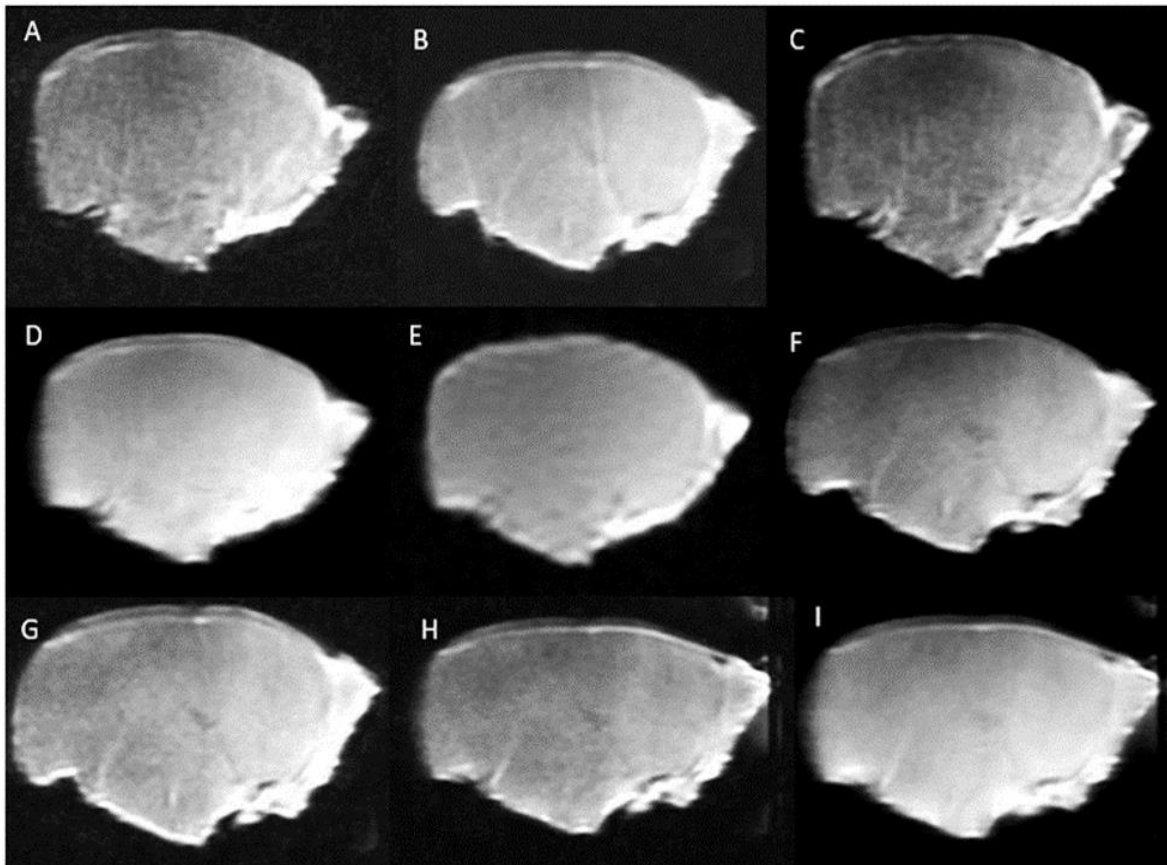


Figure 170: Coronal images of excised pork tissue acquired after sonications in a 3×3 grid pattern with a 10 mm step using a 2.75 MHz transducer ($D=50$ mm, $ROC=65$ mm) at acoustic power of 45 W and 60 W for sonication times of 60 s (Grid 1) and 100 s (Grid 2) respectively, at 20 mm focal depth. A) T2-W FSE image acquired with $TE=60$ ms, B) T2-W FSE image acquired with $TE=30$ ms, C) T2-W FSE image acquired with $TE=70$ ms, D) T2-W FSE image acquired with $TE=10$ ms, E) T1-W FSE image acquired with $TR=300$ ms, F) T2-W FSE image with fat suppression acquired with $TE=10$ ms, G) T2-W FSE image with fat suppression acquired with $TE=50$ ms, H) T2-W FSE Oblique image with fat suppression acquired with $TE=50$ ms, and I) T2-W FSE Oblique image with fat suppression acquired with $TE=10$ ms.

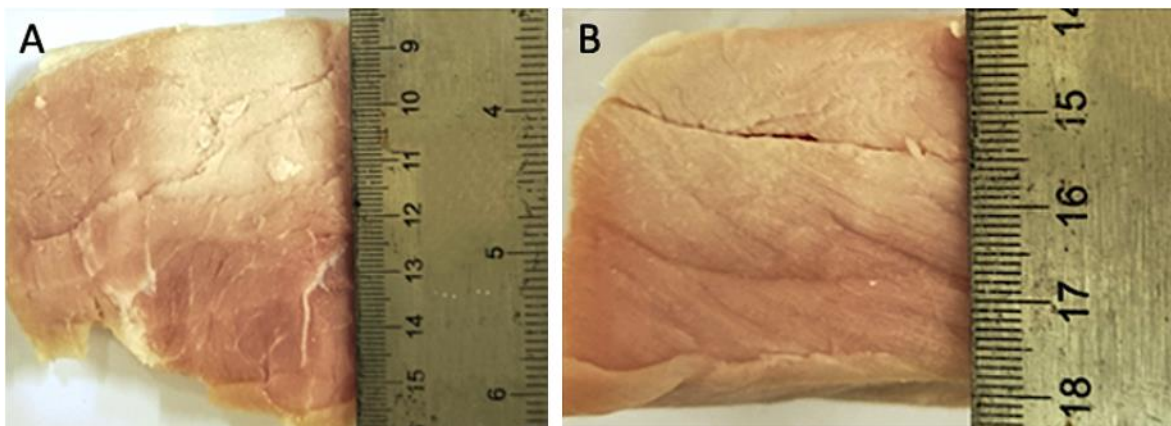


Figure 171: Photo of overlapping lesions formed on excised pork tissue after sonications with a 2.75 MHz transducer ($D=50$ mm, $ROC=65$ mm) in two 3×3 grids using acoustic power of 45 W for a sonication time of 60 s (Grid 1) and acoustic power of 60 W for a sonication time of 100 s (Grid 2) at 20 mm focal depth. A) Lesions formed in plane perpendicular to the beam, and B) Lesions formed in plane parallel to the beam.

Subsection Conclusions

From Figure 167 and Figure 168, it was observed that MRI-based treatment planning and monitoring executed with the new software was effective and provides superior accuracy of transducer movement compared to the previous software. Thermal heating at all focal spots was clearly visible on the acquired images for both Grid 1 (Figure 167) and Grid 2 (Figure 168) sonications.

Three lesions of the same grid row were visible on the axial T2-W FSE image acquired post-sonications (Figure 169). Contrary, coronal T1-W and T2-W FSE images acquired post-sonications had no visible lesions (Figure 170). The overlapping lesion formed as a result of the two grid sonications was found to have an area of $28 \times 30 \text{ mm}^2$, and a length of 26 mm as measured with a ruler at the end of the experiment (Figure 171).

Examining the effect of power on lesion detection based on T1-W and T2-W images

The purpose of this experiment was to assess the effect of the acoustic power on lesion detection using T1-W and T2-W FSE images. Movement of the robotic device was performed for execution of two 3×3 grid sonications using varied acoustical power. The SOUNDPET robot (version 2) was placed on the table of the 1.5 T MRI (Signa HD16, GE Healthcare). A piece of excised pork tissue was placed on the acoustic window of the robot and stabilized with tapes to reduce movement artifacts as shown in Figure 172. A body coil (Signa 1.5 T 12 Channel, GE Healthcare) was placed on top of the experimental set-up for MR image acquisition. The 2.75 MHz transducer (D=50 mm, ROC=65 mm) integrated within the robot was connected to an amplifier (AG1016, T & C Power Conversion).

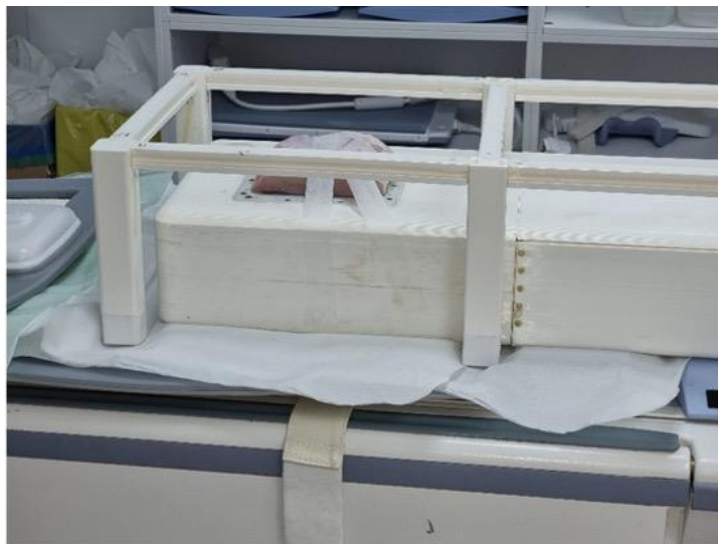


Figure 172: Experimental set-up with the SOUNDPET robot (version 2) positioned on the table of the 1.5 T MRI scanner with a piece of excised pork tissue placed on the acoustic window and stabilized with tapes to reduce movement artifacts.

The second version of the software (Deliverable 5.1) was used to control the robotic movement and the sonication parameters. Robotic motion was initiated in two 3×3 grids using a 10 mm step between successive grid points. Sonications during the first 3×3 grid operation (Grid 1)

were executed at an acoustic power of 30 W for a sonication time of 60 s at 20 mm focal depth. A T1-W FSE Fat suppression (FS) sequence (TR=300 ms, TE=11 ms, FOV=260×260 mm², Slice thickness=10 mm, Matrix=128×128, ETL=1, NEX=1, Flip angle=90°, Pixel bandwidth=32 Hz/pixel) was used for imaging the thermal heating during Grid 1 sonications.

Similarly, sonications during the second 3×3 grid operation (Grid 2) were performed at an acoustic power of 60 W for a sonication time of 90 s at 20 mm focal depth. A T2-W FSE FS sequence (TR=2000 ms, TE=50 or 100 ms, FOV=260×260 mm², Slice thickness=10 mm, Matrix=224×192, ETL=12, NEX=2, Flip angle=90°, Pixel bandwidth=27 Hz/pixel) was used for imaging during the Grid 2 sonications.

Results

Figure 173 shows the T1-W FSE FS images acquired during Grid 1 sonications (30 W for 60 s). Before the Grid 2 3×3 operation, a single sonication (60 W for 90 s) was performed at the initial (zero) position of the transducer. Thereafter, the grid operation was executed. Figure 174 shows the T2-W FSE FS images acquired during Grid 2 sonications (60 W for 90 s). Grid 2 sonications were sufficient to inflict lesions on the tissue. Coronal T2-W FSE FS images acquired after Grid 2 sonications imaged the formed lesions in a plane perpendicular to the beam as shown in Figure 175.

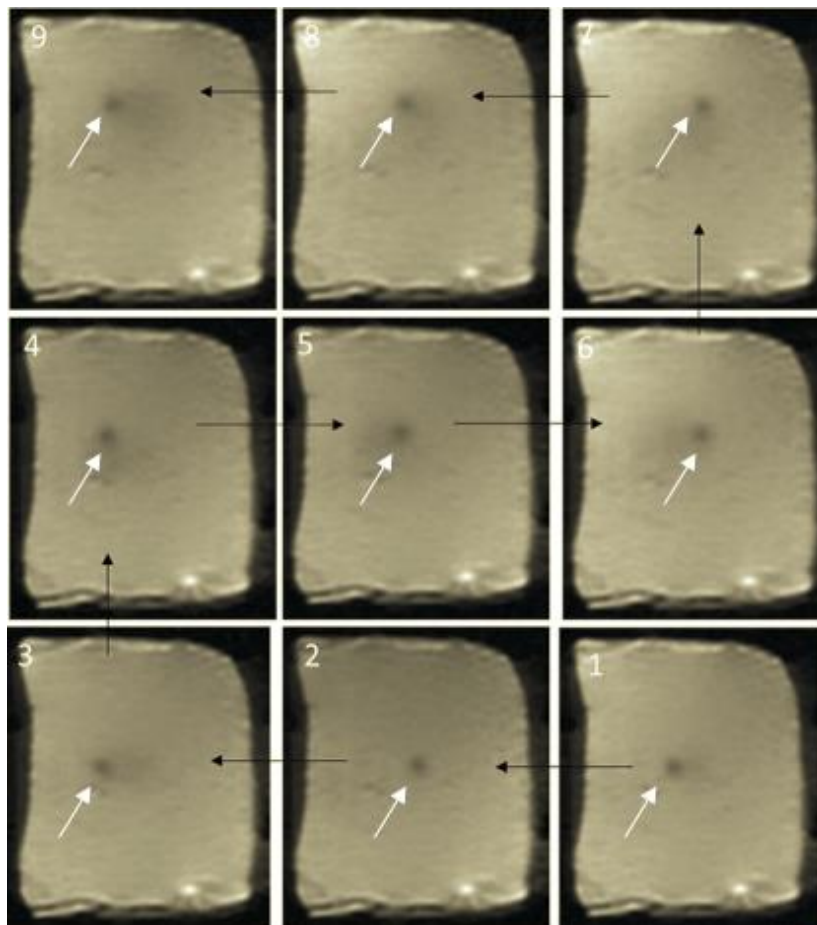


Figure 173: Coronal T1-W FSE FS images acquired during sonications on excised pork tissue in a 3×3 grid pattern with a 10 mm step using a 2.75 MHz transducer (D=50 mm, ROC=65 mm) at acoustic power of 30 W for a sonication time of 60 s at 20 mm focal depth (Grid 1). White arrows indicate thermal heating.

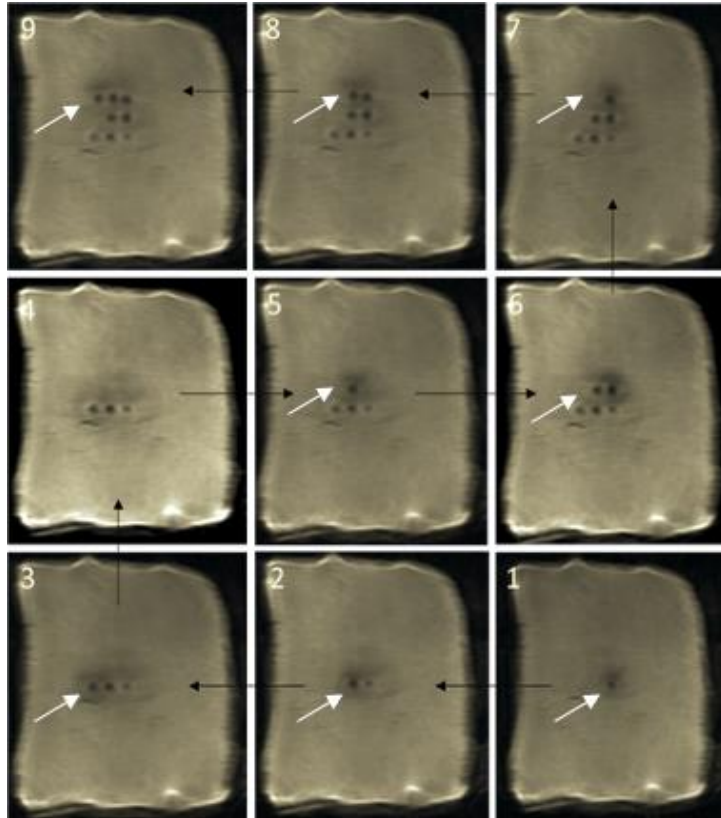


Figure 174: Coronal T2-W FSE FS images acquired with TE=50 ms during sonications on excised pork tissue in a 3×3 grid pattern with a 10 mm step using a 2.75 MHz transducer (D=50 mm, ROC=65 mm) at acoustic power of 60 W for a sonication time of 90 s at 20 mm focal depth (Grid 2). White arrows indicate thermal heating.

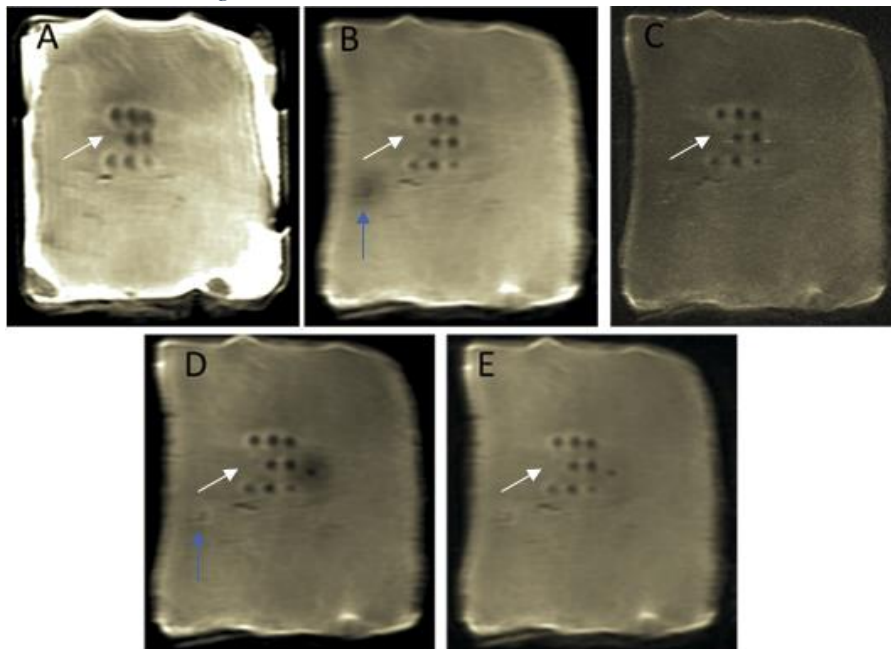


Figure 175: Coronal T2-W FSE FS images acquired after sonications on excised pork tissue in a 3×3 grid with a 10 mm step using a 2.75 MHz transducer (D=50 mm, ROC=65 mm) at acoustic power of 60 W for a sonication time of 90 s at 20 mm focal depth. Images acquired with A) TE=50 ms, B) TE=50 ms showing transducer initial-point lesion (blue arrow), C) TE=100 ms, D) TE=50 ms showing transducer initial-point lesion (blue arrow), and E) TE=50 ms 4 minutes after the previous sonication in order to minimize heating of the beam.

Figure 176 shows the excised pork tissue after the sonications. The tissue was sliced at 10 mm and the lesions formed on a plane perpendicular to the beam were exposed as shown in Figure 176B. Figure 176C, Figure 177A, Figure 177B and Figure 177C show the initial-point, first row, second row and third row lesions respectively, as formed on a plane parallel to the beam. A ruler was used to measure the lesion dimensions (diameter and length) as shown in Table 53.

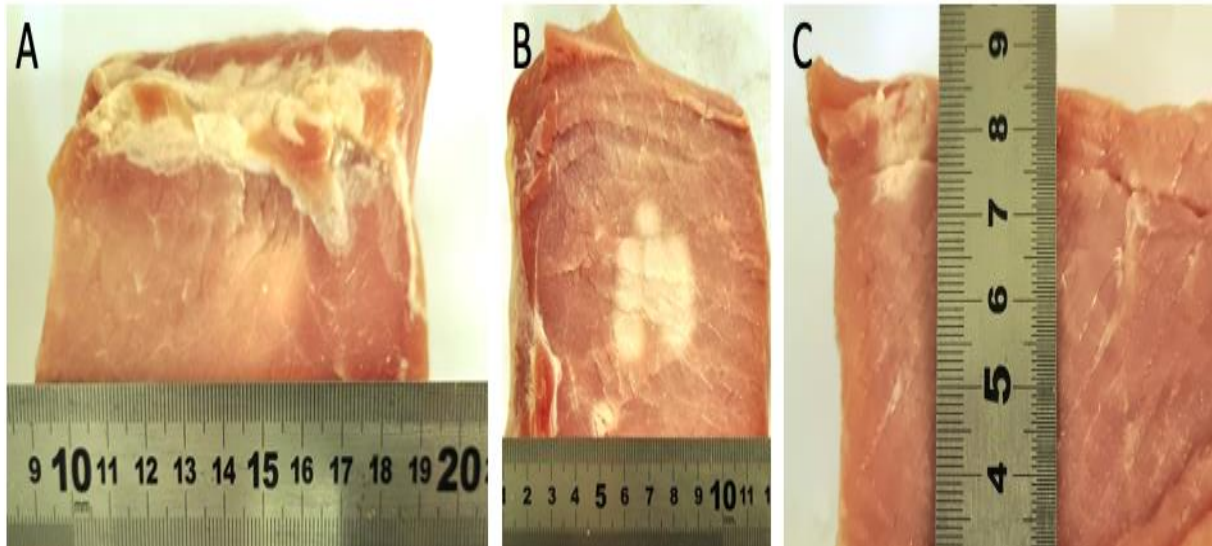


Figure 176: Photo of excised pork tissue after sonications with a 2.75 MHz transducer ($D=50$ mm, $ROC=65$ mm) in a 3×3 grid with a 10 mm step using acoustic power of 60 W for a sonication time of 90 s at 20 mm focal depth (Grid 2). A) Surface of the excised tissue, B) Slice of tissue at 10 mm showing lesions formed on plane perpendicular to the beam, and C) Measurements for initial-point lesion as formed on plane parallel to the beam.

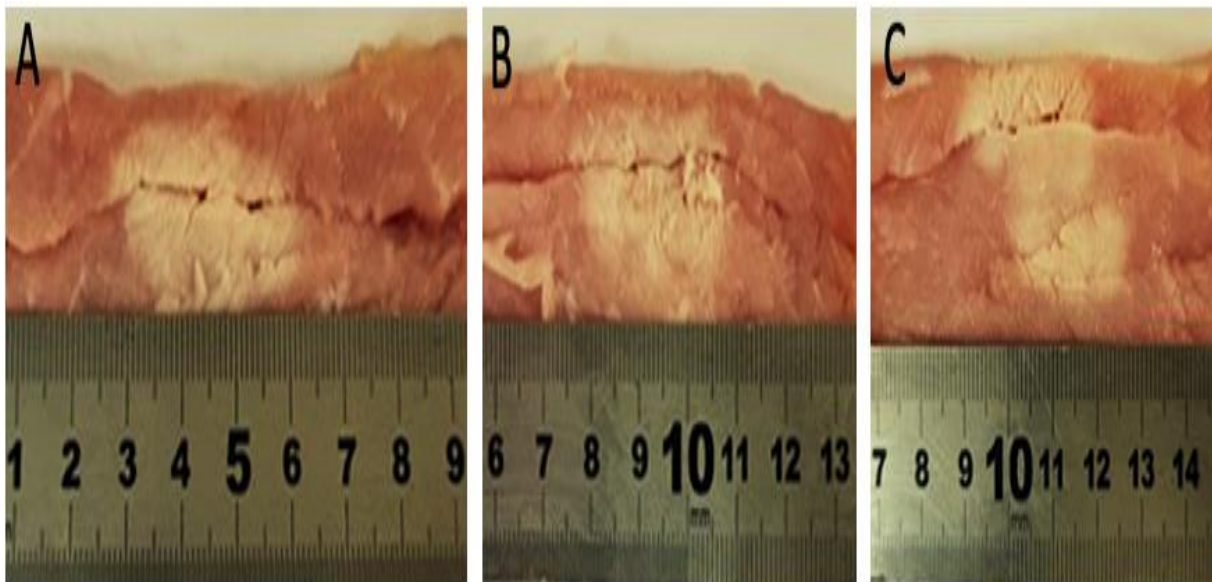


Figure 177: Photo of lesions formed on plane parallel to the beam on excised pork tissue after sonications with a 2.75 MHz transducer ($D=50$ mm, $ROC=65$ mm) in a 3×3 grid with a 10 mm step using acoustic power of 60 W for a sonication time of 90 s at 20 mm focal depth (Grid 2). Measurements for A) first row of lesions, B) second row of lesions, and C) third row of lesions.

Table 53: Dimensions of lesions formed on excised tissue after sonications in a 3×3 grid with a 10 mm step using a 2.75 MHz transducer (D=50 mm, ROC=65 mm) at acoustic power of 60 W for a sonication time of 90 s at 20 mm focal depth (Grid 2).

Lesion	Diameter (mm)	Length (mm)
Initial point	8	13
1	12	11
2	12	12
3	11	10
4	10	14
5	9	14
6	10	14
7	10	11
8	11	13
9	11	13

Subsection Conclusions

MRI plannings with the software were effective and with superior accuracy of transducer movement compared to the first version of the software used in previous experiments. Thermal heating at all nine locations of Grid 1 sonications (30 W for 60 s) was clearly visible in T1-W images (Figure 173). Thermal heating was visible at eight locations of the Grid 2 sonications (60 W for 90 s) in T2-W images (Figure 174). Grid 2 sonication protocol inflicted lesions on the excised tissue, with 8 out of 9 lesions as well as the initial-point lesion clearly visible in T2-W images acquired post-sonication (Figure 175). The lesion at point 4 of Grid 2 was not visible in either the T2-W images (Figure 175) nor the photos (Figure 176B).

Moreover, it was noticed that when the power was set to 60 W, the CNR was higher than in the case of the 30 W power. T2-W FSE images acquired with TE=50 ms offered the best CNR (Figure 175), substantiating the results of previous assessments for optimal lesion detection with T2-W FSE sequences (section: Optimizing the echo time (TE) and repetition time (TR) in T1-W and T2-W sequences for enhanced lesion detection). Nevertheless, coronal T2-W FSE images acquired with TE=100 ms at the end of the experiment showed the 8 lesions clearly (Figure 175), since the TE was within the range proposed for T2-W sequences (section: Optimizing the echo time (TE), repetition time (TR) and echo train length (ETL) of T1-W and T2-W sequences for lesion detection). As seen in photos of the tissue acquired at the end of the experiment (Figure 176 and Figure 177), the length and diameter of the lesions were fairly consistent (Table 53).

Assessment of the SOUNDPET version 2 robotic system for 2×2 and 3×3 grid sonications

The purpose of the experiment was to assess the movement of the robotic device by performing two 2×2 and one 3×3 grid sonications on excised pork tissue using different acoustic power. Figure 178 shows the setup of the experiment. The SOUNDPET robot (version 2) was placed on the table of the 1.5 T MRI scanner (Signa HD16, GE Healthcare). A piece of excised pork tissue was placed on the acoustic window of the robot with tapes used to reduce movement

artifacts as shown in Figure 178. The 2.75 MHz transducer (D=50 mm, ROC=65 mm) integrated within the robot was connected to an amplifier (AG1016, T & C Power Conversion).

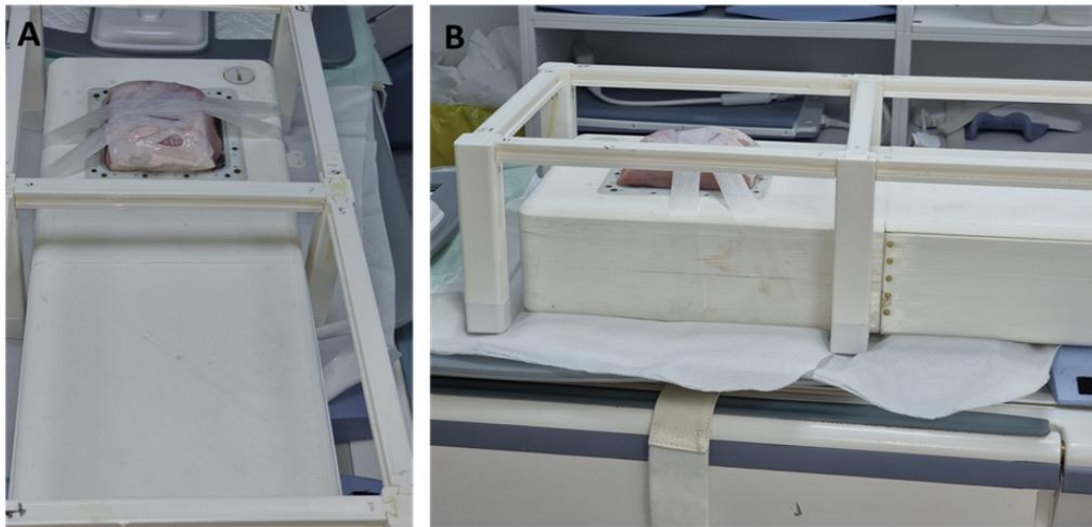


Figure 178: Experimental set-up with the SOUNDPET robot (version 2) positioned on the table of the 1.5 T MRI scanner with a piece of excised pork tissue placed on the acoustic window and stabilized with tapes to reduce movement artifacts. A) Anterior-Posterior view, and B) Lateral view.

On top of the excised tissue a body coil (Signa 1.5 T 12 Channel, GE Healthcare) was positioned for MR image acquisition. The second version of the software was used to control the transducer movement as well as the sonication parameters. Robotic motion was performed in two 2×2 grid patterns with a 15 mm step between successive points (Grid 1 and Grid 2) and in one 3×3 grid with a 10 mm step (Grid 3). Sonications during the three grid operations were performed as shown in Table 54.

Table 54: Motion and sonication parameters for three grid operations executed with a 2.75 MHz transducer (D=50 mm, ROC=65 mm) at 20 mm focal depth.

Grid	Grid pattern	Step (mm)	Acoustic power (W)	Sonication time (s)
1	2×2	15	30	60
2	2×2	15	54	120
3	3×3	10	54	120

Grid 1 sonications were imaged using a T1-W FSE sequence (TR=300 ms, TE=11 ms, FOV=260×260 mm², Slice thickness=10 mm, Matrix=128×128, ETL=3, NEX=1, Flip angle=90°, Pixel bandwidth=32 Hz/pixel), while Grid 2 and Grid 3 sonications were imaged using a T2-W FSE sequence (TR=2000 ms, TE=59 ms, FOV=260×260 mm², Slice thickness=6 mm, Matrix=224×192, ETL=1, NEX=2, Flip angle=90°, Pixel bandwidth=27 Hz/pixel).

Results

Figure 179 shows the T1-W FSE images acquired during the Grid 1 2×2 sonications (30 W for 60 s). Figure 180 shows the T2-W FSE images acquired during the Grid 2 2×2 sonications (54 W for 120 s). Before execution of Grid 3, a sonication (54 W for 120 s) was executed at the initial (zero) position of the transducer. Thereafter, the grid operation was initiated. Figure 181 and Figure 182 show the T2-W images acquired during and after the Grid 3 3×3 sonications (54 W for 120 s) respectively.

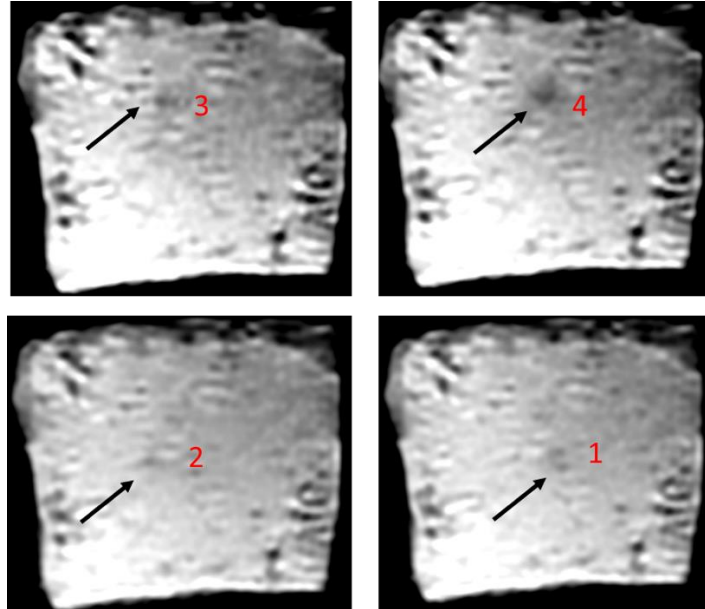


Figure 179: Coronal T1-W FSE images acquired during sonications on excised pork tissue in a 2×2 grid pattern with a 15 mm step using a 2.75 MHz transducer ($D=50$ mm, $ROC=65$ mm) at acoustic power of 30 W for a sonication time of 60 s at 20 mm focal depth (Grid 1). Arrows indicate thermal heating.

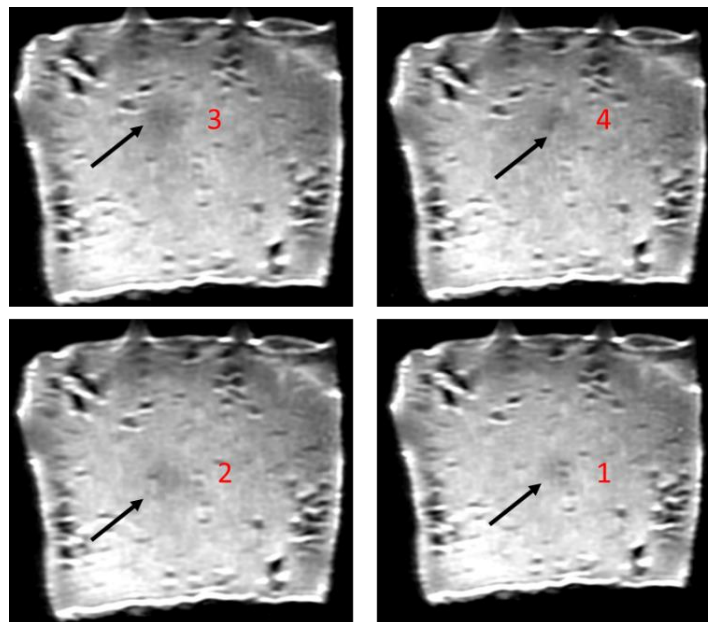


Figure 180: Coronal T2-W FSE images acquired during sonications on excised pork tissue in a 2×2 grid pattern with a 15 mm step using a 2.75 MHz transducer ($D=50$ mm, $ROC=65$ mm) at acoustic power of 54 W for a sonication time of 120 s at 20 mm focal depth (Grid 2). Arrows indicate thermal heating.

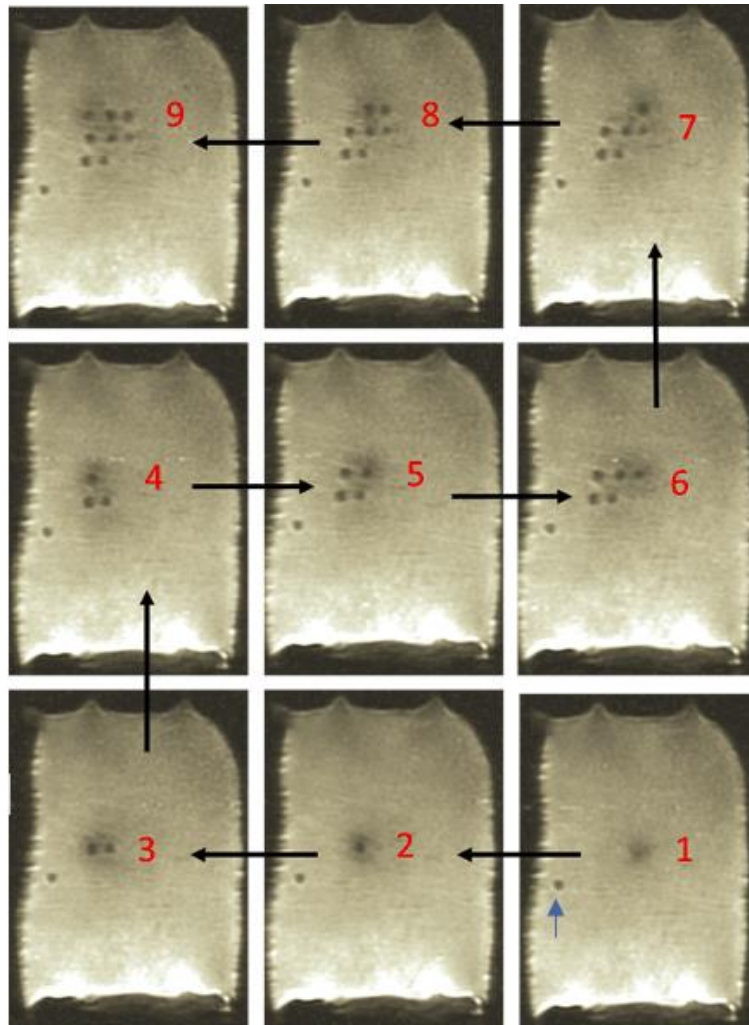


Figure 181: Coronal T2-W FSE images acquired during sonications on excised pork tissue in a 3×3 grid pattern with a 10 mm step using a 2.75 MHz transducer ($D=50$ mm, $ROC=65$ mm) at acoustic power of 54 W for a sonication time of 120 s at 20 mm focal depth (Grid 3). Numbers indicate thermal heating at grid locations from initial position (blue arrow).

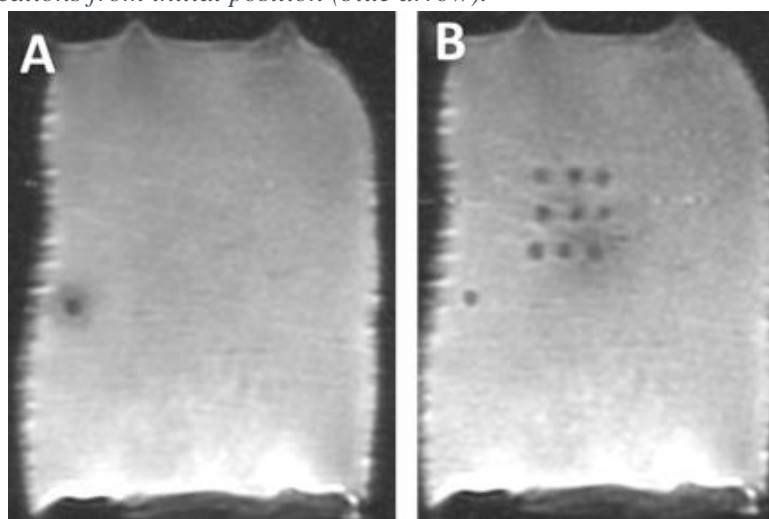


Figure 182: Coronal T2-W FSE images acquired after sonications on excised pork tissue using a 2.75 MHz transducer ($D=50$ mm, $ROC=65$ mm) at acoustic power of 54 W for a sonication time of 120 s at 20 mm focal depth. A) Lesion formed at initial-position, and B) Lesions formed after operation of the 3×3 grid with a 10 mm step (Grid 3).

The pieces of excised tissue were sliced after the sonications. Figure 183 shows indicative photos of the excised pork tissue after the Grid 3 sonications. Figure 183B shows the lesions formed at the initial-point of the transducer and at the 9 locations of the 3×3 grid on a plane perpendicular to the beam. Figure 183C, Figure 184A, Figure 184B and Figure 184C show the initial-point, first row, second row, and third row lesions respectively as formed on a plane parallel to the beam. A ruler was used to measure the lesion dimensions (diameter and length), with measurements for Grid 3 lesions shown in Table 55.

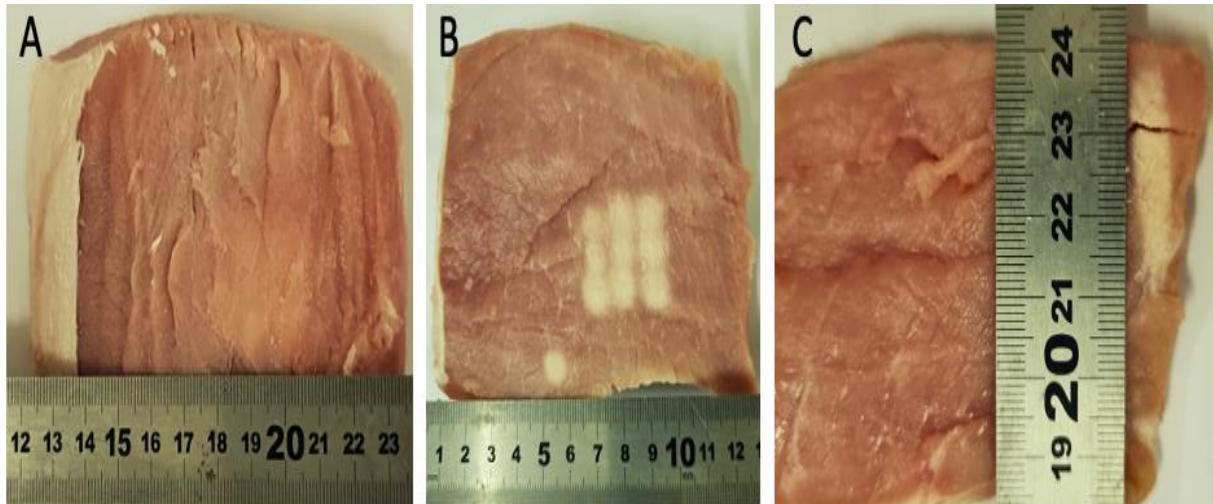


Figure 183: Photo of excised pork tissue after sonications with a 2.75 MHz transducer ($D=50$ mm, $ROC=65$ mm) in a 3×3 grid with a 10 mm step using an acoustic power of 54 W for a sonication time of 120 s at 20 mm focal depth (Grid 3). A) Surface of the excised tissue, B) Slice of tissue at 10 mm showing lesions formed on plane perpendicular to the beam, and C) Initial-point lesion as formed on plane parallel to the beam.

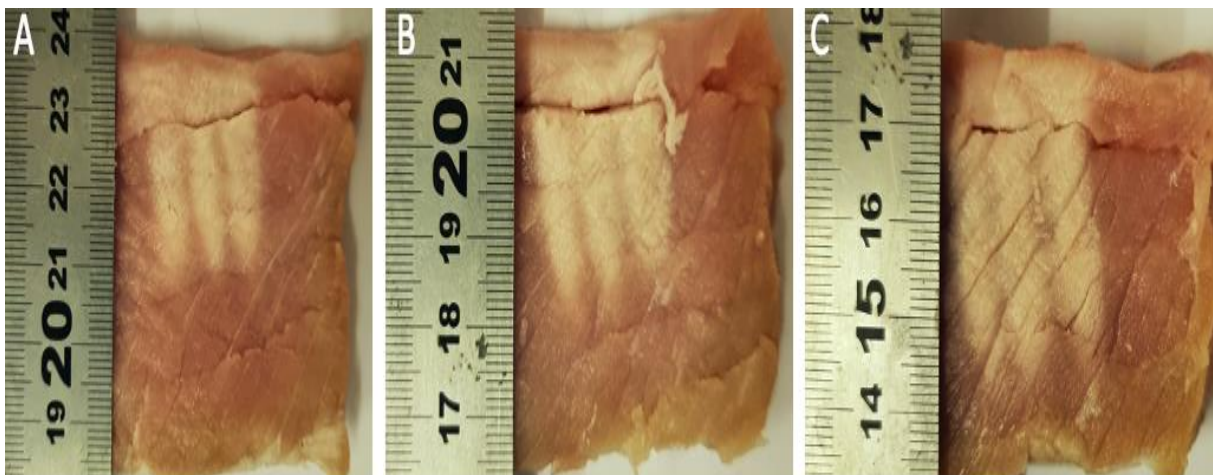


Figure 184: Photo of lesions formed on plane parallel to the beam on excised pork tissue after sonications with a 2.75 MHz transducer ($D=50$ mm, $ROC=65$ mm) in a 3×3 grid with a 10 mm step using acoustic power of 54 W for a sonication time of 120 s at 20 mm focal depth (Grid 3). A) Lesions of the first grid row, B) Lesions of the second grid row, and C) Lesions of the third grid row.

Table 55: Dimensions of lesions formed on excised tissue after sonications in a 3×3 grid with a 10 mm step using a 2.75 MHz transducer (D=50 mm, ROC=65 mm) at acoustic power of 54 W for a sonication time of 120 s at 20 mm focal depth (Grid 3).

Lesion	Diameter (mm)	Length (mm)
Initial point	8	27
1	8	29
2	8	29
3	8	29
4	8	30
5	8	30
6	8	30
7	8	32
8	8	32
9	8	32

Subsection Conclusions

In this experiment, the image quality was satisfactory without any noticeable artifacts, even when the transducer was activated during the acquisition. The transducer movement presented high accuracy in accordance to the grids defined by the software, as evident from the lesions formed at the initial position of the transducer and at the grid locations (Figure 183B).

Thermal heating at the focal spots was clearly visible at all sonication points for all three grids (i.e. 2×2 and 3×3) (Figure 179, Figure 180 and Figure 181). Additionally, the lesion formed at the initial-point was clearly visible in all T2-W FSE images of Grid 3 (Figure 181). Finally, as seen in photos of the excised tissue acquired at the end of the experiment (Figure 183 and Figure 184), the length and diameter of the lesions was fairly consistent (Table 55).

Assessment of lesion detection using a 3 T MRI scanner

The purpose of the experiment was to assess lesion detection during sonications on excised pork tissue using a 3 T MRI scanner (Magnetom Vida, Siemens Healthineers, Erlangen, Germany). The SOUNDPET robot (version 2) was placed on the table of the 3 T MRI (Magnetom Vida, Erlangen) with a piece of excised tissue positioned on the acoustic window of the robot as shown in Figure 185. The 2.75 MHz ultrasonic transducer (D=50 mm, ROC=65 mm) integrated in the robot was connected to an amplifier (AG1016, T & C Power Conversion).



Figure 185: Experimental set-up with the SOUNDPET robot (version 2) positioned on the table of the 3 T MRI scanner with a piece of excised pork tissue placed on the acoustic window for assessing lesion detection using T2-W imaging.

A series of four grid sonications were performed on two pieces of excised pork tissue at an acoustic power of 45 W for varied sonication times as shown in Table 56. Two grid sonications were performed on the first piece of the tissue at a focal depth of 30 mm, while two grid sonications were performed on the second piece of tissue at a focal depth of 35 mm. Three grids were performed by initiating a grid operation using the second version of the software (Deliverable 5.1) while one grid (Grid 2) was performed by initiating manual motion of the transducer. An 18-channel body coil (Body18, Siemens Healthineers) was positioned on top of the experimental set-up and the excised tissue for MR image acquisition during sonications. A T2-Weighted Turbo Spin Echo (T2-W TSE) sequence was used with varied parameters for detecting and imaging the lesions inflicted by the sonications.

Table 56: Motion and sonication parameters for the four grid operations executed with a 2.75 MHz transducer ($D=50$ mm, $ROC=65$ mm).

Grid	Grid pattern	Step (mm)	Acoustic power (W)	Sonication time (s)	Focal depth (mm)
1	2×3	10	45	60	30
2	2×3 (Manual)	10, 15		10, 20, 30, 40, 50, 60	
3	3×3	10		40	35
4	3×3	5		40	

Results

Figure 186 shows the T2-W TSE images (TR=4000 ms, TE=52 ms, FOV=200×200 mm², Slice thickness=10 mm, Matrix=256×256, ETL=36, NEX=1, Flip angle=180°, Pixel bandwidth=50 Hz/pixel) acquired after the Grid 1 2×3 sonications (45 W for 60 s), showing the inflicted lesions. Prior the grid operation a sonication was also performed at the initial position of the transducer for lesion creation at the initial point (number 0 in Figure 186). Figure 187 and Figure 188 show photos of the excised tissue after the sonications showing the lesions formed in planes perpendicular and parallel to the beam respectively.

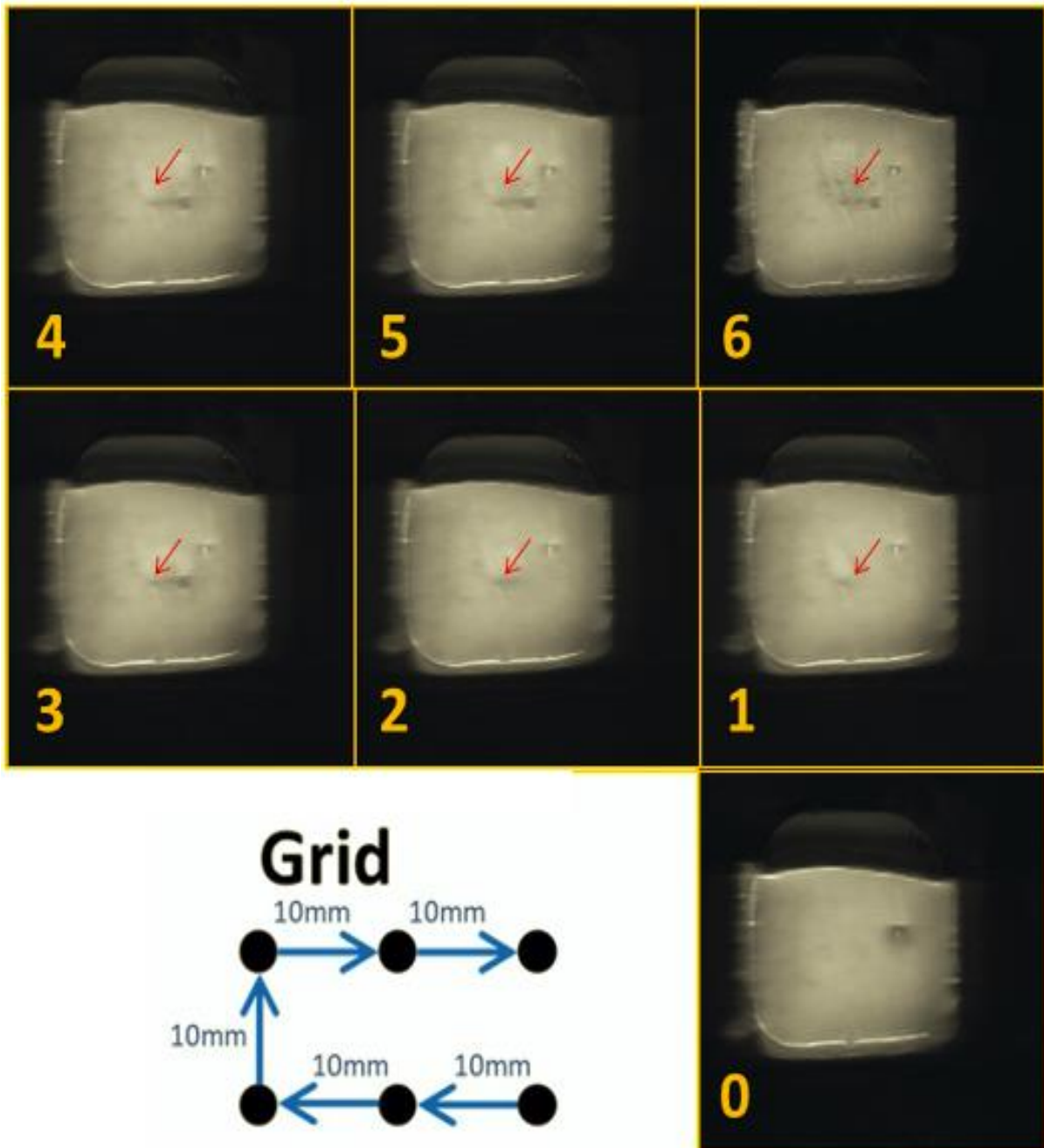


Figure 186: Coronal T2-W TSE images showing lesions (red arrow) inflicted on excised pork tissue after sonications executed in a 2×3 grid with a 10 mm step using a 2.75 MHz transducer ($D=50$ mm, $ROC=65$ mm) at acoustic power of 45 W for a sonication time of 60 s at 30 mm focal depth (Grid 1).

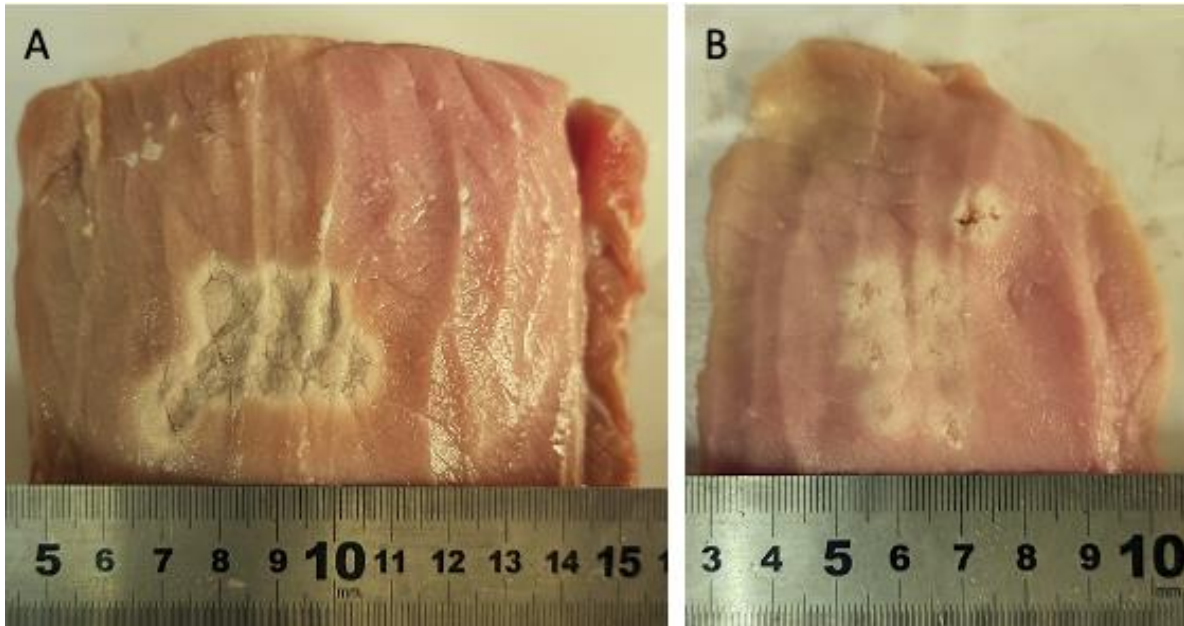


Figure 187: Photo of lesions formed on plane perpendicular to the beam on excised pork tissue after sonications in a 2×3 grid with a 10 mm step using a 2.75 MHz transducer ($D=50$ mm, $ROC=65$ mm) at acoustic power of 45 W for a sonication time of 60 s at 30 mm focal depth (Grid 1). A) Surface of the tissue, and B) Slice of the tissue at 10 mm showing the 2×3 grid and initial-point lesions.

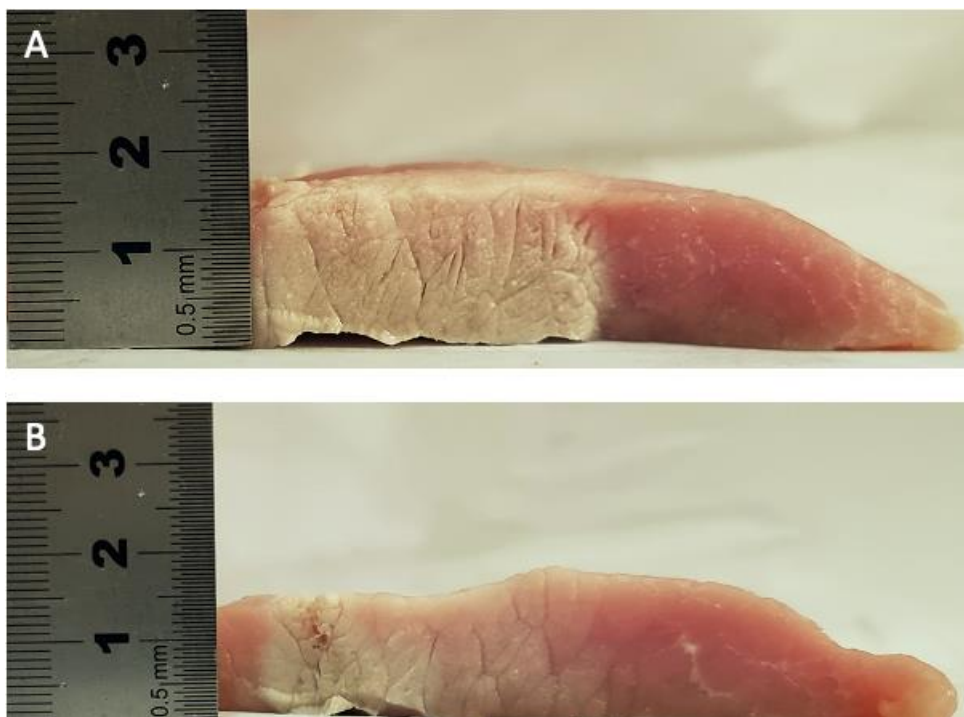


Figure 188: Photo of lesions formed on plane parallel to the beam on excised pork tissue after sonications in a 2×3 grid with a 10 mm step using a 2.75 MHz transducer ($D=50$ mm, $ROC=65$ mm) at acoustic power of 45 W for a sonication time of 60 s at 30 mm focal depth (Grid 1). A) Lesions 1, 2 and 3, and B) Lesions 4, 5 and 6.

Figure 189 shows the T2-W TSE images ($TR=2500$ ms, $TE=48$ ms, $FOV=200\times 200$ mm², Slice thickness=10 mm, Matrix=256×256, ETL=20, NEX=1, Flip angle=180°, Pixel bandwidth=50 Hz/pixel) acquired for the manual Grid 2 2×3 sonications, showing the lesions formed using an acoustic power of 45 W for varied sonication times. Figure 190 and Figure 191 show photos

of the excised tissue after the sonications showing the lesions formed in planes perpendicular and parallel to the beam respectively. The diameters of lesions formed using the acoustic power of 45 W for varied sonication times are shown in Table 57.

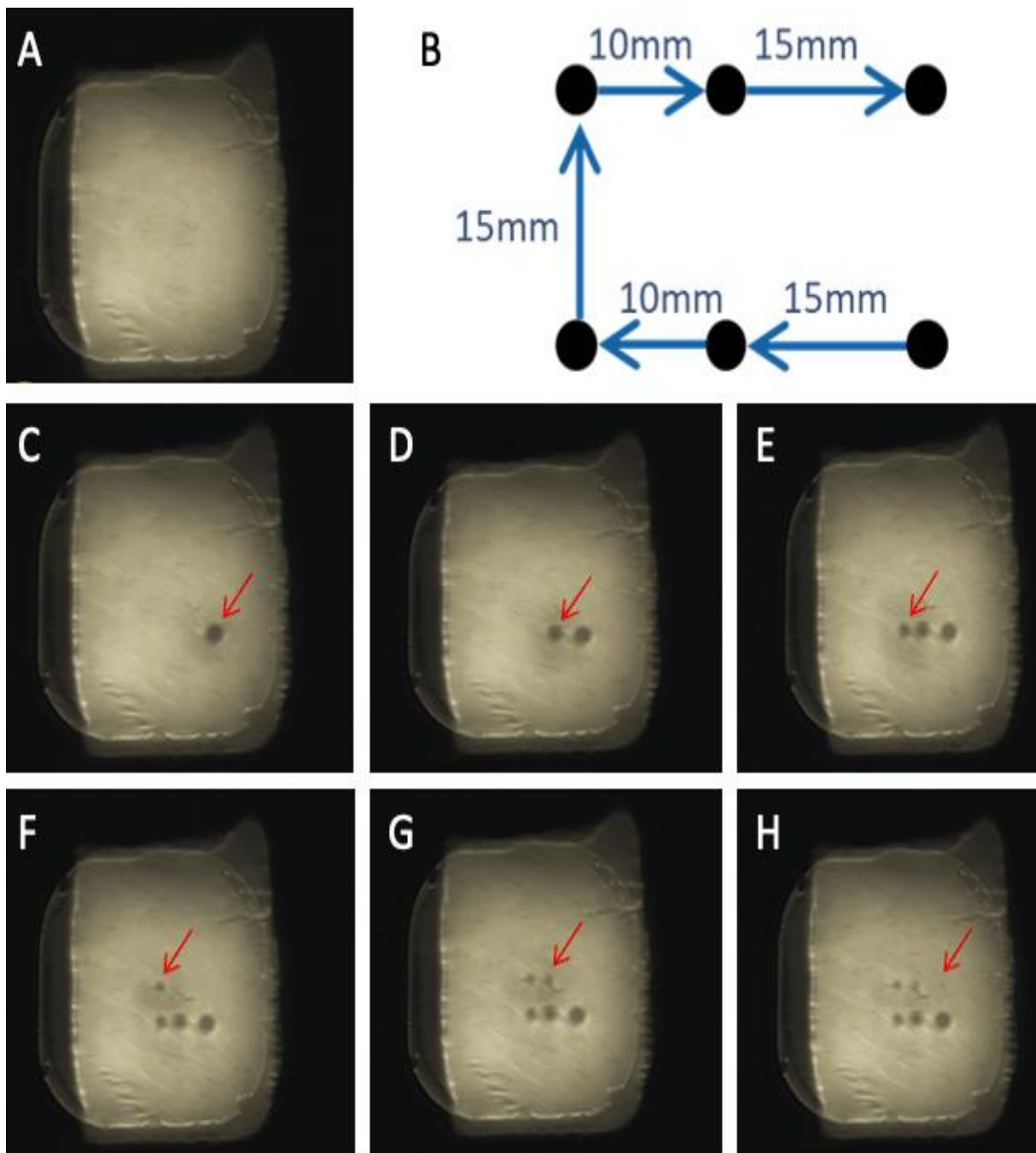


Figure 189: Coronal T2-W TSE images showing lesions (red arrow) inflicted on excised tissue after sonications executed in a manual 2×3 grid with 10 mm and 15 mm steps using a 2.75 MHz transducer ($D=50$ mm, $ROC=65$ mm) at acoustic power of 45 W for varied sonication times (10-60 s) at 30 mm focal depth (Grid 2). Images acquired A) before grid sonications, B) showing schematic representation of the 2×3 grid, C) after sonication at 1st grid point using a 60 s sonication time, D) after sonication at 2nd grid point using a 50 s sonication time, E) after sonication at 3rd grid point using a 40 s sonication time, F) after sonication at 4th grid point using a 30 s sonication time, G) after sonication at 5th grid point using a 20 s sonication time, and H) after sonication at 6th grid point using a 10 s sonication time.

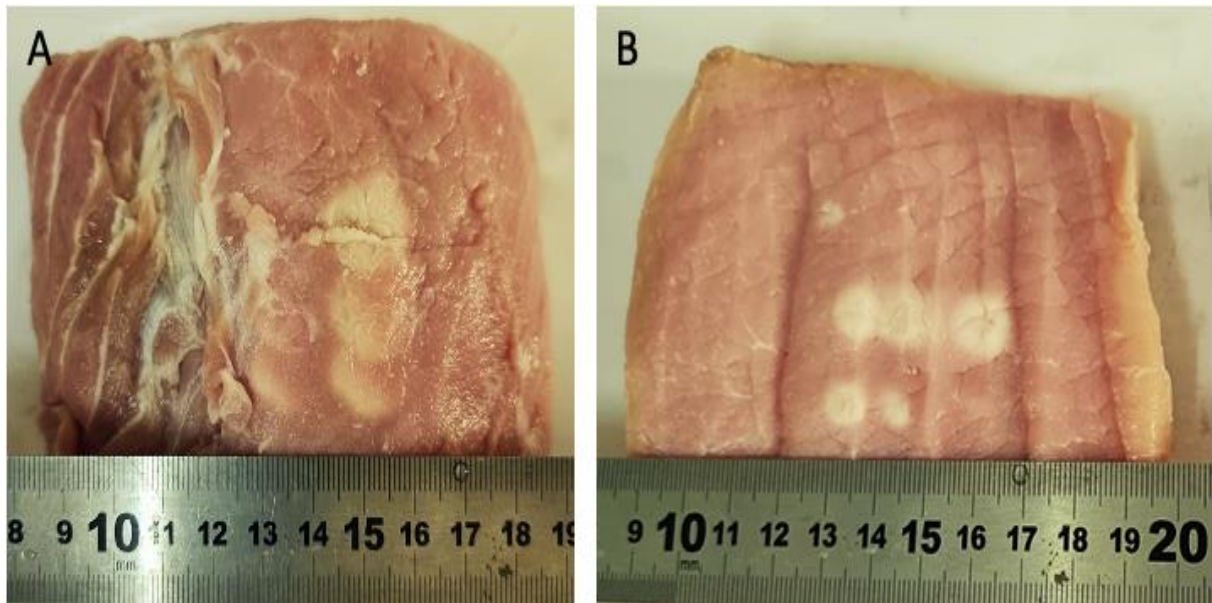


Figure 190: Photo of lesions formed on plane perpendicular to the beam on excised pork tissue after sonications in a manual 2×3 grid with 10 mm and 15 mm steps using a 2.75 MHz transducer ($D=50$ mm, $ROC=65$ mm) at acoustic power of 45 W for varied sonication times (10-60 s) at 30 mm focal depth (Grid 2). A) Surface of the tissue, and B) Slice of the tissue at 10 mm showing the 2×3 grid lesions.

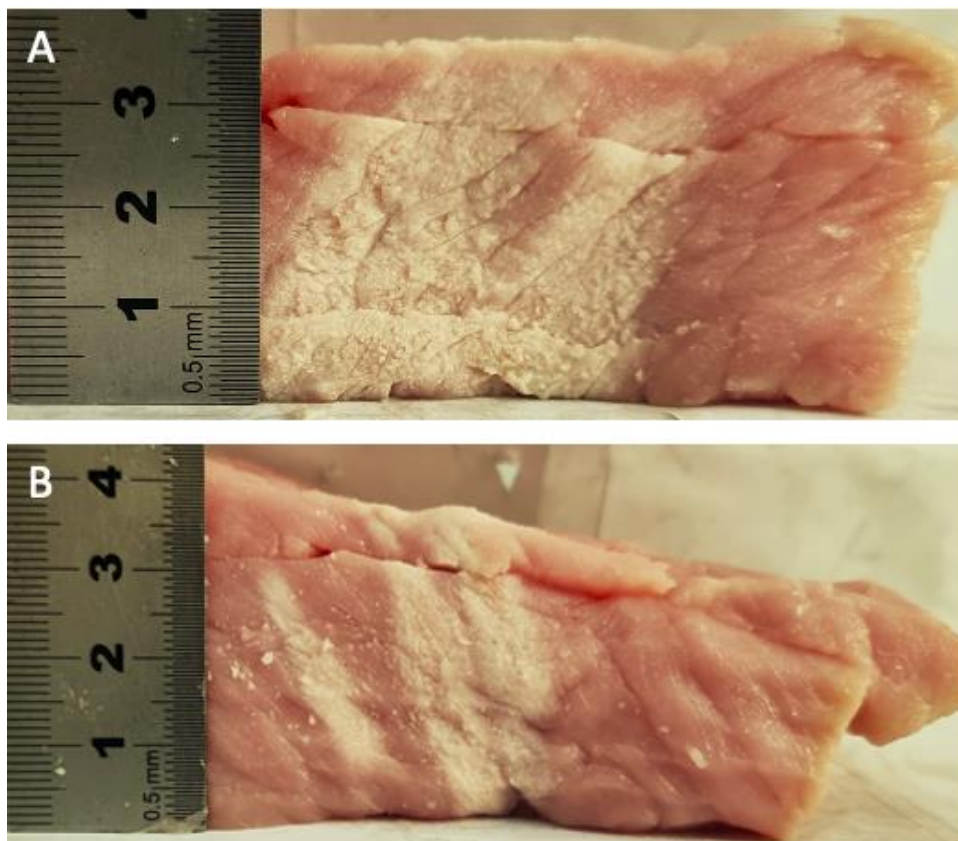


Figure 191: Photo of lesions formed on plane parallel to the beam on excised pork tissue after sonications in a manual 2×3 grid with 10 mm and 15 mm steps using a 2.75 MHz transducer ($D=50$ mm, $ROC=65$ mm) at acoustic power of 45 W for varied sonication times (10-60 s) at 30 mm focal depth (Grid 2). A) Lesions 1, 2 and 3, and B) Lesions 4, 5 and 6.

Table 57: Diameter of lesions formed on excised tissue after sonications in a manual 2×3 grid with 10 mm and 15 mm steps using a 2.75 MHz transducer (D=50 mm, ROC=65 mm) at acoustic power of 45 W for varied sonication times at 30 mm focal depth.

Lesion	Sonication time (s)	Diameter (mm)
1	60	9
2	50	8
3	40	7
4	30	6
5	21	6
6	10	3

Figure 192 and Figure 193 show the T2-W TSE images (TR=2500 ms, TE=48 ms, FOV=200×200 mm², Slice thickness=10 mm, Matrix=256×256, ETL=20, NEX=1, Flip angle=180°, Pixel bandwidth=50 Hz/pixel) respectively acquired after the Grid 3 (10 mm step) and Grid 4 (5 mm step) 3×3 sonications (45 W for 40 s) executed on the second tissue, showing the inflicted lesions.

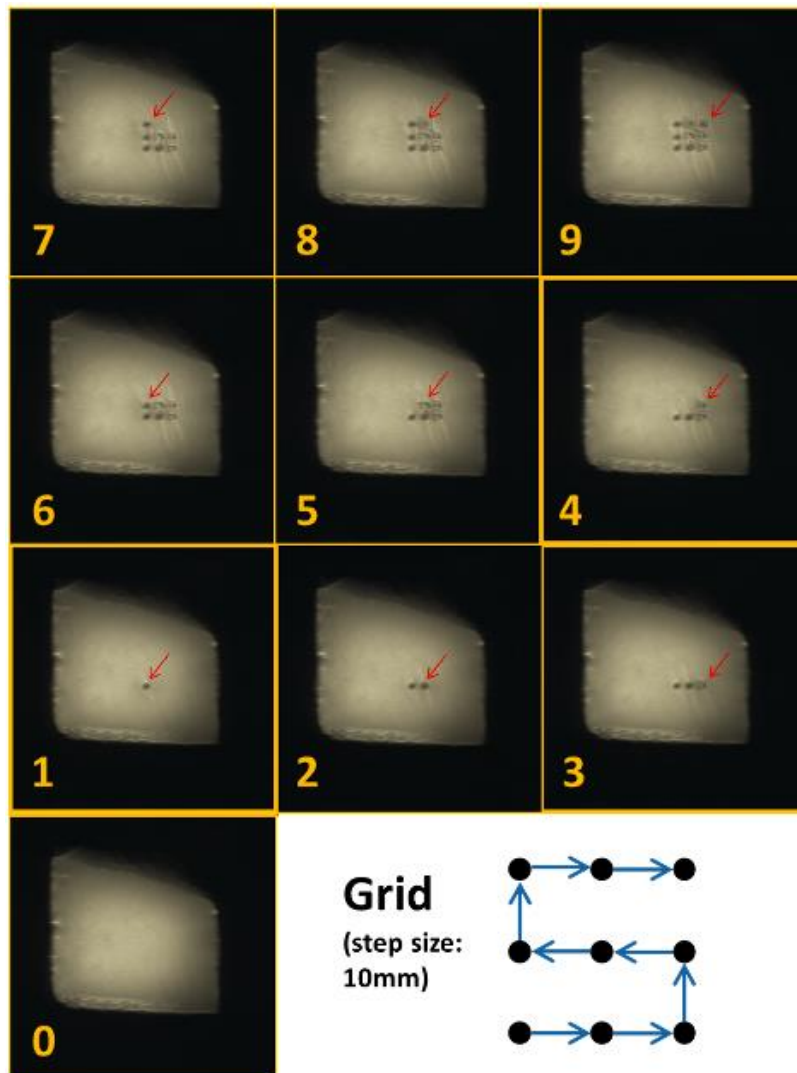


Figure 192: Coronal T2-W TSE images showing lesions (red arrow) inflicted on excised pork tissue after sonications executed in a 3×3 grid with a 10 mm step using a 2.75 MHz transducer (D=50 mm, ROC=65 mm) at acoustic power of 45 W for a sonication time of 40 s at 35 mm focal depth (Grid 3).

Grid

(step size:
5mm)

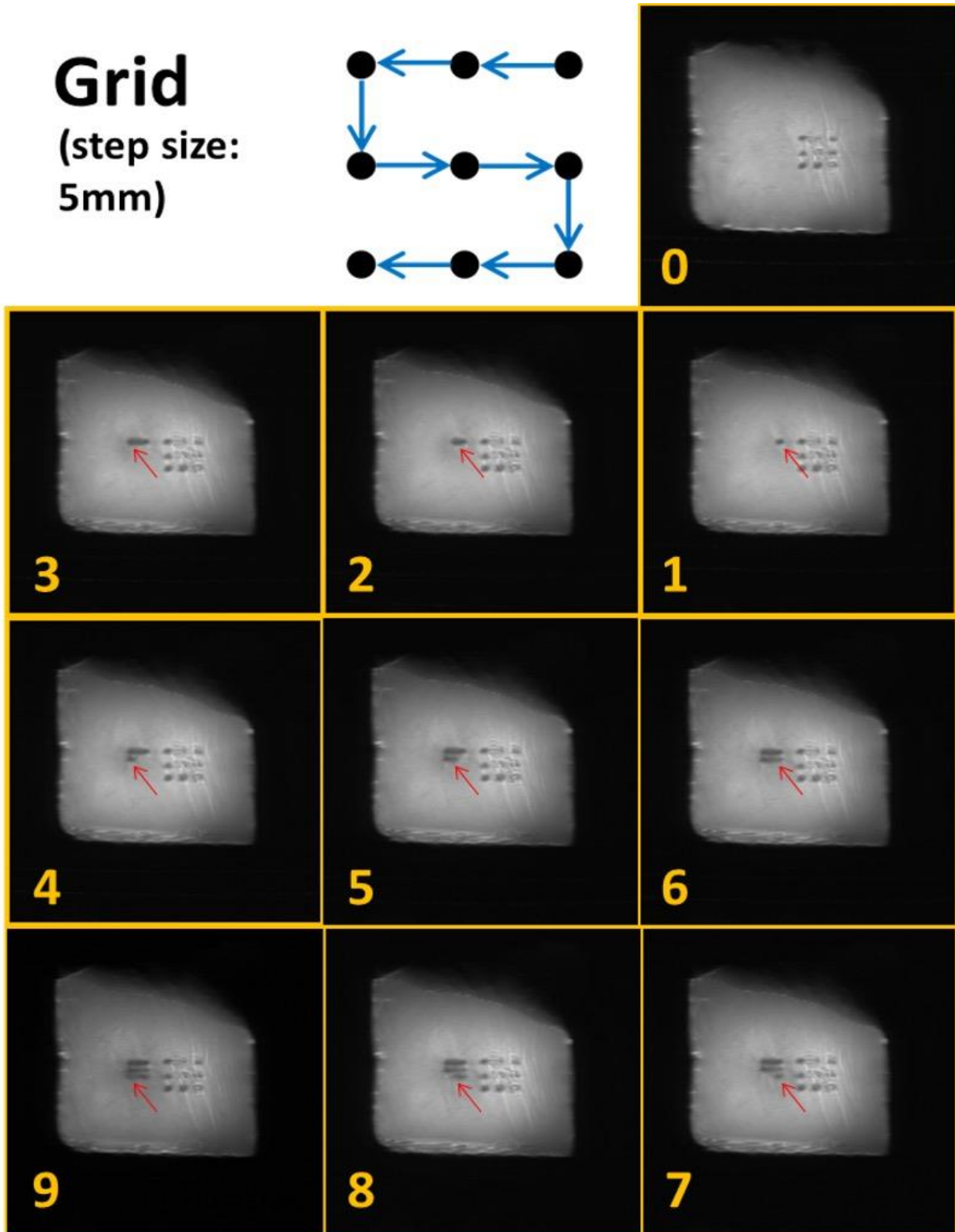
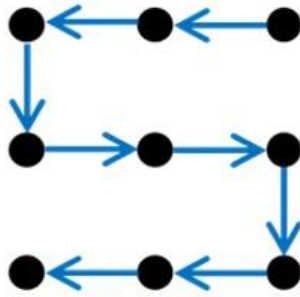


Figure 193: Coronal T2-W TSE images showing lesions (red arrow) inflicted on excised pork tissue after sonications executed in a 3×3 grid with a 5 mm step using a 2.75 MHz transducer ($D=50$ mm, $ROC=65$ mm) at acoustic power of 45 W for a sonication time of 40 s at 35 mm focal depth (Grid 4).

Figure 194 shows photos of the excised tissue after the Grid 3 and Grid 4 sonications, showing the two grid lesions formed in a plane perpendicular to the beam. Figure 195 and Figure 196 show the Grid 3 and Grid 4 lesions respectively, formed in a plane parallel to the beam. The diameters of the formed discrete Grid 3 lesions are shown in Table 58.

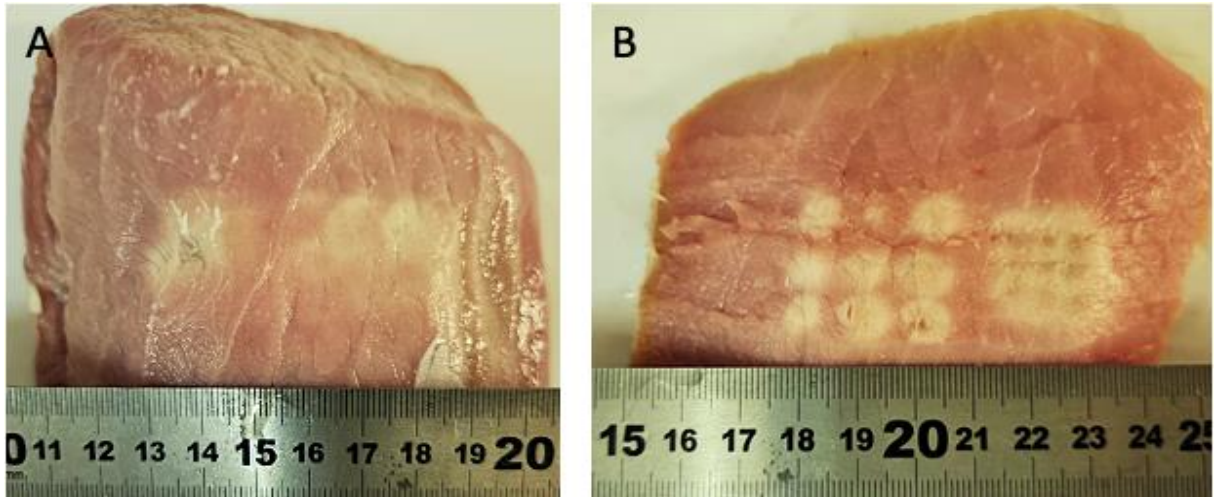


Figure 194: Photo of lesions formed on plane perpendicular to the beam on excised pork tissue after sonications in two 3×3 grids one with 5 mm step (Grid 4) and one with 10 mm step (Grid 3) using a 2.75 MHz transducer ($D=50$ mm, $ROC=65$ mm) at acoustic power of 45 W for a sonication time of 40 s at 35 mm focal depth. A) Surface of the tissue with the Grid 4 lesions (left) and the Grid 3 lesions (right), and B) Slice of the tissue at 25 mm showing the two 3×3 Grid 3 (left) and Grid 4 (right) lesions.

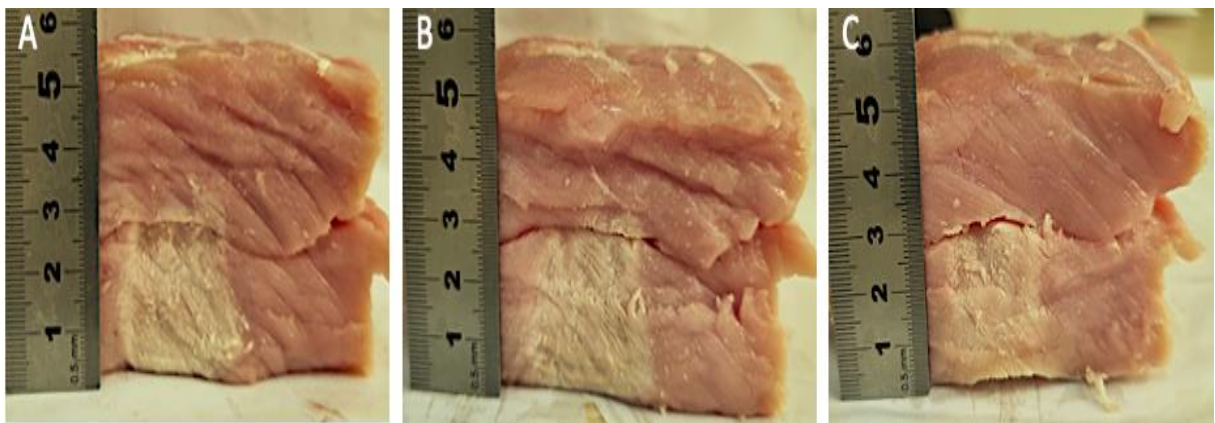


Figure 195: Photos of lesions formed on plane parallel to the beam on excised pork tissue after sonications in a 3×3 grid with a 10 mm step using a 2.75 MHz transducer ($D=50$ mm, $ROC=65$ mm) at acoustic power of 45 W for a sonication time of 40 s at 35 mm focal depth (Grid 3). A) Lesions 1, 6 and 7, B) Lesions 2, 5 and 8, and C) Lesions 3, 4 and 9.

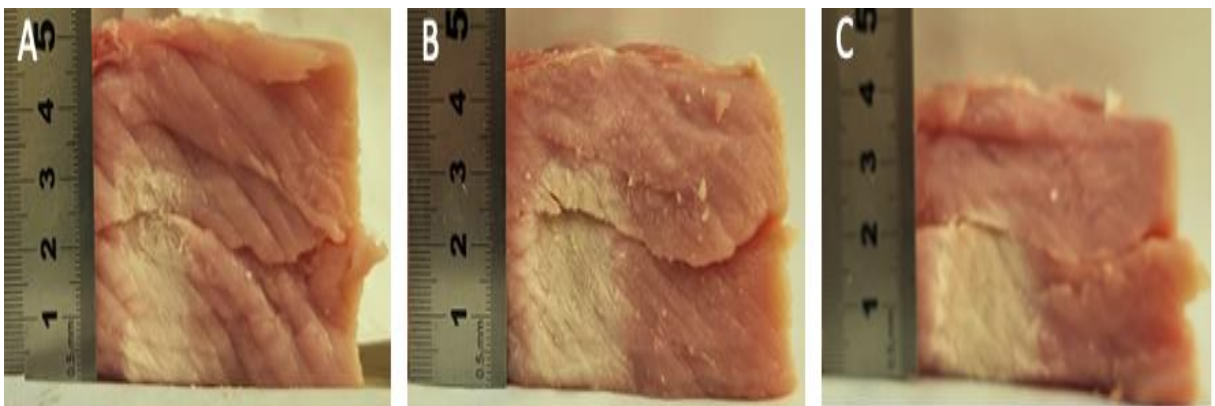


Figure 196: Photos of lesions formed on plane parallel to the beam on excised pork tissue after sonications in a 3×3 grid with a 5 mm step using a 2.75 MHz transducer ($D=50$ mm, $ROC=65$ mm) at acoustic power of 45 W for a sonication time of 40 s at 35 mm focal depth (Grid 4). A) Lesions 1, 6 and 7, Lesions 2, 5 and 8, and C) Lesions 3, 4 and 9.

Table 58: Diameter of lesions formed on excised tissue after sonications in a 3×3 grid with a 10 mm step using a 2.75 MHz transducer (D=50 mm, ROC=65 mm) at acoustic power of 45 W for a sonication time of 40 s at 35 mm focal depth (Grid 3).

Lesion	Diameter (mm)
1	6
2	6
3	6
4	7
5	8
6	5
7	6
8	4
9	6
<i>Average</i>	<i>6 ± 1.1</i>

Subsection Conclusions

As shown in photos of the two tissues acquired after the experiment, all four grid sonications led to clearly visible lesions (Figure 187, Figure 190 and Figure 194). The grid lesions could also be observed in the T2-W images acquired post-sonication (Figure 189, Figure 192 and Figure 193), with the exception of the first grid sonication (Grid 1) where the lesions could be barely seen (Figure 186).

For the second 2×3 grid sonications, the sonication time varied between 10 s and 60 s (Grid 2) for a constant acoustic power of 45 W. The six sonications were sufficient for the formation of six lesions as clearly seen in photos of the tissue (Figure 190). The six lesions could also be detected in the T2-W images (Figure 189), except for the lesion formed using a sonication time of 10 s which could hardly be seen in the T2-W image (Figure 189H). Nevertheless, it was concluded that the diameter of the lesions was proportional to the sonication time (Table 57). For instance, a lesion with a 9 mm diameter was formed with a sonication time of 60 s, whereas a 3 mm lesion diameter was observed with the shorter sonication time of 10 s.

In the case of the second piece of tissue and the first 3×3 grid sonications performed with a 10 mm step using a sonication time of 40 s (Grid 3), the nine formed lesions presented similar diameters, with an average diameter of 6±1 mm (Table 58). Using a smaller grid step size (5 mm) for performing the second 3×3 grid sonications (Grid 4), overlapping lesions were formed having an area of 170×200 mm². Overall, the step size in the grid sonications was sometimes fixed to 5 mm (Figure 193) or 10 mm (Figure 186), and other times varied between 10 mm and 15 mm (Figure 189). In this regard, the MRI planning and monitoring software was effective and was characterized by great accuracy of transducer movement.

Measurement of MR relaxation times of tumor-like phantom and lesion at 1.5 T and 3 T MRI scanners

The T1 and T2 relaxation times of an agar-based phantom with a tumor-like material and of a lesion inflicted on excised pork tissue were measured. Different MRI scanners were used to assess the effect of the varied magnetic field strength (1.5 or 3 T) on the T1 and T2 relaxation times of the phantoms and lesions.

Regarding T1 and T2 relaxation measurements of phantoms inside a 1.5 T MRI scanner (Signa HD16, GE Healthcare), 10 homogeneous phantoms were developed in individual inserts, containing different percentage concentrations of agar (Merck KGaA, Darmstadt, Germany), silica (Sigma Aldrich, Missouri, USA), evaporated milk (Nounou, Friesland Campina, Marousi, Greece) and wood powder (Swedish pine) as shown in Figure 197A. Pure water and oil were also inserted in two inserts acting as reference values. Relaxation measurements of phantoms inside the 3 T MRI scanner (Magnetom Vida, Siemens Healthineers) were executed for an agar-based phantom (6 % w/v agar) with a tumor-like material (6 % w/v agar, 4 % w/v silica) in the centre as shown in Figure 197B. Correspondingly, in both 1.5 T (SignaHD16, GE) and 3 T (Magnetom Vida, Siemens Healthineers) scanners, relaxometry measurements were performed for a lesion inflicted on excised pork tissue as shown in Figure 197C. Notably, at 1.5 T (SignaHD16, GE), relaxometry measurements for the excised tissue, were acquired for both a single lesion and an area of overlapping lesions (25). Either of the materials (10 homogeneous phantoms, agar-based phantom with tumor-like material, excised tissue with inflicted lesions) were placed on the table of the MRI scanner with an imaging coil placed on top for MR image acquisition as typically shown in Figure 197D.

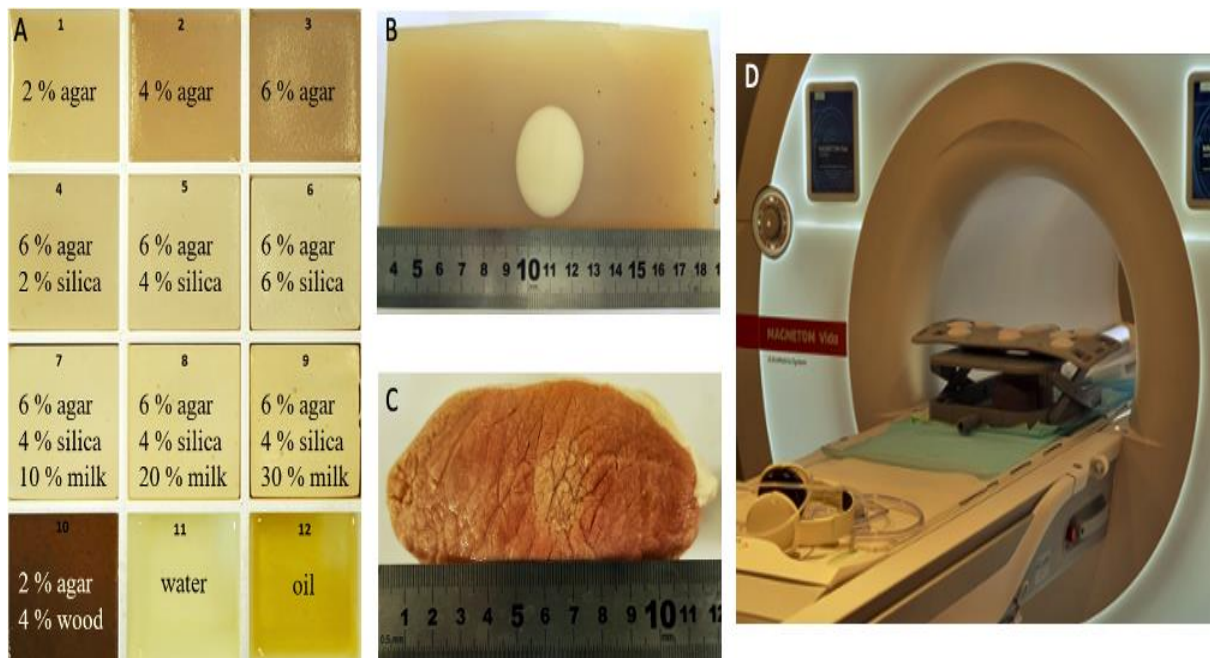


Figure 197: A) Photo of the 10 homogeneous phantoms and their compositions, B) Cross-section of an agar-based phantom (6 % w/v agar) with a tumor-like material (6 % w/v agar, 4 % w/v silica), C) Lesion formed on excised porcine tissue, and D) Typical experimental set-up inside the 3 T MRI scanner with the agar-based phantom or the excised tissue placed on the table of the MRI scanner and an imaging coil placed on top for MR image acquisition.

Regarding measurements in the 1.5 T MRI scanner, the 10 homogeneous phantoms and the area of overlapping lesions on excised tissue were scanned using the posterior head and face part of a head/neck/spine (HNS) coil (Signa 1.5 T, 16 channel, GE Healthcare), while the single lesion inflicted on excised tissue was scanned using a GPFLEX coil (Signa 1.5 T Receiver only, GE Healthcare). Correspondingly, inside the 3 T MRI scanner scans for both the single lesion and the agar-based phantom with a tumor-like material (6 % w/v agar, 4 % w/v silica) were executed using an 18-channel body coil (Body18, Siemens Healthineers).

For either of the investigated materials, in both 1.5 T (Signa HD16, GE Healthcare) and 3 T (Magnetom Vida, Siemens Healthineers) scanners, a series of MR images were acquired. The acquired MRI images were inserted in a DICOM software (MicroDicom, MicroDicom Ltd., Sofia, Bulgaria) for post-processing. DICOM software tools were utilised for measuring the signal intensity in the agar-based phantoms and the excised pork tissue using a Region of Interest (ROI) approach. For the homogeneous phantoms, mean signal intensities (SI) were measured in a ROI set within the agar phantom, while in the tumor-like agar-based phantom, mean SI were measured for ROIs in both the tumor-like material and the agar-background. Correspondingly, for the pork excised tissue SI were measured in ROIs taken in both the inflicted lesion and the surrounding intact tissue.

T1 Relaxation time measurements

For T1 relaxation time measurements, images of the agar-based phantoms or excised tissue were acquired using a T1-W Inversion Recovery (IR) Spin Echo (SE) sequence at variable inversion times (TI). The IR sequence is the standard method for T1 relaxation time measurements because of its large dynamic range and insensitivity to pulse sequence parameter imperfection. For each investigated material, the mean SI measured from the image in the corresponding ROI was plotted as a function of the varied TI used for image acquisition. The nulling TI (SI is zero) was interpolated from the graphs and the T1 relaxation time was calculated using Equation 1:

$$TI = 0.693 \times T1 \quad (1)$$

T1 relaxation measurements inside the 3 T MRI scanner (Magnetom Vida, Siemens Healthineers) were additionally performed using a voxel-by-voxel approach. In this regard, parametric maps were generated from the acquired MRI images using automated algorithms integrated in the MRI scanner.

T2 Relaxation time measurements

For T2 relaxation time measurements, images of the agar-based phantoms or excised tissue were acquired using a T2-W SE sequence at variable TE. For each investigated material, the mean SI measured from the image in the corresponding ROI was plotted as a function of the varied TE that was used for image acquisition. The plotted SI data were compared to the following Equation 2:

$$M_{xy} = M_o e^{-\frac{TE}{T2}} \quad (2)$$

where M_{xy} is the transverse magnetization and M_0 is the maximum transverse magnetization following the RF pulse. In this regard, following regression analysis, an exponential trendline was fitted to the plotted data and T2 relaxation time calculations were performed by taking the inverse of the exponent of the exponential fit.

Results

T1 relaxation time calculations

The 10 homogeneous agar-based phantoms were scanned inside the 1.5 T MRI scanner (Signa HD16, GE Healthcare) with an IR sequence (TR=5000 ms, TE=10 ms, FOV=260×260 mm², Slice thickness=7 mm, Matrix=192×128, NEX=0.5, ETL=15, Flip angle=90°) and TI values ranging from 50-1050 ms. Regarding both the single lesion and area of overlapping lesions inflicted on excised pork tissue, these were scanned inside the 1.5 T MRI scanner (Signa HD16, GE Healthcare) using an IR sequence (TR=5000 ms, TE=10 ms, FOV=260×260 mm², Slice thickness=7 mm, Matrix=192×128, NEX=0.5, ETL=15, Flip angle=90°) and TI values ranging from 50-800 ms. Concerning measurements in the 3 T MRI scanner, the agar-based phantom (6 % w/v agar) with a tumor-like material (6 % w/v agar, 4 % w/v silica) and the excised tissue with the single lesion were scanned using an IR sequence (TR=6320 ms, TE=9 ms, FOV=200×200 mm², Slice thickness=10 mm, Matrix=128×96, NEX=1, ETL=3 Flip angle=180°) and TI values ranging from 150-3000 ms. Figure 198A and Figure 198B show typical MRI images of the agar-based phantom (6 % w/v agar) with the tumor-like material (6 % w/v agar, 4 % w/v silica) and the single lesion inflicted on excised pork tissue acquired with the IR sequence inside the 3 T scanner (Magnetom Vida, Siemens Healthineers).

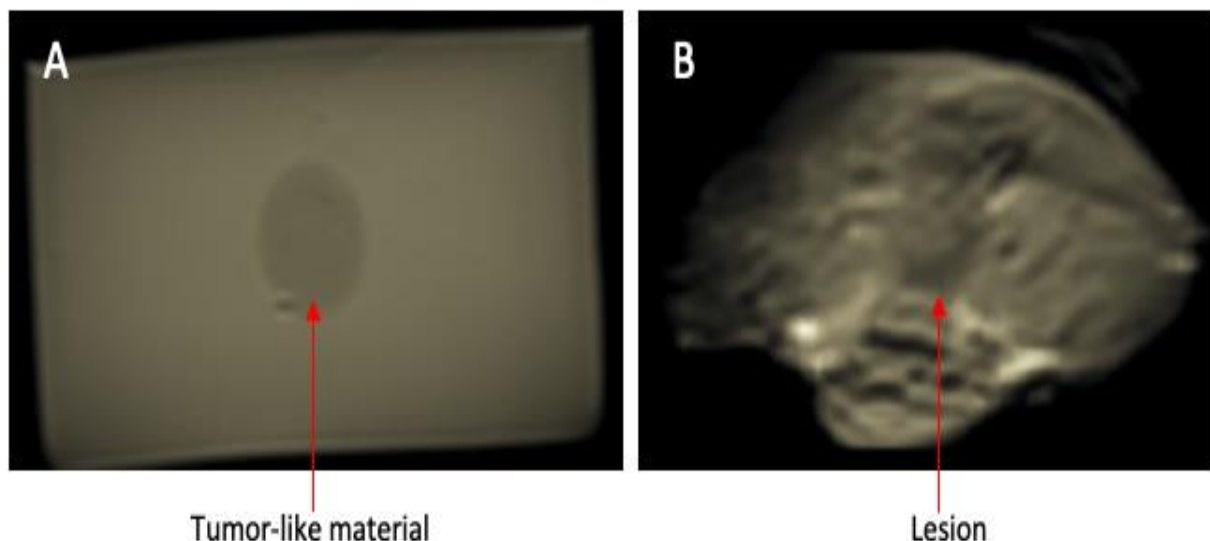


Figure 198: Coronal IR images of A) an agar-based phantom (6 % w/v agar) with a tumor-like material (6 % w/v agar, 4 % w/v silica) acquired using a TI of 400 ms, and B) a lesion inflicted on excised pork tissue acquired using a TI of 2000 ms, inside a 3 T MRI scanner (Magnetom Vida, Siemens Healthineers).

Figure 199 shows typical plots of the mean SI measured in each of the ROIs within the tumor-like material (6 % w/v agar, 4 % w/v silica), the agar-based background (6 % w/v agar), the inflicted lesion and the surrounding pork tissue as a function of the varied TI (150-3000 ms), showcasing magnetization decay inside the 3 T MRI scanner (Magnetom Vida, Siemens

Healthineers). Table 59 shows the T1 relaxation times as calculated from the plotted mean SI from images acquired inside the 1.5 T MRI scanner (Signa HD16, GE Healthcare) for the 10 homogeneous phantoms developed with different compositions. The T1 times of water and oil are also reported. Additionally, Table 59 includes T1 calculations for the single lesion inflicted on excised tissue, the area of overlapping lesions as well as the surrounding excised tissue.

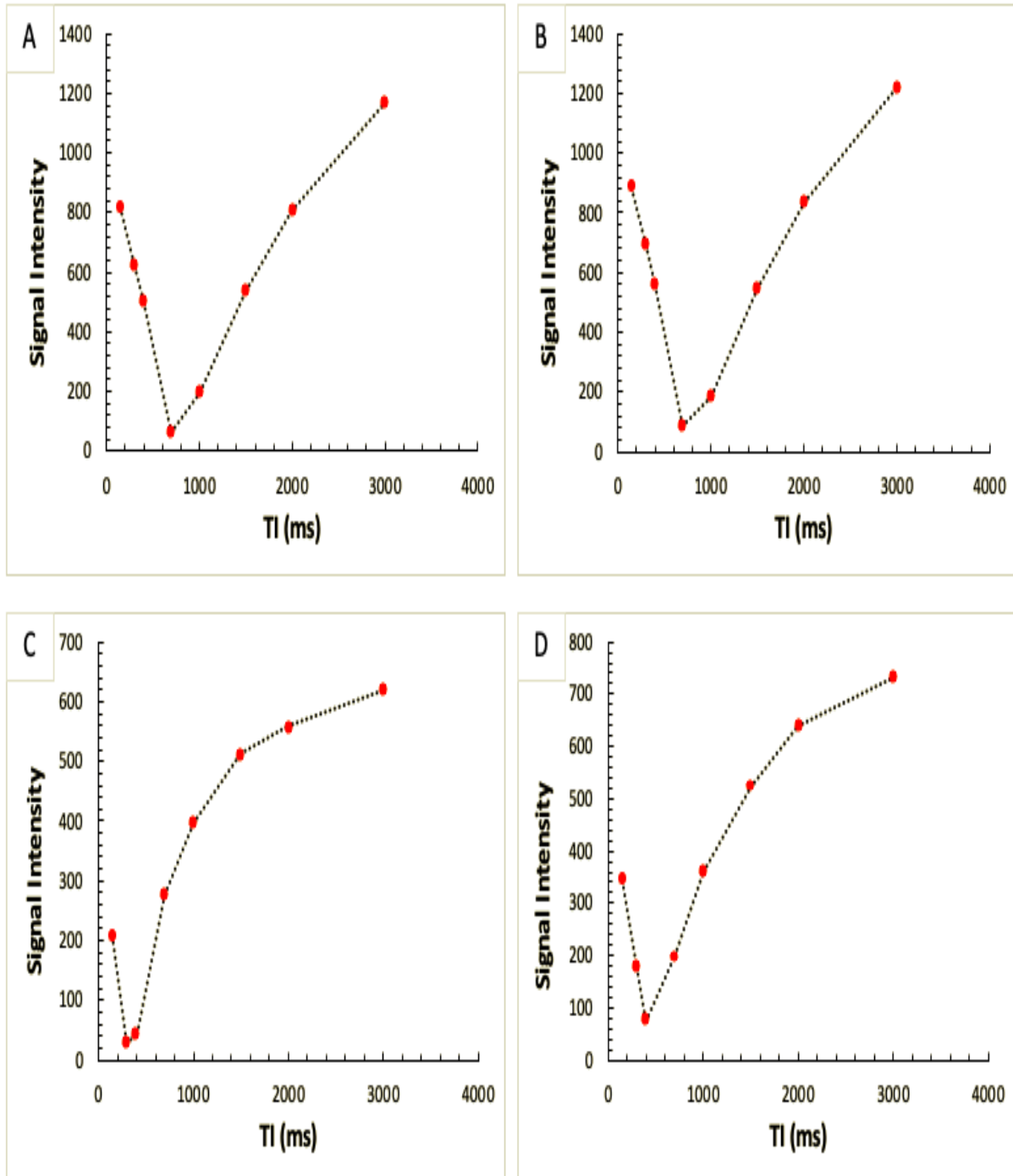


Figure 199: Signal intensities as measured from images acquired with an Inversion Recovery sequence inside a 3 T MRI scanner (Magnetom Vida, Siemens Healthineers) using varied TI values (150-3000 ms) for A) a tumor-like material (6 % w/v agar, 4 % w/v silica), B) an agar-based phantom (6 % w/v agar), C) a lesion inflicted on excised pork tissue, and D) a piece of excised pork tissue.

Table 59: T1 relaxation times as measured using IR sequences inside a 1.5 T MRI scanner (Signa HD16, GE Healthcare) for 10 homogeneous phantoms with different inclusions, a single lesion and an area of overlapping lesions inflicted on excised pork tissue as well as for the intact excised tissue surrounding the lesions.

Material	Nulling TI (ms)	T1 (ms)
Phantom (2 % w/v agar)	985	1431.06
Phantom (4 % w/v agar)	850	1228.25
Phantom (6 % w/v agar)	725	1051.46
Phantom (6 % w/v agar, 2 % w/v silica)	700	987.55
Phantom (6 % w/v agar, 4 % w/v silica)	675	976.4
Phantom (6 % w/v agar, 6 % w/v silica)	700	990.04
Phantom (6 % w/v agar, 4 % w/v silica, 10 % v/v milk)	600	862.98
Phantom (6 % w/v agar, 4 % w/v silica, 20 % v/v milk)	525	756.16
Phantom (6 % w/v agar, 4 % w/v silica, 30 % v/v milk)	500	698.15
Phantom (2 % w/v agar, 4 % w/v wood)	525	757.95
Water	-	1767.65
Oil	100	164.9
Single Lesion	300	408.3
Tissue surrounding single lesion	375	511.4
Area of overlapping lesions	250	349.5
Tissue surrounding overlapping lesions	375	535.4

Table 60 shows the T1 relaxation time calculations as measured inside the 3 T MRI scanner (Magnetom Vida, Siemens Healthineers) for the tumor-like phantom (6 % w/v agar, 4 % w/v silica), the agar-background (6 % w/v agar), the lesion and the surrounding excised tissue using the ROI approach.

Table 60: T1 relaxation times as measured using IR sequences inside a 3 T MRI scanner (Magnetom Vida, Siemens Healthineers) for an agar-based phantom (6 % w/v agar) with a tumor-like material (6 % w/v agar, 4 % w/v silica) and a single lesion inflicted on excised pork tissue.

Material	Nulling TI (ms)	T1 (ms)
Tumor-like phantom (6 % w/v agar, 4 % w/v silica)	750	1082.25
Phantom (6 % w/v agar)	765	1103.9
Lesion	325	468.98
Tissue surrounding lesion	465	671

Correspondingly, Table 61 shows the T1 relaxation time for the tumor-like phantom (6 % w/v agar, 4 % w/v silica), the agar-background (6 % w/v agar), the lesion and the surrounding excised tissue as measured from the parametric map using the voxel-by-voxel approach.

Table 61: T1 relaxation times as measured from a parametric map using voxel-by-voxel approach inside a 3 T MRI scanner (Magnetom Vida, Siemens Healthineers) for an agar-based phantom (6 % w/v agar) with a tumor-like material (6 % w/v agar, 4 % w/v silica) and a single lesion inflicted on excised pork tissue.

Material	T1 (ms)
Tumor-like phantom (6 % w/v agar, 4 % w/v silica)	2099.2
Phantom (6 % w/v agar)	2135.76
Lesion	751.33
Tissue surrounding lesion	1177.85

T2 relaxation time calculations

The 10 homogeneous agar-based phantoms were scanned inside the 1.5 T MRI scanner (Signa HD16, GE Healthcare) with a T2-W SE sequence (TR=2500 ms, FOV=260×260 mm², Slice thickness=7 mm, Matrix=192×128, NEX=2, ETL=14, Flip angle=90°) and TE values ranging from 52.2-243.5 ms. Correspondingly, the single lesion and area of overlapping lesions inflicted on excised pork tissue, were scanned inside the 1.5 T MRI scanner (Signa HD16, GE Healthcare) using a T2-W SE sequence (TR=2500 ms, FOV=260×260 mm², Slice thickness=7 mm, Matrix=192×128, NEX=2, ETL=14, Flip angle=90°) with TE values ranging from 17.38-156.46 ms and 17.5-227.14 ms respectively. For measurements inside the 3 T MRI scanner, the agar-based phantom (6 % w/v agar) with a tumor-like material (6 % w/v agar, 4 % w/v silica) and the excised tissue with the single lesion were scanned using two T2-W SE sequences with different parameters; one named as T2map_anatomical with TR=1910 ms, FOV=220×220 mm², Slice thickness=5 mm, Matrix=208×208, NEX=1, ETL=10, Flip angle=180° and TE values ranging from 13.8-138 ms, and one sequence named as t2_tse_cor_128 with TR=250 ms, FOV=260×260 mm², Slice thickness=10 mm, Matrix=128×128, NEX=2, ETL=12, Flip angle=180° and TE values ranging from 8.6-69 ms. Figure 200A and Figure 200B show typical MRI images of the agar-based phantom (6 % w/v agar) with the tumor-like material (6 % w/v agar, 4 % w/v silica) and the single lesion inflicted on excised pork tissue acquired with the two T2-W SE sequences inside the 3 T scanner (Magnetom Vida, Siemens Healthineers).

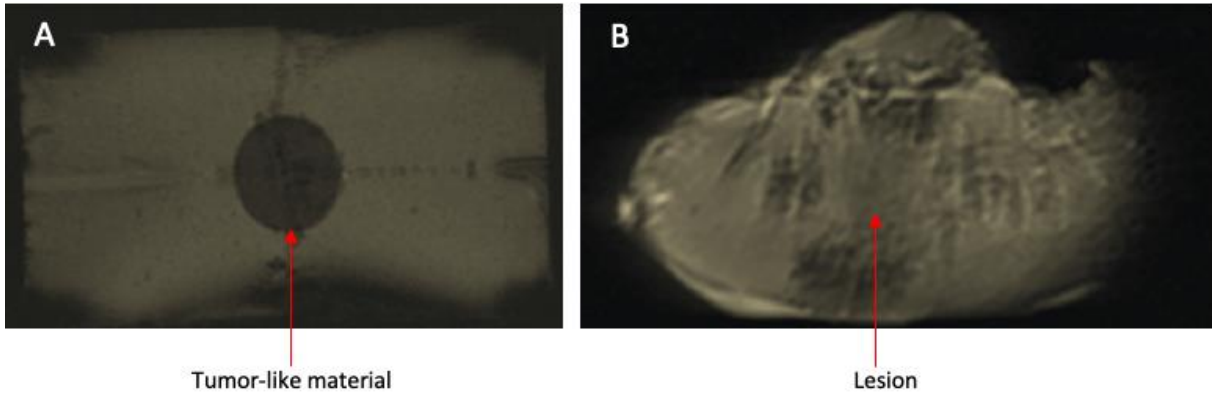


Figure 200: Coronal T2-W SE images of A) an agar-based phantom (6 % w/v agar) with a tumor-like material (6 % w/v agar, 4 % w/v silica) acquired using a TE of 34.52 ms, and B) a lesion inflicted on excised pork tissue acquired using a TE of 13.8 ms, inside a 3 T MRI scanner (Magnetom Vida, Siemens Healthineers).

Figure 201 shows typical plots of the mean SI measured in each of the ROIs set within the tumor-like material (6 % w/v agar, 4 % w/v silica), the agar-based background (6 % w/v agar), the inflicted lesion and the surrounding pork tissue as a function of the varied TE (13.8-138 ms), showcasing magnetization decay inside the 3 T MRI scanner (Magnetom Vida, Siemens Healthineers).

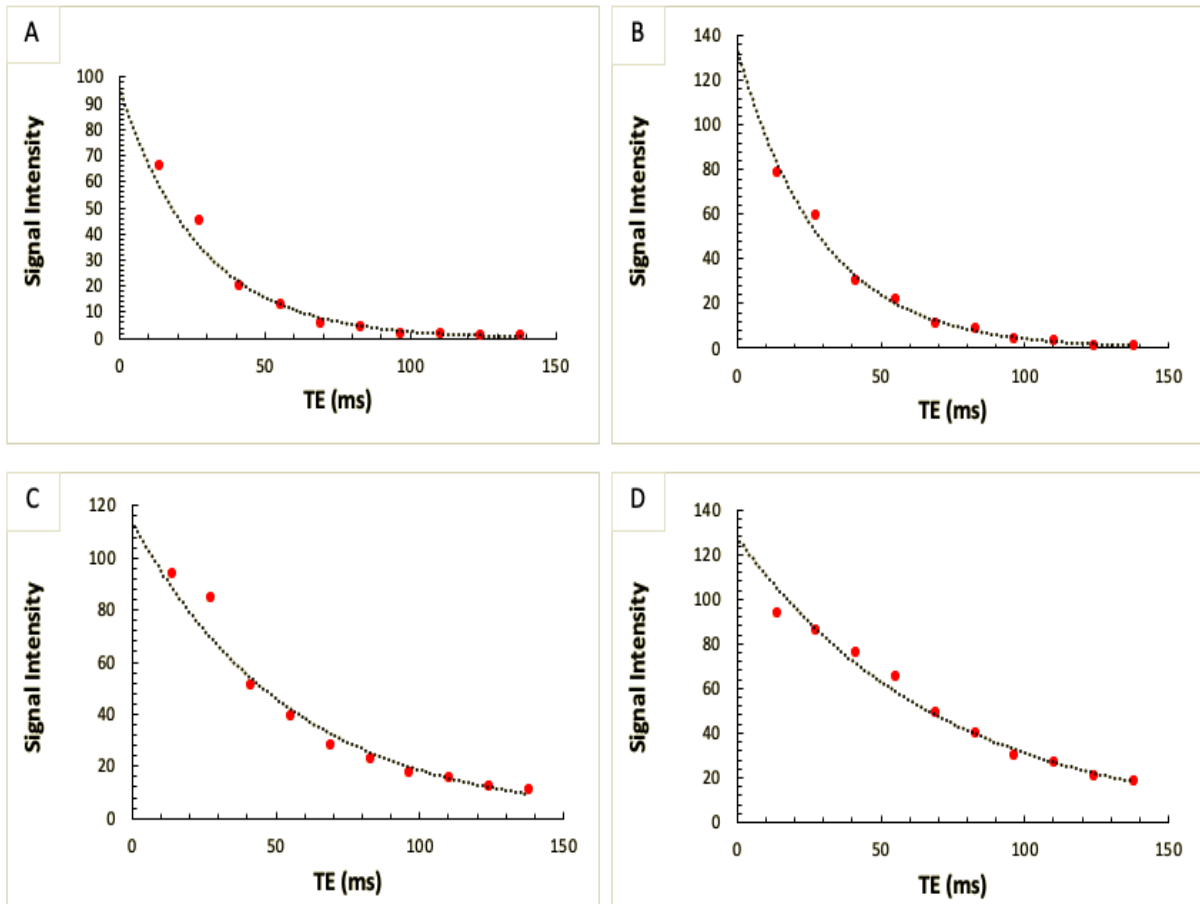


Figure 201: Signal intensities as measured from images acquired with a T2-W SE sequence inside a 3 T MRI scanner (Magnetom Vida, Siemens Healthineers) using varied TE values (13.8-138 ms) for (a) a tumor-like material (6 % w/v agar, 4 % w/v silica), (b) an agar-based phantom (6 % w/v agar), (c) a lesion inflicted on excised pork tissue, and (d) a piece of excised pork tissue.

Table 62 shows the T2 relaxation times as calculated from the exponential fit of the plotted mean SI for images acquired inside the 1.5 T MRI scanner (Signa HD16, GE Healthcare) for the 10 homogeneous phantoms developed with different compositions, the single lesion inflicted on excised tissue, the area of overlapping lesions and the surrounding excised tissue.

Table 62: T2 relaxation times as measured using T2-W SE sequences inside a 1.5 T MRI scanner (Signa HD16, GE Healthcare) for 10 homogeneous phantoms with different inclusions, a single lesion and an area of overlapping lesions inflicted on excised pork tissue as well as the intact excised tissue surrounding the lesions.

Material	T2 (ms)
Phantom (2 % w/v agar)	94.4
Phantom (4 % w/v agar)	74.5
Phantom (6 % w/v agar)	45.7
Phantom (6 % w/v agar, 2 % w/v silica)	40.2
Phantom (6 % w/v agar, 4 % w/v silica)	43.7
Phantom (6 % w/v agar, 6 % w/v silica)	39.6
Phantom (6 % w/v agar, 4 % w/v silica, 10 % v/v milk)	40.2
Phantom (6 % w/v agar, 4 % w/v silica, 20 % v/v milk)	42
Phantom (6 % w/v agar, 4 % w/v silica, 30 % v/v milk)	38.5
Phantom (2 % w/v agar, 4 % w/v wood)	86
Water	1308.9
Oil	80
Single Lesion	54.8
Tissue surrounding single lesion	72
Area of overlapping lesions	50.5
Tissue surrounding overlapping lesions	54.5

Table 63 shows the T2 relaxation time calculations as measured inside a 3 T MRI scanner (Magnetom Vida, Siemens Healthineers) for the tumor-like phantom (6 % w/v agar, 4 % w/v silica), the agar-background (6 % w/v agar), the lesion and the surrounding excised tissue using the two different T2-W SE sequences.

Table 63: T2 relaxation times as measured using T2-W SE sequences inside a 3 T MRI scanner (Magnetom Vida, Siemens Healthineers) for an agar-based phantom (6 % w/v agar) with a tumor-like material (6 % w/v agar, 4 % w/v silica) and a single lesion inflicted on excised pork tissue.

Material	T2 (ms)	
	T2map_anatomical sequence	t2_tse_cor_128
Tumor-like phantom (6 % w/v agar, 4 % w/v silica)	27.78	35.71
Agar-phantom (6 % w/v agar)	29.4	40
Lesion	55.56	45.45
Tissue	71.43	58.82

Subsection Conclusions

In this experiment, the T1 and T2 relaxation times of agar-based phantoms and lesions inflicted on excised tissue were measured inside two MRI scanners of different magnetic field strength (1.5 and 3 T). Specifically, inside the 1.5 T MRI scanner, 10 homogeneous agar-based phantoms having different compositions were imaged, while within the 3 T MRI scanner an agar-based phantom (6 % w/v agar) with a tumor-like material (6 % w/v agar, 4 % w/v silica) was correspondingly imaged. Analogously, in both scanners, excised pieces of pork tissue with inflicted lesions (single or multiple) were utilised for imaging.

A series of T1-W IR sequences at different TI and a series of T2-W sequences at different TE were performed for T1 and T2 relaxation time calculations, respectively. T1 and T2 relaxation time calculations were performed by fitting the SI measured from specific ROIs in the acquired images to the mathematical exponential decays of transverse and longitudinal magnetizations. Moreover, T1 relaxations within the 3 T MRI scanner were also performed using a voxel-by-voxel approach and generating parametric maps. Table 64 summarizes the T1 and T2 relaxation time calculations of the agar-based phantom (6 % w/v agar) with a tumor-like material (6 % w/v agar, 4 % w/v silica) and of the single inflicted lesion and its surrounding excised tissue as measured at both 1.5 T and 3 T MRI scanners. Regarding the 1.5 T, measurements as acquired for the two homogeneous phantoms having identical concentrations of inclusions with the tumor-like phantom (6 % w/v agar, 4 % w/v silica) and its agar-based background (6 % w/v agar) are reported.

Generally, for the four investigated materials (tumor-like phantom, agar-background, lesion and tissue) T1 and T2 relaxation times measured with the ROI approach differed between the two magnetic field strengths. Specifically, T1 relaxation time was generally longer (6-30 %), while T2 relaxation time was lower (13-22 %) at 3 T compared to 1.5 T, with the degree of change varying with the type of the investigated material, thus corroborating similar relaxometry trends reported in previous studies [1], [2] executed on human tissues at similar magnetic field strengths.

Table 64: T1 and T2 relaxation time as measured within a 1.5 T (Signa HD16, GE) and a 3 T MRI scanner (Magnetom Vida, Siemens Healthineers) for an agar-based phantom (6 % w/v agar) with a tumor-like material (6 % w/v agar, 4 % w/v silica) and a single lesion inflicted on excised pork tissue.

Material	T1 (ms)			T2 (ms)		
	1.5 T (ROI approach)	3 T (ROI approach)	3 T (Voxel approach)	1.5 T (ROI approach)	3 T (ROI approach)	
					T2map_anatomical sequence	t2_tse_cor_128
Tumor-like phantom (6 % w/v agar, 4 % w/v silica)	976.4	1082.25	2099.2	43.7	27.78	35.71
Agar-phantom (6 % w/v agar)	1051.46	1103.9	2135.76	45	29.4	40
Lesion	408.3	468.98	751.33	54.8	55.56	45.45
Tissue	511.4	671	1177.85	72	71.43	58.82

Moreover, at both 1.5 and 3 T, the estimated T1 and T2 relaxation times of lesions were lower than the respective relaxation time of the surrounding excised pork tissue as expected from the literature [3]. Additionally, a greater difference in the T1 relaxation time was observed, at both 1.5 T and 3 T, between the lesion and the surrounding tissue compared to the T2 relaxation time, with the T2 relaxation time of the lesion as estimated at 1.5 T being proximal to T2 relaxation times previously reported for HIFU lesions inflicted on excised porcine liver [4]. Correspondingly, T1 and T2 relaxation times of the agar-phantom (6 % w/v agar) at both 1.5 T and 3 T were higher than the tumor-like material (6 % w/v agar, 4 % w/v silica), since the

addition of silica has been previously shown to have a negative effect on the relaxation times [5].

Noteworthy, the T1 relaxation times as measured at 3 T using a voxel-by-voxel approach were higher than the respective measurements obtained with the ROI approach. Nevertheless, this might be attributed to the fact the parametric maps are susceptible to a higher degree of noise in the parameter estimates since the analysis is based on a voxel-by-voxel basis. Future experiments will investigate this further.

References

- [1] C. M. J. De Bazelaire, G. D. Duhamel, N. M. Rofsky, and D. C. Alsop, "MR Imaging Relaxation Times of Abdominal and Pelvic Tissues Measured in Vivo at 3.0 T: Preliminary Results," *Radiology*, vol. 230, no. 3, 2004, doi: 10.1148/radiol.2303021331.
- [2] R. Rakow-Penner, B. Daniel, H. Yu, A. Sawyer-Glover, and G. H. Glover, "Relaxation times of breast tissue at 1.5T and 3T measured using IDEAL," *J. Magn. Reson. Imaging*, vol. 23, no. 1, 2006, doi: 10.1002/jmri.20469.
- [3] V. Hadjisavvas, K. Ioannides, M. Komodromos, N. Mylonas, and C. Damianou, "Evaluation of the contrast between tissues and thermal lesions in rabbit in vivo produced by high intensity focused ultrasound using fast spin echo MRI sequences," *J. Biomed. Sci. Eng.*, vol. 04, no. 01, 2011, doi: 10.4236/jbise.2011.41007.
- [4] A. Eranki *et al.*, "Mechanical fractionation of tissues using microsecond-long HIFU pulses on a clinical MR-HIFU system," *Int. J. Hyperth.*, vol. 34, no. 8, 2018, doi: 10.1080/02656736.2018.1438672.
- [5] A. Antoniou *et al.*, "MR relaxation times of agar-based tissue-mimicking phantoms," *J. Appl. Clin. Med. Phys.*, vol. 23, no. 5, May 2022, doi: 10.1002/acm2.13533.